

ON THE CRANIAL OSTEOLOGY OF THE AFRICAN PALM CIVET,  
*NANDINIA BINOTATA* (GRAY, 1830)  
(MAMMALIA, CARNIVORA, FELIFORMIA)

JOHN R. WIBLE

Curator, Section of Mammals

Carnegie Museum of Natural History, 5800 Baum Boulevard, Pittsburgh, Pennsylvania 15206  
wiblej@carnegiemnh.org

MICHELLE SPAULDING

Rea Postdoctoral Fellow, Section of Mammals

Carnegie Museum of Natural History, 5800 Baum Boulevard, Pittsburgh, Pennsylvania 15206  
spauldingm@carnegiemnh.org

ABSTRACT

The external and endocranial surfaces of the skull of the African palm civet, *Nandinia binotata* (Gray, 1830), are described and illustrated in detail based on 30 specimens (from Carnegie Museum of Natural History and American Museum of Natural History). With the inclusion of a newborn and six juveniles with deciduous dentitions, a reasonable ontogenetic series is represented. The bone-by-bone descriptions are primarily based on the condition in an adult female and the newborn with consideration of variation across the sample. The principal cranial foramina are treated in a glossary, and the hyoid apparatus and larynx are described from a single specimen. The sample exhibits a remarkable degree of variability in cranial features that are often used as different states of characters in phylogenetic analysis (e.g., number and position of palatal foramina, the orbital mosaic, and composition of the lacrimal foramen).

*Nandinia binotata*, the only taxon in the Nandiniidae, has been identified as the most basal extant feliform in recent phylogenetic analyses of both molecular and morphological data. It has long been recognized that its ear region with its uninflated auditory bulla exhibits a primitive level of organization. To assess the primitive nature of the skull of *N. binotata*, comparisons are made with three extant carnivorans, the felid *Felis catus* Linnaeus, 1758, the viverrid *Genetta genetta* (Linnaeus, 1758), and the canid *Canis lupus* Linnaeus, 1758. Of the three, *N. binotata* shares numerous resemblances across the skull with *G. genetta*, which accounts for its historical inclusion in the Viverridae. Whereas aspects of the ear region of *N. binotata* are clearly unique among extant carnivorans, the rest of its skull is not similarly so.

KEY WORDS: African palm civet, auditory ossicles, Carnivora, endocranium, foramina, hyoid, mandible, skull

INTRODUCTION

The placental order Carnivora is divided into two main subclades, the ‘cat-like’ Feliformia and the ‘dog-like’ Caniformia. The nominal members of these two, the domestic cat, *Felis catus* Linnaeus, 1758, and dog, *Canis lupus familiaris* Linnaeus, 1758, have been subjects of numerous anatomical treatises (e.g., Mivart 1881; Ellenberger and Baum 1891; Jayne 1898; Baum and Zietzschmann 1936; Evans 1993). These reference works are frequently used in comparative studies throughout Mammalia. However, this reliance on domestic forms may not be well justified for studies of mammals far afield taxonomically from Carnivora. There is little choice, though, as so few non-human species have been studied to the same level of detail as the cat and dog.

Based upon our knowledge of stem fossil carnivoramorphans (Flynn and Wesley-Hunt 2005; Flynn et al. 2010), the dog family Canidae, including its less transformed domestic breeds, offers a reasonable model for the primitive carnivoran bauplan. This family is generally found to be the sister taxon to all other caniforms (e.g., Wesley-Hunt and Flynn 2005; Agnarsson et al. 2010; Eizirik et al. 2010). In contrast, members of the cat family Felidae are strikingly different from stem fossil taxa and there is unambiguous agreement that Felidae is not the first feliform family to diverge. The extant clade in that position in recent morphological and molecular analyses (e.g., Wesley-Hunt

and Flynn 2005; Agnarsson et al. 2010; Eizirik et al. 2010; Meredith et al. 2011) is the monotypic Nandiniidae, which contains the African palm civet, *Nandinia binotata* (Gray, 1830). In addition, previous morphological studies have proposed *N. binotata* as somewhat of a living fossil as it retains many primitive anatomical features, especially in its ear region (Hunt 1989, 1998, 2001). Consequently, in Feliformia, *N. binotata* likely represents a more reasonable morphological model of the common ancestor of Carnivora than *F. catus*.

*Nandinia binotata* has not always been recognized as the basalmost member of Feliformia. In 1830, John Edward Gray, later to be Keeper of Zoology at the British Museum, named the two-spotted civet from Ghana, *Viverra binotata* Gray, 1830, relating it to the large Indian civet, *Viverra zibetha* (Linnaeus, 1758) (see Rosevear 1974:230, for the confusing story on the attribution of authorship for *V. binotata*). Two years later, Gray suggested *Paradoxurus? binotatus* (Gray, 1832), in reference to similarities with the Asian palm civet and also named another taxon, *Paradoxurus hamiltonii* Gray, 1832. He finally synonymized these taxa within the new monotypic genus, *Nandinia* Gray, 1843. In 1864, Gray formally united *Nandinia* with the Asian palm civets *Paradoxurus* F. Cuvier, 1821, *Paguma* Gray, 1831, and *Arctogale* Peters, 1864, in the tribe Paradoxurina within the family Viverridae. Close relationships

between *N. binotata* and the Asian palm civets have been supported by various workers nearly to the present day (e.g., Flower 1869; Mivart 1882; Gregory and Hellman 1939; Simpson 1945; Honacki et al. 1982; Bininda-Emonds et al. 1999).

Nevertheless, soon after its discovery, numerous observations demonstrated that *N. binotata* differed from other paradoxurines. For example, Flower (1869, 1872) first noted that the posterior part of the auditory bulla is cartilaginous and that the cecum is absent in *N. binotata* compared to the entirely bony bulla and well-developed cecum of the Asian palm civets. In contrast to the prevailing paradoxurine paradigm, several authors promoted other relationships for *N. binotata*. Winge (1941 translation of his 1895 book in Danish) identified it as the only extant member of his Amphictididae, which included *Miacis* Cope, 1872, and *Didymictis* Cope, 1875, among other early Paleogene forms. He observed (p. 217) that “The skull, particularly in the structure of *Proc. jugularis* and the tympanic cavity, is almost identical with that of *Amphictis*.” This fossil form was later considered as an Oligocene-Miocene procyonid (McKenna and Bell 1997). In response to Winge, Carlsson (1900) produced the most comprehensive description of the anatomy of *N. binotata* to date. She addressed aspects of the skeleton, dentition, musculature, stomach, liver, brain, and larynx. Her conclusion was that in the majority of features *N. binotata* is a viverrid, but a possible link between viverrines and herpestids. She found no specific relationship with paradoxurines. Pohle (1920) revisited the features of *Nandinia* studied by Carlsson and concluded that Winge was correct, formally placing *Nandinia* within the Miacidae, along with *Viverravinae* and *Miacinae*. Even though Pocock (1915) found oddities of the perineal scent glands in *N. binotata*, he ultimately concluded that *N. binotata* belonged with the paradoxurines; however, in 1929, he reconsidered and placed the African palm civet in the monotypic family *Nandiniidae*, noting that its auditory and mastoid regions were unique among feliforms. He also noted (p. 898) that *N. binotata* “is an extremely interesting primitive type, resembling in many cranial and dental characters, especially the structure of the bulla, the extinct *Miacidae* of the Eocene.”

Gregory and Hellman (1939) published a revision of the *Viverridae* and a new classification for *Carnivora*. They acknowledged the features that Pocock (1929) used to distinguish *N. binotata* from the paradoxurines, but identified these differences as specializations of the African palm civet that occurred after the common viverrid ancestry. They reconfigured the *Viverridae* into four sections, one being the *Paradoxurida* with the subfamilies *Paradoxurinae*, *Arcotalidiinae*, and *Nandiniinae*. Their most radical conclusion was their treatment of various early Paleogene taxa; they placed fossils within the *Viverridae* that today are identified as *carnivoramorphans* falling outside of crown *Carnivora* (Wesley-Hunt and Flynn 2005; Spaulding et al. 2010; Spaulding and Flynn 2012) within the section *Viverrida* in the subfamilies *Miacinae* and *Viverrinae*. The for-

mer was wholly extinct, but the latter included *Viverravus* Marsh, 1872, and *Didymictis* along with extant viverrines.

For carnivoran systematics, the ear region and neighboring basicranium have long been a focus of study (e.g., Turner 1848; Flower 1869; Hough 1948), and *N. binotata* has held a central role as it is the only extant carnivoran with a cartilaginous entotympanic in the adult, a rare condition among placental mammals in general (Kampen 1905; Klaauw 1931; Novacek 1977; MacPhee 1979). The researcher that has made the most substantive contributions on the ear region of *N. binotata*, and in many other extant and extinct carnivorans, is R.M. Hunt, Jr. In 1974, Hunt made detailed observations about the elements of the auditory bulla and carotid vasculature in extant representatives of all carnivoran families, including *N. binotata* as a representative of *Viverridae*. In 1987, Hunt conducted a character analysis of various ear region features and concluded that *N. binotata* is the living carnivoran closest to the projected feliform morphotype; he identified *N. binotata* as the sister group of other extant feliforms and resurrected Pocock’s (1929) *Nandiniidae*. Hunt (1989, 1998, 2001) reinforced this position with further studies of various extinct and extant feliforms. Subsequently, phylogenetic analyses of morphological (e.g., Véron 1995; Spaulding and Flynn 2012) and DNA data (e.g., Gaubert et al. 2005; Flynn et al. 2005) have supported Hunt’s position for *N. binotata* as sister to other extant feliform, which as noted above is widely held today (see also, Wozencraft 2005; Gaubert 2009).

Since 2003, the senior author has published a series of descriptions of the skull within various mammalian clades (Wible 2003, 2007, 2008, 2011; Wible and Gaudin 2004; Giannini et al. 2006). In choosing a carnivoran for this series, *N. binotata* seemed an obvious choice, due to its position as sister to all other feliforms and its purported resemblance to plesiomorphic extinct *carnivoramorphans*. Although aspects of the hard- and soft-tissue cranial anatomy of *N. binotata* have been investigated previously (e.g., Tandler 1899; Carlsson 1900; Pocock 1916; Allen 1924; Gregory and Hellman 1939; Davis and Story 1943; Van Valen 1963; Chapuis 1966; Rosevear 1974; Hunt 1974, 1989, 1998, 2001; Wozencraft 1984; Wible 1984), a detailed and illustrated description of the whole skull has not been accomplished. It is the goal of this report to fill this void.

## MATERIALS AND METHODS

The specimens studied here are from the collections of the American Museum of Natural History (AMNH) and the Carnegie Museum of Natural History (CM). The majority of the AMNH specimens are from the sample of 73 *N. binotata* collected by the American Museum Congo Expedition (Allen 1924), the same sampling that Gregory and Hellman (1939) and Hunt (1974, 1989, 1998, 2001) used for their studies. The majority of the CM specimens are from Cameroon, with two each from both Ivory Coast and Malawi. Some authors (e.g., Ellerman et al. 1953; Meester

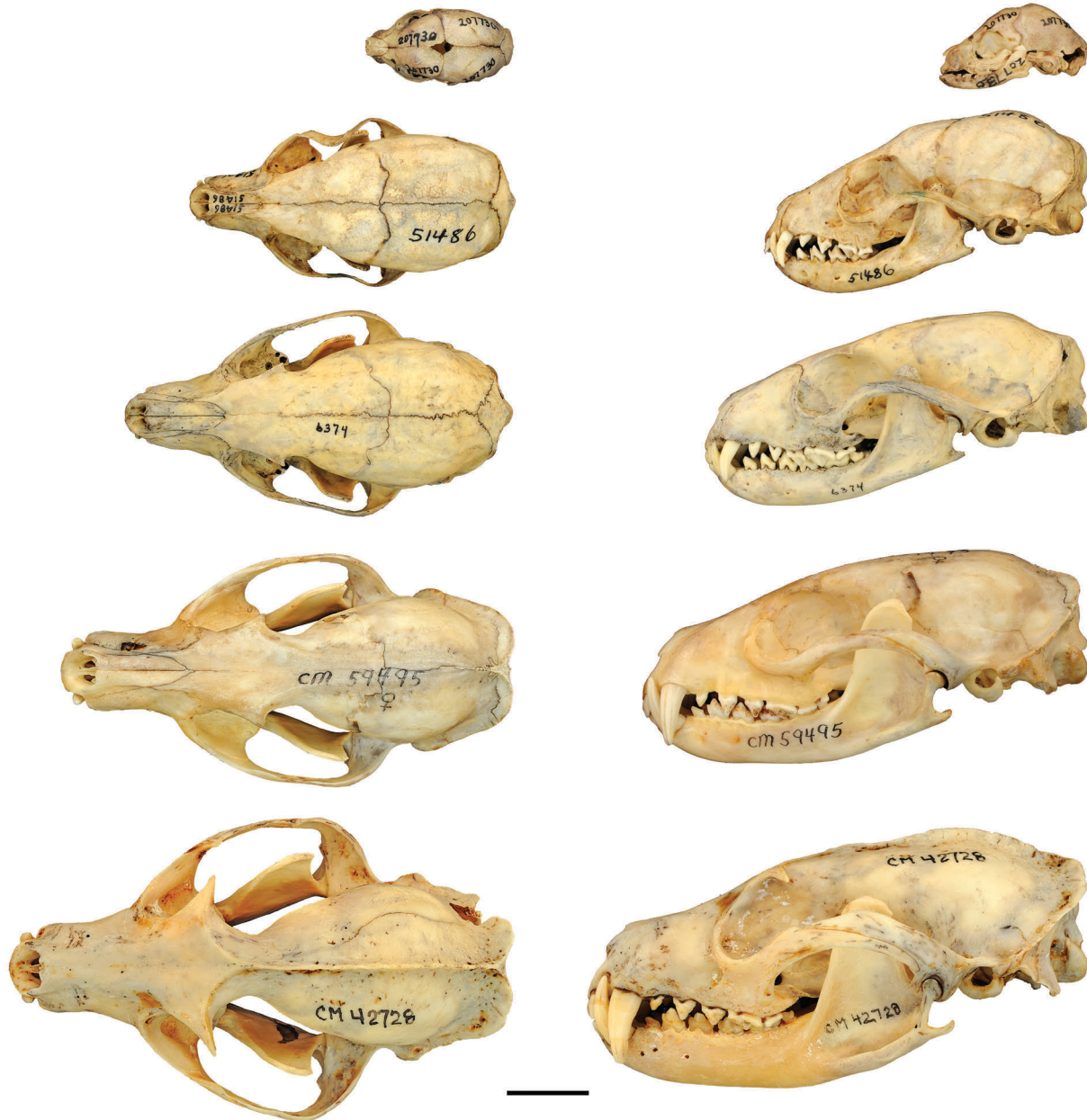


Fig. 1—Skulls and lower jaws of *Nandinia binotata* in dorsal and left lateral views. From top to bottom, newborn of unknown sex, AMNH 207730; juveniles, AMNH 51486, a female, and CM 6374, a male; and adult females, CM 59495 and CM 422782. Scale = 20 mm.

et al. 1986; Kingdon 1997) recognize two subspecies, grouping the East African isolates into *N. binotata gerrardi* (Thomas, 1893), and those from the main Central and West African forest block into *N. binotata binotata* (Gray, 1830). Other authors (e.g., Allen 1939; Meester and Setzer 1971; Rosevear 1974; Gaubert 2009) recognize four subspecies by further subdividing the East African and Central/West African populations. Of the 30 specimens examined here, 26 are from localities in the distribution area of *N. b. binotata*. The two from Malawi are in the distribution area of *N. b. gerrardi*, which also includes Mozambique,

and southern and eastern Tanzania, northeastern Zambia, and eastern Zimbabwe, and the remaining two specimens are from the New York Zoological Society. Thomas (1893) named *N. gerrardi* as a second species of the genus, but it has not been so recognized by subsequent authors. *Nandinia b. arborea* Heller, 1913, is from Kenya, southern Sudan, northern Tanzania, and Uganda, and *N. b. intensa* Cabrera and Ruxton, 1926, is from southern Congo, Angola, and northwestern Zambia.

The 30 specimens range from a newborn to advanced adults with few open cranial sutures (Fig. 1). The specimens

**TABLE 1.** Status of sutures of selected cranial bones in the *Nandinia binotata* specimens studied here: 0, open; 1, partially closed; 2, fully closed. Abbreviations: **FR**, interfrontal; **NA**, internasal; **PA**, inter-parietal; **FR/NA**, frontonasal; **PAL**, interpalatine; **PAL/MX**, palatomaxillary; **BS/BO**, basisphenoid/basioccipital; **PA/OC**, parietoccipital; **FR/LAC**, frontolacrimal; **FR/PA**, frontoparietal; **OC**, intra-occipital; **PT**, pterygosphenoidal.

Specimen	FR	NA	PA	FR/NA	PAL	PAL/MX	BS/BO	PA/OC	FR/LAC	FR/PA	OC	PT
AMNH 207730	0	0	0	0	0	0	0	0	0	0	0	0
AMNH 51471	0	0	0	0	0	0	0	0	0	0	0	0
AMNH 51486	0	0	0	0	0	0	0	0	0	0	1	1
CM 6371	0	0	0	0	0	0	0	0	0	0	1	1
AMNH 51488	0	0	0	0	0	0	0	0	0	0	2	1
CM 6374	0	0	0	0	0	0	0	0	0	0	2	1
AMNH 201513	0		0	0	0	0	0	0	0	0	2	1
AMNH 51448	0	0	0	0	0	0	0	0	0	0	2	1
CM 42281	0	0	0	0	0	0	0	0	0	0	2	1
CM 5157	0	0	0	0	0	0	0	0	0	0	2	1
CM 2356	0	0	0	0	0	0	0	0	0	0	2	1
CM 59497	0	0	0	0	0	0	0	0	0	0	2	1
AMNH 51503	0	0	0	0	0	0	0	0	0	0	2	1
CM 59495	1	0	0	0	0	0	0	1	0	0	2	1
AMNH 134969	1	0	1	0	0	0	0	0	0	0	2	1
CM 59496	1	1	1	0	0	0	0	0	0	0	2	1
CM 42727	1	1	1	0	0	0	0	0	0	0	2	1
CM 3693	2	0	2	0	0	0	0	0	0	0	2	1
CM 42725	2	1	1	0	0	0	0	0	0	1	2	2
CM 42726	2	1	1	0	0	0	0	0	0	0	2	1
CM 42282	2	1	1	0	0	0	0	0	0	0	2	1
CM 69365	2	1	2	0	0	0	1	1	0	0	2	1
CM 69366	2	1	2	0	0	0	1	1	0	1	2	1
AMNH 51510	2	1	2	2	0	0	1	1	1	2	2	1
CM 16103	2	1	2	1	1	0	1	2	1	2	2	2
AMNH 51494	2	2	2	2	0	0	2	1	0	2	2	2
AMNH 51445	2	2	2	2	0	0	2	1	2	2	2	2
CM 42728	2	2	2	2	0	0	2	2	2	2	2	2
CM 5097	2	2	2	2	0	1	2	1	2	2	2	2
AMNH 5153	2	2	2	2	1	1	2	2	2	2	2	2

are listed below in order from youngest to oldest, based on our investigations of cranial sutures (see Table 1). After the newborn are six juveniles, which are identified as such because they do not have the full adult dentition; comments about their dentition are included with the following abbreviations: “d,” deciduous; “I/i,” upper/lower incisors; “C/c,” upper/lower canines; “P/p,” upper/lower premolars; and “M/m,” upper/lower molars. The remaining 25 specimens have adult dentitions. Relevant cranio-mandibular measurements are present in Table 2.

(1) AMNH 207730, sex unknown, newborn, New York

Zoological Society. The di1, di2, di1, and di2 are erupting. The di3, di3, dC, dc, P1, p1, dP2, dp2, dP4, and dp4 are visible in their crypts.

(2) AMNH 51471, male juvenile, Medje, Zaire, collected September 23, 1910. The full deciduous dentition is erupted (di1–3, dC, dP2, dP4–5, di1–3, dc, dp2, dp4–5). The p1 and P1 are just erupting; the m1 and M1 are forming in their crypts; a crypt is present for m2, but a developing tooth is not preserved.

(3) AMNH 51486, female juvenile, Niapu, Zaire, collected November 17, 1913. The full deciduous dentition

**TABLE 2.** Cranial and mandibular measurements of the *Nandinia binotata* specimens studied here. \* indicates estimate; AMNH 51445 is not included as it is too damaged even for estimates. Abbreviations: **GSL**, greatest skull length; **ZB**, greatest zygomatic breadth; **BCW**, greatest braincase width; **POB**, greatest width across postorbital process of frontal; **POC**, narrowest width at post-orbital constriction; **POL Rt**, preorbital length, right side; **ML Rt**, greatest mandibular length, right side; **BCH**, greatest braincase height.

Specimen	Sex	GSL	ZB	BCW	POB	POC	POL Rt	ML Rt	BCH
AMNH 207730	?	33.6	17.1	16	12.1	-	8.7	21.5	16.3
AMNH 51471	M	69.2	36.0	29.5	16.4	15.8	18.9	43.5	24.5
AMNH 51486	F	70.0	36.3	28.5	17.9*	17.3	20.6	44.9	25.9
CM 6371	F	72.4	38.7	30.2	18.3	16.4	21.9	48.3	24.9
AMNH 51488	F	73.2	37.4	29.4	16.6	14.6	21.5	47.6	24.6
CM 6374	M	81.6	43.1	29.7	20.7	17.0	25.8	54.4	24.9
AMNH 201513	?	76.5*	-	30.5	22.4	17.5	25.6	-	27.7
AMNH 51448	F	85.7*	-	31.3	22.0	16.7	27.2	59.7	26.6
CM 42281	?	95.7	48.1	-	24.2*	14.9	31.4	64.6	27.9
CM 5157	?	93.9	49.9	31.5	23.6	14.7	31.9	63.7	27.0
CM 2356	M	92.8	47.2	30.5	24.2	15.1	29.8	63.5	27.1
CM 59497	M	96.9	53.3	30.2	28.2	15.0	31.4	68.7	29.2
AMNH 51503	F	94.3	47.3	30.0	20.9*	13.9	30.8	65.6	27.7
CM 59495	F	92.6	47.9	29.7	22.2	13.8	31.4	63.5	26.9
AMNH 134969	?	103.8*	58.2	28.5	29.2	14.1	34.8	71.2	-
CM 59496	F	100.0	51.5	30.4	29.7	14.5	31.6	68.9	29.0
CM 42727	F	88.7	50.6	-	27.4	14.1	28.2	60.6	29.0
CM 3693	?	98.3	55.7	31.4	27.7	13.4	31.4	68.6	30.0*
CM 42725	F	91.1	53.8	30.9	30.8	14.3	30.1	62.1	28.6
CM 42726	M	101.2	57.5	32.0	28.8	13.7	32.5	70.1	28.1
CM 42282	F	103.6	58.0	32.2	30.6	13.0	33.5	73.9	28.4
CM 69365	M	97.0	54.8	32.2	25.0	13.4	33.1	68.7	29.1
CM 69366	F	87.6	50.7	30.6	25.6	14.4	29.1	60.8	27.4
AMNH 51510	F	93.6	52.6	31.7	28.9	14.7	29.5	66.1	27.0
CM 16103	F	90.7	53.1	31.0	29.9	13.9	27.6	65.2	28.7
AMNH 51494	M	99.7	53.6	29.6	30.4	14.1	32.4	70.0	28.0
CM 42728	M	99.3	60.9	30.6	33.9	11.6	33.3	70.5	29.4*
CM 5097	M	100.2	57.6	30.1	33.6	14.6	32.9	69.7	29.4
AMNH 5153	F	96.2	54.2	30.1	28.0*	13.0	32.1	67.6	27.8

and the P1 and p1 are erupted. Crypts for I1–2 and i1 are open. The m1 is in its crypt; the M1 and m2 are forming in crypts.

(4) CM 6371, female juvenile, Cholo, Malawi, collected March 28, 1926. The I1 is erupted bilaterally and the right i1 is erupting; the deciduous predecessors at both loci are shed. The M1 and m1 are in crypts; the m2 is forming.

(5) AMNH 51488, female juvenile, Niapu, Zaire, collected November 25, 1913. The I1–2 and i1 are erupted; the i2 is erupting and its deciduous predecessor is still in place. The M1, m1, and m2 are in crypts. The left ear region

was figured in Hunt (1987: fig. 16A).

(6) CM 6374, male juvenile, Cholo, Malawi, June 18, 1927. The dI3, di3, dC, dc, dP2, dp2, dP4, dp4 are still in their alveoli; the P5, p5, M1, m1, and m2 are erupted; and the M2 is forming in its crypt.

(7) AMNH 201513, sex unknown, juvenile, Djaiposten, Cameroon, collected September 1929. The mandible is missing. Most upper teeth have fallen out of their alveoli; only the dP4 and dP5 remain. The left I2 is erupting; the I3, C, and P2 are in their crypts; and the P5 is erupting.

(8) AMNH 51448, female, Akenge, Zaire, collected

October 7, 1913. The C is erupting.

(9) CM 42281, sex unknown, Eseka, Cameroon, collected March 8, 1974.

(10) CM 5157, sex unknown, Cameroon, collected 1920.

(11) CM 2356, male, Batanga, Cameroon, collected April 30, 1912.

(12) CM 59497, male, Ambam, Cameroon, collected August 1, 1978.

(13) AMNH 51503, female, Niapu, Zaire, collected December 4, 1913.

(14) CM 59495, female, Ambam, Cameroon, collected July 28, 1978.

(15) AMNH 134969, sex unknown, New York Zoological Society, received December 1946.

(16) CM 59496, female, Ambam, Cameroon, collected July 30, 1978.

(17) CM 42727, female, Kribi, Cameroon, collected August 11, 1944.

(18) CM 3693, sex unknown, Cameroon.

(19) CM 42725, female, Ebolowa, Cameroon, collected March 18, 1945.

(20) CM 42726, male, Ebolowa, Cameroon, collected April 5, 1941.

(21) CM 42282, female, Eseka, Cameroon, collected May 8, 1974.

(22) CM 69365, male, Lakota, Ivory Coast, collected October 23, 1971.

(23) CM 69366, female, Lakota, Ivory Coast, collected October 23, 1971.

(24) AMNH 51510, female, Niapu, Zaire, collected December 24, 1913.

(25) CM 16103, female, Lolodorf, Cameroon, collected June 8, 1937.

(26) AMNH 51494, male, Niapu, Zaire, collected November 28, 1913.

(27) AMNH 51445, male, Akenge, Zaire, collected October 3, 1913.

(28) CM 42728, male, Kribi, Cameroon, collected August 11, 1944.

(29) CM 5097, male, Metet, Cameroon, collected January 9, 1919.

(30) AMNH 51513, female, Niapu, Zaire, collected January 22, 1914.

The terminology employed here follows that in prior similar publications by the senior author and collaborators, with English equivalents of the *Nomina Anatomica Veterinaria* (Fifth Edition 2005) and *Nomina Anatomica* (Fifth Edition 1983) used when appropriate; the former is abbreviated NAV in this report. In instances when the *Nominae* are inadequate (e.g., auditory ossicles), the most appropriate terms from the comparative literature are employed. Appendix 1 is a list of anatomical terms used along with references and equivalents; preceding it is a glossary of osseous structures associated with nerves, arteries, and/or veins.

Adult *N. binotata* have a dental formula in the upper

and lower jaws of three incisors, a canine, four premolars, and two molars, with variation in the presence of the upper second molar reported (Gaubert 2009). Teeth in classes of multiples (i.e., incisors, premolars, and molars) can be numbered from one anteriorly to the last number in the class (e.g., P1, P2, P3, P4, for upper premolars), or teeth can be numbered with a hypothesis of homology with reference to an ancestral condition with more teeth. It is generally held (e.g., Kielan-Jaworowska et al. 2004; Wible et al. 2007, 2009; but see O'Leary et al. 2013) that the primitive formula for Eutheria for teeth in the classes of multiples has five upper and lower premolars, three upper and lower molars, and five upper and four lower incisors. It has long been recognized that the missing molar in forms such as *N. binotata* is the ancestral ultimate one (see Wesley-Hunt and Flynn 2005; Spaulding et al. 2010; Spaulding and Flynn 2012); therefore, the appropriate numeration for the molars of *N. binotata* is M1/m1 and M2/m2. Regarding the incisors, there is no generally accepted model of incisor loss in placentals (see discussion in Wible 2008) and we simply number these teeth in *N. binotata* as I1/i1, I2/i2, and I3/i3 without a hypothesis of incisor loss. In the premolar series it is widely accepted that the reduction from the ancestral condition of five to the maximum of four occurring in placentals occurred at the middle locus (Nessov et al. 1998; Wible et al. 2007, 2009; Archibald and Averianov 2012). In light of this hypothesis, we number the premolars of *N. binotata* as P1/p1, P2/p2, P4/p4, and P5/p5.

## DESCRIPTIONS

The descriptions begin with an overview of the external surfaces of the principal adult and neonatal skulls, CM 59495 and AMNH 207730, to highlight features that span multiple cranial bones and differ ontogenetically. The overview is in five views: dorsal, anterior, lateral, ventral, and posterior. The five figures that accompany these views (Figs. 2–4, 6, 29) do not follow the usual sequential numerical citation that is found elsewhere. Our goal is to place figures with or near their primary textual references, and the last two (Figs. 6, 29) illustrate structures that appear later. Following the overview is a bone-by-bone description that considers the anatomy in the principal adult, the neonate, and others. The last includes comparisons across the entire study sample. In citing specimens, numbers followed by “(R)” or “(L)” signify the occurrence of a feature on only the “right” or “left” side. The order of bone descriptions follows that in prior works by the senior author (e.g., Wible 2008, 2011), which is roughly anterior to posterior through the rostrum, palate, braincase roof, mesocranium, orbit, basicranium, occiput, mandible, and hyoid apparatus. Finally, there is a treatment of the endocranium as a whole. The nasal cavity will not be treated in this report as the authors intend to address it separately.

### Overview

**Dorsal View.**—The adult skull (Figs. 2A–B) is comprised of three roughly subequal parts: the rostrum, the orbitotemporal region, and the braincase. The projecting rostrum has sub-parallel sides and premaxillae that extend anteriorly well beyond the nasals. The orbitotemporal region is bordered laterally by the gently curved zygomatic arch; the orbital fossae are delimited from the much larger temporal fossae by both the well-developed postorbital processes of the frontals and a pronounced postorbital constriction. The mildly bulging braincase supports the prominent zygomatic processes of the squamosals and terminates posteriorly with a pronounced nuchal crest. Weak temporal lines extend from the postorbital processes to the nuchal crest; they converge near their posterior end to form a short, weak sagittal crest (these features of the temporal lines and sagittal crest vary in the studied adult sample).

The newborn (Figs. 2C–D), in contrast is largely braincase, with a short rostrum and orbitotemporal region. Compared to the adult, the snub-nosed rostrum of the newborn is more rounded with little disparity in the rostral projection of the nasals and premaxillae. The orbits are little delimited from the much smaller temporal fossae; the postorbital processes are minute and postorbital expansion is present rather than constriction. The temporal fossae and zygomatic processes of the squamosal are largely hidden by the braincase. The nuchal and sagittal crests are absent, and weak temporal lines are not visible in this view. Finally, the center of the skull has a large fontanel where the sagittal and coronal sutures meet.

**Anterior View.**—In the adult skull (Figs. 3A–B), the rostrum holds the upper dentition, with the dagger-like canines the most prominent teeth. The width across the postcanine teeth is greater than that across the braincase. Visible through the external nasal aperture, which is taller than wide, are the delicate scrolls of the maxillo- and ethmoturbinates. The zygomatic arches arise low and curve dorsolaterally, creating space for the occupants of the temporal fossae. The dorsalmost point on the zygoma is roughly near mid-height of the skull.

In the newborn (Figs. 3C–D), the deciduous upper dentition is largely unerupted and the facial bones are relatively smaller elements. Visible through the external nasal aperture, which is wider than tall, is an empty nasal fossa; the cartilaginous maxillo- and ethmoturbinates are not ossified. The zygomatic arches barely project away from the braincase and are situated well below skull mid-height. Parts of the basicranium are visible as a result of the greater basicranial flexion.

**Lateral View.**—In the adult skull (Figs. 4A–B), the braincase and orbitotemporal region are roughly tubular, with a gently concave dorsal contour. The greatest height is on the braincase at the external acoustic meatus. The rostrum is dorsoventrally shorter than the orbitotemporal region

and braincase, but it is a gradual decrease in height and not abrupt. The external nasal aperture is sloped from anteroventral to posterodorsal. The incisors are taller than the postcanine dentition. Most of the orbit is encircled by bone, more than 270° of its rim. The zygomatic arch is concave ventrally. The prominent nuchal crest delimits the sidewall of the braincase from the occiput and slightly overhangs the occiput. Dorsal to the prominent occipital condyles, the occiput is roughly vertical.

In the newborn (Figs. 4C–D), the lateral profile is more rounded, with strong slopes between the orbitotemporal region and rostrum as well as between the braincase and occiput. Several fontanelles are present, including a large one in the posteroventral corner, where the ossified pars canalicularis of the petrosal is located in older specimens. Several structures are strikingly larger relatively in the newborn, including the orbit and the ear region (e.g., the ectotympanic ring). A nuchal crest does not delimit the occiput, which is not tall and slopes slightly posterodorsally. The weak temporal lines are situated much lower on the braincase.

**Ventral View.**—In the adult skull (Figs. 6A–B), the incisors are in a gently curved arch; the postcanine dentition diverges posteriorly, measured at its lingual margin. A short postdental palate extends a short distance posterior to the last molars. In the mesocranium, the entopterygoid processes are subparallel. The length of the basipharyngeal canal is roughly two-thirds that of the basicranium posterior to it. The well-developed postorbital constriction and gently curved zygomatic arches emphasize the size of the temporal fossae. The jaw joints are largely situated lateral to the braincase. The greatest width of the braincase is posterior to the external acoustic meatus. At that point, the width across the central stem between the ear regions is much greater than the width of the choanae, which in turn is subequal to that of the foramen magnum.

In the newborn (Figs. 6C–D), the hard and postdental palates are proportionally similar to those in the adult, but the braincase extends much farther anteriorly. This is the source of the relatively smaller temporal fossae. The entopterygoid processes are not straight and the length of the basipharyngeal canal is roughly one-third that of the basicranium posterior to it. The width of the foramen magnum is greater than that of the choanae, which is greater than that of the central stem between the ear regions. The ear region with its simple ectotympanic ring is proportionally strikingly larger than in the adult, whereas the jaw joint is strikingly smaller.

**Posterior View.**—In the adult (Figs. 29A–B), the rounded braincase is flanked posteriorly by the gently arched nuchal crest and laterally by the prominent zygomatic arches. The gap between the braincase and zygoma accommodates the temporalis muscle. The foramen magnum is wider than high and the occipital condyles extend dorsally as high as the foramen. Each side of the occiput comes to a point

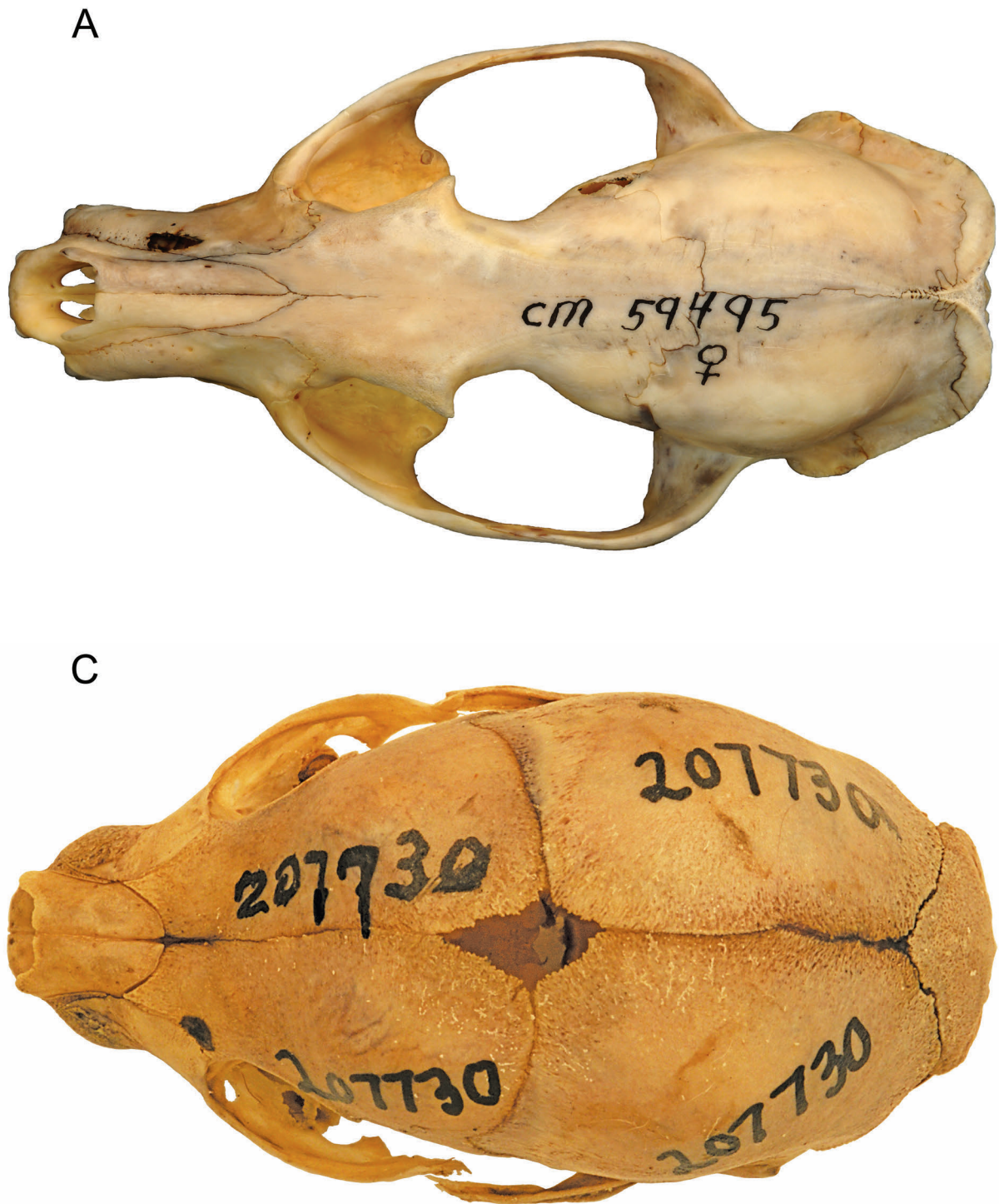
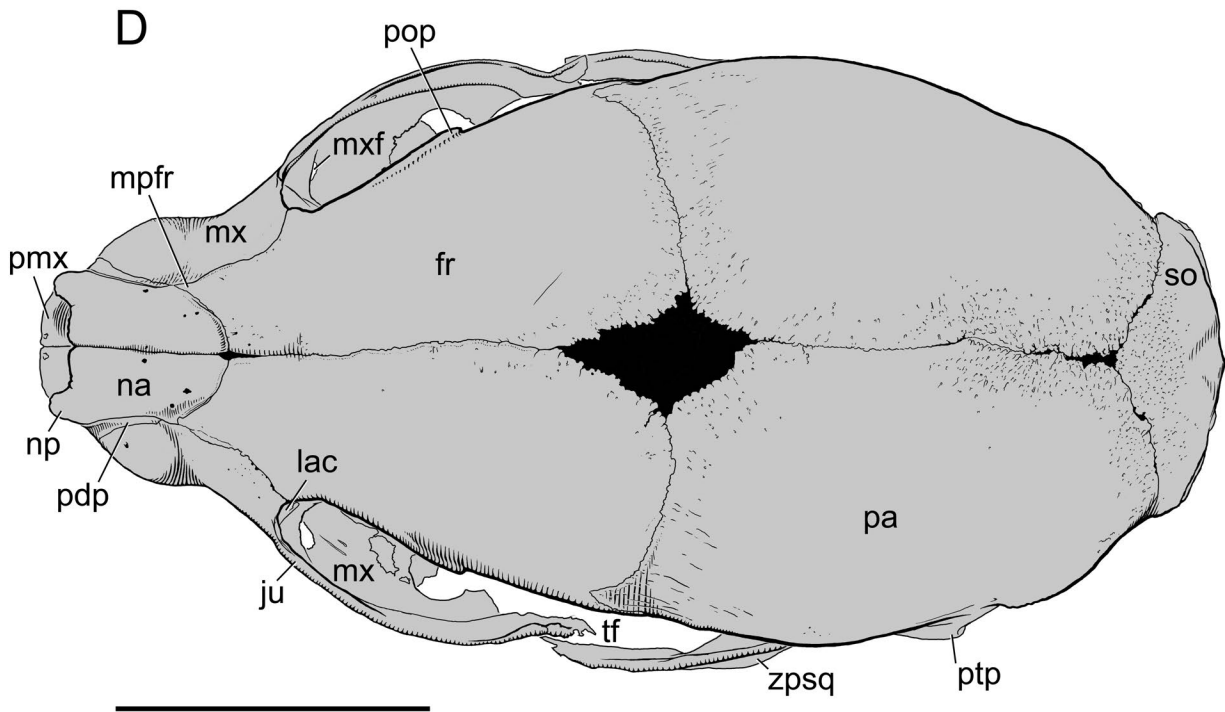
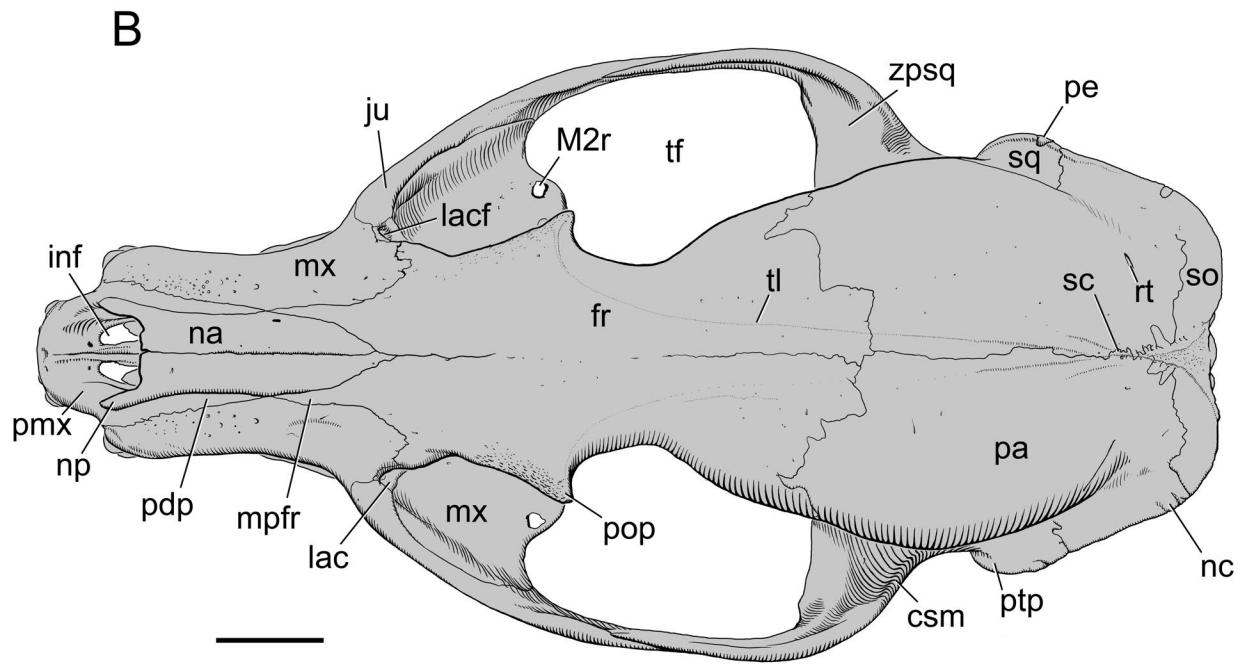


Fig. 2—Skulls of *Nandinia binotata* in dorsal view. **A, B**, adult, CM 59495; **C, D**, newborn, AMNH 207730. Scale = 10 mm. Abbreviations: **esm**, crista supramastoideus; **fr**, frontal; **ju**, jugal; **inf**, incisive foramen; **lac**, lacrimal; **lacf**, lacrimal foramen; **M2r**, root of upper second molar; **mpfr**, maxillary process of frontal; **mx**, maxilla; **mxl**, maxillary foramen; **na**, nasal; **nc**, nuchal crest; **np**, nasal process of nasal; **pa**, parietal; **pdp**, posterodorsal process of premaxilla; **pe**, petrosal; **pmx**, premaxilla; **pop**, postorbital process of frontal; **ptp**, posttympanic process of squamosal; **rt**, foramen for ramus temporalis; **sc**, sagittal crest; **so**, supraoccipital; **sq**, squamosal; **tf**, temporal fossa; **tl**, temporal line; **zpsq**, zygomatic process of squamosal.



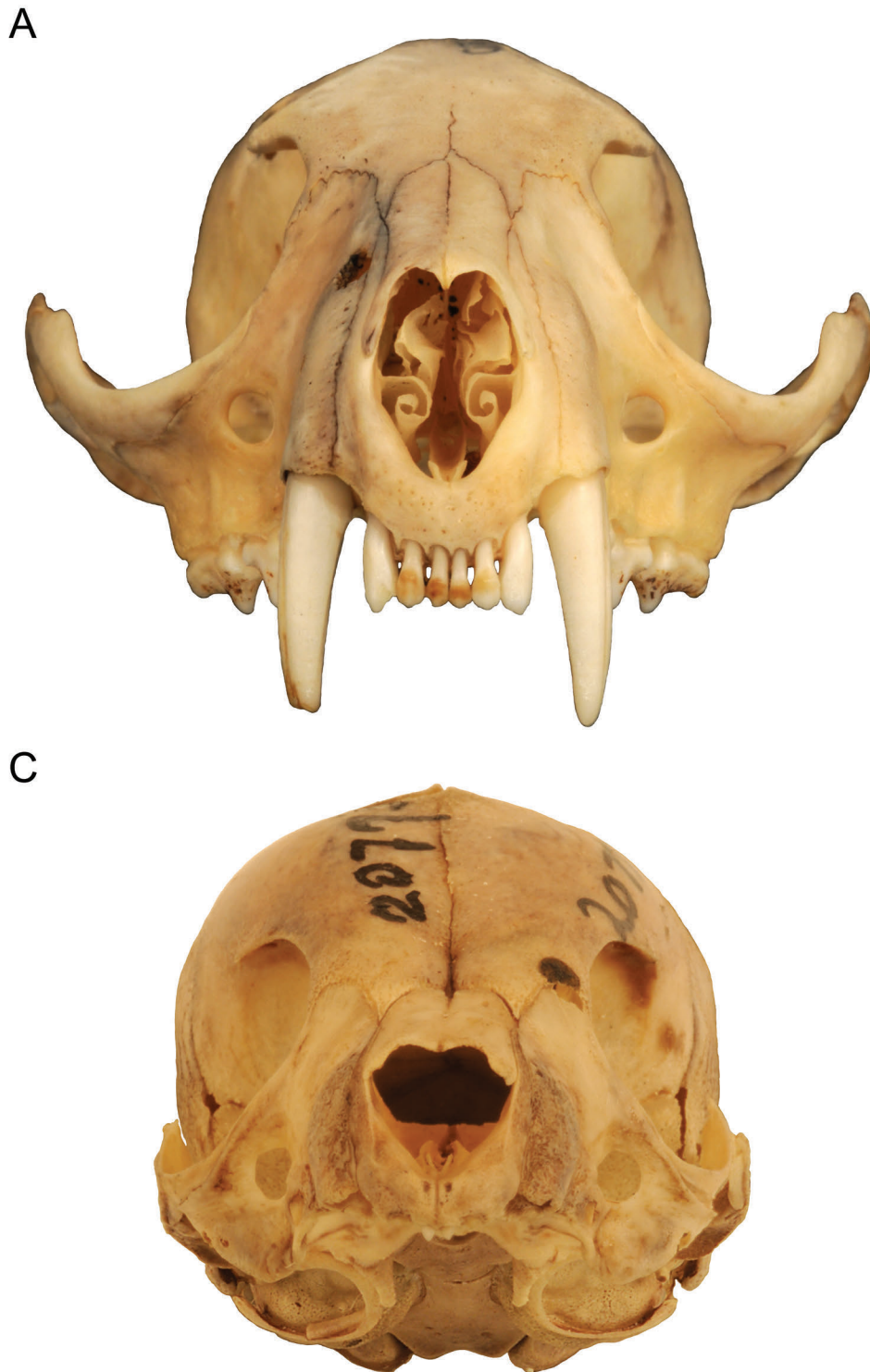
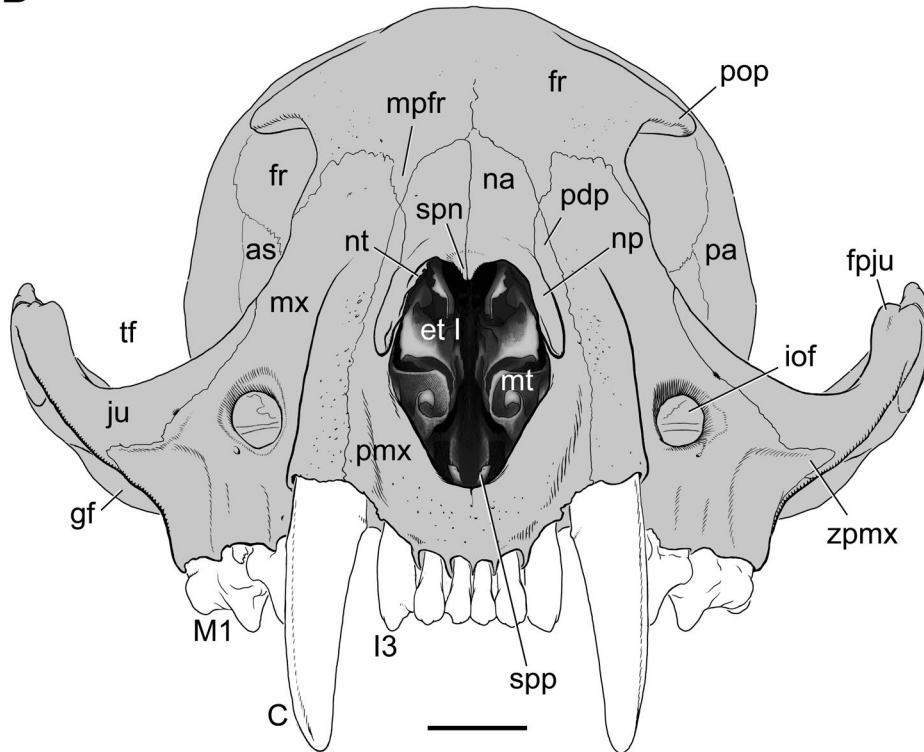
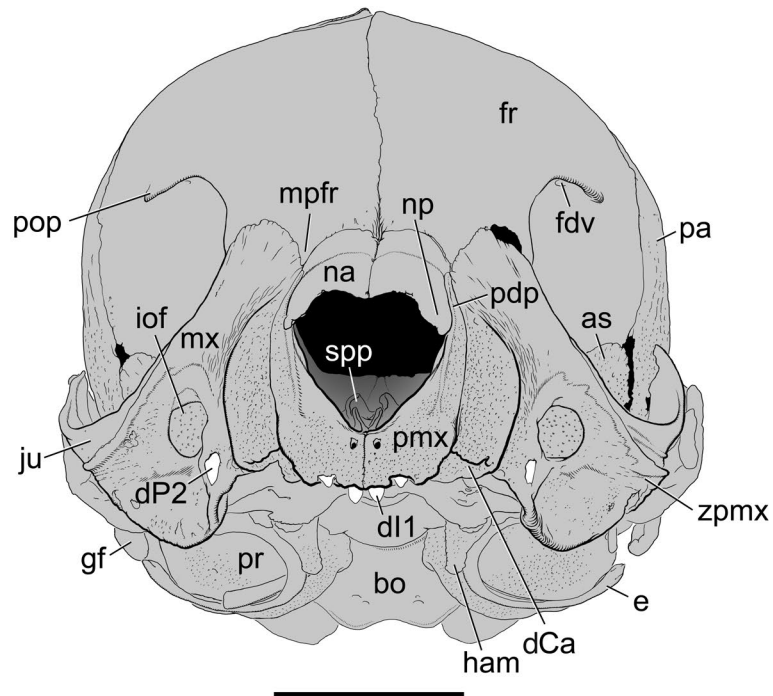


Fig. 3.—Skulls of *Nandinia binotata* in anterior view. **A, B**, adult, CM 59495; **C, D**, newborn, AMNH 207730. Scale = 5 mm. Abbreviations: **as**, alisphenoid; **bo**, basioccipital; **C**, upper canine; **dCa**, deciduous upper canine alveolus; **dI1**, deciduous upper first incisor; **dP2**, deciduous upper second premolar; **e**, ectotympanic; **et I**, ethmoturbinate I; **fdv**, frontal diploic vein foramen; **fpju**, frontal process of jugal; **fr**, frontal; **gf**, glenoid fossa; **ham**, pterygoid hamulus; **I3**, upper third incisor; **iof**, infraorbital foramen; **ju**, jugal; **M1**, upper first molar; **mpfr**, maxillary process of frontal; **mt**, maxilloturbinate; **mx**, maxilla; **na**, nasal; **np**, nasal process of nasal; **nt**, nasoturbinate; **pa**, parietal; **pdp**, posterodorsal process of premaxilla; **pmx**, premaxilla; **pop**, postorbital process of frontal; **pr**, promontorium of petrosal; **spn**, septal process of nasal; **spp**, septal process of premaxilla; **tf**, temporal fossa; **zpmx**, zygomatic process of maxilla.

B



D



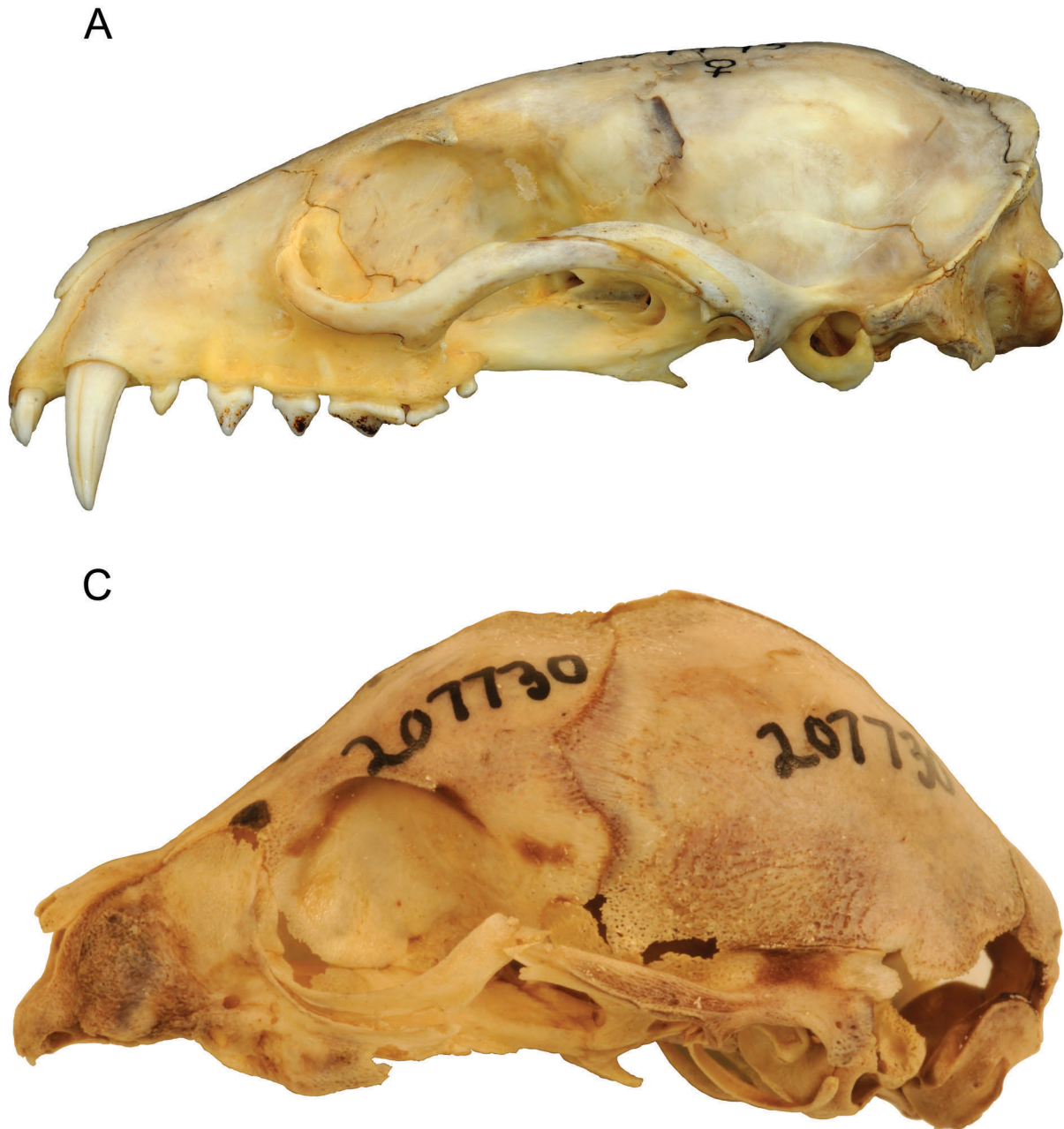
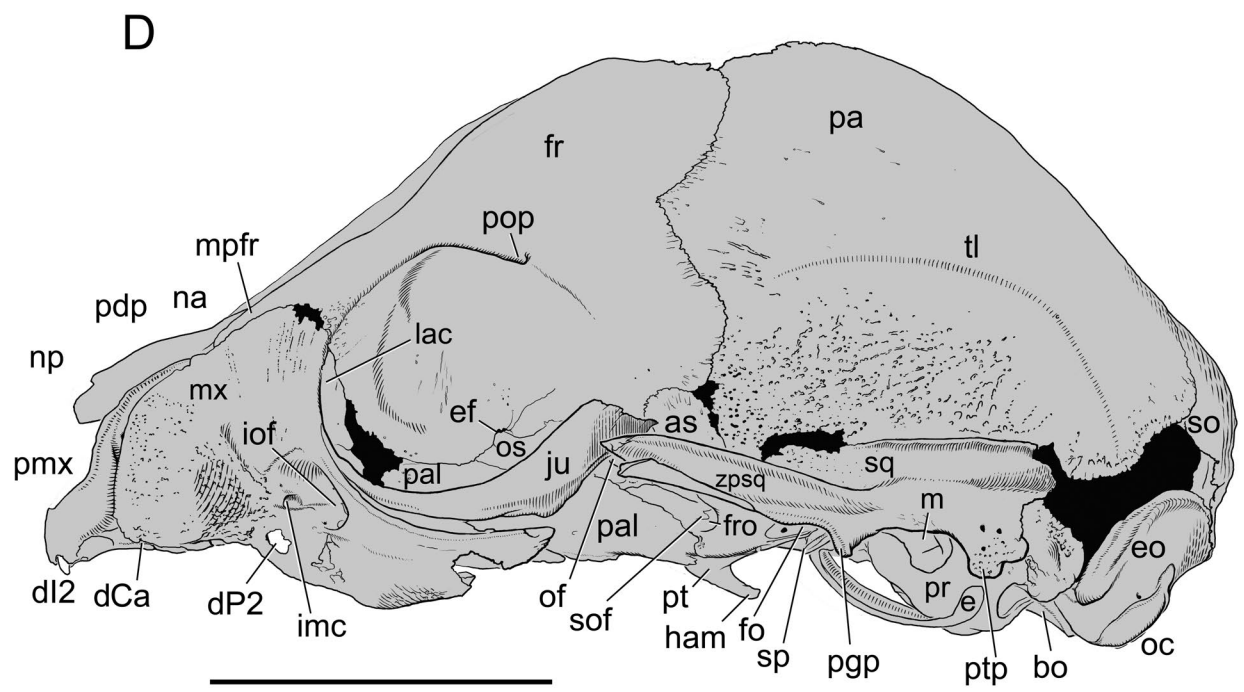
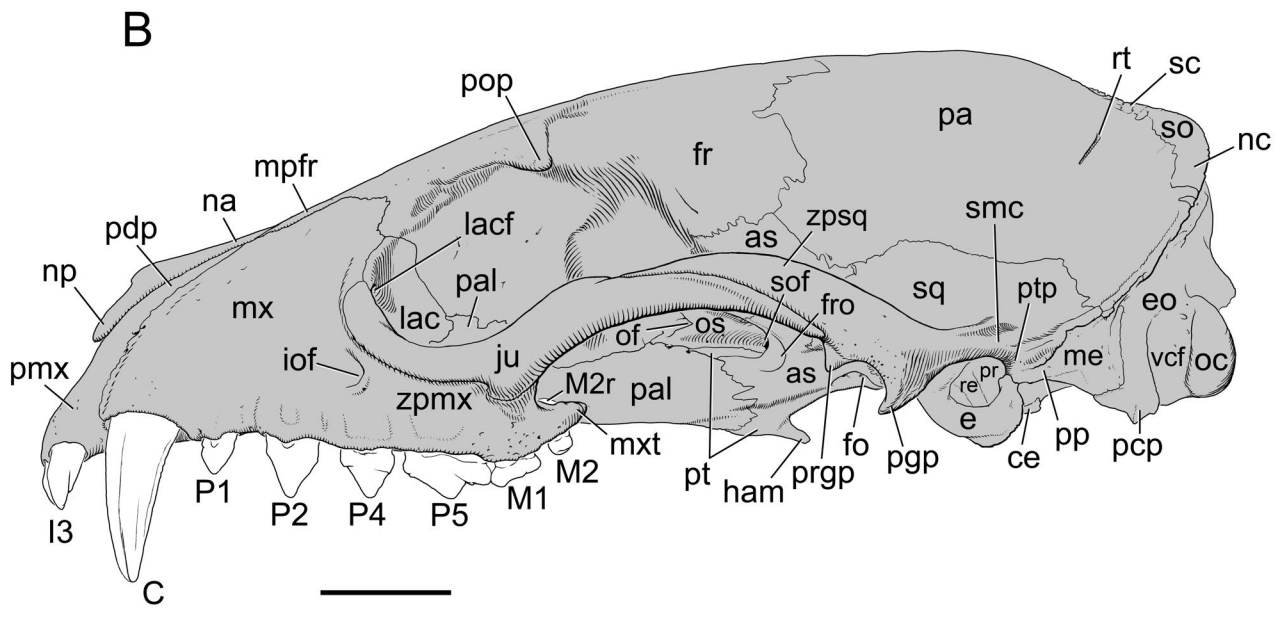


Fig. 4—Skulls of *Nandinia binotata* in lateral view. **A, B**, adult, CM 59495; **C, D**, newborn, AMNH 207730. Scale = 10 mm. Abbreviations: **as**, alisphenoid; **bo**, basioccipital; **C**, upper canine; **Ca**, upper canine alveolus; **ce**, caudal entotympanic; **dCa**, deciduous upper canine alveolus; **dl2**, deciduous upper second incisor; **dp2**, deciduous upper second premolar; **e**, ectotympanic; **ef**, ethmoidal foramen; **eo**, exoccipital; **fo**, foramen ovale; **fr**, frontal; **fro**, foramen rotundum; **ham**, pterygoid hamulus; **I3**, upper third incisor; **imc**, incisivomaxillary canal; **iof**, infraorbital foramen; **ju**, jugal; **lac**, lacrimal; **lacf**, lacrimal foramen; **m**, malleus; **M1**, upper first molar; **M2**, upper second molar; **M2r**, root of upper second molar; **me**, mastoid exposure of petrosal; **mpfr**, maxillary process of frontal; **mx**, maxilla; **mxt**, maxillary tuberosity; **na**, nasal; **nc**, nuchal crest; **np**, nasal process of nasal; **oc**, occipital condyle; **of**, optic foramen; **os**, orbitosphenoid; **P1**, upper first premolar; **P2**, upper second premolar; **P4**, upper penultimate premolar; **P5**, upper ultimate premolar; **pa**, parietal; **pal**, palatine; **pcp**, paracondylar process of exoccipital; **pdp**, posterodorsal process of premaxilla; **pgp**, postglenoid process; **pmx**, premaxilla; **pop**, postorbital process of frontal; **pp**, paroccipital process of petrosal; **pr**, promontorium of petrosal; **prgp**, preglenoid process; **pt**, pterygoid; **ptp**, posttympanic process of squamosal; **re**, rostral entotympanic; **rt**, foramen for ramus temporalis; **sc**, sagittal crest; **smc**, suprameatal crest; **so**, supraoccipital; **sof**, superior orbital fissure; **sp**, spine of rostral process of malleus; **sq**, squamosal; **tl**, temporal line; **vcf**, ventral condyloid fossa; **zpmx**, zygomatic process of maxilla; **zpsq**, zygomatic process of squamosal.



ventrally as the paracondylar process of the exoccipital.

In the newborn (Figs. 29C–D), the rounded braincase is not flanked posteriorly or laterally; the nuchal crest is absent and the zygomatic arch does not extend away from the braincase. The large openings in the posteroventral corners of the occiput are the result of the non-ossification of the pars canalicularis of the petrosal. The foramen magnum is wider and shorter than in the adult, and the occipital condyles do not extend as far dorsally. Although present, the paracondylar processes of the exoccipitals are weak, and the most ventral point on the occiput is on the condyle. The erupting anterior dentition is visible as a result of the greater basicranial flexion.

#### Nasal (“na” in figures)

The paired nasals are the principal elements of the roof of the rostrum and the nasal cavity.

**CM 59495, Principal Adult.**—In dorsal view (Figs. 2A–B), the nasals extend just posterior to the level of the anterior orbital rim and their midline length is 21% of greatest skull length. These elements are widest anteriorly and taper to a point posteriorly, with the left nasal extending farther than the right. The anterior two-thirds of the lateral margins are subparallel and contact both the facial processes of the premaxillae and their narrow posterior continuations, the posterodorsal processes (“pdp” in Fig. 2B). The posterior third of the lateral margins has a gentle and then a sharp convergence toward the midline and contacts the maxillary processes of the frontals (“mpfr” in Fig. 2B). In between the premaxilla and frontal (“pmx” and “fr” in Fig. 2B, respectively), the lateral margin bulges where it has a point contact with the facial process of the maxilla (“mx” in Fig. 2B). The anterior margins, which form the roof of the external nasal aperture, are straight medially but with elongate, digitiform nasal processes of the nasals present laterally, ending in a rounded prong (“np” in Fig. 2B). The dorsal surface of the nasal is flat anteriorly, but one-third into its length a slight midline depression begins. This depression does not continue onto the frontals. Several tiny foramina are present on either side of the midline, and a more substantial foramen with a groove extending posteriorly lies on the right element near the maxillary contact.

In anterior view (Figs. 3A–B), the nasal process extends ventrolaterally nearly to the midpoint of the external nasal aperture. The dorsal margin of the external nasal aperture is bi-concave with a midline projection from the ventral surface of both nasals, the septal processes (“spn” in Fig. 3B). This projection can be traced posteriorly roughly half the length of the nasals until it is covered ventrally by the perpendicular plate of the ethmoid (not visible in the figures). The lateral margin of the ventral surface of the nasals has a low longitudinal crest that is recessed in from the external nasal aperture, the nasoturbinates (“nt” in Fig. 3B).

In lateral view (Figs. 4A–B), the dorsal margin of the

nasal is straight. The anteroventral end of the nasal process is not flush with the premaxilla but overlies the anterior edge of the facial process.

**AMNH 207730, Newborn.**—In dorsal view (Figs. 2C–D), the nasals do not reach to the level of the anterior orbital rim; the midline nasal length is 14.6% of greatest skull length. On the lateral margin, the nasal has a narrow contact with the maxilla on the left side, but these two bones are separated by a point contact between the premaxilla and frontal on the right side. The nasal processes are not as elongate and narrow as in the adult, but they still are not flush with the premaxilla anteriorly. The nasals do not taper to a point posteriorly nor contact on the midline at their posterior margin; the frontal is visible between them. A slight midline depression begins in the posterior one-third of the nasals and continues onto the frontals. Several substantial foramina are asymmetrically arranged, four on the right and two on the left.

In anterior view (Figs. 3C–D), the nasal processes do not extend as far ventrally along the external nasal aperture, only reaching down roughly one-third the height of the opening. The structures on the internal surface of the nasal are not visible in direct anterior view. The septal processes extend the length of the nasal but are not as prominent as in the adult, and the nasoturbinates are likewise not as well developed; it is broader the crest-like adult structure and does not reach far posteriorly.

In lateral view (Figs. 4C–D), the dorsal margin of the nasal is convex anteriorly and concave posteriorly.

**Others.**—The series in Figure 1 illustrates some ontogenetic changes of the nasals. The external nasal aperture is more vertical in the newborn with the body of the premaxilla hidden in dorsal view and becomes more oblique through the series. The length of the nasal as a percentage of greatest skull length increases from 14.6% in the newborn, to 17.5 and 18% in the juveniles, to 21 and 22% in the adults.

We recorded the incidence of two features of the nasals across the study sample:

(1) Contact between the lateral margin of the nasal and the facial process of the maxilla: (a) no contact - AMNH 207730(R) (Figs. 2C–D), CM 6371, AMNH 51488, CM 6374, AMNH 51503, CM 3693, 42725, 69365(R), AMNH 51510; (b) point contact - AMNH 207730(L) (Figs. 2C–D), 51486, CM 59495 (Figs. 2A–B), AMNH 134969, CM 69365(L); (c) contact - AMNH 51471, 201513, 51448, CM 42281, 5157, 2356, 59497, 59496, 42727, 42282, 69366. This distribution shows no obvious correlation with geography, ontogeny, and sex.

(2) Nasal depression: (a) shallow - CM 6371, 6374, 42281, 5157, 59497, 59495, AMNH 134969, CM 59496, 3693, 42725, 42726, 42282, 69365, 69366, 16103; (b) deep and extending onto the frontal - AMNH 207730, 51471, 51486, 51488, 51448, CM 2356, AMNH 51503, CM 42727, AMNH 51510, 51494, CM 42728. This

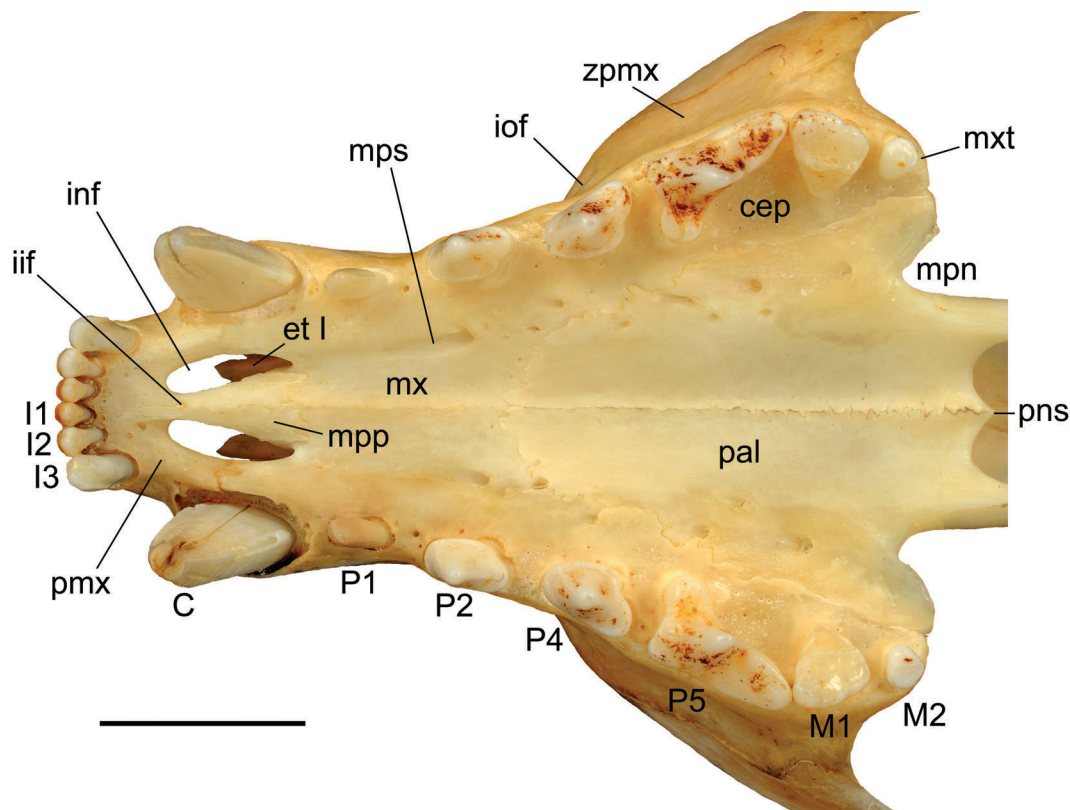


Fig. 5.—Palate of adult *Nandinia binotata*, CM 59495, in ventral view. Scale = 10 mm. Abbreviations: C, upper canine; cep, carnassial embrasure pit; et I, ethmoturbinate I; I1, upper first incisor; I2, upper second incisor; I3, upper third incisor; iif, interincisive foramen; inf, incisive foramen; M1, upper first molar; M2, upper second molar; mpn, minor palatine notch; mpp, medial palatine process of premaxilla; mps, major palatine sulcus; mx, maxilla; mxt, maxillary tuberosity; P1, upper first premolar; P2, upper second premolar; P4, upper penultimate premolar; P5, upper ultimate premolar; pal, palatine; pmx, premaxilla; pns, posterior nasal spine; zpmx, zygomatic process of maxilla.

distribution shows no obvious correlation with geography, ontogeny, and sex.

In addition, we also noted the number and position of foramina on the nasal. All specimens have at least one per side with the majority showing an asymmetrical distribution in number and position. The greatest number of foramina occurred in CM 69366(L), with three small ones centrally, three tiny ones posteriorly, and four even smaller ones anteriorly.

#### Premaxilla (“pmx” in figures)

The paired premaxillae contribute to the lateral wall and floor of the anterior rostrum and nasal cavity, and house the three upper incisors (I1, I2, and I3). In addition, in the specimens where the suture with the maxilla can be followed (i.e., AMNH 207730, 51486, 201513, 51503, 134969; CM 6374, 3693), the premaxilla closes the anteromedial border of the canine alveolus.

**CM 59495, Principal Adult.**—In lateral view (Figs. 4A–B), the body and facial process of the premaxilla make a minor contribution to the rostrum. The body extends well

rostral to the nasal bone and is thickest dorsoventrally at the I3. The facial process tapers along its length, grading seamlessly into the narrow posterodorsal process (“pdp” in Fig. 4B), which ends dorsal to the diastema between the P1 and P2. The posterodorsal process does not contact the maxillary process of the frontal, as a small slip of maxilla intervenes. The suture with the nasal is simple, whereas the suture with the maxilla is complex except in its most posterior part. Two small foramina are found in the suture between the premaxilla and maxilla near the base of the posterodorsal process. A slight paracanine fossa is predominantly on the facial process of the premaxilla but spans onto the maxilla.

In ventral view (Figs. 5, 6A–B), the alveolar process of the premaxillary body houses three incisors that are in a gentle arc and increase in size laterally. The medial palatine process (“mpp” in Fig. 5) extends from the body on the midline and broadens posteriorly, reaching even with the back edge of the canine alveolus. The interpremaxillary suture runs along the length of the left and right medial palatine processes, but does not extend anteriorly onto the body. There are several small foramina on the midline suture; the largest of these, the interincisive foramen (“iif”

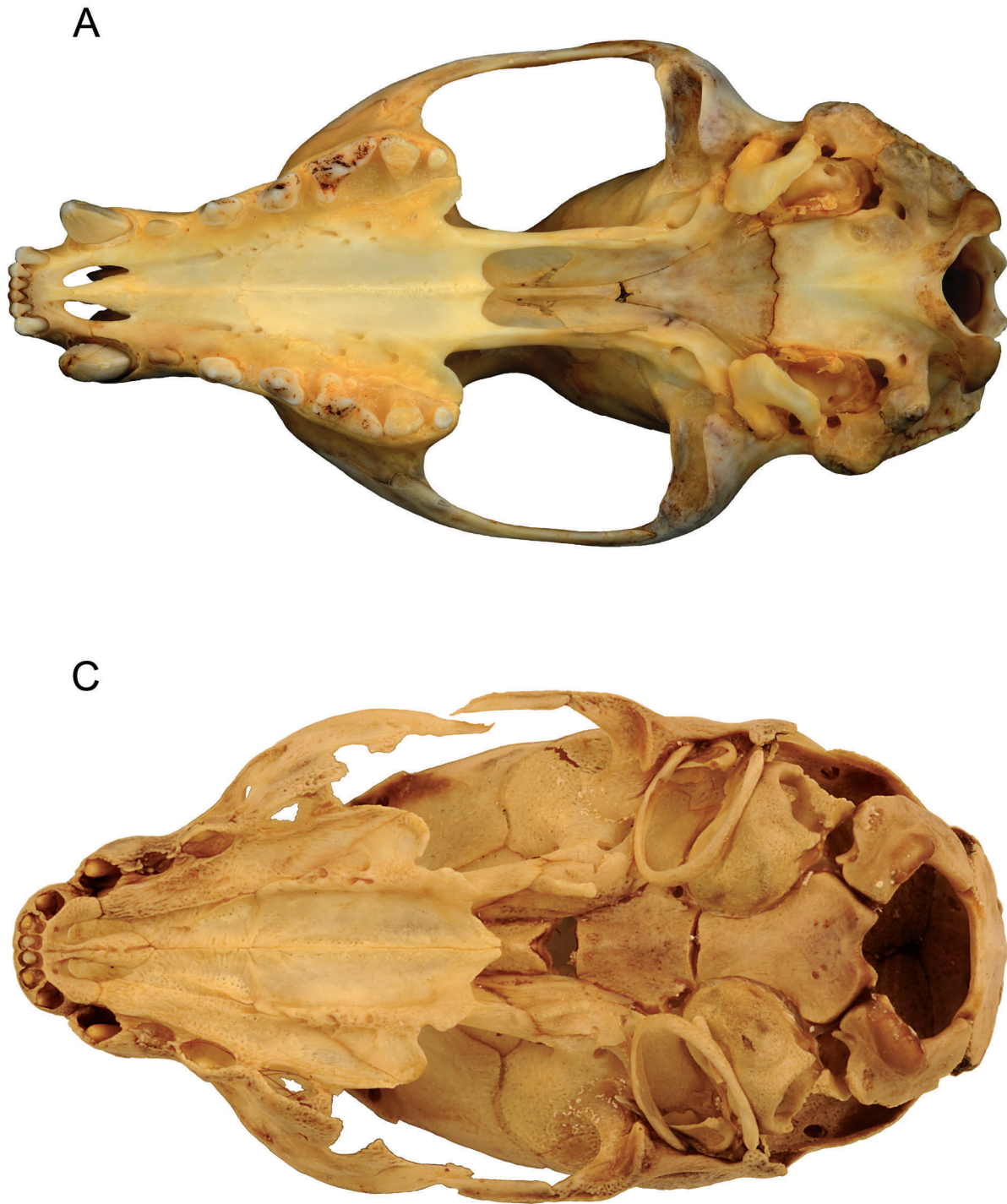
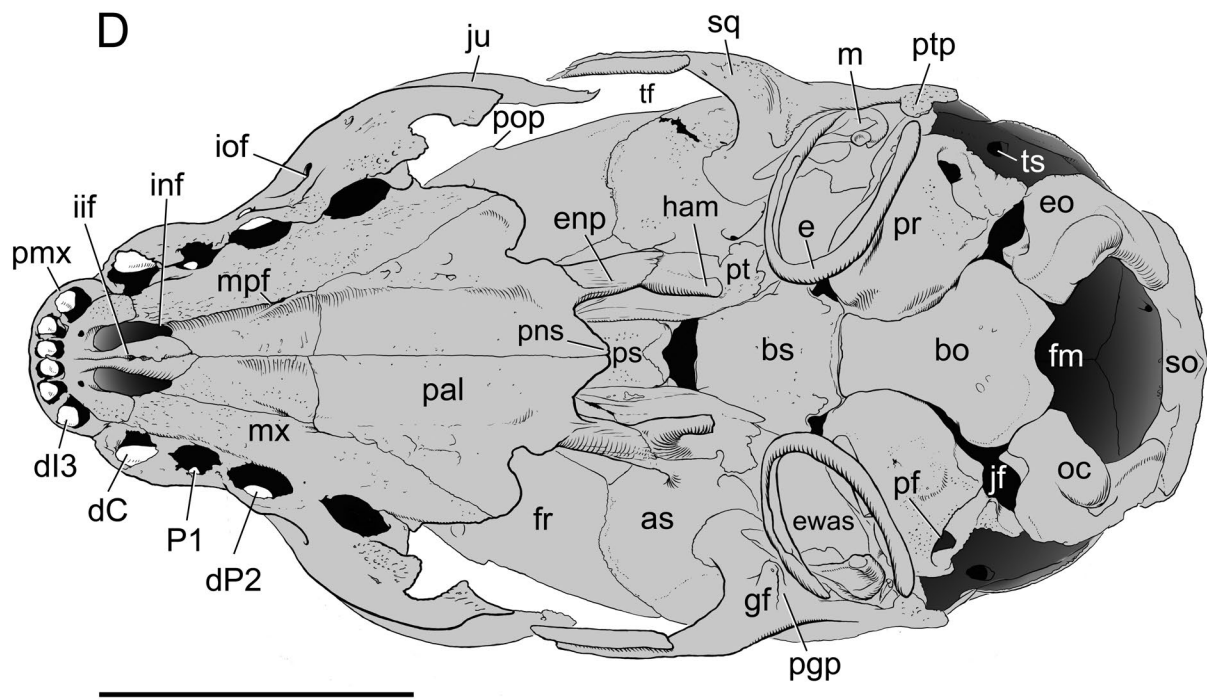
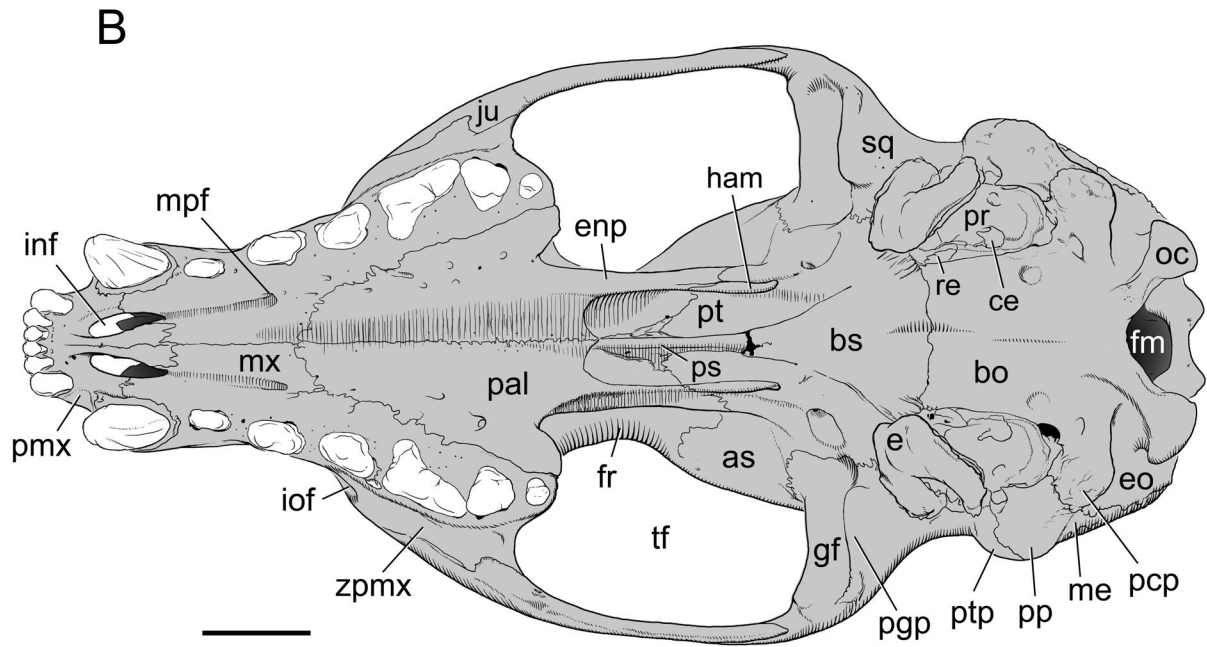


Fig. 6—Skulls of *Nandinia binotata* in ventral view. **A, B**, adult, CM 59495; **C, D**, newborn, AMNH 207730. Scale = 10 mm. Abbreviations: **as**, alisphenoid; **bo**, basioccipital; **bs**, basisphenoid; **ce**, caudal entotympanic; **dC**, deciduous upper canine; **dI3**, deciduous upper third incisor; **dP2**, deciduous upper second premolar; **e**, ectotympanic; **enp**, entopterygoid process; **eo**, exoccipital; **ewas**, epitympanic wing of alisphenoid; **fm**, foramen magnum; **fr**, frontal; **gf**, glenoid fossa; **ham**, pterygoid hamulus; **iif**, interincisive foramen; **inf**, incisive foramen; **iof**, infraorbital foramen; **jf**, jugular foramen; **ju**, jugal; **m**, malleus; **me**, mastoid exposure of petrosal; **mpf**, major palatine foramen; **mx**, maxilla; **oc**, occipital condyle; **P1**, upper first premolar; **pal**, palatine; **pcp**, paracondylar process of exoccipital; **pf**, perilymphatic foramen; **pgp**, postglenoid process; **pmx**, premaxilla; **pns**, posterior nasal spine; **pop**, postorbital process of frontal; **pp**, paroccipital process of petrosal; **pr**, promontorium of petrosal; **ps**, presphenoid; **pt**, pterygoid; **ptp**, posttympanic process of squamosal; **re**, rostral entotympanic; **so**, supraoccipital; **sq**, squamosal; **tf**, temporal fossa; **ts**, opening for transverse sinus; **zpmx**, zygomatic process of maxilla.



in Fig. 5), is directed anteriorly. The medial palatine process forms almost the entire medial margin of the incisive foramen (“inf” in Figs. 5, 6B); at the extreme posterior end there is a small piece of maxilla. The midline length of the premaxilla is 26.2% of the hard palate length.

The bone between I3 and the canine is the continuation of the alveolar process (Fig. 5). This part of the premaxilla extends close to the anteroposterior midpoint of the medial side of the canine, which is also roughly the anteroposterior midpoint of the lateral margin of the incisive foramen. A lateral palatine process is essentially absent and the alveolar process walls the incisive foramen laterally. It is unclear in CM 59495 if the premaxilla contributes to the canine alveolus, as the suture between the premaxilla and maxilla in the alveolus is fused. Rostral to the anterior edge of the incisive foramen is a fossa that contains small foramina of unknown function: two on the right and one on the left (Fig. 5). The incisive foramen is an elongate oval that is narrowest posteriorly; its long axis is not parasagittal but angled slightly from anteromedial to posterolateral.

In dorsal view (Figs. 2A–B), the interpremaxillary suture extends farther anteriorly than in ventral view, but still does not fully reach the tip of the body. At the anteromedial aspect of the incisive foramen is a small foramen that lies posterior to the small foramina on the ventral surface described above; nevertheless, it is possible that these communicate through the premaxilla. Immediately posterior to this foramen is the septal process of the premaxilla (see below).

In anterior view (Figs. 3A–B), the interpremaxillary suture is visible at the ventral margin of the external nasal aperture. The body of the premaxilla is more substantial than necessary for housing the roots of the incisors and is riddled with numerous small foramina. Within the nasal fossa, the dorsal ends of the septal processes of the premaxillae are visible and diverge from each other at 45° (“spp” in Fig. 3B). The septal processes are continuous posteriorly with the lateral laminae of the vomer (not visible in the figures); the suture with the vomer is W-shaped with the bottom of the W pointed posteriorly. The septal process has no base and thus is V-shaped, rather than Y-shaped as it is in *Solenodon paradoxus* Brandt, 1833 (Wible 2008). The anterior base of the maxilloturbinate (“mt” in Fig. 3B) extends onto the premaxilla just rostral to the premaxillary-maxillary suture.

**AMNH 207730, Newborn.**—In lateral view (Figs. 4C–D), the premaxillary body is distinct from the facial process and the posterodorsal process is distinct from the facial process, unlike the condition seen in the adult. The left side has a small foramen in the facial process adjacent to the maxillary suture near the base of the posterodorsal process; the right side has two foramina.

In ventral view (Figs. 6C–D), the maximum midline length of the premaxilla is 28.2% of the hard palate length. The medial palatine process forms the entire medial mar-

gin of the incisive foramen. The midline suture with the maxilla reaches posteriorly to the anterior P1 alveolus, in contrast to the adult condition where it terminates at the posterior margin of the canine alveolus. The interpremaxillary suture, as in the adult, does not extend all the way to the tip of the rostrum; it ends posterior to the dI1 alveolus. The dI1 is erupting, the dI2 is just starting to erupt, and the dI3 is visible in its crypt. The dC is in a crypt that is enclosed by the maxilla, but if the tooth had fully erupted, the premaxilla would form the anteromedial corner of the alveolus. The interincisive foramen is present, and a single small foramen occurs in the small fossa anterior to the incisive foramen.

In dorsal view (Figs. 2C–D), the interpremaxillary suture runs the whole anteroposterior length of the premaxilla. The small foramen anterior to the incisive foramen lies at about the same level as the one described on the ventral surface, whereas in the adult it is farther posterior.

In anterior view (Figs. 3C–D), the interpremaxillary suture runs the entire dorsoventral extent of the premaxillary body. The body consists of little more than the bone required for housing the deciduous incisor roots. There is a hole on each side just off the midline in the dorsal margin of the body that appears to represent an area of incomplete bone deposition.

**Others.**—We recorded the incidence of two features of the premaxilla across the study sample:

(1) Posterior extent of the medial palatine process: (a) extends posterior to the incisive foramen - AMNH 207730 (Fig. 6D), 51471, CM 6371, 6374, AMNH 51448, CM 42281, 5157, 2356, 59497, 59495 (Fig. 5), 59496, 42727, 3693, 42725, 42726, 42282, 69365, 69366, AMNH 51510, CM 16103, AMNH 51494, CM 42728, 5097; (b) does not extend posterior to the incisive foramen - AMNH 51486, 51488, 201513, 51503, 134969. This distribution shows no obvious correlation with geography, ontogeny, and sex.

(2) Position of the interincisive foramen to the suture between the premaxilla and maxilla lateral to the incisive foramen: (a) even with or anterior to - AMNH 207730 (Fig. 6D), 51471, CM 6371, 6374, AMNH 201513, 51448, CM 42281, 5157, 2356, 59497, 59495 (Fig. 5), AMNH 134969, CM 59496, 3693, 42725, 42726, 42282, 69365, 69366, AMNH 51510, CM 16103, AMNH 51494, CM 42728, 5097; (b) posterior to - AMNH 51486, 51488, 51503, CM 42727. This distribution shows no obvious correlation with geography, ontogeny, and sex.

We also found that all specimens have at least one small foramen near the base of the posterodorsal process either entirely within the premaxilla or in the suture with the maxilla; nine specimens showed an asymmetrical pattern in the bone(s) enclosing this foramen.

#### Maxilla (“mx” in figures)

The paired maxillae contribute to the lateral wall and floor of the rostrum and nasal cavity, and house the canine (C),

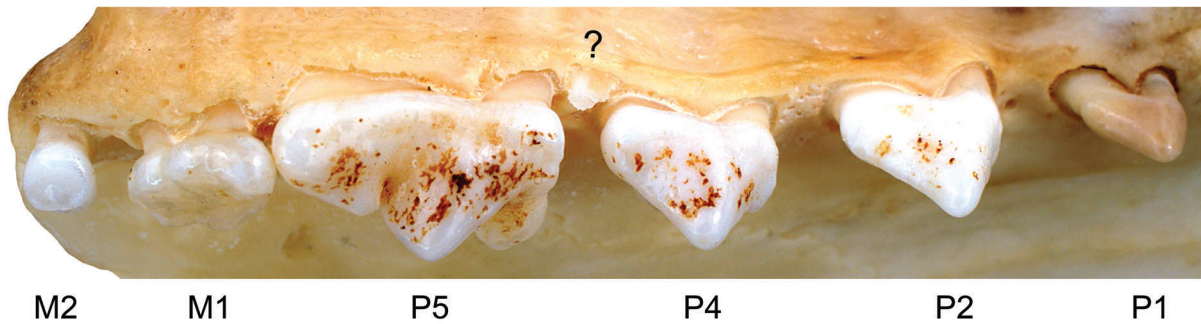


Fig. 7—Right postcanine dentition of adult *Nandinia binotata*, CM 59495, in lateral view. Scale = 5 mm. Question mark is the unusual toothlet described in the text. Abbreviations: **M1**, upper first molar; **M2**, upper second molar; **P1**, upper first premolar; **P2**, upper second premolar; **P4**, upper penultimate premolar; **P5**, upper ultimate premolar.

four premolars (P1, P2, P4, and P5), and two molars (M1 and M2) in the adult. As noted above, the premaxilla contributes to the anteromedial closure of the canine alveolus.

**CM 59495, Principal Adult.**—In oblique lateral view (Fig. 7), on the right side a “toothlet,” which is not found in any other specimen, is present along the alveolar margin in the diastema between P4 and P5. This “toothlet” fills the interdental space, does not extend ventrally as far as the crown of P5, and appears to be covered in enamel. At its alveolus, the “toothlet” is ellipsoidal, longer than wide; it tapers to a longitudinal crest with an irregular edge that is highest posteriorly. On the left side (not figured), there is a smaller structure in the same diastema, but it fills only the posterior half of the interdental space and is barely erupted below the alveolar margin. Only the tip of the crest is exposed, it is smooth, and the presence of enamel is uncertain. There is a second similar structure lateral to the anterior root of the left P4, which differs in having a more irregular edge. It is a bit larger than the other example on this side, but smaller than the “toothlet” on the right. The significance of these structures is unknown.

In lateral view (Figs. 4A–B), the P5 abuts M1, but diastemata are present between the remaining maxillary teeth. The alveolar margin is relatively straight from P1 to P5 and bends posterodorsally at the buccal midpoint of the M1. The margin is again straight from this bend to its termination posterior to the M2. Most of what is visible of the maxilla in lateral view is the facial process; however, dorsolateral to the last two premolars and the molars is the zygomatic process (“zpmx” in Fig. 4B). From anterior to posterior, the facial process contacts the premaxilla, nasal, frontal, lacrimal (“lac” in Fig. 4B), and jugal (“ju” in Fig. 4B). These contacts are in the form of a smooth curve, except for that with the frontal dorsal to the anterior orbital rim, which has two sharp angles. At the contact with the lacrimal, the maxilla forms the anterior orbital rim. There are numerous small foramina in the facial process of the maxilla, especially along its dorsal aspect. The eminence over the root of the canine is prominent, but there are smaller eminences (alveolar juga) over the anterior root of

the P2 and the anterobuccal roots of the P4 and P5. Dorsal to the P4 is the infraorbital foramen (“iof” in Fig. 4B), which is C-shaped in lateral view, with its lateral margin posterior to its medial margin. The infraorbital foramen is well ventral to the dorsoventral midpoint of the snout, but close to the jugal bone. Anterior to the infraorbital foramen is a slight depression accommodating the contents of the foramen. Ventrolateral to the infraorbital foramen is a tiny foramen of unknown function.

The zygomatic process has a bifurcate contact with the jugal, with the posterior component much smaller. The maxillary tuberosity (“mxt” in Fig. 4B), visible posterior to the zygomatic process, is very weak and does not fully contain the root of M2, which is visible in the floor of the orbit in lateral view (“M2r” in Fig. 4B). The maxilla is not visible in the orbit in direct lateral view.

In ventral view (Figs. 5, 6A–B), the alveolar processes have a slight constriction behind the canine and then diverge posterolaterally, giving the maxillae a Y-shape. The midline length of the palatine process of the maxilla is 21.2% of the hard palate length. The intermaxillary suture, which extends to the level of the posterior margin of the P2, is raised in its anterior half. The suture with the horizontal process of the palatine is complex until it reaches the posterior edge of the carnassial embrasure pit (“cep” in Fig. 5). Medial and parallel to the postcanine dentition are numerous palatal foramina. These foramina follow sub-parallel lines that cross sutures; the anteriormost foramina are in the maxilla and the posteriormost ones in the palatine. Naming these foramina is not straightforward as the contents are not known. We consider the anteriormost ones the major palatine foramina and the posteriormost ones accessory palatine foramina, which would transmit nerves and vessels of the same names. The largest major palatine foramen is the anteriormost (“mpf” in Fig. 6B), which shows slight asymmetry as it is slightly more anterior on the left side. It lies medial to the P2 and has a well-developed groove, the major palatine sulcus (“mps” in Fig. 5), that extends to the incisive foramen on the left and almost so on the right; the lateral margin of the groove is more prominent than the medial. On the left side are two

additional foramina between the P2/P4 that are entirely within the maxilla; on the right side, one is entirely within the maxilla and a second is in the palatomaxillary suture. These are not at the same level on either side. On the right element is another foramen within the maxilla, medial to the P4; the corresponding structure on the left is within the palatine. In addition to these are numerous foramina in the interdental spaces; the largest of these is bilaterally between the P1 and P2. The zygomatic process of the maxilla extends from the P4 to the M1/M2 interdental space. At the anterior end of the zygomatic process, the ventral margin of the infraorbital foramen is visible (bilaterally in Fig. 5).

In dorsal view (Figs. 2A–B), the numerous small foramina in the dorsal aspect of the facial process are visible, especially those near the canine eminence.

In anterior view (Figs. 3A–B), the infraorbital foramen is essentially round, only just slightly taller than wide (more so on the right than left). There is a tiny opening in the suture with the jugal, dorsolateral to the infraorbital foramen; it is asymmetrically placed and is higher on the left side. This foramen cannot be traced into the orbit and its function is unknown.

In the anterior aspect of the orbit (Fig. 8A), the maxilla forms the bulk of the orbit floor; there is some palatine in the posteromedial floor. Only one tooth root is exposed, the single root of M2. The maxilla contacts the perpendicular process of the palatine medially and the jugal laterally. The lacrimal comprises the bulk of the anterior contact. There are numerous tiny foramina in the orbit floor, the larger ones presumably serving as passage for alveolar nerves. The maxillary foramen (“mxf” in Fig. 8A) is in the apex of the orbit floor and is entirely enclosed in the maxilla. The infraorbital canal, between the infraorbital and maxillary foramina, is short, comparable in length to M1. In the ventromedial floor of the maxillary foramen is a sizeable anteriorly-directed opening that is probably the incisivomaxillary canal (“imc” in Fig. 8A). Dorsal to the maxillary foramen is a small foramen in the complex suture with the lacrimal (two are found on the right side); it resembles the vascular foramen of the lacrimal described in *Pteropus lylei* K. Andersen, 1908, by Giannini et al. (2006). Laterally, the maxilla is upturned to meet the jugal and comprises a large portion of the anterior internal rim of the zygomatic arch. Medially, the palatomaxillary suture is in the orbit floor posteriorly, but the maxilla is upturned anteriorly to a small extent and has a minor contribution to the orbit wall. The top of the upturned maxilla forms a crest that continues posteriorly onto the palatine. On the left side, medial to this crest, is a well-developed depression between the maxilla and palatine; on the right side, rather than a depression there is a well-developed anteriorly-directed oval opening, which is taller than wide. This depression on the left is the inferior oblique muscle fossa (“iomf” in Fig. 8A) and the opening on the right is the lacrimal fenestra, which is an open inferior oblique muscle fossa.

**AMNH 207730, Newborn.**—In ventral view (Figs. 6C–D), the dC is in its crypt, the P1 is represented by a nubbin of a cusp in its crypt, the dP2 is represented by more of a cusp in its crypt, the dP4 is slightly more of a cusp in its crypt (not visible in direct ventral view), and the dP5 is a nubbin on the left side in its crypt (not visible in direct ventral view). The maxilla is not fully ossified at birth as crypts for the molars have not yet formed.

In lateral view (Figs. 4C–D), the alveolar margin is not straight; it is shaped like a gently sloping upside down V, with the apex between the dC and dP2, and is not present behind the dP4. The infraorbital foramen lies dorsal to the dP2 and dP4; it is larger relatively in the newborn than in the adult. The incisivomaxillary canal (“imc” in Fig. 4D) is anterior to the infraorbital foramen. On the left side (but not on the right), there is an unossified part of the frontomaxillary contact at the posterodorsal margin of the maxilla is an unossified part of the frontomaxillary contact. The frontomaxillary suture is a smooth curve and not angled.

In ventral view (Figs. 6C–D), the midline palatine process of the maxilla is 18.9% of the hard palate length. The intermaxillary suture is raised. The anteriormost major palatine foramen is opposite the dP2, slightly anterior to the palatomaxillary suture. Two processes from the maxilla grow ventrally to enclose the anteriormost major palatine foramen and the suture between them is obvious. A second major palatine foramen is in the palatomaxillary suture opposite the dP4. The major palatine sulcus is better defined than in the adult, with a more prominent lateral margin that extends to the incisive foramen and is continuous posteriorly with an equally prominent ridge on the palatine. The medial margin of the major palatine sulcus is about half the height and length of the lateral. The palatine process medial to the lateral margin is sunken, creating a midline depression that extends from the incisive foramen to the posterior edge of the hard palate. The anterior root of the zygoma is not as laterally deflected as in the adult, and the maxilla makes up a relatively smaller contribution to the anterior internal rim of the arch.

In anterior view (Figs. 3C–D), the left infraorbital foramen is subcircular and the right is more ovoid, taller than wide.

In the anterior aspect of the orbit (Fig. 8B), the maxilla is incompletely ossified in the floor and in the anteromedial wall, with an enormous lacrimal fenestra between the maxilla, lacrimal, frontal, and palatine (“lacfe” in Fig. 8B). An infraorbital canal is essentially lacking as the maxillary and infraorbital foramina are contiguous. The suture between the lacrimal and maxilla is simple and has no foramina.

**Others.**—In the series in Figure 1, in dorsal view, in the oldest and largest specimen, CM 42728, the anterior root of the zygomatic arch, formed by maxilla and jugal, is at a higher angle to the sagittal plane as compared to the others. The other adult in the figure, CM 59495, resembles the larger juvenile, CM 6374. However, the change between

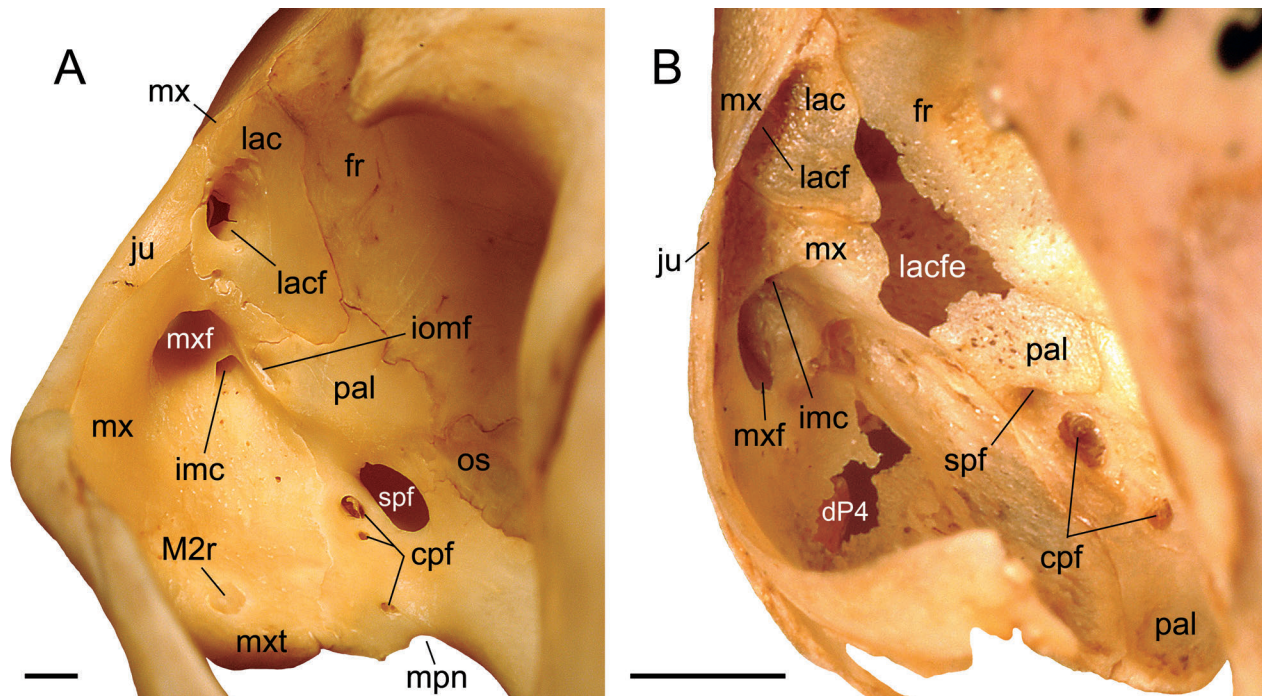


Fig. 8—Anterior wall of orbit of *Nandinia binotata* in posterior view. **A**, adult, CM 59495; **B**, newborn, AMNH 207730. Scale = 2 mm. Abbreviations: **cpf**, caudal palatine foramen; **dP4**, deciduous upper fourth premolar; **fr**, frontal; **imc**, incisivomaxillary canal; **iomf**, inferior oblique muscle fossa; **ju**, jugal; **lac**, lacrimal; **lacf**, lacrimal foramen; **lacfe**, lacrimal fenestra; **M2r**, root of upper second molar; **mpn**, minor palatine notch; **mx**, maxilla; **mx**, maxillary foramen; **mxt**, maxillary tuberosity; **os**, orbitosphenoid; **pal**, palatine; **spf**, sphenopalatine foramen.

the two adults is a continuum over the 13 specimens in our sample that fall between them. In lateral view, the infraorbital foramen shifts from a position dorsal to the anterior aspect of the dP4 in the newborn, AMNH 207730, and younger juvenile, AMNH 51486, to dorsal to the posterior aspect of the dP4 in the older juvenile, CM 6374. A position dorsal to the posterior aspect of P4 is consistently present throughout the adult sample.

We recorded the incidence of two features of the maxilla across the study sample:

(1) Openings in the floor of the orbit exposing molar roots (only sampled in specimens with adult dentition): (a) none - AMNH 134969, CM 3693, 42282, AMNH 51510, 51494(R), CM 42728, 5097(L), 51503; (b) one for the single root of M2 - CM 42281, 5157(R), 59497, AMNH 51503, CM 59495 (Fig. 2B), 59496(L), 42725, 42726, 69365, 69366, 16103, AMNH 51594(L), CM 5097(R); (c) two, for M2 and the posterobuccal root of M1 - AMNH 51448, CM 5157(L), 2356, 59496(R). This distribution shows no obvious correlation with geography, ontogeny, and sex.

(2) Position of incisivomaxillary canal: (a) posterior to or within the maxillary foramen - AMNH 51471, 51486, CM 6371, AMNH 51488, 51448, CM 42281, AMNH 51503, CM 59495 (Fig. 8A), 59496, 42727, 16103; (b) within the infraorbital canal (anterior to the maxillary foramen and posterior to the infraorbital foramen) - CM 6374, AMNH 201513, CM 2356, 5157, AMNH 134969, CM

3693, 42725, 42726, 42282, 69365, 69366, AMNH 51510, 51494, CM 42728, 5097, AMNH 51513; (c) anterior to the infraorbital foramen - AMNH 207730 (Figs. 4C–D), CM 59497. This distribution shows no obvious correlation with geography, ontogeny, and sex.

We found that all specimens have a major palatine sulcus, and also a carnassial embrasure pit (Figs. 5, 9) with the exception of the newborn, AMNH 207730. The tiny foramen in the suture between the maxilla and jugal described in the principal adult, CM 59495 (Fig. 2B), is unique to that specimen. The number of major palatine foramina varies between one and seven, with one occurring bilaterally only in AMNH 51448 and on one side only in AMNH 51488 and 51513. The anteriormost major palatine foramen is the largest in all specimens (Figs. 5, 9).

Another feature that varies, but with only a few variants, concerns the location of the principal major palatine foramen. It is well anterior to the palatomaxillary suture in all (Fig. 5) but two juveniles, AMNH 51488 and 51448, where it is just anterior to the suture.

Gaubert (2009) reported the M2 to be variably present in *N. binotata*, but we found only a single adult in our sample that has the M2 absent, and this was on just one side, the right side of AMNH 51510. This specimen has a pit on the right side in the location where the left M2 occurs, suggesting that the M2 alveolus was resorbed.

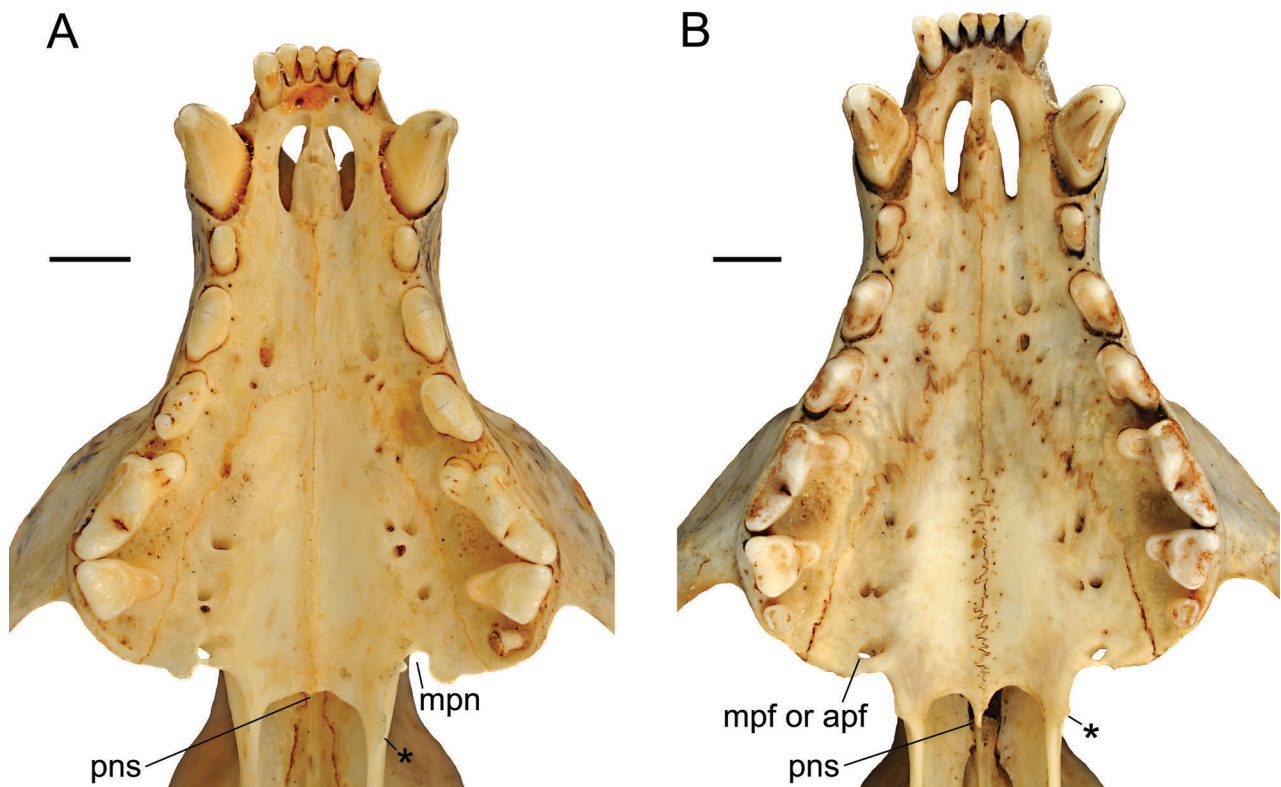


Fig. 9—Posterior hard palate of *Nandinia binotata* in ventral view. **A**, AMNH 51510; **B**, CM 42282. The asterisk is the raised ridge on the palatine lateral to the choanae (cf. Fig. 5). Scale = 5 mm. Abbreviations: **apf**, accessory palatine foramen; **mpf**, minor palatine foramen; **mpn**, minor palatine notch; **pns**, posterior nasal spine.

#### Palatine (“pal” in figures)

The paired palatines contribute to the hard palate and floor of the nasal cavity via the horizontal process, and to the orbit wall and basipharyngeal canal via the perpendicular process.

**CM 59495, Principal Adult.**—In ventral view (Figs. 5, 6A–B), the horizontal process is 52.6% of maximum hard palate length at the midline. The interpalatine suture starts anteriorly medial to the posterior margin of the P2, and becomes raised starting opposite the M1. The suture is simple anteriorly and complex from the posterior margin of the P4 and beyond. Extending forward from the entopterygoid processes (“enp” in Fig. 6B) is a low, longitudinal eminence on the horizontal process that continues anteriorly onto the maxilla as the lateral margin of the major palatine sulcus. Medial to this eminence, the horizontal process is gently concave, whereas laterally it is flat and grades into the alveolar margin. Tiny foramina occur near the midline, but the accessory palatine foramina are in the lateral flat area. The right side has three accessory palatine foramina and the posterior two have anteriorly directed grooves; the left side has seven with the second, fifth, and seventh foramina having associated grooves. On its posterior margin, the horizontal process abuts the maxillary tuberosity

laterally and extends minutely beyond it. Medial to that is a distinct notch for the minor palatine nerves and vessels (“mpn” in Fig. 5). Even further medial, the horizontal process has a short postdental palate flooring the choanae. The posterior border of the postdental palate has a distinct posterior nasal spine (“pns” in Fig. 5) that is V-shaped and flanked by a concavity. A postpalatine torus is absent.

Part of the perpendicular process is visible in ventral view (Figs. 6A–B). Its ventral border forms the anterior two-thirds of the parasagittal entopterygoid process (“enp” in Figs. 6B, 10), which is completed posteriorly by the pterygoid (“pt” in Figs. 10–11) and alisphenoid (based on the newborn, AMNH 207730) (“as” in Fig. 11). Its medial surface forms the lateral wall and much of the roof at the choanae and the anterior part of the basipharyngeal canal. The palatines approximate one another in the roof of the choanae and are narrowly separated by the presphenoid (“ps” in Figs. 6B, 10). The presphenoid exposure between the palatines is wider in the basipharyngeal canal than at the choanae (Figs. 6A–B). In the lateral wall of the basipharyngeal canal, the palatine contacts the pterygoid via a posteriorly directed V-shaped suture (Fig. 10). At the confluence of the palatine, presphenoid, and pterygoid on the left side (and of the first two bones on the right) is a small aperture of unknown function that opens into the orbit;

more anteriorly, in the suture between the palatine and presphenoid is another small foramen that also opens into the orbit in varying locations (both are labeled “?” in Fig. 10).

In lateral view (Figs. 4A–B), much of the perpendicular process is visible; only the anteroventral part is hidden by the zygoma. The perpendicular process is longer than tall and tallest anteriorly (Figs. 8A, 11). Starting from the anteroventral border, its contacts are: anteriorly (Fig. 8A), the maxilla and lacrimal; dorsally (Fig. 11), the frontal, orbitosphenoid (“os” in Fig. 11), and presphenoid; and posteriorly, the pterygoid, alisphenoid, and pterygoid again. Most of its ventral margin is free as the entopterygoid process, which posteriorly slopes ventrally. The perpendicular process extends from just posterior to the maxillary foramen to just anterior to the sphenorbital fissure and foramen rotundum (“sof” and “fro” in Figs. 10–11, respectively). The dorsal surface of the posterolateral corner of the horizontal process has a small exposure in the floor of the orbit, medial to the maxilla (Fig. 8A).

Various foramina are in or near the orbital exposure of the palatine. The lacrimal fenestra and inferior oblique muscle fossa are described above with the maxilla (Fig. 8A). Posterior to the lacrimal fenestra is a small foramen of unknown function directed posteromedially into the perpendicular process; this area is not ossified in the newborn. The large sphenopalatine foramen (“spf” in Fig. 8A) lies within the palatine dorsal to the P5/M1; it is ovoid, longer than tall, and opens posterolaterally. In the dorsal border of the sphenopalatine foramen is a suture within the palatine itself, suggesting that two processes from the palatine serve to enclose the foramen dorsally; Wible (2011) reported a similar phenomenon in treeshrews. Lateral to the sphenopalatine foramen in the roof of the horizontal process are a variable number of small caudal palatine foramina (“cpf” in Fig. 8A): the left side has two proximal to the sphenopalatine and a third positioned near the caudal border of the horizontal process, whereas the right side has one larger one near the sphenopalatine that splits into two and a second that is not located as far posteriorly as on the left side. In the suture with the orbito- and presphenoid are three tiny foramina ventral to the optic foramen (“?” in Fig. 11). The posterior two connect to openings in the basipharyngeal canal described above (Fig. 10).

**AMNH 207730, Newborn.**—In ventral view (Figs. 6C–D), the horizontal process is 52.8% of maximum hard palate length, nearly identical to the adult. The interpalatine suture is not raised. The longitudinal eminence on the horizontal process that is continuous anteriorly with the lateral margin of the major palatine sulcus on the maxilla is much more prominent. Medial to these eminences, the horizontal process is concave, and this concavity extends across the midline for all but the anteriormost part of the horizontal process. The palatomaxillary suture is relatively straight, rather than curved as it is in the adult. Five accessory palatine foramina occur within the horizontal process. Whereas the lateral border of the postdental palate is in the same

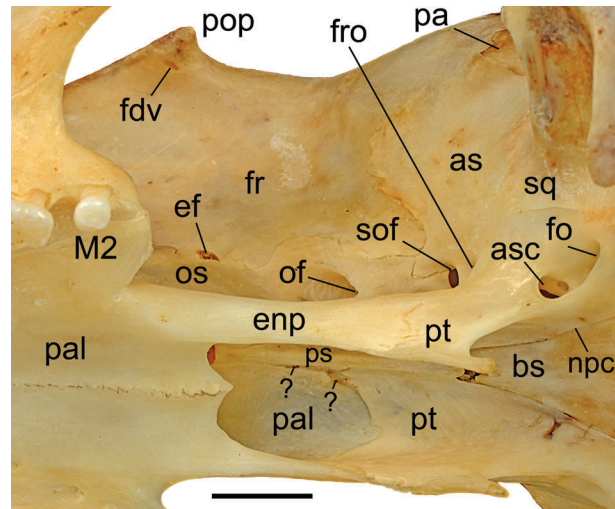


Fig. 10—Mesocranium and orbit of adult *Nandina binotata*, CM 59495, in left ventrolateral view. Question marks are small foramina of unknown function that open in the orbit. Scale = 5 mm. Abbreviations: as, alisphenoid; asc, caudal opening of alisphenoid canal; bs, basisphenoid; ef, ethmoidal foramen; enp, entopterygoid process; fdv, frontal diploic vein foramen; fo, foramen ovale; fr, frontal; fro, foramen rotundum; M2, upper second molar; npc, groove for nerve of pterygoid canal; of, optic foramen; os, orbitosphenoid; pa, parietal; pal, palatine; pop, postorbital process of frontal; ps, presphenoid; pt, pterygoid; sof, sphenorbital fissure; sq, squamosal.

parasagittal plane as the entopterygoid process in the adult, there is a small flange of the horizontal process that extends lateral to the plane of the entopterygoid process; this flange forms the medial aspect of the notch for the minor palatine nerve. The postnasal spine is proportionally larger. The entopterygoid processes diverge posteriorly and are broader than in the adult. The perpendicular process has little contribution to the roof of the basipharyngeal canal near the choanae, and more of the presphenoid is exposed.

In lateral view (Figs. 4C–D), the dorsal margin of the perpendicular process is straight; missing due to incomplete ossification is the anterodorsal part that helps to close off the lacrimal fenestra (Fig. 8B). Two caudal palatine foramina occur bilaterally (Fig. 8B), but on the right side the anterior one splits into two. There is one small foramen of unknown function within the perpendicular process halfway between the sphenopalatine and optic foramina that is not present in the principal adult (not visible in figures).

**Others.**—We recorded the incidence of one feature of the palatine across the study sample:

(1) Attachment of the inferior oblique muscle: (a) lacrimal fenestra - AMNH 51486, 51488, CM 6374 (Fig. 12B), AMNH 201513, 51448, CM 42281, 5157, 59495(R), AMNH 134969 (Fig. 12A), CM 42727, 3693, 42725, 42282, 69365, 69366, 16103, 42728, 5097; (b) muscular fossa principally on the palatine - AMNH 51471, CM 6371, 2356, 59497, AMNH 51503, CM 59495(L) (Fig. 8A), 59496, 42726; (c) muscular fossa principally on the maxilla - AMNH 51510, 51494. This distribution shows

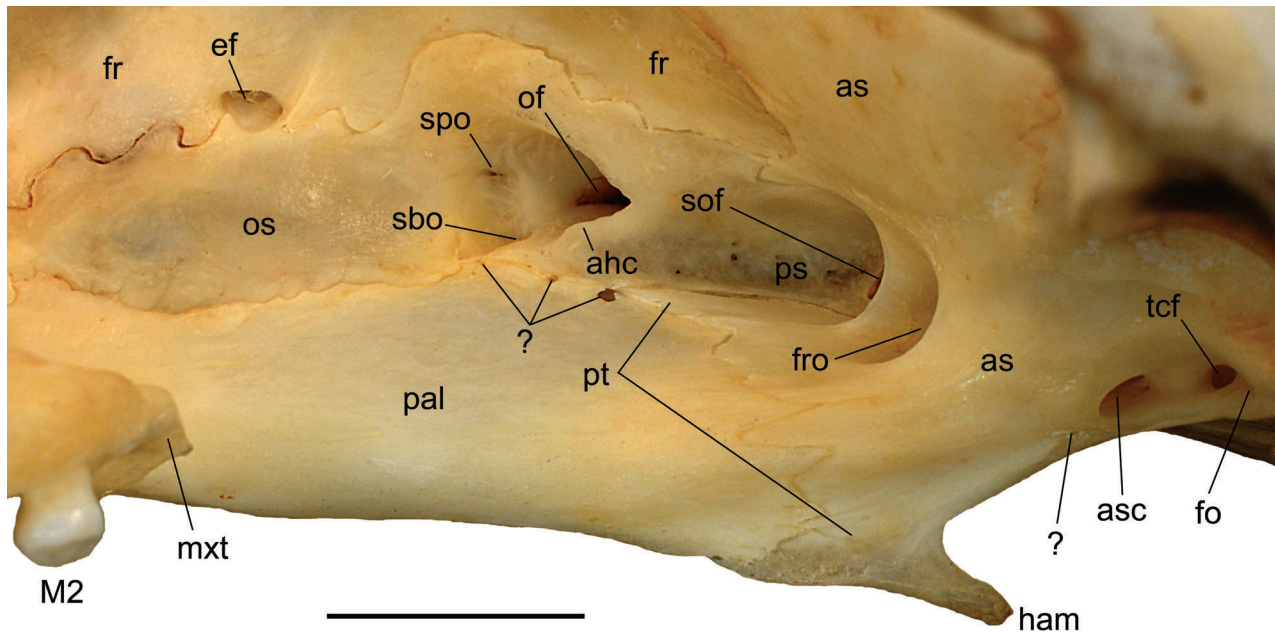


Fig. 11—Mesocranium of adult *Nandinia binotata*, CM 59495, in left lateral view. Question marks are three small foramina between the palatine and orbitosphenoid, and another anterior to the caudal opening of the alisphenoid canal. Scale = 5 mm. Abbreviations: **ahc**, ala hypochiasmatica; **as**, alisphenoid; **asc**, caudal opening of alisphenoid canal; **ef**, ethmoidal foramen; **fo**, foramen ovale; **fr**, frontal; **fro**, foramen rotundum; **ham**, pterygoid hamulus; **M2**, upper second molar; **mxt**, maxillary tuberosity; **of**, optic foramen; **os**, orbitosphenoid; **pal**, palatine; **ps**, presphenoid; **pt**, pterygoid; **sbo**, suboptic foramen; **sof**, superior orbital fissure; **spo**, supra-optic foramen; **tcf**, transverse canal foramen.

no obvious correlation with geography, ontogeny, and sex.

The number of accessory palatine foramina per side varies between four and 13 (Figs. 5, 9). Four specimens have the same number of accessory palatine foramina bilaterally, although the foramina positions are not identical. The left-right disparity in accessory palatine foramina number does not exceed three. The size of the posterior nasal spine shows a continuum from a tiny spine in AMNH 51510 (Fig. 9A) to a spine projecting 3 mm beyond the posterior margin of the palate in CM 42282 (Fig. 9B); the remaining specimens, including the principal adult, CM 59495 (Fig. 5), fall between these extremes.

The majority of specimens show a distinct minor palatine notch lateral to the choanae (Fig. 5). However, roughly a third of the study sample shows varying degrees of closing this notch, with the growth of bony lappets from the medial and/or lateral margin of the notch (see the left notch in Fig. 9A). In three specimens, these lappets meet to enclose a foramen, bilaterally in CM 42282 and on the right sides of AMNH 51471 and 51510 (Fig. 9). There are two possible interpretations for the contents of this foramen: it is a minor palatine foramen containing the minor palatine nerve and vessels or it is an accessory palatine foramen containing an accessory palatine nerve with the minor palatine nerve running posterior to it.

In describing the palatine of the newborn, AMNH 207730, we noted the presence of a small horizontal flange lateral to the anterior root of the entopterygoid process that forms the medial margin of the minor palatine notch (Figs.

6C–D). Roughly half the sample, including males and females, juveniles and adults, has only a faint vertical ridge in the comparable position (Figs. 5, 6A–B). The remaining specimens show some elevation and lateral protrusion as noted in the newborn (“\*” in Fig. 9), with one specimen, CM 63966, having the elevation on one side only. The lateral protrusion is similar to the lateral flare of the postdenal palate described in some *Bassaricyon* Allen, 1876, by Helgen et al. (2013)

The number of caudal palatine foramina varies between two and six, with 11 specimens showing the same number bilaterally. Of the remainder, the right and left sides differ by only one foramen in the vast majority.

The suture within the palatine dorsal to the sphenopalatine foramen reported in the principal adult, CM 59495, is present throughout the study sample.

#### Lacrimal (“lac” in figures)

The paired lacrimals are small elements confined to the anterior orbit.

**CM 59495, Principal Adult.**—The lacrimal is a roughly quadrangular element in the anterior orbit, longer than tall (Fig. 8A). Anteriorly, in the narrow interval between the frontal and jugal, it contacts the facial process of the maxilla to form a weakly delimited anterior orbital rim. A lacrimal facial process is entirely absent. Laterally, the lacrimal contacts the jugal and makes no contribution to

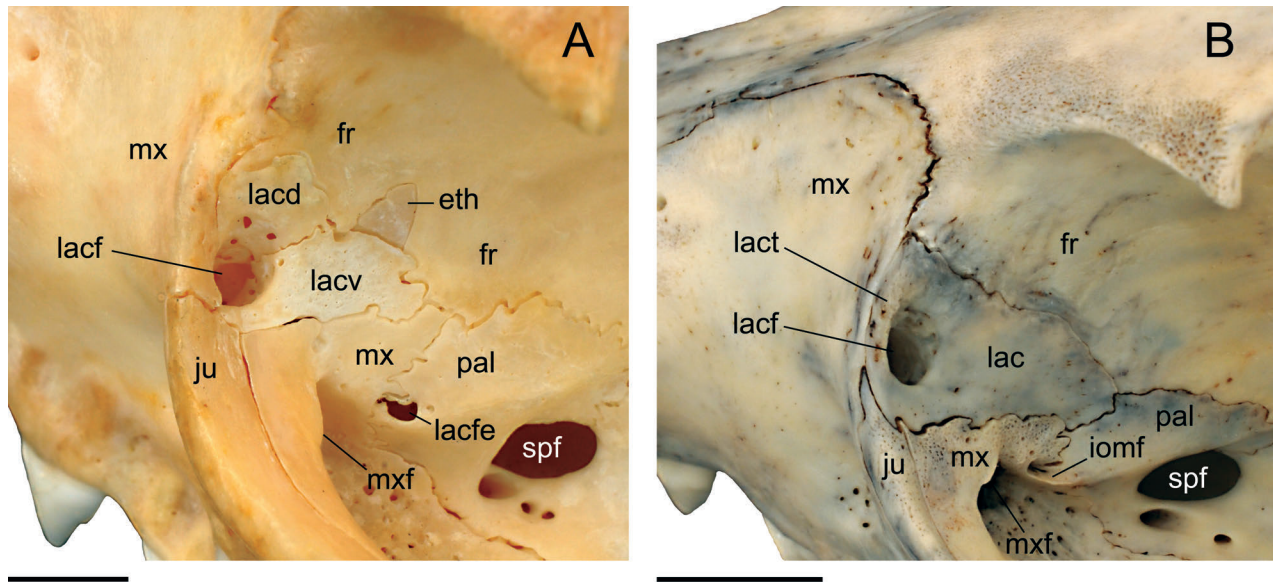


Fig. 12—Anterior wall of left orbit of *Nandinia binotata* in oblique posterior view. **A**, adult, AMNH 134969; **B**, juvenile, CM 6374. Scale = 5 mm. Abbreviations: **eth**, ethmoid exposure; **fr**, frontal; **iomf**, inferior oblique muscle fossa; **ju**, jugal; **lac**, lacrimal; **lacd**, “dorsal lacrimal”; **lacf**, lacrimal foramen; **lacfe**, lacrimal fenestra; **lact**, lacrimal tubercle; **lacv**, “ventral lacrimal”; **mx**, maxilla; **mx**, maxillary foramen; **pal**, palatine; **spf**, sphenopalatine foramen.

the anterior zygoma; a lacrimal zygomatic process is also lacking. Ventrally, the lacrimal contacts the maxilla dorsal to the maxillary foramen. Posteriorly, it contacts the perpendicular process of the palatine. The longest contact is the dorsal one with the orbital surface of the frontal. The sutures are all simple except for a small portion of the maxillary suture directly dorsal to the maxillary foramen that is complex. The well-developed, anteroventrally directed lacrimal foramen (“lacf” in Fig. 8A) is entirely in the orbit, situated just medial to the contact with the jugal. Only a thin layer of lacrimal excludes the jugal from the foramen’s lateral margin. A suture within the lacrimal in the lateral wall of the foramen suggests that two processes from the lacrimal meet to form the aperture. Several small foramina are present within the ventral floor of the foramen; on the left side, one is positioned just posterior to the foramen’s rim. Posteromedial to the lacrimal foramen is a slight lacrimal fossa.

**AMNH 207730, Newborn.**—The lacrimal is a small triangular wedge confined to the anterior orbit (Fig. 8B). It does not contribute to the anterior orbital rim nor does it contact the palatine or jugal. Its anterolateral and ventral edges contact the maxilla. The dorsal half of its posterolateral edge contacts the frontal, and the ventral half does not contact any bone. All sutures are simple. The lateral wall of the lacrimal foramen is formed by the maxilla.

**Others.**—The lacrimal is by far the most variable cranial bone in *N. binotata*, showing differences in its contribution to the anterior orbital rim and to the orbital wall (Figs. 8, 12). These differences affect the lacrimal’s sutural rela-

tions with its neighbors and the composition of the lacrimal foramen. We recorded the distribution of six features of the lacrimal in the study sample:

(1) Composition of the anterior rim of the orbit between the frontal and jugal: (a) maxilla only - AMNH 51471, 51486, 51488, AMNH 201513, 51448, CM 42281, 5157, 2356, 59497, AMNH 51503, 134969 (Fig. 12A), CM 59496, 3693, 42725, 42726, 42282, 69365, 69366; (b) maxilla and lacrimal - CM 59495 (Figs. 4A–B, 8A); (c) lacrimal only - CM 6371, 6374 (Fig. 12B). The principal adult, CM 59495, is not representative of the vast majority of specimens as its lacrimal buttresses the maxilla. The two juvenile specimens of *N. b. gerardi*, CM 6371 and 6374, differ from the others, *N. b. binotata*, in the presence of a small facial process of the lacrimal with a weak lacrimal tubercle.

(2) Composition of the lacrimal foramen: (a) lacrimal only - CM 6371, 6374 (Fig. 12B), AMNH 201513, CM 42727; (b) lacrimal and maxilla - AMNH 207730 (Fig. 8B), 51471, 51486, 51488, 51448, CM 42281, 5157(L), 2356, 59497(R), AMNH 51503, CM 59495, CM 59496, 3693, 42725, 42282(R), 69365, 69366, AMNH 51510, CM 16103(L), AMNH 51494; (c) two “lacrimals” and maxilla - CM 5157(R), 59497(L), AMNH 134969 (Fig. 12A), CM 42726, 16103(R), 42282(L). Of the four specimens with the foramen entirely in the lacrimal, the two juvenile specimens of *N. b. gerardi*, CM 6371 and 6374, differ in that they do not have a seam in the anterolateral margin that suggests enclosure by the union of two lacrimal processes. In light of their juvenile stage, if the foramen had formed in that manner, a seam would be expected to occur.

Most specimens have the foramen between the lacrimal and maxilla, with a contribution of roughly 40% and 60% from these two bones, respectively. The principal adult, CM 59495, is unusual in that there is only a tiny bit of maxilla (Fig. 8A). The final variant includes the presence of two distinct ossifications of the lacrimal, dorsal and ventral parts, bilaterally in one specimen, AMNH 134969 (“lacd” and “lacr” in Fig. 12A), and four specimens on one side only. We are not aware of similar reports in other mammals of this phenomenon.

(3) Lacrimal-jugal contact: (a) present - AMNH 51486, CM 6374 (Fig. 12B), 59495 (Fig. 8A), AMNH 134969(L) (Fig. 12A); (b) absent - AMNH 207730 (Fig. 8B), 51471, 51488, CM 6371, AMNH 201513, 51448, CM 42281, 5157, 2356, 59497, AMNH 51503, 134969(R), CM 59496, 42727, 2356, 42725, 42726, 42281, 69365, 69366. This distribution shows no obvious correlation with geography, ontogeny, and sex.

(4) Lacrimal-palatine contact: (a) present - CM 6371, 6374 (Fig. 12B), AMNH 201513, 51448, CM 42281, 2356, AMNH 51503, CM 59495 (Fig. 8A), 59496, 42272(L), 3693, 42726, 42282, 69365, 69366, AMNH 51510, CM 16103, AMNH 51494; (b) point contact - AMNH 51471, 51486, 51488, CM 59497(L), 42272(R), 42725(R); (c) absent - AMNH 207730 (Fig. 8B), CM 5157, 59497(R), AMNH 134969 (Fig. 12A), CM 42725(L). This distribution shows no obvious correlation with geography, ontogeny, and sex.

(5) Posterior extent of the lacrimal relative to the sphenopalatine foramen: (a) extends even with or posterior to - CM 6374(R), 59496, 42282, AMNH 51494; (b) does not reach to - AMNH 207730 (Fig. 8B), 51471, 51486, CM 6371, AMNH 51488, CM 6374(L) (Fig. 12B), AMNH 201513, 51448, CM 42281, 5157, 2356, 59497, AMNH 51503, CM 59495 (Fig. 8A), AMNH 134969 (Fig. 12A), CM 42727, 3693, 42725, 42726, 69365, 69366, AMNH 51510, CM 16103. This distribution shows no obvious correlation with geography, ontogeny, and sex.

(6) Dorsal extent of the lacrimal: (a) equal to or more than twice the height of the lacrimal foramen - AMNH 207730 (Fig. 8B), 51471, 51486, CM 6371, AMNH 201513, CM 2356, 59495 (Fig. 8A), 59496, 42282(R), 69365, 69366, AMNH 51510; (b) less than twice the height of the lacrimal foramen - AMNH 51488, CM 6374 (Fig. 12B), AMNH 51448, CM 42281, 5157, 59497, AMNH 51503, 134969 (Fig. 12A), CM 42727, 3693, 42725, 42726, 42282(L), 16103. This distribution shows no obvious correlation with geography, ontogeny, and sex.

#### Jugal (“ju” in figures)

The paired jugals are the principal elements of the zygoma and form the infraorbital margin.

**CM 59495 - Principal Adult.**—In dorsal view (Figs. 2A–B), the jugal is a long, thin bone. Anteriorly, it is curved medially to form the infraorbital margin; it straightens

posteriorly to form the beginning of the zygomatic arch. It is of relative uniform mediolateral width, except at its anteromedial end where it is thickened. It contacts the anterolateral margin of the lacrimal anteromedially, overlies the zygomatic process of the maxilla anteriorly, and underlies the zygomatic process of the squamosal posteriorly (“zpsq” in Fig. 2B). Between the zygomatic processes of the maxilla and squamosal, the freestanding portion of the jugal forms just less than half the zygoma.

In lateral view (Figs. 4A–B), the jugal is concave dorsally in the infraorbital margin and concave ventrally in the zygoma. Its contact with the zygomatic process of the maxilla is bifurcate; the anterodorsal process is relatively long, curving to reach the lacrimal, and the posteroventral process is very short, anteroventrally directed, and lies above the M1. Anterior to the terminus of the zygomatic process of the squamosal is a weak, blunt frontal process of the jugal (best seen in anterior view; “fpju” in Fig. 3B). Posteriorly, the jugal tapers to a point and ends just anterior to the preglenoid process of the squamosal (“prgp” in Fig. 4B). Muscular fossae are not developed on the jugal.

In ventral view (Figs. 6A–B), the two jugals are subparallel in the zygoma, with only a small degree of divergence. Although the posterior extent of the jugal in lateral view is near the level of the preglenoid process of the squamosal, the two are quite separated in ventral view and the jugal does not contribute to the glenoid fossa.

In anterior view (Figs. 3A–B), as previously documented above, a tiny foramen of unknown function is in the maxillary suture.

**AMNH 207730, Newborn.**—The jugal is broken bilaterally anterior to the zygomatic process of the squamosal (Figs. 6C–D). The portion in the infraorbital margin tapers to a point anteriorly and does not reach the lacrimal (Fig. 8B). The bifurcate contact with the maxilla is incipient, with a tiny posteroventral process (Figs. 4C–D). The jugal does not extend as far posteriorly as in the adult, ending well before the preglenoid level (Figs. 6C–D).

**Others.**—We sampled the incidence of one feature of the jugal in the study sample:

(1) Posterior extent of the jugal relative to the preglenoid process: (a) anterior to - AMNH 207730 (Fig. 4D), 51471, 51486, CM 6371, AMNH 51448, CM 6374, CM 42281, CM 5157, 59497, AMNH 51503, CM 3693, 42725, 42726, 69366, AMNH 51510, CM 16103, AMNH 51494; (b) even with or posterior to - AMNH 201513, CM 2356, 59495 (Fig. 4B), AMNH 134969, CM 59496, 42727, 42282, 69365, 42728, 5097, AMNH 51513. This distribution shows no obvious correlation with geography, ontogeny, and sex.

We also noted two other features with only a few variants. First, the contact of the jugal with the lateral aspect of the zygomatic process of the maxilla is typically bifurcated (Fig. 4B). However, the size of the posteroventral process of the jugal is a continuum from large and rounded

(e.g., CM 42281), to large and pointed (e.g., CM 16103), to three specimens with almost no posteroventral process (CM 59497, 69365, 69366). Second, the frontal process of the jugal is typically weak (Fig. 3B), but in two of the five juveniles preserving the jugal, the frontal process is absent (AMNH 51471 and 51488).

#### Frontal (“fr” in figures)

The paired frontals consist of a squama that forms the roof of the anterior braincase and an orbital surface that is the major element of the orbit wall and contributes to the anterior temporal fossa.

**CM 59495, Principal Adult.**—In dorsal view (Figs. 2A–B), the frontals comprise 39.6% of the midline skull length. The interfrontal suture is partially fused; it fades in and out from the level of the mid-orbit posteriorly. At its posterior extent, the fusing interfrontal suture lies to the left of the sagittal suture between the parietals (“pa” in Fig. 2B). Anteriorly, the frontals have long maxillary processes that taper to a point (“mpfr” in Fig. 2B) and almost meet the posterodorsal processes of the premaxillae. The maxillary process contacts the nasal medially and the maxilla laterally. Posterolateral to the maxillary process, the frontal forms the supraorbital margin without a supraorbital crest. Demarcating the posterior extent of the orbit is a prominent postorbital process (“pop” in Fig. 2B); it is triangular, the posterior margin is strongly concave, and the anterior edge is a weak, gently concave crest. Temporal lines (“tl” in Fig. 2B) begin at the apex of the postorbital processes and curve posteromedially; they converge, but do not meet, and continue posteriorly onto the parietals. A prominent postorbital constriction begins level with the space between the optic and ethmoidal foramina, well anterior to the frontals’ suture with the parietals. The posterior suture with the parietal is irregular, and the posterior-most extent of the frontal lies on the midline.

In lateral view (Figs. 4A–B, 11), the orbital surface of the frontal contacts (from anterior to posterior) the facial process of the maxilla at the orbital rim, the lacrimal, the perpendicular process of the palatine, the orbitosphenoid, and in the temporal fossa the alisphenoid and the parietal. The only angular suture is with the lacrimal. The ventral border with the palatine and orbitosphenoid is roughly longitudinal, with the posteroventralmost extent nearly into the sphenorbital fissure. The suture with the parietal trends vertical its whole length, while the suture with the alisphenoid is a V with its apex pointing anteriorly. The orbital surface of the frontal is gently concave up to and including the area of the postorbital constriction; posterior to that, the frontal strongly bulges out in the temporal fossa.

The ethmoidal foramen (“ef” in Figs. 10–11) lies between the ventral margin of the orbital surface and the orbitosphenoid, at a level just posterior to the postorbital process. The foramen is directed dorsally into the braincase and is hidden in lateral view by the zygoma (Figs.

4A–B). A short but well-developed sulcus on the frontal runs to the foramen from above and behind. On the right side, a tiny opening anterior to the ethmoidal foramen lies in the suture with the orbitosphenoid. The only other foramen associated with the orbital surface is the frontal diploic vein foramen on the undersurface of the root of the postorbital process (“fdv” in Fig. 10). The foramen is directly posteriorly into the frontal and has a short sulcus leading anteriorly into it.

**AMNH 207730, Newborn.**—In dorsal view (Figs. 2C–D), the frontals are 38.1% of the midline skull length. The interfrontal suture is present save for posteriorly where there is a fontanel between the frontal and parietal. The postorbital process is a tiny, sharp bump at the posterior end of the well-developed supraorbital crest (“soc” in Fig. 4D). No temporal lines are evident. A postorbital constriction is lacking, but there is a pronounced frontal eminence at the level of the postorbital process.

In lateral view (Figs. 4C–D), the anteroventral margin of the frontal does not contact its neighboring bones (i.e., the lacrimal and palatine) and the opening thus formed represents a large lacrimal fenestra. The frontal’s ventral suture is less longitudinal than in the adult. A small fontanel occurs at the juncture of the frontal, alisphenoid, and parietal. The ethmoidal foramen does not have a sulcus associated with it. The frontal diploic vein foramen is relatively larger (about the same actual size as in the adult) and is dorsally directed into the braincase. It is medial to the supraorbital crest, anterior to the tiny postorbital process (Figs. 3C–D).

**Others.**—In the series in Figure 1, the major stages of the ontogeny of the temporal lines on the frontal can be traced. Lines are absent in the newborn, AMNH 207730, and present but are faint in the younger juvenile, AMNH 51486, where the distance between the lines is greater at the frontoparietal suture than at the postorbital processes. In the older juvenile, CM 6374, the lines are more developed, they diverge posteriorly, but the distance between them is greater at the postorbital processes than at the frontoparietal suture. In the younger adult female, CM 59495, the more prominent lines strongly converge posteriorly, and in the older adult female, CM 42728, the lines meet on the midline just posterior to the postorbital processes to create a sagittal crest. In our study sample organized by age (see Table 1), we identified 13 adults between the two in Figure 1. Of these 13, the older eight have sagittal crests, including both males and females. The younger five include two specimens of unknown sex with sagittal crests and three females without. Therefore, it is likely that a sagittal crest distinguishes sex in a certain age window of young adulthood, but not throughout the ontogenetic series.

Figure 1 also shows ontogenetic changes in two other features of the frontals: the postorbital constriction and the postorbital processes. The measurements in Table 2 (POC) reveal that the width of the frontals posterior to the post-

orbital processes is actually absolutely greater in the juveniles and young adults than in the older specimens. As the skull gets longer, the postorbital constriction increases. In addition, as the skull gets longer, the postorbital processes become more prominent, irrespective of sex. The extreme size of the postorbital processes seen in the adult female CM 42728 is characteristic of most adults, and the principal adult, CM 59495, has small postorbital processes relative to others in its age cohort.

We sampled the incidence of one feature of the frontal in the study sample:

(1) Composition of the ethmoidal foramen: (a) between the frontal and orbitosphenoid - AMNH 207730 (Fig. 4D), 51471, 51486, 51488, 51448, CM 5157, 2356, 59497, AMNH 51503, CM 59495 (Fig. 11), 42727(L), 42725, 42726, 42282, 69365, 69366; (b) within the frontal - CM 6371, 6374, AMNH 201513, 134969, CM 59496, 42727(R), 3693. All specimens have only one ethmoidal foramen except for two on the right side of CM 59496. This distribution shows no obvious correlation with geography, ontogeny, and sex.

We also noted variation in the occurrence, number, and position of the frontal diploic vein foramen. The usual pattern is to have one comparable in size and position to that in the principal adult, CM 59495 (Fig. 10). However, four specimens (AMNH 51448, CM 59497(L), 42727(R), 3693(R)) have two foramina on at least one side, and five specimens (CM 6371(R), AMNH 51503(L), CM 16103(L), AMNH 51445, CM 42728) have only minute foramina on at least one side. The position of the foramina across the study sample is also variable, from nearer the orbital rim anterior and medial to the postorbital process to more medially positioned. One specimen has the foramen on the orbital rim, CM 16103(R).

#### Parietal ("pa" in figures)

The paired parietals are the principal elements of the roof and sidewall in the posterior two-thirds of the braincase. In addition, they have an unusual exposure on the floor of the basicranium in the form of an epitympanic wing.

**CM 59495, Principal Adult.**—In dorsal view (Figs. 2A–B), the parietals are quadrangular and are 22.2% of the midline skull length. The parietal contacts the frontal anteriorly, the squamosal posterolaterally ("sq" in Fig. 2B), and posteriorly the mastoid exposure of the petrosal ("pe" in Fig. 2B), the exoccipital (not visible in dorsal view), and the supraoccipital ("so" in Fig. 2B). The last two bones are fused to each other, but their positions are based on juvenile specimens that still retain the suture (e.g., AMNH 51486). The back of the braincase is marked by a well-developed nuchal crest ("nc" in Fig. 2B), which curves anteroventromedially from the midline and ends as the post-tympanic process of the squamosal ("ptp" in Fig. 2B). The nuchal crest is formed by various bones along its length: at its dorsal origin it is formed by the supraoccipital alone,

next jointly by the parietal on the anterior surface and the exoccipital on the posterior, then via the parietal anteriorly and the mastoid exposure of the petrosal posteriorly, and finally the squamosal comprises the front of the crest and the mastoid exposure of the petrosal completes the structure. The parietal's suture with the supraoccipital is complex along the midline and simplifies laterally; on the right side the two are fused at the lateral extreme of the contact. Lateral to the main exposure of the supraoccipital in the nuchal crest is a second very small intrusion of this bone bilaterally that is surrounded by the parietal. The temporal lines that originate on the frontal continue onto the parietal and converge posteriorly at the supraoccipital suture; only a very small part of the minute sagittal crest is present on the parietal ("sc" in Fig. 2B). Anterior to the supraoccipital suture are small parietal foramina, three on the left and one on the right. Lateral to these structures is a small foramen for the ramus temporalis that has a sulcus extending posterodorsally ("frt" in Fig. 2B).

In lateral view (Figs. 4A–B), the parietal contacts the frontal anteriorly, the alisphenoid anteroventrally, and ventrally it predominantly contacts the squamosal with an additional contact with the mastoid exposure of the petrosal in the nuchal crest.

**AMNH 207730, Newborn.**—In dorsal view (Figs. 2C–D), the parietals are 36.2% of the midline skull length. There is no nuchal crest or identifiable parietal foramina. The posterior suture with the supraoccipital has a broader V-shaped incursion of the latter bone. A low parietal eminence is present, more so than in the adult.

In lateral view (Figs. 4C–D), the parietal does not reach to the petrosal as it is not fully ossified and only contacts the squamosal anterior to its posttympanic process. The roughly horizontal suture with the alisphenoid and the anterior part of the squamosal is partially incomplete, more so on the left side. A low, curved line is visible on the parietal, roughly in the same vertical plane as the tiny post-orbital process. This line is best expressed in the posterior half of the parietal where it curves down towards the occipital condyles. A tiny foramen on the posterior part of this curved line is in the position of the foramen for the ramus temporalis in the adult. Although this line is low on the braincase wall, based on the juvenile specimens (e.g., AMNH 51486), we identify it as the temporal line.

In ventral view (Fig. 13), the parietal has an unusual exposure on the basicranium, which, if present in the principal adult, CM 59495, is hidden in ventral view by the ectotympanic and rostral process of the malleus. In the newborn, this flat, three-sided exposure lies in the anterolateral roof of the middle ear ("ewpa" in Fig. 12); it contacts the epitympanic wing of the alisphenoid medially ("ewas" in Fig. 12), the squamosal laterally, and the tegmen tympani of the petrosal posteriorly ("tt" in Fig. 12). Its posterolateral corner appears to have no osseous contact, but this is obscured by the malleus. We refer to this structure as the epitympanic wing of the parietal as it is exposed in

the middle-ear roof. Contacting the ventral surface of the parietal epitympanic wing and adjacent squamosal is a well-developed malleolar hook of the rostral process of the malleus (“mh” in Fig. 12; Wible and Spaulding 2012). The posterolateral corner of the parietal epitympanic wing roofs the malleolar-incudal articulation, i.e., the epitympanic recess.

**Others.**—The series in Figure 1 reveals that the relative anteroposterior length and mediolateral width of the parietals becomes proportionally smaller with age. Additionally, the major ontogenetic changes in the formation of the sagittal crest on the parietal are shown. The newborn, AMNH 207730, has faint temporal lines that are very low on the braincase ventral to the parietal eminence and that curve ventrally at the posterior end (see also Figs. 4C–D). The younger juvenile, AMNH 51486, has faint temporal lines that cross the parietal eminence and intersect with the developing nuchal crest posteriorly. A similar pattern occurs in the older juvenile, CM 6374, although the temporal line passes medial to the parietal eminence. In the principal adult, CM 59495, the more distinct temporal lines are more medially placed and converge across the length of the parietal, ultimately joining together anterior to the nuchal crest to create a short, low sagittal crest (see also Figs. 4A–B). The older adult, CM 42728, has a prominent sagittal crest running the length of the parietal. Our observations on the sagittal crest of the frontals recorded above hold for the parietals as well; that is, there is a window in young adulthood where the parietal sagittal crest likely distinguishes males and females, but it does not over the whole ontogenetic series.

We noted that all specimens, except two juveniles (AMNH 51488 and 201513), have foramina in the same general vicinity as those identified as for the ramus temporalis in the principal adult, CM 59495 (Figs. 2A–B, 4A–B). These foramina are not substantial and are asymmetric in number and position. Interestingly, the two juvenile *N. b. gerardi*, CM 6371 and 6374, are the only specimens with a foramen in the parietosquamous suture, but then on only one side in each.

The epitympanic wing of the parietal was first noted in specimens where the ectotympanic and rostral process of the malleus had been removed (Figs. 14–17). A detailed survey of all specimens reveals that in six with the ectotympanic and rostral process removed, a parietal epitympanic wing is clearly present (i.e., AMNH 51488, 201513, CM 2356, AMNH 51503, CM 3693, 69366). The epitympanic wing is also clearly visible in ten other specimens with the ectotympanic and rostral process still in place. Of the remaining specimens, the condition is hidden by the ectotympanic and/or soft tissues in eight, and the relevant sutures are fused in six. Given its incidence in all specimens that can be assessed for this feature (including juveniles and adults from Ivory Coast, Cameroon, Zaire, and Malawi), this condition is not considered anomalous or a variant, but the standard morphology for *N. binotata*.

Three specimens with damaged braincases show that the epitympanic wing of the parietal is continuous with the parietal in the skull roof via the tentorial process of the parietal (AMNH 51448, 201513, and 134969). The second of these specimens is illustrated in Figure 14. This specimen’s right petrosal is isolated from the skull, allowing a glimpse into the endocranium. On the right side, the well-developed tentorial process of the parietal (“tpa” in Fig. 14) occupies the endocranial space dorsal to the absent petrosal, and the ventral part of the tentorial process bears a facet for the petrosal (“pef” in Fig. 14). Ventrolateral to the petrosal facet is an irregular quadrangular shape that is exposed on the basicranium on the right side; this is the epitympanic wing.

The condition of the epitympanic wing in CM 3693 (Fig. 15) is described, with differences to others noted below. The epitympanic wing is roughly quadrangular, with a central, oval depression (longer than wide) demarcated by a high medial crest and a low lateral one (“mhf” in Fig. 15). The steep medial slope of the medial crest abuts the epitympanic wing of the petrosal (“ewpe” in Fig. 16B); the lateral crest overlies what constitutes a narrow epitympanic wing of the squamosal. Anteriorly, the parietal has an interdigitating suture with the epitympanic wing of the alisphenoid, and posteriorly, it abuts the tegmen tympani of the petrosal. A smooth depression on the parietal slopes posteroventrally onto the rough anterior face of the tegmen tympani. The smooth surface on the parietal and the rough one on the tegmen tympani contact a well-developed malleolar hook of the rostral process of the malleus. This broken process was found in place attached by soft tissue on CM 69366(L). Running on the lateral side of the medial crest on the parietal is a groove interpreted to be for the lesser petrosal nerve (based on *F. catus*, Davis and Story 1943; *C. lupus familiaris*, Evans 1993; “lpn” in Figs. 15, 18). The morphology of the passage for the nerve that enters this groove posteriorly differs on the two sides; it is a notch between the parietal and tegmen tympani on the left, but a short canal in the parietal on the right. In the anterolateral surface of the parietal are two small areas where the overlying squamosal bone is exposed. In contrast to the condition in the newborn, the epitympanic wing of the parietal does not contribute to the epitympanic recess (“er” in Fig. 15), which is formed by both the petrosal and the squamosal.

As in the newborn, the other ontogenetically young specimens (AMNH 201513 and 51448) have a parietal exposure that is relatively flat and featureless (Fig. 14), with the area exposed in the former specimen double that of the latter. The two also differ regarding the course of the lesser petrosal nerve. In AMNH 201513 (Fig. 14), an open groove runs the anteroposterior length of the parietal on the right side, but the posterior half is enclosed in a canal on the left side. In AMNH 51448, the nerve course is indicated with an open groove on the alisphenoid and not the parietal. Unlike the newborn and like the adult condition, the parietal in both does not contribute to the epitympanic recess. As in CM 3693, the remaining adult specimens,

CM 2356 and 69366 (Fig. 16B) and AMNH 51503 (Fig. 17), have medial and lateral crests, but there are differences in the structure of both crests as the overall exposure of the parietal is smaller. The lateral crest is formed entirely by the squamosal, and the medial is half parietal and half alisphenoid. Additionally, none of these specimens has an exposure of the overlying squamosal as present in CM 3693.

#### Interparietal

In light of the distribution of an interparietal in Carnivora (Koyabu et al. 2012), *N. binotata* likely has this midline skull roof element present between the parietals anteriorly and the supraoccipital posteriorly. If indeed present, this element is already seamlessly fused to the supraoccipital in the newborn, AMNH 207730. Consequently, a separate interparietal is not described.

#### Pterygoid (“pt” in figures)

The paired pterygoids are only fully delimited from their neighbors in the newborn, AMNH 207730, and are fully fused in the oldest adults (e.g., AMNH 51513). These elements contribute to the walls and roof of the posterior basipharyngeal canal and form the posterior entopterygoid processes.

**CM 59495, Principal Adult.**—In oblique ventral view (Fig. 11), in the mesocranium, the pterygoid has a vertical component that forms the posterior entopterygoid process (“enp” in Fig. 11) and a horizontal component contributing to the roof of the basipharyngeal canal. The pterygoid contacts the perpendicular process of the palatine anteriorly, and the latter contacts the pre- and basisphenoid (“bs” in Fig. 11) medially. In the contact between the pterygoid, presphenoid, and palatine is an opening of unknown function into the orbit (described above; “?” in Fig. 11). The posterior extent of the pterygoid (the caudal process of the pterygoid) is uncertain, as the posterior part of its suture with the basisphenoid is fused, more so on the right side (Figs. 6A–B). In the newborn, the caudal process (“cppt” in Fig. 13) extends even with the posterior margin of the foramen ovale (“fo” in Fig. 13). In CM 59495, the position of the posterior basisphenoid contact is marked by the course of the nerve of the pterygoid canal (“npc” in Fig. 19). On the right side, a narrow groove for the nerve runs to a foramen between the pterygoid and basisphenoid at the level of the pterygoid hamulus. Anterior to this foramen is an open seam between the pterygoid and anterior basisphenoid. The left side differs in that the portion of what is an open groove on the right side is enclosed in a short canal, medial and slightly posterior to the foramen ovale; the floor for this may be entirely basisphenoid based on the position of the pterygoid in the newborn.

The pterygoid forms the posterior third of the ento-

pterygoid process behind the perpendicular process of the palatine and ends as the hamulus (“ham” in Fig. 12), which extends nearly to the level of the caudal opening of the alisphenoid canal (“asc” in Fig. 12). The entopterygoid processes are essentially parallel, with the tips of the hamuli very slightly everted (Figs. 6A–B). Within the lateral wall of the basipharyngeal canal, the anterior contact between the pterygoid and palatine is V-shaped, with the base of the V directed posteriorly (Fig. 10). The suture with the palatine can be followed laterally across the ventral surface of the entopterygoid process into the infratemporal fossa. In the newborn, the suture between the pterygoid and alisphenoid runs posteriorly, perpendicular to the pterygopalatine suture (Fig. 13), but it is fused in CM 59495.

In lateral view (Fig. 12), the vertical part of the pterygoid is fully fused to the alisphenoid dorsally, but features aid in delimiting the two. A shallow muscular fossa, longer than tall, is found on the back of the palatine and on the pterygoid; based on *F. catus*, this is the origin of the medial (internal) pterygoid muscle (Jayne 1898). A low, oblique ridge extends from the palatine posterodorsally toward the caudal opening of the alisphenoid canal and marks the dorsal limit of this muscle fossa. In juvenile *N. binotata* (e.g., AMNH 51486), this ridge is on the alisphenoid, and that bone’s suture with the pterygoid is immediately ventral to the ridge. Additionally, in CM 59495, a small foramen (two on the right side) is anteroventral to the caudal opening of the alisphenoid canal (“?” in Fig. 12); in the newborn what appears to be the same opening is between the pterygoid and alisphenoid on the left and within the pterygoid on the right.

On the ventral margin, the pterygoid minutely underlies the palatine (Fig. 12). Posterior to the termination of the palatine, the ventral margin of the pterygoid is not straight, but has a slight convexity followed by a slight concavity. In the former, the ventral margin is thicker, demarcating the ventral limit of the fossa for the medial pterygoid muscle. The finger-like pterygoid hamulus is directed posteriorly and slightly ventrally. The posterior margin of the pterygoid is U-shaped.

The pterygoid also has an exposure in the rear of the orbit (Figs. 4A–B, 12) between the pre- and alisphenoid, representing the lateral surface of the horizontal component in the roof of the basipharyngeal canal. It is longer than tall, extending from the level of the rear of the optic foramen into the sphenorbital fissure, where it forms the ventromedial floor. Its dorsal, convex margin contacts the presphenoid; its straight ventral margin contacts the alisphenoid; and its narrow posterior and anterior margins contact the alisphenoid and palatine, respectively.

**AMNH 207730, Newborn.**—In ventral view (Figs. 6C–D), the pterygoid extends into the choanae, whereas in the adult it lies well posterior to that opening. The suture with the palatine is oblique and not U-shaped. More of the presphenoid is exposed in the roof of the basipharyngeal canal, as the pterygoid is not as extensively ossified medially

as in the adult. The course of the nerve of the pterygoid canal cannot be determined, as it is not indicated by grooves, canals, or foramina. The caudal process of the pterygoid nearly contacts the ectotympanic (“e” in Fig. 13), whereas the inferred position of the caudal process in the adult is well anterior. The entopterygoid processes are not sub-parallel and instead converge medially. The pterygoid hamuli are stouter than in the adult (Figs. 6C–D).

In lateral view (Figs. 4C–D), a muscular fossa with demarcating ridges is absent. The pterygoid does not underlie the palatine on the straight ventral margin, and the hamulus is at a sharper angle, extending more ventrally. The orbital exposure is relatively larger in the newborn and forms the entire ventral floor of the sphenorbital fissure (not visible in the figures).

**Others.**—The orbital exposure of the pterygoid is present in nearly all specimens. Three of the oldest adults do not show a separate pterygoid in the orbit (AMNH 51510, 51494, 51513), but we cannot rule out that this is the result of sutural fusion between the pterygoid and alisphenoid. There are only two specimens that we are certain lack the orbital exposure, the juvenile *N. b. gerardi*, CM 6371 and 6374, where the pterygoid is fully covered by the alisphenoid. Regarding the specimens with an orbital exposure, we recorded the following feature of the study sample:

(1) Orbital exposure of the pterygoid-palatine contact: (a) present - AMNH 207730, 51486, 51488, 201513, 51448, CM 42281, 59497, AMNH 51503(L), CM 59495 (Figs. 4A–B, 12), AMNH 134969, CM 59496, 42727, 42726, 42282, 69365, 69366, 16103, AMNH 51445; (b) absent - CM 5157, 2356, AMNH 51503(R), CM 3693, 42725, AMNH 51595. In the specimens without contact, the orbital exposure of the pterygoid is present, but the alisphenoid overlies it at the palatine suture.

We also noted that the muscle fossa on the lateral side of the pterygoid (Figs. 4C–D), which we reported as absent in the newborn, AMNH 207730, is present in the rest of the study sample. Also, the canal enclosing the nerve of the pterygoid canal near the foramen ovale on the left side of the principal adult, CM 59495, is uncommon, only occurring in CM 42727 and AMNH 201513(R) (Fig. 14). As an indicator of the fragility of the hamulus, we found exactly half the sample had this structure damaged bilaterally.

#### Ethmoid (“eth” in figures)

The unpaired ethmoid is the principal element of the nasal cavity. It is not exposed on the exterior of the skull except in two specimens. Its morphology within the nasal cavity will not be described here.

**AMNH 134969 and CM 63966.**—In the adult New York Zoological Society specimen, AMNH 134969, the ethmoid has a small triangular exposure in the orbit (Fig. 12A). In the right orbit, the ethmoid lies at the junction of the lacrimal, frontal, and maxilla; anteriorly and posteriorly it con-

tacts the frontal, and ventrally it contacts the lacrimal and has a point contact with the maxilla. In the left orbit (Fig. 12A), the ethmoid is a bit more anteriorly positioned and contacts only the frontal and lacrimal.

On the right side of another adult, CM 63966, there is a narrow sliver of ethmoid exposed in the posterior suture between the lacrimal and frontal. The left side is too damaged to see whether this condition is bilateral.

#### Vomer

The unpaired vomer lies in the floor of the nasal cavity and the roof of the nasopharyngeal meatus, and has no exposure on the exterior of the skull. Only limited observations on CM 59495 are included below.

**CM 59495, Principal Adult.**—The lateral laminae of the vomer, which define the V-shaped sulcus septi nasi, lie immediately posterior to the V-shaped septal process of the premaxilla. The premaxilla obscures the vomer in direct anterior view (Figs. 3A–B). The narrow, elongate, pointed wings or alae of the vomer can be seen with effort through the choanae (but are not visible in any figures). They are separated on the midline by a narrow, open sphenoidal incisure and nearly extend to the presphenoid. Lateral to the wings and separated by sutures are the external laminae of the ethmoid. Together, the vomerine wings and external laminae form the transverse lamina, the roof of the nasopharyngeal meatus.

#### Sphenoid Complex

The bones of the sphenoid complex contribute to the roof of the mesocranium and the walls of the orbitotemporal region, and are underlain by the paired pterygoid bones described above. The sphenoid complex is divided into anterior and posterior parts, each of which includes an unpaired element in the mesocranial roof and a pair of wings in the orbitotemporal walls: unpaired presphenoid and paired orbitosphenoids for the anterior part, and unpaired basisphenoid and paired alisphenoids for the posterior part. The number of ossification centers forming the sphenoid complex varies among mammals (De Beer 1937; Moore 1981), and it is uncertain how many occur in *N. binotata*. Based on the newborn, AMNH 207730, there are a minimum of four. The anterior part (presphenoid and orbitosphenoids) appears to be a single ossification; the underlying palatine and pterygoid hide their continuity in ventral view (Figs. 6C–D). The posterior part is composed of three ossifications, with a complete suture separating the basisphenoid from the paired alisphenoids (Fig. 13). However, the juvenile, AMNH 201513, shows a remnant of a suture on the endocranial surface of the presphenoid (see Endocranium), which is not accessible in the newborn. This necessitates a minimum of five centers. The newborn beagle figured by Evans (1993: fig. 2–47) shows

the same arrangement as the newborn *N. binotata*; however, in fetal stages of the beagle, the anterior part has as many as six centers: two for the presphenoid and two for each orbitosphenoid.

#### Presphenoid ("ps" in figures)

The presphenoid and paired orbitosphenoids are not separated by sutures in any specimens. As is standard, the presphenoid is identified as the midline element of the anterior part of the sphenoid complex in the mesocranial roof.

**CM 59495, Principal Adult.**—In ventral view (Figs. 6A–B), the presphenoid is a narrow midline rod that forms a low ridge in the basipharyngeal canal. The rod is uniform except at its anterior and posterior ends where it is slightly mediolaterally thicker. It extends from just within the choanae to nearly the rear of the entopterygoid processes. The presphenoid is separated from the body of the vomerine wings anteriorly and the basisphenoid posteriorly by narrow gaps, and is covered laterally by the perpendicular process of the palatine anteriorly and by the horizontal part of the pterygoid posteriorly. Roughly at the midpoint of the midline rod, a small triangular exposure of the presphenoid is visible in a gap at the dorsomedial juncture of the palatine and pterygoid; it is here that small paired openings to the orbit are present (described above; Fig. 10). Anterior to this are additional paired foramina in the presphenoid of unknown function that open in the orbit (Fig. 10).

In lateral view (Fig. 11), the body of the presphenoid is visible in the ventromedial floor of the sphenorbital fissure. It is vertically oriented with a pronounced concavity in its posterior half. It is separated from the basisphenoid behind by a narrow gap (not visible in the figures), and ventrally it contacts the orbital exposure of the pterygoid and, anterior to this, the perpendicular process of the palatine. Dorsally, the body flares dorsolaterally as the orbitosphenoid. As interpreted here, the presphenoid forms the floor of the optic foramen, but this is best described together with the orbitosphenoid. On the right side (not visible in the figures) is a large opening medially directed into the middle of the presphenoid and with a groove directed posteriorly from it; there are also three minute openings at the posterior end of the presphenoid and two anteriorly. The left side lacks the large opening, but has half a dozen minute ones asymmetrically arranged (Fig. 11).

**AMNH 207730, Newborn.**—In ventral view (Figs. 6C–D), the presphenoid comprises more of the width of the roof of the basipharyngeal canal than in the adult; however, it is relatively much shorter anteroposteriorly as it barely extends beyond the choanae. The presphenoid is rounder and not ridge-like. The gaps separating it from the vomer anteriorly and the basisphenoid posteriorly are larger. At its posterior border, the presphenoid is V-shaped, with the arms of the V directed posteriorly.

Little presphenoid is exposed in lateral view as it lies

deep within the sphenorbital fissure. In contrast to the adult, the presphenoid does not contact the palatine.

**Others.**—The exposure of the presphenoid in the basi-pharyngeal canal shows some differences across the study sample. In general, most specimens resemble the principal adult, CM 59495 (Figs. 6A–B). Only the narrow midline rod of the presphenoid is exposed between the pterygoids, but more is exposed between the palatines, with the greatest width of exposure just anterior to pterygopalatine suture and then tapering anteriorly. There are two specimens that have only the narrow midline rod of the presphenoid exposed the entire length of the bone, CM 6371 and AMNH 59496.

#### Orbitosphenoid ("os" in figures)

As noted above, a real boundary between the paired orbitosphenoids and the presphenoid cannot be identified, as they are not separated by sutures, even in the newborn. As is standard, the orbitosphenoid is identified as the dorsolaterally directed wing of the anterior part of the sphenoid complex in the rear of the orbit.

**CM 59495, Principal Adult.**—In lateral view (Fig. 11), the orbitosphenoid is roughly quadrangular; it is long, extending above the posterior edge of the sphenopalatine foramen (Fig. 8A) into the sphenorbital fissure (Fig. 11). Its dorsal border is predominantly with the frontal; posteriorly, it has a narrow contact with the alisphenoid at the sphenorbital fissure. Anterior to the optic foramen ("of" in Fig. 11), the ventral border of the orbitosphenoid contacts the palatine; posterior to the optic foramen, it contacts the presphenoid. Its anterior and posterior borders are in contact with the palatine and basisphenoid, respectively. Posterior to the anteroposterior center of the orbitosphenoid is the optic foramen. This foramen is oval in anterior view, slightly wider than tall, and predominantly directed anteriorly. The lateral margin of the optic foramen is V-shaped in lateral view; the ventral leg of the V is thickened and projects forward with a slight bulge along its margin ("ahc" in Fig. 11). The dorsomedial edge of the ventral leg is set off by a distinct seam from the adjacent part of the orbitosphenoid. This bulge represents the ossified ala hypochiasmatica. Anterior to the optic foramen is a small depression, which includes two small foramina ("spo" and "sbo" in Fig. 11). These resemble foramina described by Gregory (1910) in *Solenodon paradoxus*; the dorsal one is in the area of a supra-optic foramen and the ventral one the suboptic foramen. Both foramina occur bilaterally, but the dorsal one on the right side is more anteriorly placed than on the left. At this depression, the orbitosphenoid is at its greatest dorsoventral extent as there is a slight dorsal expansion into the orbitotemporal fossa. The ethmoidal foramen, located in the suture of the orbitosphenoid with the frontal, is halfway between the optic foramen and the anterior margin of the orbitosphenoid; there is a small de-

pression on the orbitosphenoid immediately ventral to the foramen. Other small foramina have been described above between the orbitosphenoid and palatine.

**AMNH 207730, Newborn.**—In ventral view (Figs. 6C–D), a small sliver of orbitosphenoid between the frontal and alisphenoid is visible lateral to the entopterygoid process, whereas the orbitosphenoid is entirely obscured by this process in the adult. The orbitosphenoid in lateral view (not visible in the figures) is shaped like a half moon, with a very slightly curved dorsal border, whereas the bone is more quadrangular in the adult. The optic foramen is more anteroventrolaterally directed. The ossified ala hypochiasmatica is more prominent, but relatively much shorter.

**Others.**—We recorded the incidence of four features of the orbitosphenoid across the study sample:

(1) Depression anterior to the optic foramen: (a) absent - AMNH 207730, 5147, 51486, 201513, CM 42281, 2356, AMNH 51503, CM 59496, 3693, 42725, 42726, 42282, AMNH 51510, CM 16103, AMNH 51594, CM 42728, 5097, AMNH 51513; (b) present - CM 6371, 6374, AMNH 51448, CM 5157, 59497, 59495 (Fig. 11), AMNH 134969, CM 42272, 69365, 69366. This distribution shows no obvious correlation with geography, ontogeny, and sex.

(2) Supra-optic foramen: (a) absent - AMNH 207730, 51471, 51486, CM 6371, 6374, AMNH 51448, CM 42281, 5157(L), AMNH 51503, CM 69366(L), AMNH 51510(L), CM 16103(L), 42728(L); (b) present - AMNH 51488, 201513, CM 5157(R), 59497, 59495 (Fig. 11), AMNH 134969, CM 59496, 3693, 42725, 69365, 69366(R), AMNH 51510(R), CM 16103(R), AMNH 51494, CM 42728(R), 5097. This distribution shows no obvious correlation with geography, ontogeny, and sex.

(3) Suboptic foramen: (a) absent - AMNH 207730, 51471, 51486, CM 6371, AMNH 51488, CM 6374, AMNH 201513, 51448, CM 42281, 5157(L), 2356, 59497(L), AMNH 51503, 134969, CM 42727, 3693, 42725, 42726, 42282, 16103, AMNH 51494, CM 42728, 5097, AMNH 51513; (b) present - CM 59497(L), 59495 (Fig. 11), 59496, 69365, 69366, AMNH 51510. This foramen is not present in any juveniles and has a spotty distribution in adults.

(4) Anterior extent of the orbitosphenoid: (a) posterior to the sphenopalatine foramen - AMNH 207730 (Fig. 8B), 51471, 51486, CM 6371, 6374, AMNH 201513, 51448, CM 5157, 2356, 59497, AMNH 51503, 134969, CM 59496, 42727, 42725, 42726, 42282, 69365, 69366, AMNH 51510, 41494, CM 42728, 5097; (b) even with the sphenopalatine foramen - AMNH 51488, CM 42281, 59495 (Fig. 8A), 3693, 16103. Of the five specimens with the orbitosphenoid even with the sphenopalatine foramen, in CM 16103 the orbitosphenoid actually contributes to the posterodorsal margin of the foramen between the palatine and frontal.

We also noted that a low orbital crest, which delimits the orbital and pterygopalatine fossae, is present in the older adult specimens. It extends anteriorly from the ventral

margin of the optic foramen to dorsal to the sphenopalatine foramen; most of its course is on the orbitosphenoid, but it is also on the palatine and variably on the frontal. The principal adult, CM 59495, is the youngest adult with an indication and it is so faint that it does not show in the photograph in Figure 11.

#### Basisphenoid (“bs” in figures)

The basisphenoid is separated from the paired alisphenoids by sutures only in the newborn, AMNH 207730, and the descriptions in the adult are based on that.

**CM 59495, Principal Adult.**—In ventral view (Figs. 6A–B), the basisphenoid is funnel-shaped, with the narrow end directed anteriorly towards the presphenoid. It is separated from this bone anteriorly by a narrow gap, which presumably was completed by cartilage in life. Posteriorly, the basisphenoid contacts the basioccipital via an irregular, transverse suture (“bo” in Figs. 6B, 19). This suture is depressed centrally and gently rises laterally; this topography extends anteriorly onto the basisphenoid a short distance and posteriorly onto the basioccipital (“mt” in Fig. 19). The raised area on the basioccipital corresponds to the muscular tubercle of *C. lupus familiaris*, which is the site of attachment of the longus capitis muscle (Evans 1993). The raised area on the basisphenoid is interpreted as a weak tympanic process (“tpbs” in Fig. 19), as the back of the surface contacts the anterior face of the rostral entotympanic (blue bone in Fig. 19). The tympanic process curves anterolaterally in front of the ear region and its ventral surface is rugose with several obliquely oriented slits. Any basisphenoid contact with the petrosal is hidden by the rostral entotympanic. Anterolateral to the rostral entotympanic on the basisphenoid is the back of the groove for the nerve of the pterygoid canal (“npc” in Fig. 19), which curves anteromedially to a foramen in the basipharyngeal canal at the level of the pterygoid hamulus (described above). In light of the newborn, we interpret the alisphenoid to be immediately lateral to the groove for the nerve of the pterygoid canal. Anterior to its fusion with the alisphenoid, the basisphenoid is underlain by the pterygoid.

**AMNH 207730, Newborn.**—In ventral view (Figs. 6C–D, 13), the basisphenoid is not funnel-shaped, but hexagonal. Most of the ventral surface is composed of a broad, convex, longitudinal ridge that flattens as the bone reaches its lateral neighbors. Its suture with the basioccipital is likewise convex ventrally due to this ridge. Anterolateral to the basioccipital suture is a narrow contact with the promontorium of the petrosal, and anterolateral to that is a gap between these two bones that is partially closed by connective tissue. In the middle of this gap is a round opening in the connective tissue that is approximately two-thirds surrounded by bone, namely the basisphenoid anteriorly and the petrosal posteriorly; this is the carotid foramen (“cf” in Fig. 13). As is described below, the carotid foramen in

the adult is enclosed in the basisphenoid, but a small remnant of the gap between the basisphenoid and petrosal in the newborn is present posterior to the adult carotid foramen. The condition in the newborn is the same as the adult condition in *F. catus* and *C. lupus familiaris*, where this gap including the carotid foramen is called the middle lacerated foramen (Jayne 1898) or foramen lacerum (Evans 1993).

A basisphenoid tympanic process is not developed. The suture with the alisphenoid is visible lateral to the carotid foramen and is covered more anteriorly by the caudal process of the pterygoid. No particular evidence for the passage of the nerve of the pterygoid canal is present. In light of the endocranial position of the hiatus Fallopii in the adult (see Petrosal), the greater petrosal nerve must have exited the cranial cavity in the gap between the basisphenoid and petrosal lateral to the carotid foramen (hidden by the ectotympanic in Fig. 13).

**Others.**—The triangular-shaped posterolateral corner of the basisphenoid is nearly completely covered by the intact rostral entotympanic (compare Figs. 16A and 16B; see the blue shaded area in Fig. 20). The following specimens with the rostral entotympanic removed reveal details of the posterolateral corner: AMNH 51503(R), CM 3693(R) (Figs. 15, 16A, 20), CM 16103, AMNH 51494(R), CM 5097(R), AMNH 201513 (Fig. 14), 51448(R), 51445; the last three are damaged and of less utility. The posterolateral surface has medial and lateral vertical walls that converge anteriorly, and an irregular central area that ends posteriorly as a narrow horizontal shelf. The higher, parasagittal medial wall is the lateral face of the basisphenoid tympanic process (Fig. 20); the oblique lateral wall is the raised ridge associated with the course of the nerve of the pterygoid canal (see below). At the juncture of the medial and lateral walls, halfway between the ventral surface of the basisphenoid tympanic process and the horizontal shelf is the anteromedially directed carotid foramen (“cf” in Figs. 16A, 20), which is hidden in direct ventral view (as in Fig. 15). A groove begins at the anterior aspect of the carotid foramen and curves posterolaterally (“cg” in Figs. 16A, 20); this groove continues posteriorly onto the rostral entotympanic in those specimens retaining that element (see below). Posterior to the carotid foramen is a seam in the basisphenoid that extends posterolaterally onto the horizontal shelf (Fig. 16A), suggesting that the carotid foramen was enclosed by two spurs of the basisphenoid. The surface immediately posterodorsal to the carotid foramen is concave, and it and the horizontal shelf are also covered by the rostral entotympanic, based on AMNH 134969, CM 69366 (Fig. 16A), and CM 42728 (right side). The anterior face of the in situ rostral entotympanic forms the posterior border of the carotid foramen, underlying the basisphenoid (Figs. 16B, 20).

In all specimens exposing this triangular posterodorsal surface of the basisphenoid, there is a small gap between the horizontal shelf and the anterior pole of the promon-

torium (“\*” in Figs. 15, 16A, 17, 20); the extent of this ranges from absolutely no contact between the two bones (i.e., AMNH 201513, CM 16103, AMNH 51503) to limited contact between the lateral aspect of the basisphenoid and the promontorium (i.e., CM 3693, 5097), and finally to a medial and lateral contact between these bones (i.e., AMNH 51494). This variable gap is floored by the rostral entotympanic (“re” in Fig. 16B).

MacPhee (1981:59) used the term piriform fenestra to include a “large gap, seen in all fetal and a few adult mammals, that lies between the auditory capsule and its dorsal outgrowths (tegmen tympani, epitympanic wing of petrosal) on the one hand and the epitympanic wings of the sphenoid and squamosal on the other.” In MacPhee’s accompanying illustration (his fig. 1), the piriform fenestra is shown as the gap lateral to the alicochlear commissure, which is the cartilage forming the lateral border of the carotid foramen. The gap described above between the basisphenoid and petrosal in adult *N. binotata* (“\*” in Figs. 15, 16A, 17) differs from the piriform fenestra in that it would lie posteromedial to the ossified alicochlear commissure. This gap is the posterior remnant of the larger gap described above in the newborn, AMNH 207730 that includes the carotid foramen (Fig. 13), and as noted above, this larger gap is also the adult condition in *F. catus* and *C. lupus familiaris* where it is termed the middle lacerated foramen (Jayne 1898) or foramen lacerum (Evans 1993). A more laterally positioned, narrow gap we identify as the piriform fenestra is present in the newborn, AMNH 207730 (“\*” in Fig. 13).

The lateral margin of the triangular basisphenoid surface provides additional details of the course of the nerve of the pterygoid canal, which can be studied even in specimens retaining the ectotympanic. Two major patterns occur with additional variants of both resulting from differing degrees of development of the basisphenoid, petrosal, and rostral entotympanic. The first pattern (AMNH 207730, 51486, CM 6371, AMNH 51488, CM 6374, AMNH 201513, 51448, CM 42281, 5157, 59497, AMNH 134969, CM 59496(L), 42727, 42725, 69365, AMNH 51510, CM 16103, 42728) has a foramen situated near the back of the ridge associated with the course of the nerve of the pterygoid canal (“gpn” in Fig. 14). This foramen leads forward into the anteromedially-directed groove for the nerve of the pterygoid canal (“npc” in Fig. 14). This foramen is the exit from the cranial cavity for the greater petrosal nerve, which joins the deep petrosal (internal carotid) nerve below the foramen, and together they run forward in the groove as the nerve of the pterygoid canal. The composition of this foramen varies: within the basisphenoid (three specimens), between the basisphenoid and petrosal (seven; Fig. 14), between the basisphenoid and rostral entotympanic (two), and between the basisphenoid, petrosal, and rostral entotympanic (five); one specimen, CM 42282, has the second arrangement on one side and the fourth on the other.

The remaining specimens (AMNH 51471, CM 2356,

AMNH 51503, CM 59495, 59496(R), 3693, 42726, 42282, 69366, AMNH 51494, CM 5097, AMNH 51513) exhibit a second pattern where the foramen for the greater petrosal nerve is not visible in ventral view, as it is obscured by a basisphenoid floor, creating a canal of varying length. Additionally, a separate opening leads into the canal from behind (“dpn” in Figs. 15–16); this opening transmits the deep petrosal nerve from the middle ear into the canal where it joins the greater petrosal nerve. The two nerves then run together in the canal as the nerve of the pterygoid canal (Fig. 18). The composition of the foramen for the deep petrosal nerve varies: within the basisphenoid (two specimens), between the basisphenoid and petrosal (five; Fig. 18), between the basisphenoid and rostral entotympanic (one; Fig. 16A), and between the basisphenoid, petrosal, and rostral entotympanic (one); two specimens have different compositions on the right and left sides.

The first pattern, a foramen for the greater petrosal nerve, is taken as the ontogenetically prior condition as it occurs in the newborn, AMNH 207730. Unexpectedly, the youngest juvenile, AMNH 51471, has the second pattern, a foramen for the deep petrosal nerve, whereas the remaining juveniles have the first one.

A craniopharyngeal canal centrally placed in the basisphenoid is found in only one juvenile, AMNH 201513 (Fig. 14), and in seven adults, AMNH 51503, 134969, CM 42725, 42282, 69365, 69366, AMNH 51510.

#### Alisphenoid (“as” in figures)

As noted above, the paired alisphenoids are separated from the basisphenoid in only the newborn, AMNH 207730. Our interpretation of the limits of this bone in the remaining specimens is based upon observations of the newborn.

**CM 59495, Principal Adult.**—In ventral view (Figs. 6A–B, 19), much of the alisphenoid is hidden by the pterygoid, to which it is seamlessly fused, and the ectotympanic. The alisphenoid is dominated by a large, obliquely oriented, oval opening. This is the combined foramen ovale (“fo” in Fig. 19) and the caudal opening of the alisphenoid canal (“asc” in Fig. 19; caudal alar foramen of Evans 1993), the contents of which are more readily visible in lateral view and are considered below. Lateral to this opening is the suture with the squamosal, which is parasagittal, complex posteriorly, and smooth anteriorly (Fig. 19). Anteromedial to this opening is the small foramen (two on the right side in the ridge line anterior to “asc” in Fig. 19) mentioned above that in the newborn lies in or near the suture between the pterygoid and alisphenoid. Posterior to the large combined opening, the alisphenoid and the immediately adjacent squamosal slope posterodorsally into the ear region. The low ridge marking the change in slope represents a weak tympanic process of the alisphenoid (“tpas” in Fig. 19) and an even smaller entoglenoid process of the squamosal (“eng” in Fig. 19). On the slope immediately posterior to the foramen ovale is a weak, broad sulcus that

curves from posterolateral to anteromedial (“ats” in Fig. 16); it transmits the auditory tube from the middle ear to the nasopharynx. The slope behind the alisphenoid tympanic process is the epitympanic wing of the alisphenoid; it is described below in specimens with the ectotympanic and rostral process of the malleus removed.

In lateral view (Figs. 4A–B, 10), from anterior to posterior in the temporal fossa, the alisphenoid contacts the orbitosphenoid in the roof of the sphenorbital fissure, the frontal, the parietal, and finally the squamosal. In the infratemporal fossa (Fig. 11), it contacts the palatine anteriorly and the pterygoid dorsally; it is also fused to the basisphenoid in the floor of the sphenorbital fissure (not visible in the figures) and to the pterygoid ventrally. Separating the temporal and infratemporal fossae is a faint infratemporal crest that can be traced back to the glenoid fossa on the squamosal. Ventral to the infratemporal crest are two large, anteriorly directed, subcircular foramina. The posterolateral one is slightly the smaller of the two; it is entirely within the alisphenoid and is the foramen rotundum (“fro” in Figs. 10–11; rostral alar foramen of Evans 1993). As the foramen rotundum merges with the alisphenoid canal internally, the foramen rotundum also includes the rostral opening of the alisphenoid canal. The larger anteromedial foramen, between the alisphenoid, orbitosphenoid, presphenoid, and pterygoid, is the sphenorbital fissure. Posterolateral to the foramen rotundum is the combined opening for the foramen ovale and the caudal opening of the alisphenoid canal; the former is recessed in the posterodorsal aspect of the combined opening and the latter is in the anteroventral aspect. Looking into these two respective foramina, additional openings are visible. In the floor of the foramen ovale vestibule are three openings on the right and one on the left (“tcf” in Fig. 11); in the posterior wall of the caudal opening of the alisphenoid canal vestibule are two asymmetrically arranged openings. The significance of these openings is unclear, but they resemble transverse canal foramina reported in other placentals by Wible (2008, 2011) and are treated as such here. Also, visible within the roof of the caudal opening of the alisphenoid canal is a large opening into the middle cranial fossa; this is the internal opening of the foramen rotundum.

**AMNH 207730, Newborn.**—In ventral view (Fig. 13), the foramen ovale and the caudal opening of the alisphenoid canal share a depression. The squamosal is nearly in the lateral wall of the foramen ovale, and the caudal process of the pterygoid is nearly in the medial wall of the combined opening. Within the combined opening are two additional foramina anteriorly, in the posterior wall of the caudal opening of the alisphenoid canal vestibule and one posteriorly in the floor of the foramen ovale vestibule. The tympanic process of the alisphenoid is even weaker than in the adult, and the infratemporal crest and sulcus for the auditory tube are absent. Sloping posterodorsally from the tympanic process is the epitympanic wing. It is separated from the promontorium and tegmen tympani by a narrow

gap, a piriform fenestra (“\*” in Fig. 13), which is continuous medially with the gap between the basisphenoid and promontorium containing the carotid foramen, and laterally is overlain by the epitympanic wing of the parietal.

In lateral view (Figs. 4C–D), most of the lateral wall of the foramen rotundum is anterior to its medial wall. The latter is also the lateral wall of the sphenorbital fissure; in the adult, the lateral wall of the foramen rotundum is posterior to the medial wall. Viewed anteriorly, the sphenorbital fissure is more than twice the size of the foramen rotundum; they are subequal in the adult.

**Others.**—The following specimens in which the ectotympanic is removed reveal details of the epitympanic wing of the alisphenoid: CM 2356, AMNH 51503(R), CM 3693(R) (Figs. 15, 16A, 20), 69366 (Fig. 14B), 16103, 42728(R), 5097(R), AMNH 51448(R), 201513 (Fig. 14), 51494(R); the last three are damaged and of less utility. The first four are the most helpful as they preserve sutures delimiting the alisphenoid from the squamosal, parietal, and petrosal.

The epitympanic wing of the alisphenoid (Fig. 14) slopes posterodorsally from the weak alisphenoid tympanic process into the interval between the basisphenoid medially, the epitympanic wing of the petrosal posteriorly, the epitympanic wing of the parietal posteriorly and medially, and the epitympanic wing of the squamosal medially. The size of the epitympanic wing of the alisphenoid, along with the parietal and squamosal epitympanic wings, varies both within and between specimens. For example, in CM 69366(L), the alisphenoid epitympanic wing forms the entire anterior border of the parietal, but on the right side (Fig. 16B) it forms less than half that border, with the squamosal completing the remainder. The crest demarcating the medial border of the fossa on the parietal epitympanic wing for the malleolar hook of the tympanic plate continues onto the alisphenoid epitympanic wing in CM 2356, as does the groove for the lesser petrosal nerve. However, this does not occur in AMNH 51503, CM 3693 (Fig. 16A), or 69366 (Fig. 16B). Additionally, in CM 42281, 2356, and 3693 (Fig. 16A), the fossa on the epitympanic wing of the parietal continues onto a concave surface on the epitympanic wing of the alisphenoid, roughly doubling the area of that fossa; this houses the anterior crus of the ectotympanic (see Ectotympanic and Malleus). This same surface is flat and shows no specific evidence of ectotympanic contact in AMNH 201513 (Fig. 14), 51448, and 51503. The weak sulcus for the auditory tube is best developed on the alisphenoid epitympanic wing medial to the malleolar head facet (Figs. 14–15, 16A). Its medial border, formed by the groove for the nerve of the pterygoid canal, is more pronounced than its lateral one.

Above we recorded a difference regarding the walls of the foramen rotundum between the principal adult, CM 59495, and the newborn, AMNH 207730, with the adult having the lateral wall posterior to the medial one and the newborn having the reverse (Fig. 4). This appears to be an ontogenetic difference, as all adults have the same condi-

tion as the principal adult and the juveniles show a mixture: the newborn condition is present in AMNH 51471, CM 6371, and 6374, while the adult condition is present in AMNH 51486, 51488, and 210513.

We noted that the formation of the foramen ovale varies in the studied sample. Most specimens resemble the principal adult, CM 59495 (Fig. 19), with the foramen entirely in the alisphenoid and the squamosal well away from it (Fig. 14). In AMNH 51503, the posterolateral margin of the foramen is formed by the squamosal, and in three others (AMNH 51488, CM 6374(L), 42281) the squamosal makes a smaller contribution in the same area.

We also noted that the number and position of transverse canal foramina varies in the studied sample. However, in only one specimen, CM 59496, are transverse canal foramina entirely absent.

#### Squamosal (“sq” in figures)

The paired squamosals contribute to the ventrolateral aspect of the sidewall of the braincase, to the lateral margin of the basicranium, and to the posterior zygoma. The squamosal houses the glenoid fossa, which is the cranial component of the temporomandibular joint.

**CM 59495, Principal Adult.**—In dorsal view (Figs. 2A–B), the most visible part of the squamosal is the zygomatic process (“zpsq” in Fig. 2B). It has a triangular base that juts out laterally and slightly anteriorly from the braincase. The posterior wall of the base, the crista supramastoidea (“csm” in Fig. 2B), is high and the surface anterior to that is gently concave. Within this concave surface are one small and several minute foramina. Extending anteriorly and slightly medially from the base is the narrow contribution to the zygomatic arch. This projection continues forward for more than half the length of the arch, overlying the jugal and tapering to a point. Also visible in dorsal view is the squamosal’s contribution to the ventral end of the nuchal crest (“nc” in Fig. 2B), which forms the posttympanic process (“ptp” in Fig. 2B).

In lateral view (Figs. 4A–B), the squamosal contacts the alisphenoid both anteriorly and anteroventrally, the parietal dorsally, the mastoid exposure of the petrosal posteriorly (“me” in Fig. 4B), and the ectotympanic posteroventrally; the last will be treated with the ventral view. The base of the zygomatic process occupies the anterior half of the squamosal in lateral view. The narrow strip of squamosal on the braincase wall anterior to the zygomatic process is the squama, and the broad area posterior to the zygomatic process is the caudal process. As noted above, the squamosal overlies the jugal in the zygoma; the lateral view shows that the squamosal zygomatic process is curved gently upward.

Three processes are visible along the ventral margin in lateral view. The one in the middle, the postglenoid process (“pgp” in Fig. 4B), projects the farthest ventrally. It is flanked on either side by a concavity. The anterior concavity, the glenoid fossa, is deep and C-shaped; its anterior

margin has a low, but distinct preglenoid process (“prgp” in Fig. 4B). The posterior concavity, the roof of the external acoustic meatus, is shallow, and its posterior margin has a thick, rounded process that juts out laterally and represents the ventral end of the nuchal crest. Based on the specimen’s right side, the squamosal forms the anterior face of this prominence and the mastoid exposure the posterior; on the left side these two bones are fused ventrally. In the carnivoran literature (e.g., Jayne 1898), this prominence is usually referred to as the mastoid process. However, following prior usage in other taxa by the senior author (e.g., Wible 2008, 2011), we call the anterior face the posttympanic process of the squamosal and the posterior face the paroccipital process of the petrosal (“ptp” and “pp” in Fig. 4B, respectively). Dorsal to the external acoustic meatus is the suprameatal crest (“smc” in Fig. 4B), a thickened bar of squamosal connecting the zygomatic process and the posttympanic process. Dorsally, there is a short, weak extension of the crista supramastoideus (supramastoid crest) onto the caudal process. In the broad area dorsal to the suprameatal crest, the caudal process has several minute foramina asymmetrically placed.

In ventral view (Figs. 6A–B, 19), the squamosal is dominated by the glenoid fossa, which is confined to the base of the zygomatic process and does not extend onto the braincase proper. The fossa is ovoid, more than three times wider than long. The articular surface in the fossa extends onto the anterior face of the postglenoid process and the posterior face of the preglenoid process. The preglenoid process is mediolaterally wider than the postglenoid process. The former is highest laterally and gently diminishes in height medially; the latter is highest medially and diminishes more sharply laterally. Medial to the glenoid fossa is an oval depression, longer than wide, of unknown function. The medial wall of this depression slopes ventrally onto the alisphenoid. The posterior end of this sloped medial wall is the weak entoglenoid process (“eng” in Fig. 19), which buttresses the weak tympanic process of the alisphenoid. Between the postglenoid and entoglenoid processes is a U-shaped notch, which accommodates the chorda tympani (“ct” in Fig. 18) based on *F. catus* (Davis and Story 1943: fig. 2).

Behind the glenoid fossa is the postglenoid region, which is largely hidden by the ectotympanic (Fig. 19). The anterior crus of the ectotympanic (“acr” in Fig. 19; including the fused rostral process of the malleus) has a broad contact that is filled with connective tissue on the postero-medial face of the postglenoid process. In the lateral half of this contact is a small, oval opening that presumably is continuous internally with the postglenoid foramen (“pgf” in Fig. 19; see below). The posterior crus of the ectotympanic (“pcr” in Fig. 19) has a small, round contact with the ventromedial surface of the posttympanic process, just anterolateral to the tympanohyal (“th” in Fig. 19) of the petrosal. Between the two ectotympanic contacts is the gently curved roof of the external acoustic meatus (“eam” in Fig. 19). Additional details of the postglenoid region based on

specimens with the ectotympanics removed are included below.

**AMNH 207730, Newborn.**—In dorsal view (Figs. 2C–D), the base of the zygomatic process and the caudal process are almost entirely hidden from view. The section of the zygomatic process of the squamosal overlying the jugal does not extend far from the braincase.

In lateral view (Figs. 4C–D), the postglenoid process extends about as far ventrally as the posttympanic process; a preglenoid process is absent. The glenoid fossa and the roof of the external acoustic meatus are very gently concave. The zygomatic process is not gently curved upward, but relatively straight. The suprastoid and suprastoid crests are lacking, and the squamosal does not extend dorsally into the braincase far from the zygomatic base. As the pars canalicularis of the petrosal has not ossified, the posterior margin of the caudal process of the squamosal contacts no bone, and there is no ventral nuchal crest to which it can contribute.

In ventral view (Fig. 13), compared to the adult, the glenoid fossa is much flatter and set off from the braincase by a much wider, deeper notch medial to the postglenoid process. The squamosal medial to the glenoid is flatter and nearly reaches to the lateral margin of the foramen ovale; an entoglenoid process is lacking. The postglenoid region is a narrow, relatively flat ridge. The dorsomedial aspect of the postglenoid region, which contributes to the middle ear, is hidden by soft tissue, as well as by the ectotympanic and malleus. The anterior crus of the ring-shaped ectotympanic has a narrow contact with the dorsomedial postglenoid region and the posterior crus approximates but falls short of contacting the posttympanic process. The presence of a postglenoid foramen cannot be confidently ascertained.

**Others.**—The following specimens in which the ectotympanic is removed reveal details of the squamosal within the middle ear: CM 2356, AMNH 51503R (Fig. 18), CM 3693(R) (Figs. 15, 16A), 69366 (Fig. 16B), 16103, 42728(R), 5097(R), AMNH 51448(R), 201513 (Fig. 14), 51494(R); the last three are damaged and of less utility. The first four are the most helpful as they preserve sutures delimiting the squamosal from the alisphenoid, parietal, and petrosal.

The exposed dorsomedial aspect of the postglenoid region shows, from anterior to posterior, the facet for the anterior crus of the ectotympanic (“acr” in Fig. 17), the lateral wall of the epitympanic recess (“er” in Fig. 17), the lateral wall of the fossa incudis (“fi” in Fig. 17), and the ventromedial surface of the posttympanic process. The roofs of the first two structures, the anterior crus facet and epitympanic recess, are formed by the epitympanic wing of the squamosal. Medially, the epitympanic wing of the squamosal contacts the parietal epitympanic wing and the tegmen tympani. The anterior crus facet is oval (longer than wide); its lateral wall is prominent, whereas the me-

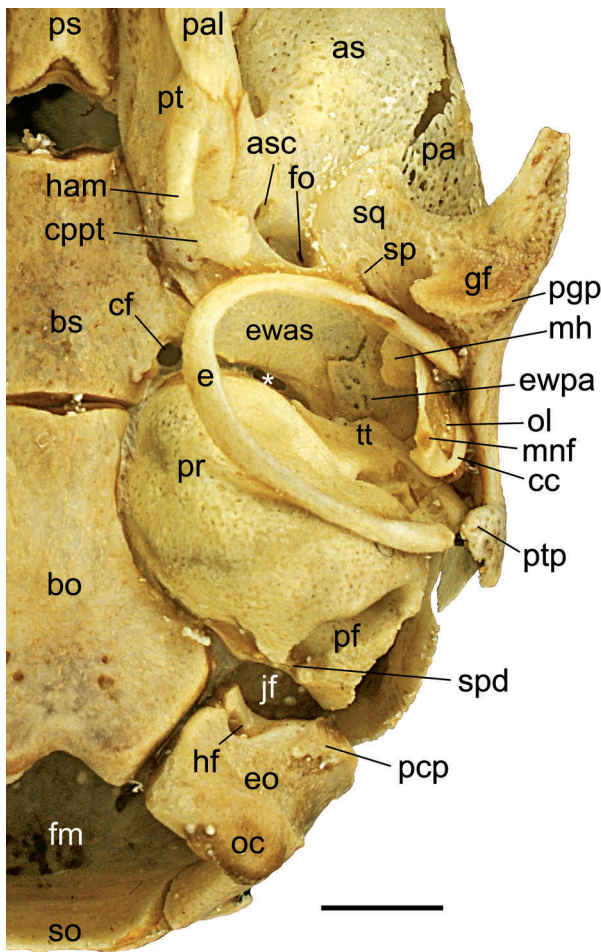


Fig. 13—Left basicranium of newborn *Nandina binotata*, AMNH 207730, in ventral view. Suture between the ali- and basisphenoid is posterior to the pterygoid and partially hidden by the ectotympanic. White asterisk is in the narrow piriform fenestra, between the promontorium of the petrosal and the epitympanic wing of the alisphenoid. Scale = 2 mm. Abbreviations: **as**, alisphenoid; **asc**, caudal opening of alisphenoid canal; **bo**, basioccipital; **bs**, basisphenoid; **cc**, capitular crest; **cf**, carotid foramen; **cppt**, caudal process of pterygoid; **e**, ectotympanic; **eo**, exoccipital; **ewas**, epitympanic wing of alisphenoid; **ewpa**, epitympanic wing of parietal; **fm**, foramen magnum; **fo**, foramen ovale; **gf**, glenoid fossa; **ham**, pterygoid hamulus; **hf**, hypoglossal foramen; **jf**, jugular foramen; **mh**, malleolar hook; **mnf**, facet for cartilaginous manubrium; **oc**, occipital condyle; **ol**, osseous lamina; **pa**, parietal; **pal**, palatine; **pcp**, paracondylar process of exoccipital; **pf**, perilymphatic foramen; **pgp**, postglenoid process; **pr**, promontorium of petrosal; **ps**, presphenoid; **pt**, pterygoid; **ptp**, posttympanic process of squamosal; **so**, supraoccipital; **sp**, spine of rostral process of malleus; **spd**, sulcus for perilymphatic duct; **sq**, squamosal; **tt**, tegmen tympani.

dial one is lower. In CM 2356, the medial wall is formed entirely by squamosal, but in CM 3693 it lies along the suture between the squamosal and parietal (Fig. 15).

Anterior to the depression for the anterior crus of the ectotympanic, foramina variable in size, number, and position occur on the posterior face of the postglenoid process (“pgf” in Figs. 14–16). These foramina are partly obscured or hidden when the ectotympanic is in place, but we were

able to verify their presence in all but one specimen, AMNH 51510, which has glue covering the area. These structures resemble postglenoid foramina in other placentals (Evans 1993; Wible 2008, 2011) and are treated as such here (see Endocranium). Their arrangement is quite variable. For example, CM 5097 has a single dorsally placed foramen 1 mm in diameter with a short sulcus extending ventrally; CM 2356 has a similar arrangement but the foramen is less than half the size of that in the previous specimen; CM 3693 has one more ventrally placed foramen on the left side and two small ones on the right (Fig. 15); AMNH 201513 has three on the right and four on the left (Fig. 14). Variable small foramina also occur in the roof of the depression for the anterior crus. CM 2356 has none; CM 3693 has one anteriorly placed on the right side only (Fig. 15); CM 5097 has two centrally placed on the left and one on the right; AMNH 16103 has three in the anterior, middle, and posterior aspects on the left side but only the last two on the right side.

Anterior to the postglenoid foramina, the surface of the entoglenoid process in the most advanced juvenile, AMNH 201513, and the adults has an indication of the course of the chorda tympani nerve. For example, on the right side of AMNH 201513, there is a distinct groove (“gct” in Fig. 14), while on the left side this is a deep notch. Posterior to the depression for the anterior crus is a second depression comparable in size and shape, but obliquely oriented (from posterolateral to anteromedial) and shared between the squamosal and petrosal (“er” in Figs. 15, 17). This is the epitympanic recess forming the roof over the malleus-incus articulation. Based on specimens with the malleus and incus in situ (e.g., CM 59497, AMNH 134969), it is clear that the bulk of the epitympanic recess is in the petrosal and that the squamosal forms the lateral wall. The concave, vertical lateral wall of the epitympanic recess is prominent, but the medial wall is relatively flat, although its development varies (see Petrosal).

Posterior to the epitympanic recess is a narrow, deep nook, the fossa incudis, which houses the crus breve of the incus (“fi” in Fig. 17). The squamosal forms only the lateral wall of this nook, with the petrosal making the remaining surfaces; the extent of the floor to the fossa is variable (see Petrosal).

The ventromedial aspect of the posttympanic process abuts the tympanohyal (“th” in Figs. 14–15, 17). Just anterolateral to this abutment is a small facet on the posttympanic process accommodating the tip of the posterior crus of the ectotympanic (“pcrf” in Figs. 15, 17). The lateral surface of the tympanohyal forms the medial wall of this facet.

We also noted features of the squamosal that changed ontogenetically in the study sample. The preglenoid process, which is absent in the newborn and younger juveniles, is first noticeable in the oldest juvenile, AMNH 201513, and then only at its lateral end (Fig. 14). In the adults, the preglenoid process shows a general ontogenetic increase in its mediolateral extent and ventral projection; the latter can

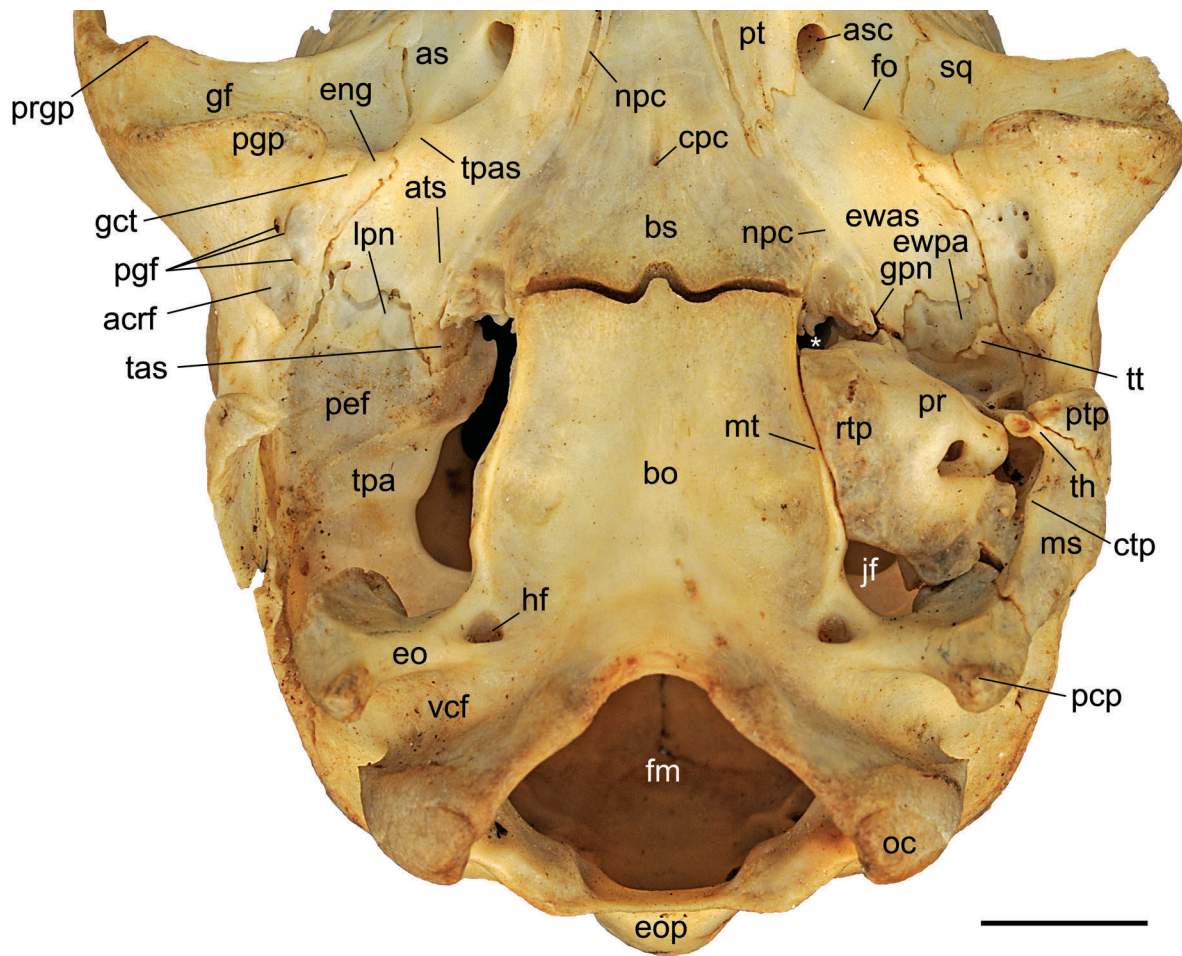


Fig. 14—Basicranium of juvenile *Nandinia binotata*, AMNH 201513, in ventral view. Right petrosal is isolated from the skull and illustrated elsewhere (Fig. 21); its absence exposes structures within the cranial cavity. White asterisk is in the gap between the basisphenoid and the promontorium of the petrosal. Scale = 5 mm. Abbreviations: **acrif**, facet for anterior crus of ectotympanic; **as**, alisphenoid; **asc**, caudal opening of alisphenoid canal; **ats**, sulcus for auditory tube; **bo**, basioccipital; **bs**, basisphenoid; **cpc**, craniopharyngeal canal; **ctp**, caudal tympanic process of petrosal; **eng**, entoglenoid process of squamosal; **eo**, exoccipital; **eop**, external occipital protuberance; **ewas**, epitympanic wing of alisphenoid; **ewpa**, epitympanic wing of parietal; **fm**, foramen magnum; **fo**, foramen ovale; **gct**, groove for chorda tympani nerve; **gf**, glenoid fossa; **gpn**, foramen for greater petrosal nerve; **hf**, hypoglossal foramen; **jf**, jugular foramen; **lpn**, groove for lesser petrosal nerve; **ms**, mastoid shelf; **mt**, muscular tubercle; **npc**, groove for nerve of pterygoid canal; **oc**, occipital condyle; **pcp**, paracondylar process of exoccipital; **pef**, petrosal facet on tentorial process of parietal; **pgf**, postglenoid foramina; **pgp**, postglenoid process; **pr**, promontorium of petrosal; **prgp**, preglenoid process; **pt**, pterygoid; **ptp**, posttympanic process of squamosal; **rtp**, rostral tympanic process of petrosal; **sq**, squamosal; **tas**, tentorial process of alisphenoid; **th**, tympanohyal; **tpa**, tentorial process of parietal; **tpas**, tympanic process of alisphenoid; **tt**, tegmen tympani; **vcf**, ventral condyloid fossa

be seen by comparing CM 59495 and 42728 in the lateral view in Figure 1. The ontogenetic increase in the mediolateral dimension of the glenoid fossa is far greater than anteroposteriorly, which is also the case for the posttympanic process (cf. Figs. 6B, D). This changes the lateral profile of the squamosal from a relatively flat parasagittal one in the newborn, AMNH 207730 (Fig. 13), to a deeply concave one at the external acoustic meatus in the adult (Fig. 16). The ventral projection of the postglenoid process changes dramatically, as evident in Figure 1. In the newborn, AMNH 207730, the postglenoid process does not project as far ventrally as the posttympanic process, and is even with the distal end of the anterior crus of the ectotympanic

(see also Fig. 4D). These relationships change such that by the older adult, CM 42728, the postglenoid projects farther ventrally than the other two processes (Fig. 1).

#### Petrosal (“pe” in figures)

The paired petrosals are the principal elements of the auditory region; they house the inner ear, contribute to the roof and walls of the middle ear, and are crisscrossed by various nerves and vessels. The petrosal is usually divided into the anteroventromedial pars cochlearis, housing the cochlear duct and saccule, and the posterodorsolateral pars canalicularis, housing the utricle and semicircular canals.

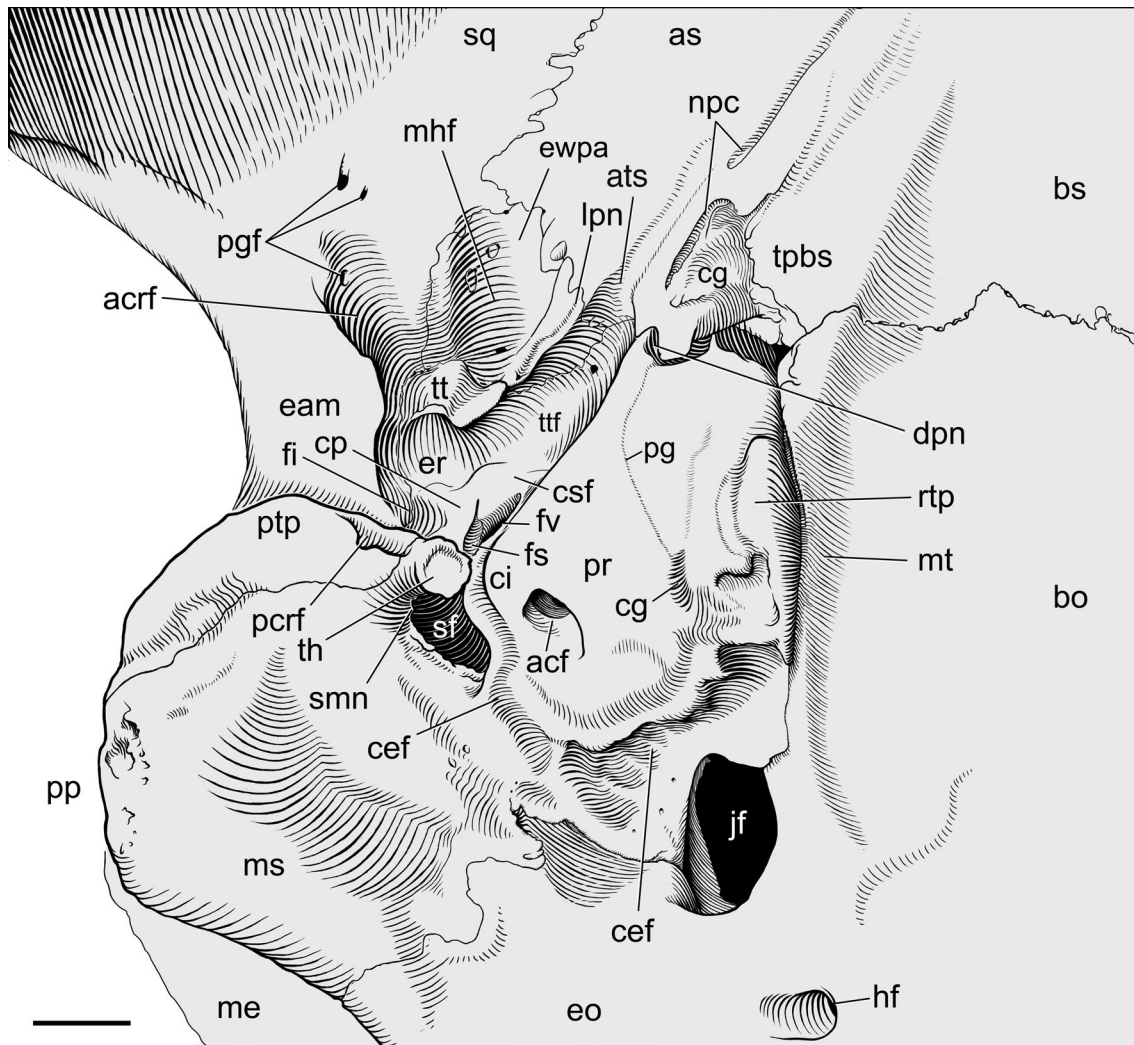


Fig. 15—Right basicranium of adult *Nandinia binotata*, CM 3693, in ventral view. The carotid foramen at the medial end of the carotid groove is hidden by the tympanic process of the basisphenoid; the epitympanic wings of the alisphenoid and squamosal are the parts of those bones abutting the epitympanic wing of the parietal. Scale = 2 mm. Abbreviations: **acf**, aperture of cochlear fossula; **acrf**, facet for anterior crus of ectotympanic; **as**, alisphenoid; **ats**, sulcus for auditory tube; **bo**, basioccipital; **bs**, basisphenoid; **cef**, facet for caudal entotympanic; **cg**, groove for internal carotid artery and nerves; **ci**, crista interfenestralis; **cp**, crista parotica; **csf**, cavum supracochleare floor; **dpn**, foramen for deep petrosal nerve; **eam**, roof of external acoustic meatus; **eo**, exoccipital; **er**, epitympanic recess; **ewpa**, epitympanic wing of parietal; **fi**, fossa incudis; **fs**, facial sulcus; **fv**, fenestra vestibuli; **hf**, hypoglossal foramen; **jf**, jugular foramen; **lpn**, groove for lesser petrosal nerve; **me**, mastoid exposure; **mhf**, facet for malleolar hook of rostral process; **ms**, mastoid shelf; **mt**, muscular tubercle; **npc**, groove for nerve of pterygoid canal; **pcrf**, facet for posterior crus of ectotympanic; **pg**, groove on promontorium for deep petrosal nerve; **pgf**, postglenoid foramina; **pp**, paroccipital process of petrosal; **pr**, promontorium of petrosal; **ptp**, posttympanic process of squamosal; **rtp**, rostral tympanic process of petrosal; **sf**, stapedius fossa; **smn**, stylomastoid notch; **sq**, squamosal; **th**, tympanohyal; **tpbs**, tympanic process of basisphenoid; **tt**, tegmen tympani; **tff**, tensor tympani fossa.

The therian petrosal presents four surfaces: tympanic/ventral, cerebellar/dorsal, squamosal/lateral, and lambdoid/mastoid (MacIntyre 1972; Wible 1990). We are fortunate that our study sample includes an isolated right petrosal of the most advanced juvenile, AMNH 201513, allowing views of all surfaces. Wible (2010a:1) has recently noted “for many mammalian lineages, more is known about the petrosal in extinct than in extant taxa, with fossilization and perhaps breakage exposing the bone.” Carnivorans are no exception, and we take this opportunity to describe the

petrosal in an extant form and begin our treatment with this isolated element.

**AMNH 201513—Isolated Right Petrosal.**—We describe and illustrate this bone in three views: ventral, oblique dorsal (to allow the internal acoustic meatus and subarcuate fossa to be seen), and lateral (Fig. 21). The fourth view, lambdoid, is not included, as it does not provide additional information beyond that gleaned from the other three orientations. The left petrosal of this specimen is preserved in

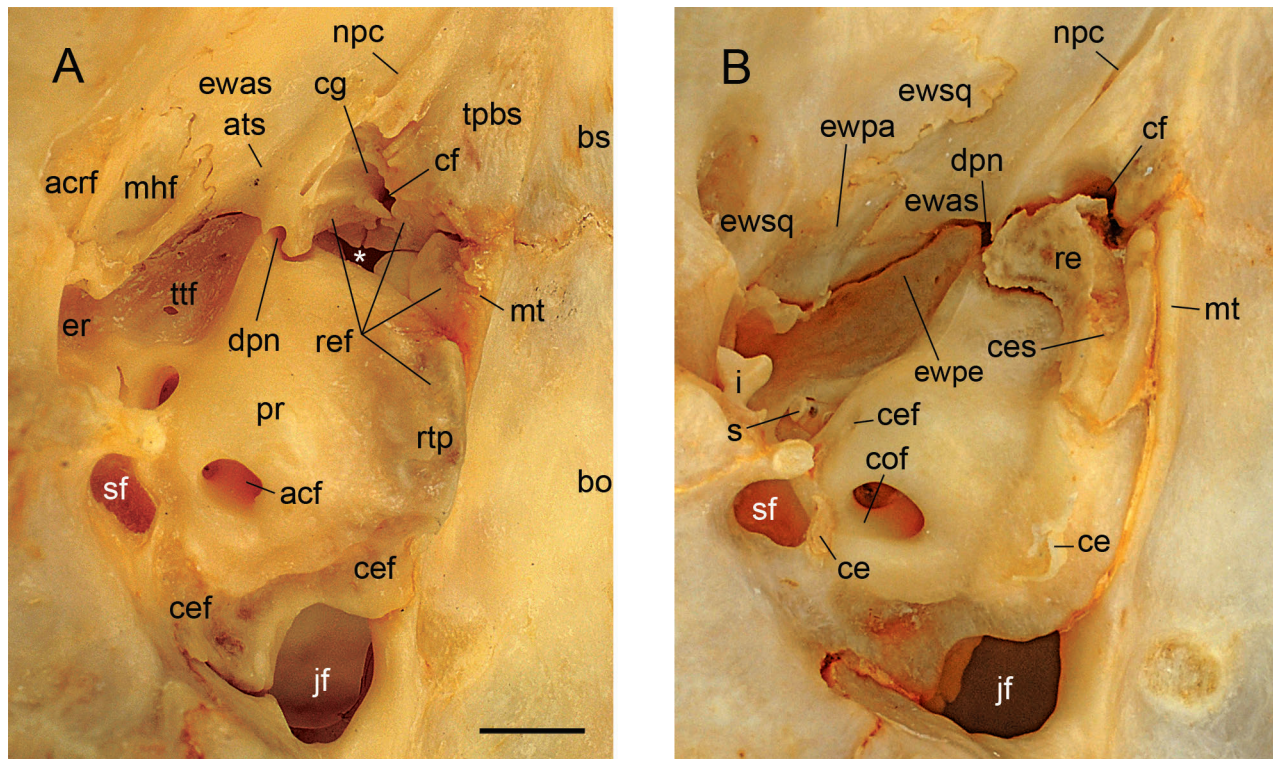


Fig. 16—Right ear regions of adult *Nandinia binotata* in oblique ventral view. **A**, CM 3693; **B**, CM 69366. White asterisk in A is in the gap between the basisphenoid and the promontorium of the petrosal, which is covered by the rostral entotympanic in B. The incus in B is displaced from its life position. Scale = 2 mm. Abbreviations: **acf**, aperture of the cochlear fossula; **acrf**, facet for anterior crus of ectotympanic; **ats**, sulcus for auditory tube; **bo**, basioccipital; **bs**, basisphenoid; **ce**, osseous caudal entotympanic; **cef**, facet for caudal entotympanic; **ces**, sulcus for caudal entotympanic; **cf**, carotid foramen; **cg**, carotid groove; **cof**, cochlear fossula; **dpn**, foramen for deep petrosal nerve; **er**, epitympanic recess; **ewas**, epitympanic wing of alisphenoid; **ewpa**, epitympanic wing of parietal; **ewpe**, epitympanic wing of petrosal; **ewsq**, epitympanic wing of squamosal; **i**, incus; **jf**, jugular foramen; **mhf**, facet for malleal hook of rostral process; **mt**, muscular tubercle; **npc**, groove for nerve of pterygoid canal; **pr**, promontorium of petrosal; **re**, rostral entotympanic; **ref**, facet for rostral entotympanic; **rtp**, rostral tympanic process of petrosal; **s**, stapes; **sf**, stapedius fossa; **tpbs**, tympanic process of basisphenoid; **ttf**, tensor tympanic fossa.

situ (Fig. 14), providing details of contacts with neighboring bones.

Ventral view (Figs. 21A, D).—The most prominent feature is the oval-shaped (longer than wide) promontorium (“pr” in Fig. 21D) - the cochlear housing, which is the manifestation of the pars cochlearis in this view. The most conspicuous feature on the promontorium is a broad, longitudinal ridge along the medial aspect that contributes to the medial bullar wall (“rtp” in Fig. 21D). In lateral view (Fig. 21F), this ridge is V-shaped, with the deepest part opposite the fenestra vestibuli (oval window; “fv” in Fig. 21F). In the intact left side of the skull, the medial surface of this ridge contacts a sharp ridge on the lateral margin of the basioccipital, the muscular tubercle (“mt” in Fig. 14), and the central part of the petrosal ridge extends ventral to that on the basioccipital. The irregular, flat ventral surface on the petrosal ridge serves as a facet for the entotympanics. The anterior slope of the V is the site of attachment for the rostral entotympanic and the posterior slope that for the caudal entotympanic. Hunt (1987) called this structure the ventral promontorial process in *N. binotata* and certain

other feliforms, but we identify this structure by the more general term rostral tympanic process (MacPhee 1981). Ontogenetically, rostral tympanic processes form in a variety of mammals as periosteal outgrowths from the pars cochlearis along the inner surface of the fibrous membrane of the tympanic cavity, the connective tissue membrane that represents the embryonic auditory bulla (MacPhee 1981). The ontogeny of the promontorial process in *N. binotata* is not known. However, the relationship between this process and the rostral and caudal entotympanics in *N. binotata* closely resembles that between the rostral tympanic process and entotympanics in other taxa (e.g., macrascalid-eans; Klaauw 1929; MacPhee 1981) where the ontogeny is known.

The surface of the promontorium lateral to the rostral tympanic process has two weak bulges, one anterior and one posterior, that are separated by a shallow, anteriorly concave surface. These bulges reflect the enclosed coils of the cochlear duct. Two openings are found on the posterior and posterolateral aspects of the promontorium, the aperture of the cochlear fossula (“acf” in Fig. 21D) and the

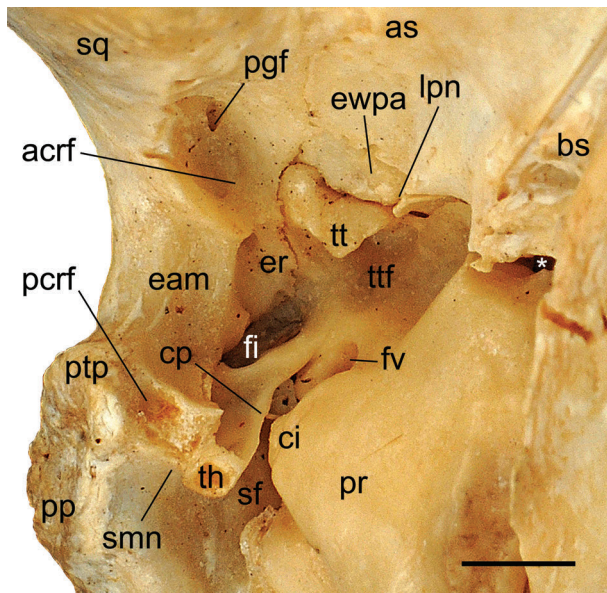


Fig. 17—Right ear region of adult *Nandinia binotata*, AMNH 51503, in oblique ventral view. Scale = 2 mm. White asterisk is in the gap between the basisphenoid and the promontorium of the petrosal. Abbreviations: **acrif**, facet for anterior crus of ectotympanic; **as**, alisphenoid; **bs**, basisphenoid; **ci**, crista interfenestralis; **cp**, crista parotica; **eam**, roof of external acoustic meatus; **er**, epitympanic recess; **ewpa**, epitympanic wing of parietal; **fi**, fossa incudis; **fv**, fenestra vestibuli; **lpn**, groove for lesser petrosal nerve; **pcrf**, facet for posterior crus of ectotympanic; **pgf**, post-glenoid foramen; **pp**, paroccipital process of petrosal; **pr**, promontorium of petrosal; **ptp**, posttympanic process of squamosal; **sf**, stapedius fossa; **smn**, stylomastoid notch; **sq**, squamosal; **th**, tympanohyal; **tt**, tegmen tympani; **tff**, tensor tympani fossa.

fenestra vestibuli, respectively. The latter accommodates the footplate of the stapes and is recessed a half millimeter in from the promontorial surface, with the resulting space representing a vestibular fossula (see Fig. 21F). The opening of the fenestra vestibuli is slightly smaller than the opening of the vestibular fossula. The fenestra vestibuli is oval (longer than wide), with a stapedial ratio (length to width) sensu Segall (1970) of 1.57 (see Fig. 21F). It is laterally and slightly anteroventrally directed. The aperture of the cochlear fossula is half moon-shaped with the dorsal margin straight. It is posteriorly and slightly ventrolaterally directed. Just within the rim of the aperture is a sulcus (faint but visible within the lateral margin in Fig. 21A) representing the point of attachment of the secondary tympanic membrane, which denotes the location of the fenestra cochleae (round window). Deep to the fenestra cochleae are the lateral opening of the cochlear canaliculus, which transmits the perilymphatic duct, and the primary and secondary osseous lamina, which curve with the coils of the cochlear duct (not shown in the figures); in life, the gap between the two laminae contains the basilar membrane. Posterior to the aperture of the cochlear fossula is a small, horizontal triangular shelf. The anterior margin of the triangle has a low raised lip with a shallow depression extending anteriorly from it towards the round window.

This depression marks the cochlear fossula (“cof” in Fig. 21D). Curving dorsomedially from behind the triangular shelf is an irregular facet contacting the caudal entotympanic (“cenf” in Fig. 21D) in the intact skull (e.g., CM 42728, AMNH 51513).

Between the oval and round windows is a thick bar of bone, the crista interfenestralis (“ci” in Fig. 21D). The crista has a prominent rounded lateral bulge that underhangs the stapedius fossa (“sf” in Fig. 21D), narrowing the gap between the promontorium and the crista parotica on the pars canalicularis (see below). This differs from the usual placental pattern in which the crista interfenestralis is a simple vertical bar with no lateral bulge (Wible 2008, 2009, 2010a, 2011, 2012). Anterior to this bulge is a shallow notch (not visible in the figures) directed toward the posterior margin of the fenestra vestibuli that accommodated the tendon of the stapedius muscle in life. On the ventral slope of this lateral bulge is a rod-shaped gutter, 2 mm in length, that is deepest at its ends and appears dumbbell-shaped. This gutter is present bilaterally and is interpreted by us to be a site of attachment for the middle-ear wall (see more below).

At the anterior pole of the promontorium is a small, narrow, quadrangular, anteromedially-directed shelf, with a rough facet on it that extends posteriorly a short distance onto the promontorium (“app” in Fig. 21D). Based on the left petrosal in the intact skull (Fig. 14), this facet contacts the basisphenoid medial to the exit of the greater petrosal nerve from the skull (see also Figs. 15, 18). This shelf resembles the apex parties petrosa identified by Giannini et al. (2006) in the megachiropteran *Pteropus* Erxleben, 1777, and is identified as such here. The bat structure differs in that it does not contact other bones.

Lateral to the apex parties petrosa is a more substantial shelf from the anterolateral surface of the promontorium, which we interpret as having a dual origin based on position: medially the epitympanic wing of the petrosal (“ew” in Fig. 21D) and laterally the tegmen tympani (“tt” in Fig. 21D), an anterior prolongation of the pars canalicularis (see below). The shelf has a comma-shaped depression with the long axis oriented transversely; this houses the tensor tympani muscle in life (“tff” in Fig. 21D) based on *F. catus* (Jayne 1898). The anterior margin of this shelf is downturned and contacts the epitympanic wings of the alisphenoid and parietal in the intact skull. Where the downturned shelf and anterolateral aspect of the promontorium meet is a small anterior projection, which lies in a more ventral plane than the apex parties petrosa. Based on specimens with the rostral entotympanic in place (Fig. 16B), this projection marks the lateral limit of the rostral entotympanic. It can also form the posterolateral border of the opening for the deep petrosal nerve (Figs. 15, 16A, 18) or that for the greater petrosal nerve (Fig. 14). It is continuous anteriorly with the upturned lateral margin of the rostral entotympanic (see below) and with the ridge on the basisphenoid associated with the nerve of the pterygoid canal (Fig. 16B). The lateral view in Figure 20 shows that

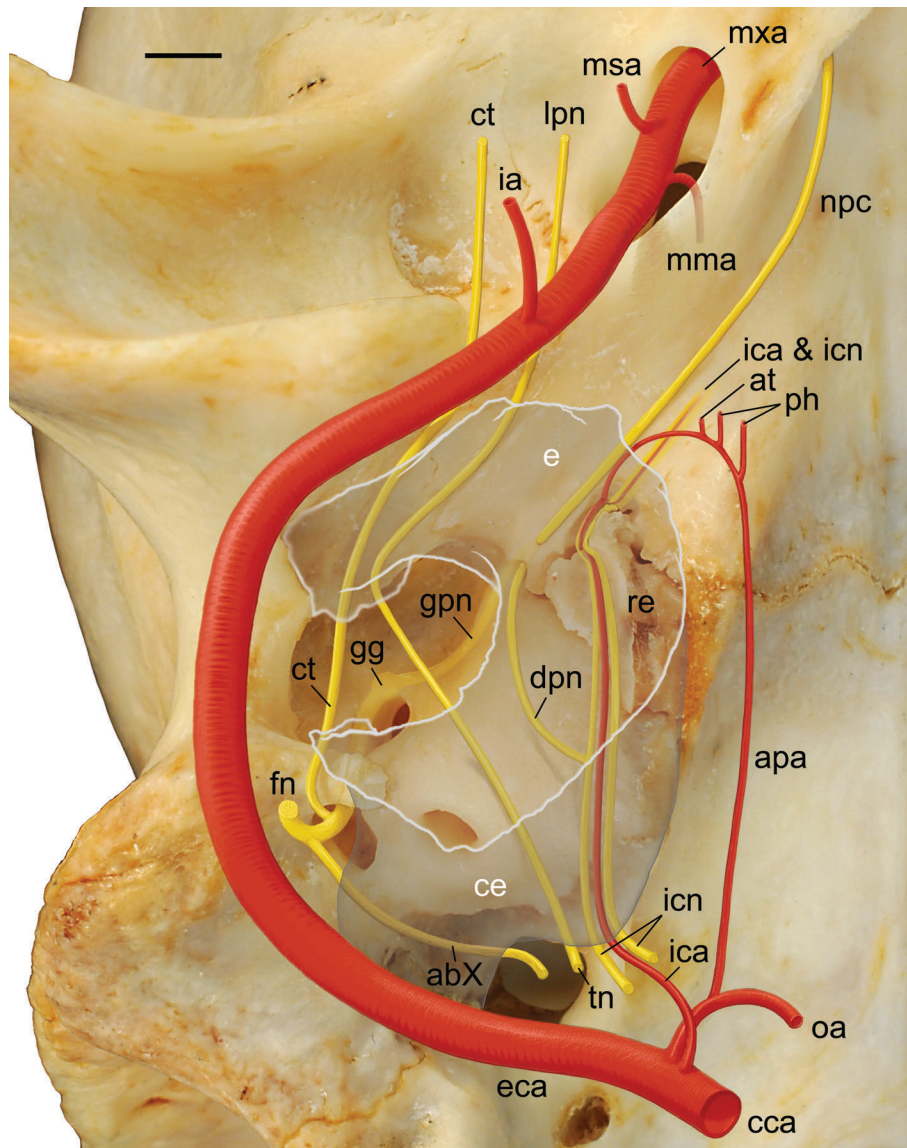


Fig. 18—Right ear region of *Nandinia binotata*, CM 3693, in ventral view (reversed from left side). The white outline delimits the ectotympanic bone, based on the isolated element with this specimen; the gray outline posterior to the ectotympanic delimits the caudal entotympanic, based on AMNH 51513. Arteries are reconstructed based on the *N. binotata* illustrated in Davis and Story (1943: fig. 9) and Hunt (1989: fig. 7); nerves are based on CM 42728, which has several dried in place, and *F. catus* (Davis and Story 1943: fig. 2). Portions of the internal carotid artery and nerve, deep petrosal nerve, tympanic-lesser petrosal nerve, and chorda tympani nerve are undercover of the ectotympanic and/or caudal entotympanic within the middle ear. The auricular ramus of the vagus is not within the middle ear, but between the caudal entotympanic and petrosal. The geniculate ganglion, the greater petrosal nerve, the intratympanic portion of the facial nerve, and the intracranial portion of the internal carotid artery and nerve are enclosed by bone. Scale = 3 mm. Abbreviations: **abX**, auricular branch of vagus nerve (cranial nerve X); **apa**, ascending pharyngeal artery; **at**, auditory tube branch; **cca**, common carotid artery; **ce**, caudal entotympanic; **ct**, chorda tympani nerve; **dpa**, deep petrosal nerve; **e**, ectotympanic; **eca**, external carotid artery; **fn**, facial nerve (cranial nerve VII); **gg**, geniculate ganglion; **gpn**, greater petrosal nerve; **ia**, inferior alveolar artery; **ica**, internal carotid artery; **icn**, internal carotid nerve; **lpn**, lesser petrosal nerve; **msa**, masseteric artery; **msa**, maxillary artery; **npc**, nerve of pterygoid canal; **oa**, occipital artery; **ph**, pharyngeal branch; **re**, rostral entotympanic; **tn**, tympanic nerve.

this projection floors the anteroventral part of the tensor tympani fossa.

Lateral and posterolateral to the pars cochlearis is the pars canicularis. The highest elevation on the pars canicularis, the tympanohyal (“th” in Fig. 21D), is po-

sitioned near the anteroposterior midpoint, opposite the round window. The tympanohyal is a ventromedially-directed process, which at its distal end has an oval facet for articulation with the rest of the hyoid apparatus that faces posteroventromedially. Posterior to the tympanohyal is a

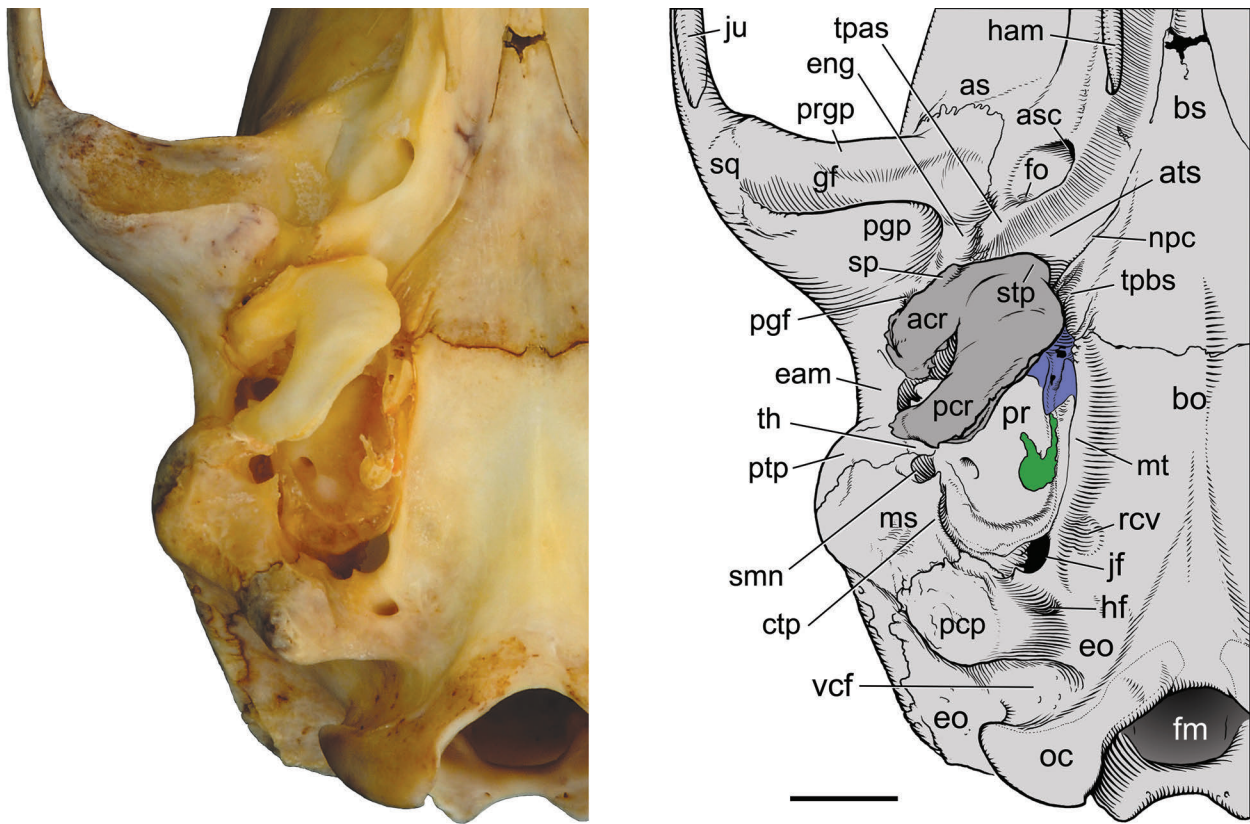


Fig. 19— Right basicranium of adult *Nandinia binotata*, CM 59495, in ventral view. In the drawing, the green is the ossified caudal entotympanic, the blue is the rostral entotympanic, and the dark gray is the ectotympanic. Scale = 5 mm. Abbreviations: **acr**, anterior crus of ectotympanic; **as**, alisphenoid; **asc**, caudal opening of alisphenoid canal; **ats**, sulcus for auditory tube; **bo**, basioccipital; **bs**, basisphenoid; **ctp**, caudal tympanic process of petrosal; **eam**, roof of external acoustic meatus; **eng**, entoglenoid process of squamosal; **eo**, exoccipital; **fm**, foramen magnum; **gf**, glenoid fossa; **ham**, pterygoid hamulus; **hf**, hypoglossal foramen; **jf**, jugular foramen; **ju**, jugal; **ms**, mastoid shelf; **mt**, muscular tubercle; **npc**, groove for nerve of pterygoid canal; **oc**, occipital condyle; **pcp**, paracondylar process of exoccipital; **pcr**, posterior crus of ectotympanic; **pgf**, postglenoid foramen; **pgp**, postglenoid process; **pr**, promontorium of petrosal; **prgp**, preglenoid process; **ptp**, posttympanic process of squamosal; **rcv**, fossa for rectus capitis ventralis; **smn**, stylomastoid notch; **sp**, spine of rostral process of malleus; **sq**, squamosal; **stp**, styliform process; **th**, tympanohyal; **tpas**, tympnic process of alisphenoid; **tpbs**, tympnic process of basisphenoid; **vcf**, ventral condyloid fossa.

broad shelf reaching posterior to the level of the jugular foramen, where it contacts the paracondylar process of the exoccipital. This mastoid shelf (“ms” in Fig. 21D) represents the ventral margin of the mastoid exposure (“me” in Fig. 21F). The lateral margin of the mastoid shelf has a prominent bulge at the location of the structure called a mastoid process in other carnivorans (Jayne 1898), which we call the paroccipital process. The medial margin of the shelf is formed by a rounded ridge (“ctp” in Fig. 18D), the caudal tympanic process (MacPhee 1981). Where the caudal tympanic process meets the tympanohyal is the stylomastoid notch (“smn” in Fig. 21D), marking the exit of the facial nerve from the middle ear (“fn” in Fig. 18). Anteromedial to the caudal tympanic process is a narrow gutter that is continuous anterolaterally with the stapedius fossa. The stapedius fossa is subcircular and has a high anterior wall formed by the gyrus of the lateral semicircular canal.

Running anteromedially from the tympanohyal is a thin, sharp crest, the crista parotica (“cp” in Fig. 21D). The crista parotica is not fully vertical but instead slanted

ventromedially and decreasing in height anteriorly. Just anterior to the tympanohyal, the crista parotica nearly contacts the lateral bulge on the crista interfenestralis. The crista parotica forms the lateral wall of the deep facial sulcus (“fs” in Fig. 21D) and ends anteriorly as the lateral margin of the secondary facial foramen (“sff” in Fig. 21D), which in turn lies lateral to the anterior margin of the fenestra vestibuli. Anterior to the secondary facial foramen is a prominence that is flanked on its anterior side by the tensor tympani fossa; this prominence represents the floor of the cavum supracochleare (“csf” in Fig. 21D), the space within the petrosal housing the geniculate ganglion of the facial nerve. The lateral surface of the crista parotica has two concavities separated by a transverse ridge. The triangular anterodorsal concavity represents the medial wall and roof of the fossa incudis (“fi” in Fig. 21D); the narrow, quadrangular posteroventral concavity is of uncertain function. Anterior to and separated by an oblique rim from the fossa incudis is a deeper triangular concavity, representing the petrosal’s contribution to the epitympanic

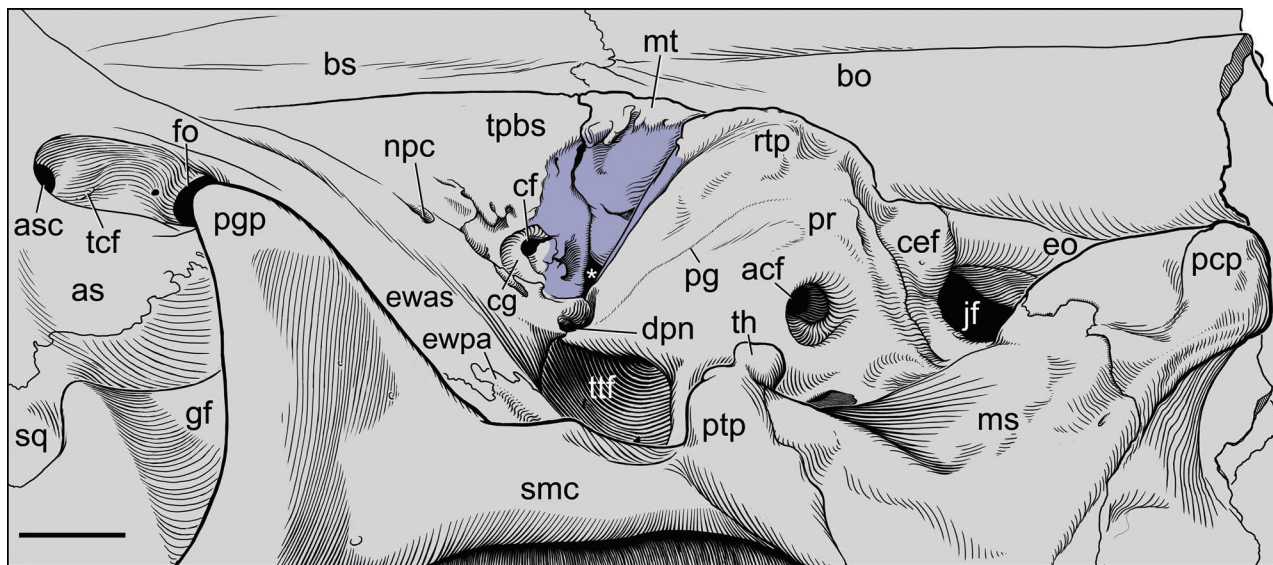


Fig. 20—Right basicranium of adult *Nandinia binotata*, CM 3693, in oblique lateral view. The area shaded blue contacts the missing rostral entotympanic. The white asterisk is in the gap between the basisphenoid and the promontorium of the petrosal. Scale = 2 mm. Abbreviations: **acf**, aperture of cochlear fossula; **as**, alisphenoid; **asc**, caudal opening of alisphenoid canal; **bo**, basioccipital; **bs**, basisphenoid; **cef**, facet for caudal entotympanic; **cf**, carotid foramen; **cg**, carotid groove; **dpn**, foramen for deep petrosal nerve; **eo**, exoccipital; **ewas**, epitympanic wing of alisphenoid; **ewpa**, epitympanic wing of parietal; **fo**, foramen ovale; **gf**, glenoid fossa; **jf**, jugular foramen; **ms**, mastoid shelf; **mt**, muscular tubercle; **npc**, groove for nerve of pterygoid canal; **pcp**, paracondylar process of exoccipital; **pg**, groove on promontorium; **pgg**, postglenoid process; **pr**, promontorium of petrosal; **ptp**, posttympanic process of squamosal; **rtp**, rostral tympanic process of petrosal; **smc**, suprameatal crest; **sq**, squamosal; **tcf**, transverse canal foramen; **th**, tympanohyal; **tpbs**, tymppanic process of basisphenoid; **ttf**, tensor tympani fossa.

recess (“er” in Fig. 21D). A high anteromedial wall separates the epitympanic recess from the fossa for the tensor tympani muscle. Anterior to the epitympanic recess and the lateral aspect of the tensor tympani fossa, the pars canalicularis ends as a ventrally projecting triangular process, which represents the distal end of the tegmen tympani (see below). The flattened distal end of this process is thickened; in the intact skull, this thickened tip forms the back of the depression for the malleolar hook of rostral process of the malleus (Fig. 14).

The final structure best described in the ventral view is the tegmen tympani, the anterior prolongation of the pars canalicularis. The term tegmen tympani is usually applied to a part of the mammalian chondrocranium (De Beer 1937; Moore 1981) where it is easily delimited from neighboring elements. However, a tegmen tympani is also identified in adults, including *F. catus* (Jayne 1898) and *C. lupus familiaris* (Evans 1993), even though such identification is often complicated by secondary fusion with neighboring elements. Following the usage of De Beer (1929, 1937) and Moore (1981), we identify the tegmen tympani in *N. binotata* as the floor of the cavum supracochleare, the adjacent facial sulcus, and the bone anterolateral to the cavum floor forming the lateral part of the tensor tympani fossa (see discussion in Wible 2008).

Oblique dorsal view (Figs. 21B, E).—The oblique dorsal view is dominated by two subequal openings, the internal acoustic meatus on the pars cochlearis and the subarcuate

fossa on the pars canalicularis (“iam” and “saf” in Fig. 21E, respectively). In AMNH 134969, which has the skull roof removed, the two openings are in the same coronal plane, with the internal acoustic meatus ventromedial to the subarcuate fossa; the former is directed medially and slightly posteriorly, whereas the latter is directed antero-medially.

The kidney-bean shaped, moderately deep internal acoustic meatus transmits the facial and vestibulocochlear nerves. A deeply recessed, obliquely oriented transverse crest (“tc” in Fig. 21E) divides the meatus into lateral and medial parts, the foramen acusticum superius and inferius, the latter twice the size of the former (“fas” and “fai” in Fig. 21E, respectively). The distribution of foramina within the internal acoustic meatus resembles that described for *F. catus* by Jayne (1898), but rather than use the terminology employed by that author, we follow that of Terry (1942). The foramen acusticum superius is the gateway for two openings: a larger anterior one leading to the facial canal for the facial nerve (not visible in the figures) and the other connecting to a cribriform pit, the superior vestibular area for nerves to the utricle and ampullae of the anterior and lateral semicircular canals (“sva” in Fig. 21E). At the posterior edge of the foramen acusticum inferius is the foramen singulare (“fsi” in Fig. 21E), which leads to a cribriform pit for nerves to the ampulla of the posterior semicircular canal. Recessed more deeply anterior to that is a smaller cribriform pit, the inferior vestibular area for nerves to the saccule (“iva” in Fig. 21E). The remainder

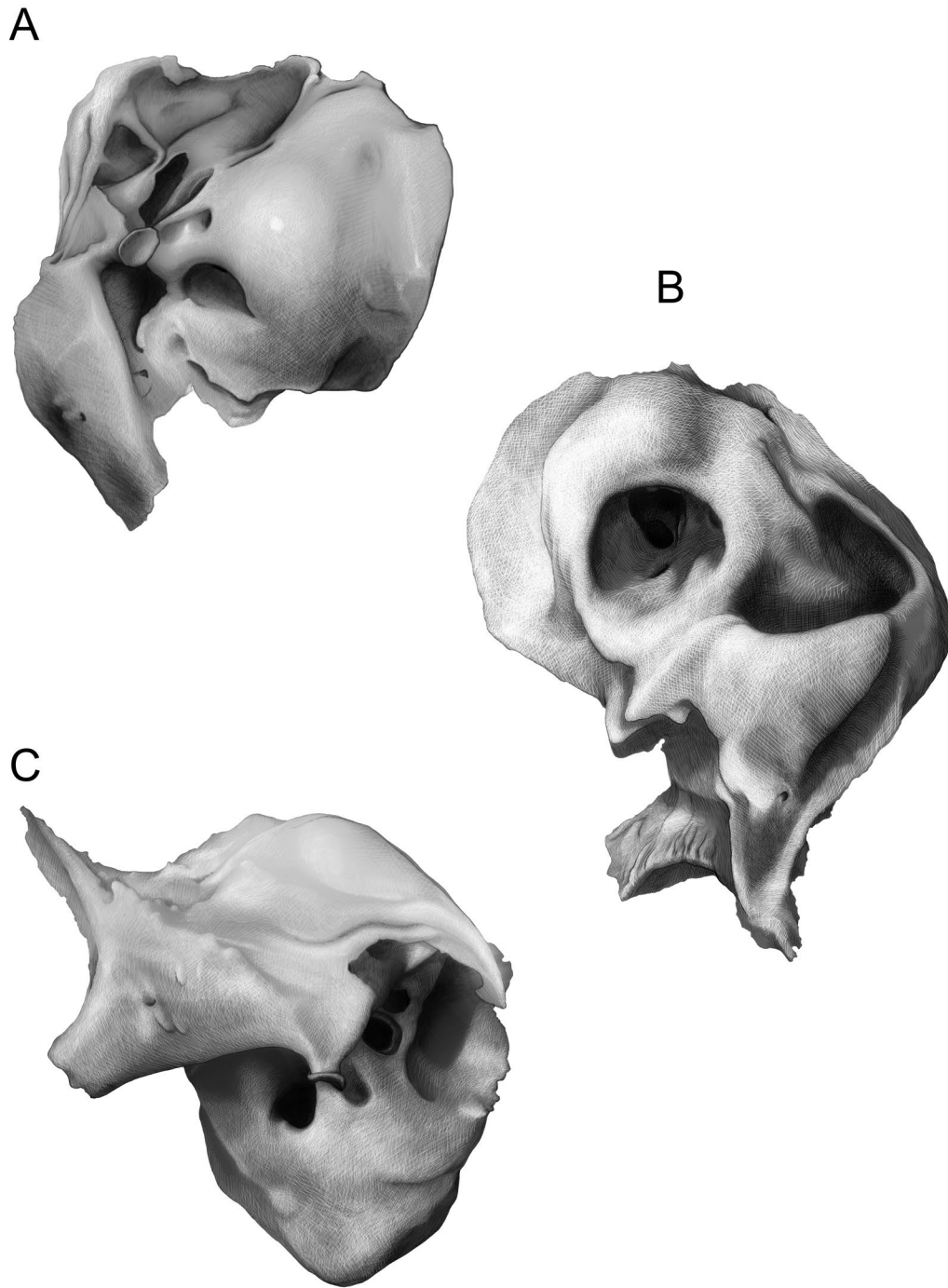
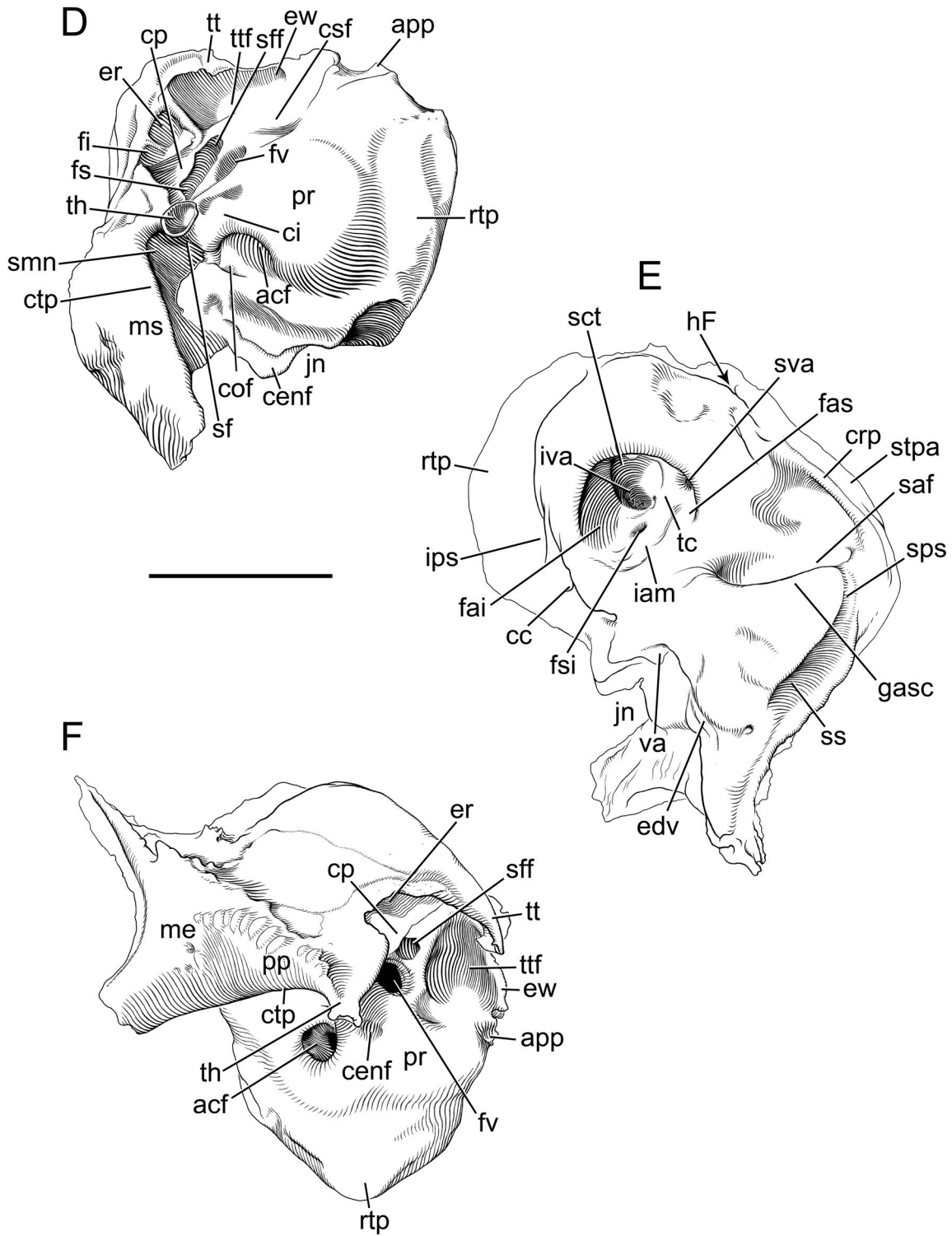


Fig. 21—Isolated right petrosal of juvenile *Nandinia binotata*, AMNH 201513. **A, D**, ventral; **B, E**, dorsal; **C, F**, lateral views. Scale = 5 mm. Abbreviations: **acf**, aperture of cochlear fossula; **app**, apex parties petrosi; **cc**, cochlear canaliculus; **cenf**, facet for caudal entotympanic; **ci**, crista interfenestralis; **cof**, cochlear fossula; **cp**, crista parotica; **crp**, crista petrosa; **csf**, cavum supracochleare floor; **ctp**, caudal tympanic process; **edv**, sulcus for vein accompanying endolymphatic duct; **er**, epitympanic recess; **ew**, epitympanic wing; **fai**, foramen acousticum inferius; **fas**, foramen acousticum superius; **fi**, fossa incudis; **fs**, facial sulcus; **fsi**, foramen singulare; **fv**, fenestra vestibuli; **gasc**, gyrus of anterior semicircular canal; **hF**, hiatus Fallopii; **iam**, internal acoustic meatus; **ips**, sulcus for inferior petrosal sinus; **iva**, inferior vestibular area; **jn**, jugular notch; **me**, mastoid exposure; **ms**, mastoid shelf; **pp**, paroccipital process; **pr**, promontorium; **rtp**, rostral tympanic process; **saf**, subarcuate fossa; **sct**, spiral cribriform tract; **sf**, stapedius fossa; **sff**, secondary facial foramen; **smn**, stylomastoid foramen; **sps**, sulcus for superior petrosal sinus; **ss**, sulcus for sigmoid sinus; **stpa**, surface for tentorial process of parietal; **sva**, superior vestibular area; **tc**, transverse crest; **th**, tympanohyal; **tt**, tegmen tympani; **tff**, tensor tympani fossa; **va**, vestibular aqueduct.



of the foramen acusticum inferius is occupied by the even more deeply recessed spiral cribriform tract (“sct” in Fig. 21E), which spirals down more than two full coils to reach the foramen centrale cochleare, the orifice of the canal of the modiolus (not visible in the figures).

The oval-shaped aperture of the subarcuate fossa leads into a deep depression that is expanded compared to its aperture in all directions except ventrally. This depression houses the paraflocculus of the cerebellum. The gyrus of the anterior semicircular canal (“gasc” in Fig. 21E) forms the rim of the aperture on the medial, dorsal, and lateral margins, with a small part of the ventromedial margin formed by the crus commune, the conjoined anterior and posterior semicircular canals. Extending ventromedially from the lateral margin of the subarcuate fossa aperture is a sharp crest, the crista petrosa (“crp” in Fig. 21E), which ends opposite the dorsal margin of the internal acoustic meatus. Based on the *in situ* left petrosal of this specimen, the crista petrosa contacts the tentorial process of the parietal (Fig. 14). Ventromedial to the terminus of the crista petrosa on the anterior face of the petrosal is the slit-like orifice for the greater petrosal nerve, the hiatus Fallopii (“hf” in Fig. 21E). A groove runs ventromedially from the hiatus Fallopii to the exit of the nerve from the cranial cavity (see Basisphenoid). The bone dorsolateral to the hiatus represents the ossified prefacial commissure of the chondrocranium. The broad, flat surface posterior to the hiatus and ventrolateral to the crista petrosa contacts the tentorial process of the parietal (“stpa” in Fig. 21E).

Posterior to the subarcuate fossa is a sharp, dorsally directed triangular spine that represents the endocranial surface of the mastoid exposure. A convex, triangular surface lies between the base of the spine and the dorsal margin of the subarcuate fossa aperture. A sharp crest runs on the lateral margin of the triangular surface and continues onto the lateral edge of the endocranial surface of the mastoid exposure. Medial to this crest is a vascular sulcus approximately 6 mm in length. The anterior third of this sulcus is narrower than the remainder, which we interpret as containing a different vessel, the superior petrosal sinus (“sps” in Fig. 21E), based on the *C. lupus familiaris* (Evans 1993); the larger posterior two-thirds contains the sigmoid sinus (“ss” in Fig. 21E). Both of these are distributaries of the transverse sinus, which runs in the ossified tentorium. At the posterior end of the sulcus for the sigmoid sinus, a much smaller sulcus runs anteromedially a short distance (“edv” in Fig. 21E) and ends in a slit-like opening into the pars canicularis that is hidden in direct dorsal view, the vestibular aqueduct (“va” in Fig. 21E). Presumably, this sulcus transmitted a vein accompanying the endolymphatic duct in the vestibular aqueduct. The surface dorsal to the sulcus leading to the vestibular aqueduct contacts the exoccipital in the intact skull.

Medial to the vestibular aqueduct is a posteromedially directed triangular spine with a gently concave surface medial to it. The concave surface is the jugular notch (“jn” in Fig. 21E), the petrosal’s contribution to the margin of

the jugular foramen (“jf” in Fig. 14). Between the jugular notch and the internal acoustic meatus is a slit-like opening into the pars cochlearis that is hidden in direct dorsal view, the cochlear canaliculus (“cc” in Fig. 21E), which contains the perilymphatic duct. Anteromedial to the cochlear canaliculus is a shallow, longitudinal sulcus for the inferior petrosal sinus along the medial surface of the pars cochlearis (“ips” in Fig. 21E). In dorsal view, the rostral tympanic process underlies this sulcus. The dorsomedial surface of the rostral tympanic process contacts the basioccipital in the intact skull.

**Lateral view (Figs. 21C, F).**—In lateral view, the pars canicularis lies lateral and posterodorsal to the pars cochlearis. On the posterior surface of the pars canicularis is the part of the mastoid exposure visible in lateral view (“me” in Fig. 21F). This three-sided exposure has concave posterior and ventral margins and an anterior margin that is gently convex. The ventral margin is the caudal tympanic process. The lateral margin contacts the squamosal; just dorsal to the midpoint of the lateral margin is a notch that is an interdigitation in the suture with the squamosal. Where the ventral and lateral margins meet is a prominence, the paroccipital process (“pp” in Fig. 21F). Lateral to the posterior margin is a narrow concavity that is the part of the mastoid exposure visible on the occiput. It contacts the exoccipital in the intact skull, confirmed by remnants of the ex- and supraoccipital suture that are preserved on the right side of AMNH 201513.

The remainder of the pars canicularis visible in lateral view is covered by the squamosal with one small exception noted below. The superior margin of the squamosal surface is formed by the crest marking the lateral margin of the sulci for the sigmoid and superior petrosal sinuses as described above. The anterior margin is the tegmen tympani, which curves anteroventrally and tapers to a point. Anteriorly, the ventral margin represents the lateral walls of the epitympanic recess and fossa incudis, and posteriorly, the unnamed crest running lateral to the crista parotica as described above. It is the ventralmost margin of this unnamed crest that is exposed and not covered by squamosal in the intact skull. This crest ends ventrally at the tympanohyal, posterior to which is the stylomastoid notch.

The main parts of the pars cochlearis visible in lateral views are the promontorium and the rostral tympanic process. The promontorium is rounded, whereas the medially placed rostral tympanic process is flatter and more vertical. The two are also distinguished by color; the pneumatized rostral process is more transparent and appears darker than the denser bone of the promontorium. The lateral view shows that the rostral process runs nearly the entire anteroposterior length of the promontorium and has its maximum depth opposite the crista interfenestralis.

Three openings in the pars cochlearis are visible: from posteroventral to anterodorsal, the aperture of the cochlear fossula, the fenestra vestibuli, and the secondary facial foramen. The fenestra vestibuli is recessed within the vestib-

ular fossula. Anterior to the fenestra vestibuli and secondary facial foramen is the epitympanic wing. The concavity in the epitympanic wing is the origin for the tensor tympani muscle.

**AMNH 207730, Newborn.**—Neither the pars cochlearis nor the pars canicularis are fully ossified, but the former is nearly almost fully formed, whereas the latter is almost entirely absent (Figs. 3C–D, 5C–D, 13). In ventral view (Fig. 13), the pars cochlearis is represented by the promontorium. The length of the promontorium as measured from the anterior pole to the ventral lip of the round window is 15.6% of greatest skull length; in the adult, AMNH 51503, it is 6.8%. The length of the promontorium in the newborn is 79.7% that of AMNH 51503.

The promontorium has no indication that the rostral tympanic process has yet formed; the ventromedial surface is smooth (Fig. 13). The anterior pole is also smooth with no indication of the apex parties petrosa. The fenestra vestibuli is nearly complete (and occupied by the stapes); only a narrow seam in the posterior border remains unossified. A vestibular fossula is lacking. A slight lateral bulge on the crista interfenestralis is present (hidden by the ectotympanic in Fig. 13). The cochlear canaliculus is an open groove with lappets partially flooring it, and not an enclosed canal as it is in the adult, in the posteromedial corner of the promontorium (“spd” in Fig. 13); consequently, the fenestra cochleae has not yet formed and the opening at the back of the promontorium is actually a perilymphatic foramen (“pf” in Fig. 13).

Lateral to the promontorium is a narrow shelf, the tegmen tympani (Fig. 13), which is all that is ossified of the pars canicularis. Anterior to the fenestra vestibuli is a small, shallow depression, the tensor tympani fossa. The secondary facial foramen lies lateral to the fenestra vestibuli. Between these two structures is the floor of the cavum supracochleare. The petrosal is not ossified lateral to the cavum supracochleare floor in the area that in the adult holds the epitympanic recess and is roofed by the epitympanic wing of the parietal.

**Others.**—Additional details of the petrosal are taken from specimens with the ectotympanic and entotympanics removed: AMNH 51448(L), 51503(R), CM 3693(R), 16103, AMNH 51445(R), CM 5097(R). The right ear region of the adult, CM 3693, is illustrated in situ in ventral and oblique lateral views in Figures 15 and 20, and is the main specimen for comparisons with the juvenile, AMNH 201513, below.

In ventral view (Fig. 15), a notable difference of the pars cochlearis when compared with the isolated petrosal of the juvenile, AMNH 201513, is the presence of two subtle grooves on the promontorium. At the posterolateral corner of the rostral tympanic process is a broad groove, 2 mm in length, that curves anterolaterally (“icg” in Fig. 15). From the anterior end of this broad groove, a second narrower groove diverges and curves across the promonto-

rium (“pg” in Fig. 15). This narrow groove ends anteriorly at a small foramen (“dpn” in Fig. 15) between the projection from the anterolateral aspect of the promontorium (described above) and the basisphenoid. The promontorial projection is larger in the adult than in the juvenile (cf. Figs. 15 and 21A, D). This foramen leads into a short canal in the basisphenoid that opens into the groove for the nerve of the pterygoid canal. In light of its position and connections, we infer that the tiny groove on the promontorium marks the course of the deep petrosal nerve, one of the internal carotid nerves (“dpc” in Fig. 18). Within the basisphenoid canal this nerve joins with the greater petrosal nerve to form the nerve of the pterygoid canal (“gpn” and “npc” in Fig. 18, respectively). The short, broad groove accommodates the internal carotid artery and nerves (see Hunt 1989: fig. 7). The internal carotid artery and nerves enter the middle ear anterolateral to the jugular foramen (“ica” and “icn” in Fig. 18; see Caudal Entotympanic below). After the divergence of the deep petrosal nerve, the internal carotid artery and nerves continue anteriorly lateral to the rostral tympanic process, without leaving any distinct impression. Upon checking the study sample, we found only one other specimen with the tiny groove on the promontorium for the deep petrosal nerve, the left side of CM 42728; the right side of this specimen has the dried nerve in place. However, more specimens have the short, broad internal carotid groove (AMNH 51488(L), CM 6374(L), AMNH 51448(L), CM 5157(R), CM 59495, AMNH 134969, CM 59496(L), 3693, 42726, 42282, 69365, AMNH 51510).

Another notable difference is the size of the facet for the caudal entotympanic. In CM 3693 (Fig. 15) as in other adults, a continuous facet curves on the posterior half of the promontorium, starting at the crista interfenestralis, extending behind the aperture of the cochlear fossula, running along the anterolateral margin of the jugular foramen, and ending at the posterior margin of the rostral tympanic process. The facet is narrow lateral to the aperture of the cochlear fossula but broad elsewhere. In the isolated petrosal of the juvenile, AMNH 201513, the part of the facet that is on the crista interfenestralis is disconnected from the remainder and the part directly posterior to the promontorium is very narrow (Figs. 21A, D). The left sides of two other juveniles, AMNH 51486 and CM 6374, also have isolated facets on the crista interfenestralis, but these are absent on the right sides of these specimens and bilaterally in the remaining juveniles.

Posterior to the round window, AMNH 201513 has a raised rim that marks the boundary of a distinct cochlear fossula (Figs. 21A, D). Only three other specimens, all adults, CM 42727, 69365 (Fig. 22), and 69366 (Fig. 16B), have a similar structure, although the rim is not as raised or the fossula as large. In contrast, the area posterior to the round window is flat in CM 3693 (Figs. 15, 16A) as in the remaining juveniles and adults (Fig. 19). On the right side of CM 3693, part of the secondary tympanic membrane is preserved in a sulcus internal to the ventral rim of the aperture

of the cochlear fossula, confirming that the opening on the promontorial surface is not the fenestra cochleae. The fenestra vestibuli in CM 3693 has a stapedial ratio of 1.59, similar to that of 1.57 seen in AMNH 201513. Twelve specimens from the study sample, including juveniles and adults, preserve an ossified cartilage of Paauw, which is a small, rod-shaped element in the tendon of the stapedius muscle near its attachment to the stapes. It is likely that this element's absence in the remaining sample is a preservation bias.

In AMNH 201513, the epitympanic recess is triangular and separated by a well-developed wall from the tensor tympani fossa (Figs. 21A, D), but in CM 3693 it is circular and is continuous with the tensor tympani fossa anteromedially (Figs. 15, 16A). The vast majority of the study sample resembles the latter condition; only two specimens, both adults, have a wall between the epitympanic recess and tensor tympani fossa, AMNH 51448 and 134969.

Compared to AMNH 210513, the tegmen tympani in CM 3693 has a much larger anteroventral surface, possessing two distinct facets that connect with depressions on the skull base anteriorly (Fig. 15). The larger medial concavity for the malleolar hook of the rostral process of the malleus faces into the depression on the epitympanic wing of the parietal, and the smaller, lateral, flat surface faces into the depression on the epitympanic wing of the squamosal for the anterior crus of the ectotympanic. All adults where the tegmen can be observed show the same pattern as CM 3963, suggesting that the simpler tegmen in AMNH 201513 is a consequence of its earlier ontogenetic age. Unfortunately, the condition in the remaining juveniles is obscured by *in situ* auditory ossicles and ectotympanics.

Two other features showing ontogenetic differences are the size of the rostral tympanic process and the mastoid shelf. In the two youngest juveniles, AMNH 51471 and 51486, the rostral tympanic process reaches as far ventrally as the rostral entotympanic. However, in an older juvenile, CM 6374, and the adult sample, the rostral tympanic process extends farther ventrally than the rostral entotympanic. In the juveniles, the mastoid shelf, the ventral part of the mastoid exposure, is narrow and not set off from the braincase wall by a distinct crest (Fig. 23). In contrast, the wider mastoid shelf in the adults is delimited from the braincase wall by a strong crest (Figs. 19-20).

We recorded the incidence of three features of the petrosal across the study sample:

(1) Crista parotica and crista interfenestralis contact: (a) absent - AMNH 51486, CM 6371, 6374, AMNH 201513, CM 2356, AMNH 51503 (Fig. 17), CM 69366(L), AMNH 51510, CM 16103, AMNH 51494(R), CM 5097, AMNH 51513; (b) present -- AMNH 51471, 51488, CM 42281, 5157, 59497, 59495, 59496, 42727, 3693, 42725, 42726, 42282, 69365, 69366(R), AMNH 51494(L), CM 42728. These two cristae are either separated by a distinct gap (Fig. 17) or they are in contact, with two specimens showing both conditions. When the two cristae meet, a canal dorsal to the contact is created, which gives passage to two

structures: dorsolaterally, the facial nerve (see Fig. 18) and ventromedially, the tendon of the stapedius muscle. In this condition, the stapedius fossa and muscle are extratympanic, outside of the middle-ear space. This distribution shows no obvious correlation with geography, ontogeny, and sex.

(2) Caudal tympanic process of the petrosal: (a) vertical ridge extending posteromedially from the tympanohyal - AMNH 51471 (Fig. 22), 51486, CM 6371, AMNH 51488 (Fig. 23), CM 6374, AMNH 201513 (Figs. 14, 21A, D), CM 59497, 42727, 42726; (b) oblique triangular process contributing to the posterolateral border of the stylomastoid notch - CM 42281, 5157, AMNH 51503, CM 59495 (Fig. 19), AMNH 134969, 51494; (c) flat - AMNH 51448, CM 2356, 59496, 42725, 3693 (Fig. 15), 42282, 69365 (Fig. 24), 69366, AMNH 51510, CM 16103, 42728, 5097, AMNH 51513. The juveniles all have a vertical ridge continuous with the base of the paracondylar process of the exoccipital. Initially, we thought this might relate to the narrower mastoid shelf in the juveniles (cf. Figs. 14 and 19). However, the juvenile condition is present in the adult sample, along with two variants, a flat caudal tympanic process that cannot be differentiated from the mastoid shelf and a triangular process walling the stylomastoid notch.

(3) Stapedius fossa: (a) open posteriorly - AMNH 201513 (Figs. 14, 21A, D), CM 42281, 2356, 59497, AMNH 51503 (Fig. 17), CM 59495, AMNH 134969(R), CM 42725, 42726, 42282, AMNH 51510, CM 16103, AMNH 51445, CM 5097(L), AMNH 51513; (b) walled posteriorly - AMNH 51486, CM 6371, AMNH 51488, CM 6374, AMNH 51448, CM 5157, AMNH 134969(L), CM 59496, 42727, 3693 (Fig. 16A), 69365 (Fig. 24), 69366 (Fig. 16B), AMNH 51494, CM 42728, 5097(R). The two conditions express the condition of the posterior wall of the stapedius fossa; it is either open to the area medial to the caudal tympanic process or separated from that area by a wall. This distribution shows no obvious correlation with geography, ontogeny, and sex.

#### Rostral Entotympanic ("re" in figures)

The paired rostral entotympanics are small osseous elements that occupy the anteromedial corner of the ear region, contributing to the formation of the auditory bulla. Of the 30 specimens studied, the rostral entotympanic is totally absent in eight, including the newborn, AMNH 207730 (Fig. 13), in which it has likely not formed, and the most advanced juvenile, AMNH 201513 (Fig. 14), where it was likely not preserved, which we assume is also true for the remaining six specimens. Therefore, we interpret the rostral entotympanic to be consistently present in juvenile and adult *N. binotata*. The rostral entotympanic is present in the principal adult, CM 59495 (Fig. 19), but is largely hidden by the ectotympanic. Therefore, we base our primary description of the rostral entotympanic on a specimen lacking the ectotympanic.

Entotympanics occur in various placentals as indepen-

dent ossifications, the majority of which have cartilaginous precursors. They form within the fibrous membrane of the tympanic cavity (MacPhee 1979, 1981), the connective tissue membrane that extends from the skull base to the ectotympanic. Two types of entotympanics were identified by Klaauw (1922) in several developing placentals based on their positions in the middle-ear wall, rostral and caudal. The existence of cartilage in the posterior wall of the auditory bulla in *N. binotata* has been recognized since Flower (1869). Kampen (1905) applied the term entotympanic to this cartilage, but also noted that a bony part was present near the carotid foramen (his foramen lacerum anticum). Klaauw (1931) noted Kampen's (1905) observations on *N. binotata*, but did not apply his terms rostral and caudal entotympanics to the bony and cartilaginous elements, respectively. The first to do so was Hunt (1974), who identified the osseous anterior element as a rostral entotympanic and the cartilaginous posterior one as a caudal entotympanic. We follow Hunt's characterization here.

**CM 69366.**—The rostral entotympanic is vaguely J-shaped in ventral view, with the curved base of the J contacting the anterior pole of the promontorium and the tail lying on the anterior slope of the rostral tympanic process (Fig. 16B). The tail does not completely cover the anterior slope, ending opposite the middle of the fenestra vestibuli. The curved anterior margin of the J abuts the basisphenoid, fitting into a facet in the bone (described above), and forming the posterior border of the carotid foramen (Fig. 16B). The ventral surface of the base of the J is concave (Fig. 16B); the internal carotid artery runs through this concavity to reach the carotid foramen (Fig. 18). Lateral to this concavity, the rostral entotympanic is raised as a low crest that increases in height anteriorly and that forms the medial border of the foramen for the deep petrosal nerve (Fig. 16B). This crest on the rostral entotympanic fills in a gap between crests on the bones anterior and posterior to it. The crest on the basisphenoid underlies the nerve of the pterygoid canal, and the crest on the petrosal marks the anteroventral limit of the tensor tympani fossa (see Fig. 20). The medial margin of the rostral entotympanic is raised, and it abuts the muscular tubercle on the basioccipital except in its most posterior extreme where it curves laterally (Fig. 16B). This posterior part of the rostral entotympanic is taller than the muscular tubercle and is visible in direct medial view, whereas the remainder of the rostral entotympanic is not taller than and hidden by the muscular tubercle. On the ventral surface of the rostral entotympanic, extending the length of the tail of the J, is an irregular sulcus ("ces" in Fig. 16B), ending anteriorly at the carotid foramen. Based on observations of specimens that preserve the cartilaginous caudal entotympanic in place, either in whole or part, e.g., AMNH 51471 (Fig. 25), 51513, CM 42728, this sulcus can be concluded to house the base of the anterior part of the caudal entotympanic. The surface of the rostral entotympanic lateral to this sulcus slopes dorsally toward the promontorium.

**Others.**—The newborn, AMNH 207730, has no indication of the rostral entotympanic or its site of attachment on the skull base (Fig. 13). Given the fine state of preservation of that specimen, it can be confidently assumed this element had failed to ossify by the newborn stage. It may be that it is even a failure to chondrify, given that cartilaginous rostral entotympanics have not yet been reported in occur in prenatal carnivorans (Wible 1984).

The youngest juvenile specimens (e.g., AMNH 51471, 51486) have a rostral entotympanic resembling that described above for CM 69366. The most noticeable difference is the greater medial exposure of the rostral entotympanic in the juveniles (Fig. 25); the muscular tubercle is not as developed as in CM 69366, exposing most of the medial aspect of the rostral entotympanic. The degree of medial exposure in most of the specimens with adult dentitions resembles that in CM 69366. There are some specimens that more closely resemble the juvenile condition, including males and females (e.g., CM 2356, 59495, AMNH 51510), and others with no medial exposure whatsoever (e.g., CM 3693, AMNH 42282).

Hunt (1987:34) noted that "study of the sample of 30 individuals of *Nandinia* from Niapu, Zaire, indicates a broad range in RE [rostral entotympanic] form, with many individuals retaining a sharp elongate ridge on the lateral face of RE. This ridge appears to be a vestige of the lateral septate margin of an originally ventrally concave RE of the type seen in *Dinictis*." We reported above the presence of such a lateral ridge in CM 69366, in line with ridges on the basisphenoid and petrosal adjacent to the foramen for the deep petrosal nerve (Fig. 16B). A review of our study sample shows that a lateral ridge is absent in the juveniles and present in the adults. However, the condition in CM 69366 differs from the other instances in its proximity to the foramen for the deep petrosal nerve. The usual adult condition for the lateral ridge is a more medial position in line with the course of the internal carotid artery and nerve en route to the carotid foramen (see Fig. 18; Hunt 1987: fig. 16B). Addressing the proposed homology between the structures in the nimravid *Dinictis* and in *N. binotata* is beyond the scope of the present study, but we reiterate that the structure in *N. binotata* is part of the internal carotid housing, not a partition of the middle ear.

#### Caudal Entotympanic ("ce" in figures)

The paired caudal entotympanics are the principal elements of the medial and posterior walls of the auditory bullae, filling the gap between the ectotympanic and petrosal. Since Flower (1869), the substance of the caudal entotympanic of *N. binotata* has been said to be cartilage. In museum osteological collections, it is difficult to distinguish cartilage from dense connective tissue, both of which are usually removed by dermestid beetle activity or by hand. The dense bullar wall tissue found in some *N. binotata* (Figs. 23, 25) is very thick and resembles tissue

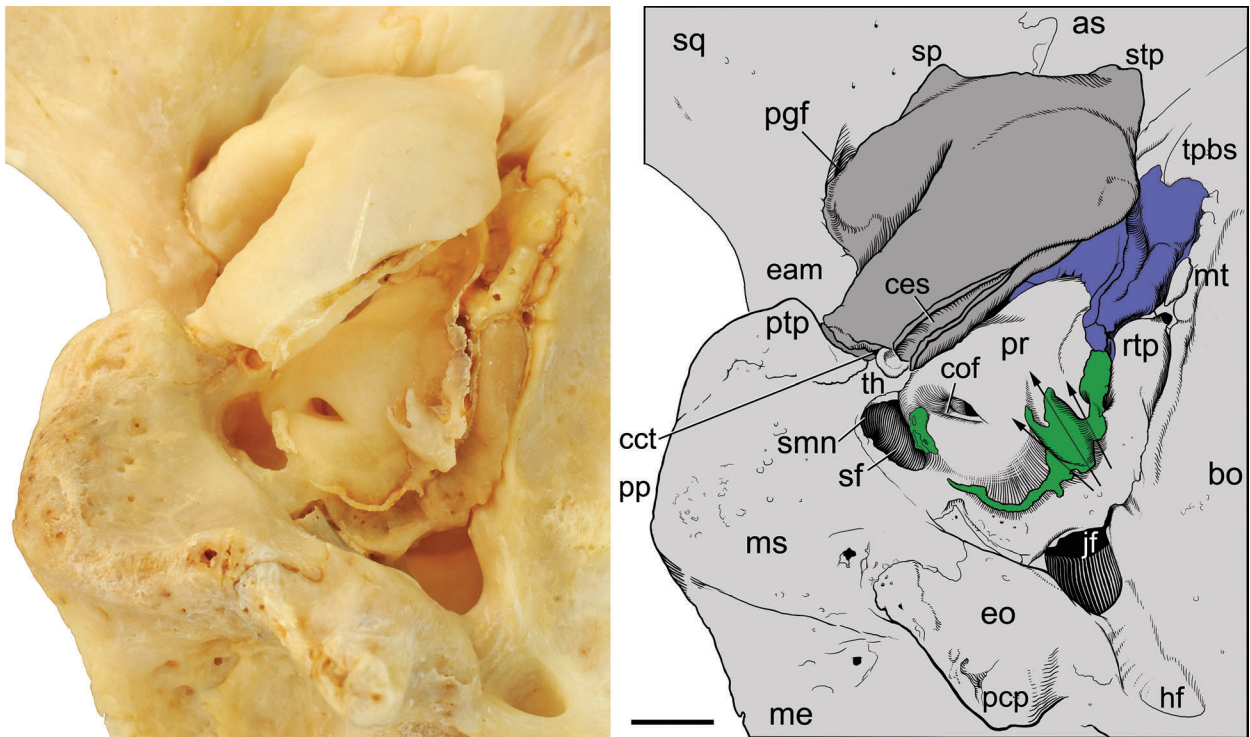


Fig. 22—Right basicranium of adult *Nandinia binotata*, CM 69365, in ventral view (reversed from left). In the drawing, the green is the ossified caudal entotympanic, the blue is the rostral entotympanic, and the dark gray is the ectotympanic (and the rostral process of the malleus). Arrows indicate three canals that run between the caudal entotympanic and petrosal (for contents see Caudal Entotympanic); the lateral and smallest canal is partially hidden by the middle one. Scale = 2 mm. Abbreviations: **as**, alisphenoid; **bo**, basioccipital; **cct**, canal for chorda tympani nerve; **ces**, sulcus for caudal entotympanic; **cof**, cochlear fossula; **eam**, external acoustic meatus; **eo**, exoccipital; **hf**, hypoglossal foramen; **jf**, jugular foramen; **me**, mastoid exposure of petrosal; **ms**, mastoid shelf; **mt**, muscular tubercle; **pcp**, paracondylar process of exoccipital; **pgf**, postglenoid foramen; **pp**, paroccipital process of petrosal; **pr**, promontorium of petrosal; **ptp**, posttympanic process of squamosal; **rtp**, rostral tympanic process of petrosal; **sf**, stapedius fossa; **smn**, stylomastoid notch; **sp**, spine of rostral process of malleus; **sq**, squamosal; **stp**, styliiform process; **tpbs**, tympanic process of basisphenoid.

preserved in the cartilaginous nasal septum in our sample. Additionally, the facets on the petrosal, ectotympanic, and rostral entotympanic for the caudal entotympanic are too large to simply accommodate dense connective tissue; clearly, a structure of considerable girth occupied these facets. In agreement with prior authors (e.g., Hunt 1974, 1987), we identify these dense tissues in specimens of *N. binotata* as cartilage. However, we found evidence of ossification within the dense tissue in numerous specimens. Of the 30 specimens studied by us, 17 have dense and/or osseous tissue in the position of the caudal entotympanic; of these, 14 have some ossification, although in only one, AMNH 51488, is most of the medial and posterior walls completed by a thin layer of bone (Fig. 24; see also Hunt 1987: fig. 16A). In light of the high incidence of some ossification, we interpret the caudal entotympanic to be a complex structure, partially cartilaginous and partially osseous, although the position and amount of ossification varies considerably. During the course of this study, we had an incident with one specimen, CM 69366, that might explain the variability of caudal entotympanic ossifications in other specimens studied by us as well as by Hunt (1974, 1987). Initially, CM 69366 had a sizeable ossifi-

cation associated with the entrance of the internal carotid artery into the posteromedial aspect of the right middle ear (Fig. 16B), but at some point this element simply fell off. Apparently, this structure was only loosely attached to the petrosal. This is likely not a unique occurrence, and thus we assume that adult specimens that appear to have no ossified portion of the caudal entotympanic actually fail to preserve the delicate ossified elements. We conclude that some ossification is generally present in the otherwise cartilaginous caudal entotympanic.

**AMNH 51488.**—On both sides, the caudal entotympanic is represented by a thin layer of bone that fills in the gap between the ectotympanic ventrally and the petrosal and rostral entotympanic dorsally in the posterior half of the medial and the posterior bullar walls (Fig. 24). There is an irregular hole in the middle of the posterior bullar wall, but Hunt (1987:33) reported that this was caused by damage during preparation. The bony layer in the medial wall on the left side (not figured) extends farther anteriorly than that on the right. The dorsal attachment is J-shaped (see Fig. 16B), first contacting the posterior half of the sulcus-like facet on the rostral entotympanic, next the broad ven-

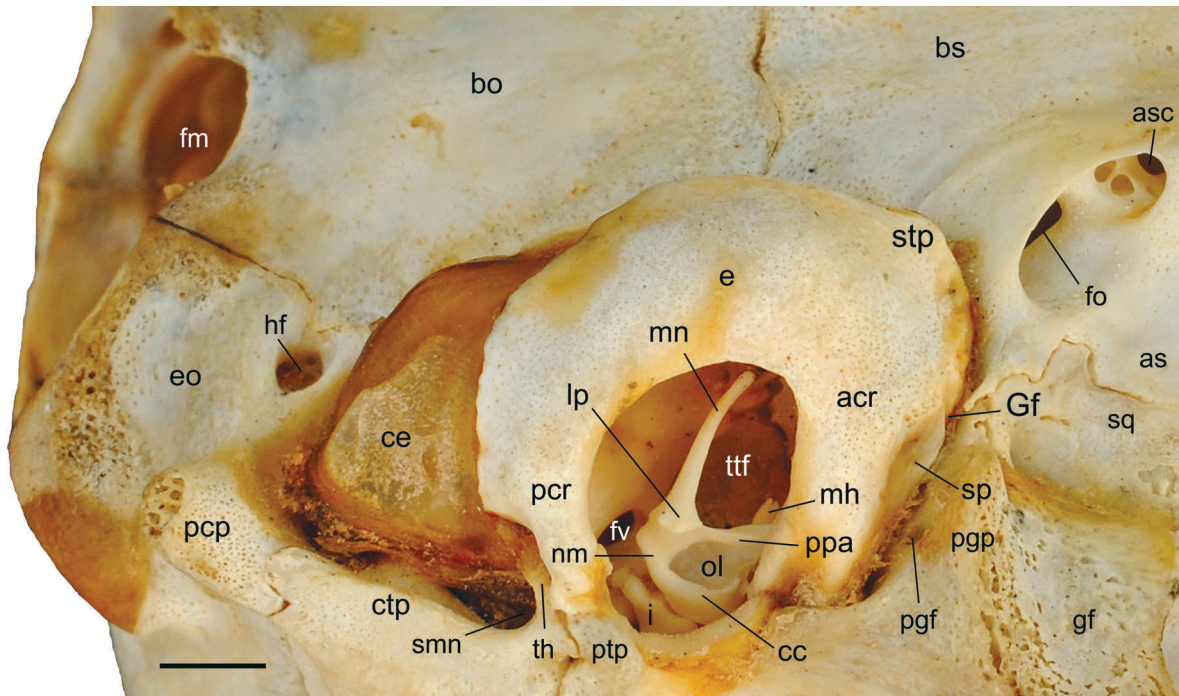


Fig. 23—Left basicranium of juvenile *Nandinia binotata*, AMNH 51471, in oblique lateral view. The malleus and incus have shifted slightly posterodorsally from their in life position. Scale = 2 mm. Abbreviations: **acr**, anterior crus of ectotympanic; **as**, alisphenoid; **asc**, caudal opening of alisphenoid canal; **bo**, basioccipital; **bs**, basisphenoid; **cc**, capitular crest; **ce**, caudal entotympanic; **ctp**, caudal tympanic process of petrosal; **e**, ectotympanic; **eo**, exoccipital; **fm**, foramen magnum; **fo**, foramen ovale; **fv**, fenestra vestibuli; **Gf**, Glaserian fissure; **gf**, glenoid fossa; **hf**, hypoglossal foramen; **i**, incus; **lp**, lateral process; **mh**, malleal hook; **mn**, manubrium; **nm**, malleal neck; **ol**, osseous lamina; **pcp**, paracondylar process of exoccipital; **pcr**, posterior crus of ectotympanic; **pgf**, postglenoid foramen; **pgp**, postglenoid process; **ppa**, pars processus anterioris; **ptp**, posttympanic process of squamosal; **smn**, stylomastoid notch; **sp**, spine of rostral process of malleus; **sq**, squamosal; **stp**, styliform process; **th**, tympanohyal; **ttf**, tensor tympani fossa.

tral surface of the rostral tympanic process behind that, then curving laterally along the broad facet on the back of the pars cochlearis, and subsequently curving anteriorly to end at the crista interfenestralis. Its ventral attachment (Fig. 24) is similarly shaped within a sulcus on the ventral surface of the corresponding parts of the ectotympanic (see Ectotympanic, below). The anterior margin is free and broken; other specimens (e.g., AMNH 51471) have membrane that fills in the entire sulcus on the rostral entotympanic and has a curved anterior border (Fig. 25), accommodating the exit of the auditory tube and nerve of the pterygoid canal from the middle ear and also the entrance of the ascending pharyngeal artery. Posterolaterally is another free edge, where the bony caudal entotympanic forms the posterior margin of the exit of the facial nerve, transforming the stylomastoid notch into a stylomastoid foramen (“smf” in Fig. 24). Here, the bone is attached to the posterior aspect of the tympanohyal. Additional attachments are on the anterior face of the caudal tympanic process and the paracondylar process of the exoccipital (Fig. 24). The middle-ear space posterior to the ectotympanic that is floored by the caudal entotympanic is the posterior chamber (Pocock 1916; Klaauw 1931). It is continuous with the anterior chamber, which overlies the ectotympanic.

From studies by Pocock (1916), Davis and Story (1943), Chapuis (1966), Hunt (1974), and Wible (1984),

*N. binotata* is known to have a transpromontorial course to the internal carotid artery. The artery enters the middle ear just in front of the jugular foramen. Dried blood in AMNH 51488 along the posterior slope of the rostral tympanic process marks the position of the posterior carotid foramen (“pcf” in Fig. 24). The bony caudal entotympanic forms the ventral margin of this opening.

**Others.**—The newborn, AMNH 207730, has no indication of the caudal entotympanic or its sites of attachment on the skull base, some of which are not even ossified: for example, the area posterior to the aperture of the cochlear fossula (Fig. 13). In other carnivorans, Wible (1984) reported the caudal entotympanic in late fetal specimens of *F. catus*, *C. lupus familiaris*, and *Aonyx cinerea* (Illiger, 1815) but did not find one in a newborn *Ursus arctos* Linnaeus, 1758.

Seventeen specimens, including AMNH 51488 (Fig. 24), show varying signs of the presence of caudal entotympanics. One specimen, AMNH 51471, has a thick membrane that fills in the posterior and medial bullar walls. In the medial wall (Fig. 25), the membrane is taut; in the posterior wall (Fig. 23), the membrane has folds in it, which we interpret as resulting from the collapse of a more convex entity during life. Because of the coverage by the membrane, it is not possible to confirm the existence

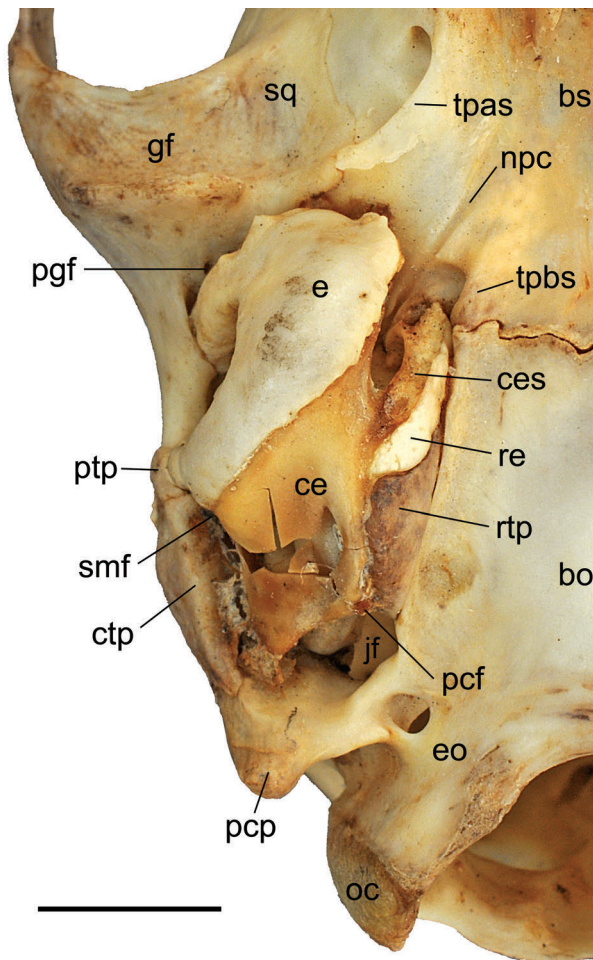


Fig. 24—Right basicranium of juvenile *Nandinia binotata*, AMNH 51488, in ventral view. A small crack is present in the posterior aspect of the tympanic process of the alisphenoid. Scale = 5 mm. Abbreviations: **bo**, basioccipital; **bs**, basisphenoid; **ce**, caudal entotympanic; **ces**, sulcus for caudal entotympanic; **ctp**, caudal tympanic process of petrosal; **e**, ectotympanic; **eo**, exoccipital; **gf**, glenoid fossa; **hf**, hypoglossal foramen; **jf**, jugular foramen; **npc**, groove for nerve of pterygoid canal; **oc**, occipital condyle; **pcf**, posterior carotid foramen; **pcp**, paracondylar process of exoccipital; **pgf**, postglenoid foramen; **ptp**, posttympenic process of squamosal; **rev**, fossa for rectus capitis ventralis; **re**, rostral entotympanic; **rtp**, rostral tympanic process of petrosal; **smf**, stylomastoid foramen; **sq**, squamosal; **tpas**, tympenic process of alisphenoid; **tpbs**, tympenic process of basisphenoid.

of any ossification in the caudal entotympanic. Fourteen others show evidence of ossification, with AMNH 51488 the most heavily ossified (Fig. 24). At the other extreme are four specimens (CM 42281, 59496, 42282, 16103) with only a small piece of bone in the caudal entotympanic facet on the back of the petrosal, lateral to the aperture of the cochlear fossula.

In between these two extremes are several other positions where bone is found. (1) CM 42725, AMNH 51510, CM 42728, and AMNH 51513 have more substantial bone filling or nearly filling the caudal entotympanic facet on the back of the petrosal either as a single piece or multiple

pieces. (2) CM 59497, 59495 (Fig. 19), 42725, 42726(R), 42728, 69365 (Fig. 22), 69366 (Fig. 16B), and AMNH 51513 have bone around the entrance of the internal carotid artery and nerves into the middle ear. In four of these, CM 59495 (Fig. 19), 42725, 69365 (Fig. 22), and AMNH 51513, this is a substantial canal (2 mm in length) accompanied by one or two smaller parallel canals. Without dissections, we are not entirely certain how to interpret these canals. CM 69365 has three canals (Fig. 22): a large middle canal slightly less than 1 mm in diameter, an intermediate medial canal slightly less than 0.5 mm, and a tiny lateral canal. We interpret the middle and medial canals as for the internal carotid artery and nerves, and the tiny lateral one for the tympanic nerve, a branch of the glossopharyngeal nerve that forms the lesser petrosal nerve anteriorly (see Fig. 18). CM 42725 also has three canals, although its medial and lateral ones are subequal. CM 59495 and AMNH 51513 preserve two canals, but in the former there is a tiny medial one and a large lateral one, while in the latter these are reversed. Are these differences in number of canals preservation biases or variation?

Regarding #2 above, Hunt (1974:33) also described this “small tubular ossification” around the internal carotid artery in *N. binotata*, but he concluded that “this ossification is not formed within the cartilage [caudal entotympanic] but lies medial [sic; it is in fact lateral] to it, and does not represent ossification of the caudal entotympanic.” The specimens studied here show otherwise, as the tubular ossification is continuous with bone within the facet for the caudal entotympanic (Fig. 22).

Another nerve of the middle ear, the auricular branch of the vagus, was found dried in situ in CM 42728; it follows an extratympanic course, between the posterior surface of the caudal entotympanic and the anterior surface of the caudal tympanic process of the petrosal (“abX” in Fig. 18). At the anteromedial aspect of the middle ear, the anterior edge of the caudal entotympanic in AMNH 51471 defines two passageways that are not fully separated (Fig. 25). The anterolateral passageway between the caudal entotympanic, ectotympanic, and alisphenoid is the musculotubal canal (“mtc” in Fig. 25), which transmits the auditory tube and tensor veli palatini muscle in *F. catus* (Davis and Story 1943: fig. 2). The posteromedial passageway between the caudal entotympanic and basisphenoid is the anterior carotid foramen (“acf” in Fig. 25), which transmits the ascending pharyngeal artery in *N. binotata* (Davis and Story 1943; “apa” in Fig. 18). This artery anastomoses with the internal carotid artery in the carotid groove in the basisphenoid (“cg” in Fig. 25).

#### Ectotympanic and Malleus (“e” and “ma” in figures)

The paired ectotympanics provide attachment for the tympanic membranes. The paired mallei articulate with the incudes, have attachments to the tympanic membranes, and are fused to the ectotympanics as early as the juvenile

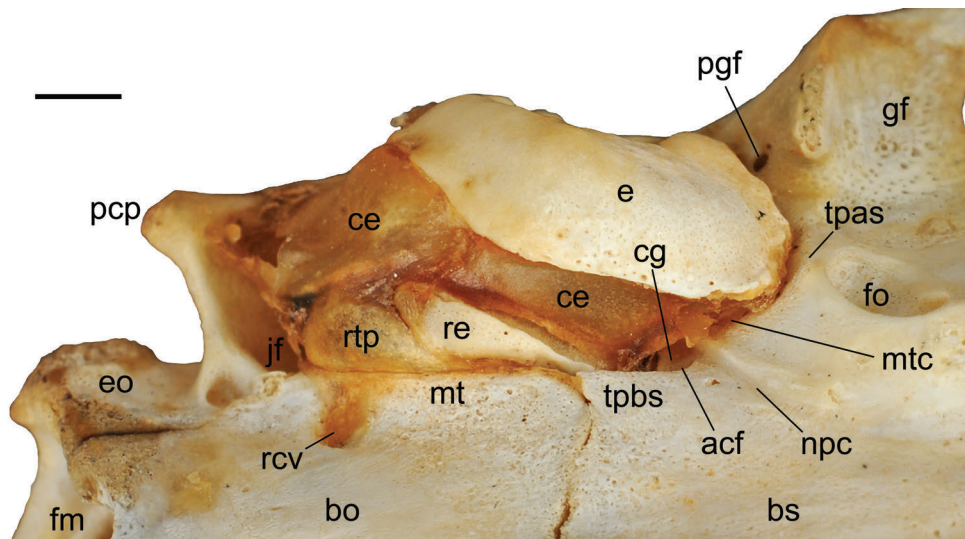


Fig. 25—Right ear region of *Nandinia binotata*, AMNH 51471, in oblique medial view. Scale = 2 mm. Abbreviations: **acf**, anterior carotid foramen; **bo**, basioccipital; **bs**, basisphenoid; **ce**, caudal entotympanic; **cg**, carotid groove; **e**, ectotympanic; **eo**, exoccipital; **fm**, foramen magnum; **fo**, foramen ovale; **gf**, glenoid fossa; **jf**, jugular foramen; **mt**, muscular tubercle; **mtc**, musculotubal canal; **npc**, groove for nerve of pterygoid canal; **pcp**, paracondylar process of petrosal; **pgf**, postglenoid foramen; **rcv**, fossa for rectus capitis ventralis; **re**, rostral entotympanic; **rtp**, rostral tympanic process of petrosal; **tpas**, tympenic process of alisphenoid; **tpbs**, tympenic process of basisphenoid.

stage. Because of the intimate relationship between the ectotympanic and malleus, these two elements are described together. Moreover, because the adult anatomy is best understood from an ontogenetic perspective, we trace these elements from the newborn to the juvenile to the adult. Aspects of the anatomy of these bones were treated in Wible and Spaulding (2012), but are augmented here.

**AMNH 207730, Newborn.**—The ectotympanic is preserved in identical fashion on the left and right sides (Figs. 6C–D), which leads us to conclude that it is in life position. It is a simple, U-shaped ring, although the arms of the U, the anterior and posterior crura, are not perfectly symmetrical (Fig. 13): the posterior crus is more curved than the anterior one. The largest dimension across the anterior and posterior crura is 16.6% of greatest skull length. The tympanic incisure between the crura is substantial and along the lateral margin. The ectotympanic lies close to the horizontal, but its medial margin is more ventrally placed than its lateral extremities. The angulation of the posterior crus from the horizontal plane is around 20°. The outer surface of the ectotympanic is convex, and much of the inner surface is concave forming the sulcus tympanicus, which serves as the attachment site of the tympanic membrane (tympanum); this concavity does not extend to the extremities (this is visible on the anterior crus in Fig. 13). Both crura have parts that are in contact with neighboring bones and parts that are suspended between these contacts (Fig. 13). The outer surface of the anterior crus has two points of contact: on the squamosal posterior to the postglenoid process and on the alisphenoid posterior to the foramen ovale. Passing through the gap between these two

contacts is the tympanic plate of the malleus (“sp” in Fig. 13; see below). The dorsal surface of the posterior crus has a broad contact with the pars cochlearis anteroventral to the round window. Its distal end approaches but does not meet the posttympanic process of the squamosal.

Only the ventral aspect of the malleus is visible (Fig. 13); the dorsal is hidden by the overlying bones and by connective tissue. The medial and lateral aspects are described separately; only the lateral can be shown in the figures. The medial aspect provides the only view of the mallear head: the head is compact with a small capitular spine. Two articular surfaces with the incus are present, with an angle greater than 90° between them; the inferior articular surface is larger than the superior one. Ventral to the head is the extensive osseous lamina (“ol” in Fig. 13), the anterior margin of which is relatively straight. Neither the ventral or posterior margins are raised; however, where these two margins meet is a slight elevation at the manubrial base, which represents the muscular process for the attachment of the tensor tympani. The manubrium has not yet ossified and a small facet marks its point of origin (“mnf” in Fig. 13).

The lateral aspect reveals a well-developed capitular crest (“cc” in Fig. 13) demarcating the head ventrally. It extends ventrally on the neck of the malleus nearly to the manubrial base. The ventral margin of the osseous lamina is very slightly thickened, representing the pars processus anterioris. Extending anteromedially from and perpendicular to the osseous lamina is the narrow, elongate tympanic plate of the rostral process. It runs in a slight depression in the dorsal surface of the anterior crus of the ectotympanic and comes to a point at its distal end, the spine of the

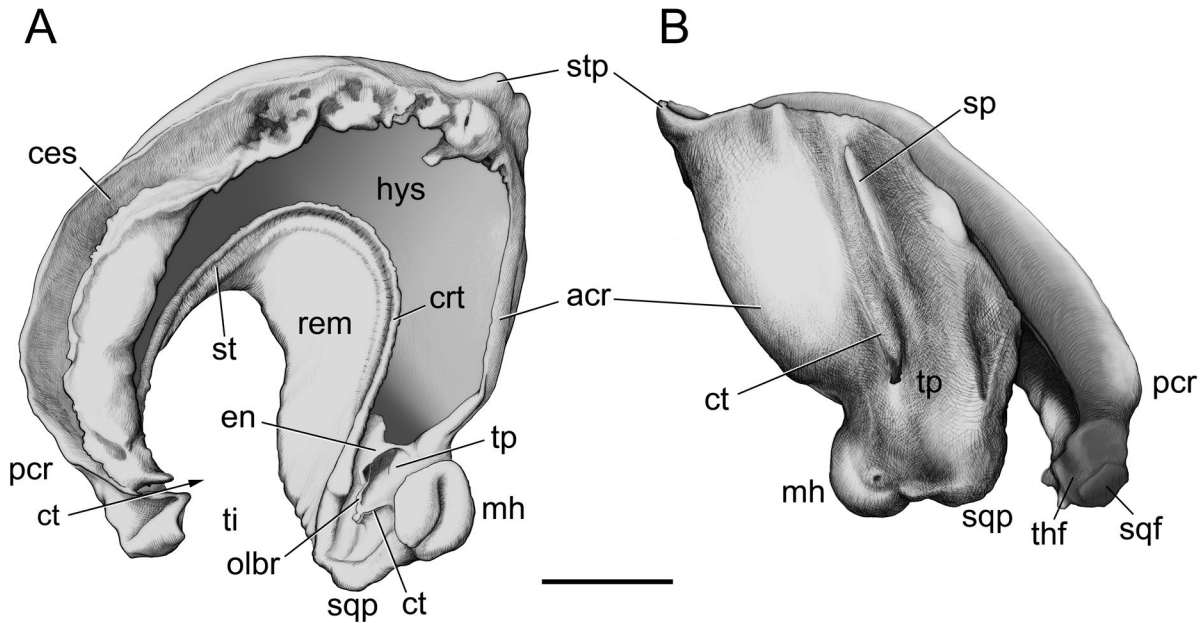


Fig. 26—Isolated right ectotympanic and malleolar tympanic plate of adult *Nandinia binotata*, CM 42728. **A**, medial; **B**, anterior views. Scale = 2 mm. Abbreviations: **acr**, anterior crus; **ces**, sulcus for caudal entotympanic; **crt**, crista tympanica; **ct**, course of chorda tympani nerve; **en**, ectotympanic notch; **hys**, hypotympanic sinus; **mh**, malleolar hook; **olbr**, osseous lamina (broken); **pcr**, posterior crus; **rem**, recessus meatus; **sp**, spine of tympanic plate; **sqf**, facet for squamosal; **sqp**, squamosal process of anterior crus; **stp**, styliiform process; **st**, sulcus tympanicus; **thf**, facet for tympanohyal; **ti**, tympanic incisure; **tp**, tympanic plate of malleus.

tympanic plate (“sp” in Fig. 13). The dorsal surface of the tympanic plate has a shallow concavity, presumably for the chorda tympani nerve, which places the Glaserian fissure between the malleus and squamosal. Extending posteriorly from the medial side of the base of the tympanic plate is a well-developed malleolar hook (“mh” in Fig. 13). The malleolar hook has a thick base, a slightly constricted neck, and a rounded distal end. The dorsal surface of the rounded distal end is connected to the tegmen tympani by connective tissue.

**AMNH 51471, Juvenile.**—The ectotympanic and malleus are illustrated in oblique lateral view in Figure 23. The ectotympanic is still U-shaped, but expanded compared to the newborn condition, with most of the expansion into the tympanic floor. The only part of the ectotympanic that is not noticeably expanded is the distal end of the posterior crus, which remains rod-like (“pcr” in Fig. 23). The anteromedial corner of the anterior crus (“acr” in Fig. 23) shows the greatest expansion, resulting in a weak styliiform process (“stp” in Figs. 23, 25). The styliiform process and the ectotympanic posterior to it contribute to the floor of the musculotubal canal, the exit of the auditory tube from the middle ear (“mtc” in Fig. 25). The ectotympanic is not as horizontal as in the newborn; the angulation of the posterior crus from the horizontal is around 35°. The tympanic incisure is narrower than in the newborn (Fig. 23). At its greatest dimension across the anterior and posterior crura, the ectotympanic is 13.8% of greatest skull length.

The skull length of the juvenile is 2.1 times that of the newborn, and its ectotympanic length is 1.7 times.

The anterior crus contacts the squamosal. Its distal end occupies a facet on the squamosal reported above in specimens lacking the ectotympanic (“acr” in Fig. 14, 16A, 17). Medial to this, the distal end has a dorsally directed process that falls short of the tegmen tympani; this observation is based on another juvenile, CM 6371, which is missing the main part of the malleus that obscures this feature in other specimens. In addition to this distal end contact, the anterior crus also meets the epitympanic wing of the alisphenoid and/or squamosal (see below). The distal end of the posterior crus contacts the tip of the post-tympanic process of the squamosal and the ventral aspect of the tympanohyal (Fig. 23). There is a small gap between the posterior crus and tympanohyal that transmits the chorda tympani nerve into the middle ear (see “cct” in Fig. 22). The caudal entotympanic, in the form of a thick membrane, is attached to the dorsal aspect of the outer circumference of the ectotympanic between the exit of the auditory tube and the tympanohyal (Figs. 23, 25).

Only the lateral surface of the malleus is fully accessible (Fig. 23). The head is demarcated by a very pronounced capitular crest, which forms the lateral wall of a deep pocket; the osseous lamina forms the medial wall. The capitular crest extends onto the neck (“nm” in Fig. 23), ventral to which is a well-developed lateral process (“lp” in Fig. 23) at the manubrial base. The thin manubrium (“mn” in Fig. 23) gently curves anteroventromedially from the ma-

nubrial base. A distinct pars processus anterioris (“ppa” in Fig. 23) forms the ventral margin of the osseous lamina; it disappears from view anteriorly, dorsal to an eminence on the inner circumference of the ectotympanic bone, which we called the ectotympanic notch (Wible and Spaulding 2012). The anterior margin of the osseous lamina lies just medial to the distal end of the anterior crus of the ectotympanic at its contact with the squamosal. Posteriorly, on the medial aspect of the malleus and adjacent to the neck is the well-developed muscular process (not visible in Fig. 23), which tapers to a rounded distal end. Anteriorly, medial to the pars processus anterioris is the malleolar hook of the tympanic plate (“mh” in Fig. 23); it is not distinguished from the ectotympanic by sutures, and its main dorsal contact is with the epitympanic wing of the parietal.

Of the remainder of the tympanic plate, only its distal end is visible (“sp” in Fig. 23). In the newborn, the spine extends well anterior to the ectotympanic (Fig. 13), but in the juvenile the spine lies on the anterior face of the anterior crus (Fig. 23). It is not distinguished from the ectotympanic by sutures but by structure; the surrounding bone is riddled with tiny holes, whereas the tympanic plate is not. The tympanic plate between the spine and the malleolar hook is hidden by the ectotympanic. Anteromedial to the tip of the spine is the Glaserian fissure (“Gf” in Fig. 23), which is between the spine, ectotympanic, and squamosal.

Anterior to the malleolar hook, the anterior crus has another contact with the skull base, the details of which are hidden by the intact ectotympanic. In specimens with the ectotympanic removed, several patterns are present. As noted above, in CM 42281, 2356, and 3693 (Fig. 16A), the fossa for the malleolar hook on the epitympanic wing of the parietal continues onto a concave surface on the epitympanic wing of the alisphenoid, which houses the anterior crus of the ectotympanic. CM 69366 (Fig. 16B), AMNH 51494, CM 42728, 5097, and AMNH 15103 have a similar arrangement, but the surface is formed by the epitympanic wing of the squamosal in the first, and the sutures between the alisphenoid and squamosal are fused in the remainder. Lastly, in AMNH 201513 (Fig. 14), 51448, 51503, the epitympanic wing of the alisphenoid anterior to the malleolar hook facet on the parietal is flat with no specific evidence of ectotympanic contact.

**CM 59495, Principal Adult.**—The ectotympanic is preserved bilaterally (Figs. 6A–B), but the tympanic plates are the only parts of the mallei present. The angulation of the posterior crus from the horizontal is around 40°, slightly higher than in the juvenile. At its largest dimension across the anterior and posterior crura, the ectotympanic is 11.6% of greatest skull length. The skull length of the adult is 1.4 times the size of the juvenile and its ectotympanic length is almost equal, at 1.1 times larger. The ectotympanic of the adult generally resembles that of the juvenile, although the styliform process is more prominent (Fig. 19). The spine of the tympanic plate in the adult is not distinguishable from the anterior crus by its bone structure, as noted for

the juvenile above; however, the spine is more prominent in the adult (Fig. 19).

**Others.**—Of the 30 specimens examined, 26 retain at least one ectotympanic, and in five of this subsample one or both ectotympanics are detached from the skull. With the exception of the newborn and juvenile described above, the tympanic plate is fused to the ectotympanic. The non-tympanic plate portion of the malleus (that is, the head, neck, manubrium, and osseous lamina) is present on at least one side in 13 specimens.

The isolated right ectotympanic and the fused tympanic plate of CM 42728 are illustrated in medial (intratympanic) and anterior (extratympanic) views in Figure 26. The medial view shows a deep hollow between the outer and inner circumference of the ectotympanic (“hys” in Fig. 26A); this accommodates the cavum tympani (the middle-ear cavity), and therefore represents a hypotympanic sinus (Klaauw 1931). The outer circumference has an irregular surface for the attachment of the caudal entotympanic extending from the styliform process nearly to the distal end of the posterior crus; the posterior half of this surface is a sulcus with dried tissue in it (“ces” in Fig. 26A). The outer circumference of the anterior crus is smooth and rounded. The inner circumference is set off from the deep hollow by a distinct crest, the crista tympanica (“crt” in Fig. 26A). Adjacent to all but the anterolateral part of the crista tympanica is a narrow sulcus, the sulcus tympanicus (“st” in Fig. 26A). These two structures, the crest and sulcus, mark the attachment of the tympanic membrane. Adjacent to the central part of the sulcus tympanicus is bone that floors the proximal part of the external acoustic meatus, forming a recessus meatus (“rem” in Fig. 26A).

Distally, the posterior crus narrows to a block-like end. Visible in anterior view are two small facet surfaces lying at an obtuse angle to each other (Fig. 26B): a smaller posterior facet that is directed dorsally and contacts the squamosal, and an anterior one that is more anteriorly directed and contacts the tympanohyal (“sqf” and “thf” in Fig. 26B, respectively). The dorsal surface of the posterior crus medial to these facets has a small channel that indicates the course of the chorda tympani nerve (arrow in 26A); this is closed to form a canal by the tympanohyal.

The anterior crus is a composite structure, part ectotympanic and part malleus. Although the two are solidly fused, their boundaries can be inferred based on the arrangement of these structures in the newborn and juvenile. In medial view, the malleus is represented by the broken stub of the osseous lamina, the proximal tympanic plate, and the malleolar hook (“olbr,” “tp,” and “mh” in Fig. 26A, respectively). The broken stub of the osseous lamina would have connected posteriorly to the rest of the malleus (including its head, neck, and manubrium; see Fig. 22). The proximal tympanic plate is flat and lies perpendicular to the osseous lamina stub. It is pierced at its dorsal end by a canal for the chorda tympani nerve (“ct” in Fig. 26A). The proximal tympanic plate runs ventromedially through a notch in the

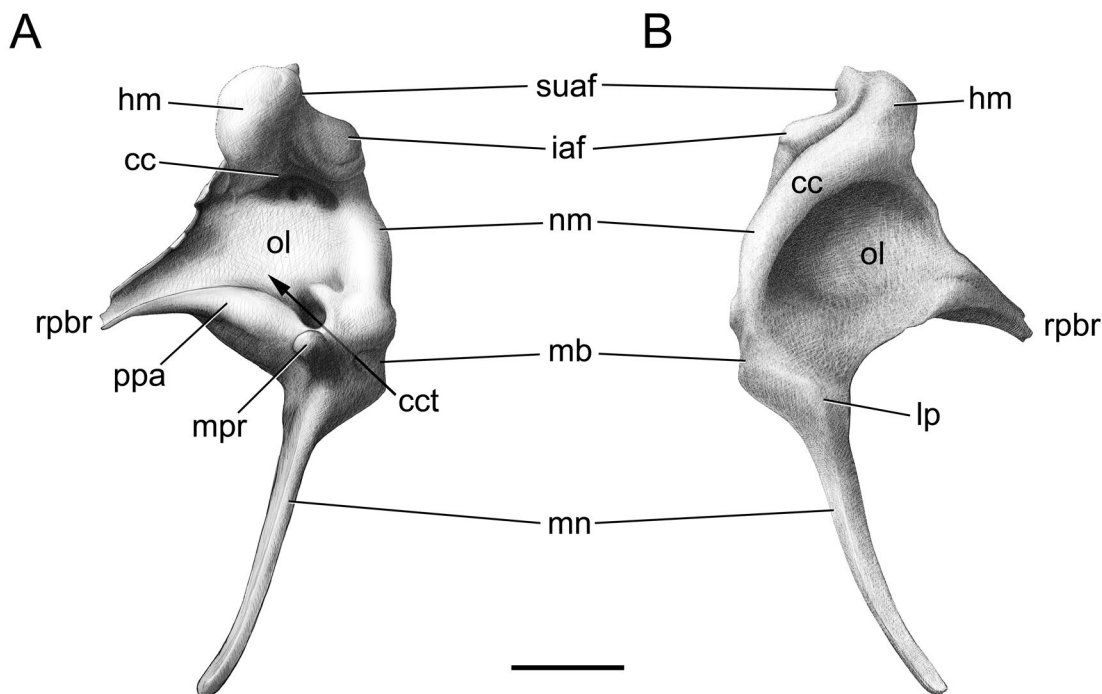


Fig. 27—Left malleus of juvenile *Nandina binotata*, CM 6371, minus the tympanic plate of the rostral process. **A**, medial; **B**, lateral surfaces. The break on the anterior aspect of the malleus is between the base of the rostral process and the tympanic plate (not shown), which is fused to the ectotympanic. Scale = 1 mm. Abbreviations: **cc**, capitular crest; **cct**, canal for chorda tympani; **hm**, head of malleus; **iaf**, inferior incudal articular facet; **lp**, lateral process; **mb**, manubrial base; **mn**, manubrium; **mpr**, muscular process; **nm**, neck of malleus; **ol**, osseous lamina; **ppa**, pars processus anterioris; **rpbr**, rostral process (broken); **suaf**, superior incudal articular facet.

ectotympanic (“en” in Fig. 26A), and its distal continuation appears on the anterior surface (marked by “tp” in Fig. 26B). The canal for the chorda tympani nerve also penetrates the tympanic plate from the medial to the anterior surface (“ct” in Fig. 26B). The malleolar hook in medial view is a rounded prominence that juts out from the proximal tympanic plate (“mh” in Fig. 26A). Its dorsomedial surface contacts the facet on the epitympanic wing of the parietal (“mhf” in Figs. 15, 16A).

In anterior view (Fig. 26B), the malleus is represented by the malleolar hook and distal tympanic plate. As in the medial view, the malleolar hook juts out from the dorsomedial surface of the distal end of the anterior crus. The distal tympanic plate includes the other orifice of the canal for the chorda tympani nerve, the groove extending from it, and a thickened area of bone adjacent (ventral) to it. The last of these ends in a point at its anteroventral end (“sp” in Fig. 26B), which is interpreted as the spine of the tympanic plate. It differs from the spine in the other specimens described above in that it does not extend anterior to the ectotympanic (see Figs. 13, 19, 22).

The remaining principle feature of the anterior crus is another prominence found on the dorsolateral aspect of its distal end, near the malleolar hook. It is more massive but less distinct than the malleolar hook. This process is termed here the squamosal process of the anterior crus (“sqp” in Fig. 26), as it fits into the facet on the squamosal in the

postglenoid region (“acrif” in Figs. 14–15, 16A, 17).

The non-tympanic plate portion of the left malleus of the juvenile, CM 6371, was removed from the middle ear and is illustrated in medial and lateral views in Figure 27. The head (“hm”) is round and its posterior surface is dominated by three incudal facets: two superiorly and one inferiorly (“suaf” and “iaf”). Details of the facets are not visible in the figures, but are detailed here. The angulation between the superomedial and inferior facets is approximately 110°, whereas that between the superolateral and inferior facets is 120°. Both of the superior facets are flat, with the medial one larger than the lateral one. The two are distinguished by their slightly different orientations. The inferior facet is saddle-shaped and longer than wide; the two superior facets together are wider than long. The head is demarcated by a capitular crest (“cc”), which is more prominent on the lateral surface where it extends along the neck (“nm”) to the manubrial base (“mb”). Ventral to the head is the osseous lamina (“ol”), which is slightly convex on the medial side and concave on the lateral. The ventral margin of the osseous lamina has a well-developed pars processus anterioris (“ppa”) on the medial side, but this is absent on the lateral. The pars processus anterioris extends onto the broken proximal part of the rostral process (“rp”). On the medial side at the manubrial base is a well-developed muscular process (“mpr”) for the tensor tympani; this process has a broad base and a cylindrical

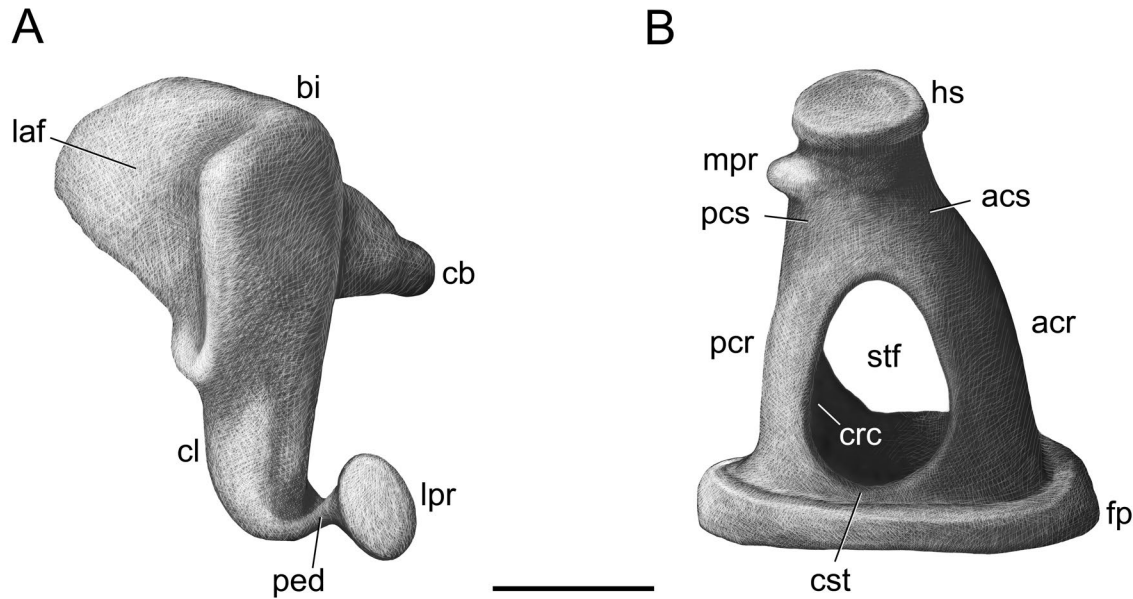


Fig. 28—Auditory ossicles of adult *Nandinia binotata*. **A**, left incus of CM 69366 in posteromedial view; **B**, left stapes of CM 42728 in ventral view. Scale = 1 mm. Abbreviations: **acr**, anterior crus of stapes; **acs**, shoulder of anterior crus; **bi**, body of incus; **cb**, crus breve; **cl**, crus longum; **crc**, crural sulcus; **cst**, crista stapedis; **fp**, footplate of stapes; **hs**, head of stapes; **laf**, lateral articular facet; **lpr**, lenticular process; **mpr**, muscular process for stapedius muscle; **pcr**, posterior crus of stapes; **pcs**, shoulder of posterior crus; **ped**, pedicle; **stf**, stapedia foramen.

tip. Just dorsal to the muscular process is a short canal for the chorda tympani (“cct”). Extending from the manubrial base is the manubrium (“mn”), which is anteroposteriorly constricted, is broadest at its base, and tapers distally. On the lateral surface, the dorsal limit of the manubrium is marked by the prominent lateral process (“lp”), which indicates the dorsalmost attachment of the tympanum to the manubrium.

#### Incus (“i” in figures)

The paired incudes are the middle of the three auditory ossicles; the incus articulates both with the malleus and stapes. Twenty specimens have at least one incus preserved. Two specimens, CM 69366 and AMNH 51513, have left incudes that are isolated from the other ossicles within the epitympanic recess and provide a view of all surfaces. The left incus of CM 69366 is photographed in ventral view in Figure 16B and drawn in ventromedial view in Figure 28A.

The body of the incus (“bi” in Fig. 28A) is dominated by the complex articular surfaces for the malleus. The lateral articular facet is convex and half-moon shaped (“laf” in Fig. 28A). The larger medial articular facet is more quadrangular and complex, with a concave posterior half and a convex anterior half (hidden from view in Fig. 28A). Extending posterodorsally from the body is the short process, crus breve (“cb” in Fig. 28A). It is cylindrical, tapering distally, and held in the fossa incudis on the skull base via the posterior ligament. The left side of CM 69366,

where the incus is missing, clearly shows that the posterior ligament attaches to the squamosal via a facet on a low prominence in the lateral wall of the fossa incudis. Extending posteroventrally from the body is the long process, crus longum (“cl” in Fig. 28A). In the left incus in AMNH 51513, the crus breve is 94% the length of the crus longum and the angle between the two is 100°. The crus longum likewise tapers distally, but it is more dorsoventrally compressed. At its distal end, the process turns medially at 90° to form the short pedicle (“ped” in Fig. 28A), which is anteroposteriorly flattened. The pedicle ends as a small foot, the lenticular process (“lpr” in Fig. 28A), with a flat oval surface that articulates with the head of the stapes.

#### Stapes (“s” in figures)

The paired stapedes are the third and final auditory ossicles. The stapes articulates with the incus and is held in the fenestra vestibuli of the petrosal by the annular ligament. Eighteen specimens have at least one stapes remaining. The vast majority are positioned within the fenestra vestibuli and, therefore, hard to see (Fig. 16B). In two specimens, AMNH 51513 and CM 42728, the stapedes have fallen out of the fenestra vestibuli and are isolated from the other ossicles exposing the entire ventral surface, making this the only surface that can be described. The left stapes of CM 42728 is drawn in ventral view in Figure 28B.

The head of the stapes (“hs” in Fig. 28B) is very narrow and set off from the rest of the bone by a slight rim. The incudal articular surface is oval and flat, mirroring that of

the lenticular process. The anterior and posterior crura meet adjacent to the head to form the shoulders of the crura (“acs” and “pcs” in Fig. 28B), which are only slightly broader than the head. The ventral aspect of the posterior shoulder has a small muscular process for the attachment of the stapedius muscle (“mpr” in Fig. 28B). Medial to the shoulders, the two crura (“acr” and “pcr” in Fig. 28B) diverge slightly from each other as they extend to the footplate (“fp” in Fig. 28B). The oval opening outlined by the shoulders, crura, and footplate is the stapedia (intracranial) foramen (“stf” in Fig. 28B). The surface of each crus facing the stapedia foramen is concave, representing the crural sulcus (“crc” in Fig. 28B). The edges that delimit the crural sulcus continue from each crus across the footplate as a low crista stapedis (“cst” in Fig. 28B). The footplate is oval, slightly broader anteriorly, and extends outward from the crura and cristae. It is flat on both its medial and lateral surfaces; the former faces into the inner ear and the latter into the stapedia foramen.

### Occipital Complex

The bones of the occipital complex contribute to the formation of the basicranium, occiput, and braincase. Typically, the mammalian occipital complex is composed of four ossifications: the median basioccipital on the skull base, the paired exoccipitals that are posterolateral to the basioccipital on the skull base and extend to the ventrolateral occiput, and the median supraoccipital that lies on the occiput and roof of the braincase. This same pattern is reported by Evans (1993) based on study of an extensive ontogenetic series of the beagle. Not all mammals follow this pattern; humans, for example, have four centers at birth, but seven in prenatal stages (Standring 2008).

Only three specimens of *N. binotata*, the newborn and two juveniles, AMNH 207730 (Figs. 4C–D, 6C–D, 29C–D), 51471 (Figs. 23, 25), and 51486, preserve sutures fully delimiting all four occipital ossifications. Remnants of the sutures between the exoccipitals and supraoccipitals are preserved in three other juveniles: CM 6371, AMNH 51488 and 201513.

### Basioccipital (“bo” in figures)

As noted above, the median basioccipital is separated from the paired exoccipitals in only the newborn, AMNH 207730, and juveniles, AMNH 51471 and 51486. The descriptions in the adult are based on the position of the basioccipital in the newborn and two juveniles.

**CM 59495, Principal Adult.**—The basioccipital is a six-sided element on the skull base (Figs. 6A–B). Its longest side is its anterior suture with the basisphenoid; this gently sinuous suture lies in a transverse plane, just posterior to the anterior limit of the rostral entotympanic. The lateral sides are gently curved, diverging slightly posteriorly, and contact the rostral entotympanic and the pars cochlearis of the pe-

trousal. The posterior extent of the basioccipital in the adult is at the fused sutures with the exoccipitals. Based on juvenile specimens, these sutures run obliquely from just anterior to the jugular foramen to the foramen magnum. Roughly the middle third of the anterior margin of the foramen magnum is basioccipital (note the position of the suture in the juvenile AMNH 51486 in Fig. 23). This anterior margin is a smooth curve, with no indication of an odontoid notch (Figs. 6A–B, 19). Overall, the midline length of the basioccipital is just slightly greater than its maximum width (Figs. 6A–B).

A prominent, funnel-shaped keel occupies the midline of the basioccipital, commencing just posterior to the suture with the basisphenoid and expanding posteriorly (Figs. 6A–B, 19). The surface lateral to the keel is relatively flat, but then turns ventrally abruptly at the lateral margin with the petrosal and rostral entotympanic to form the muscular tubercle (“mt” in Fig. 19). Based on *F. catus* (Jayne 1898; Reighard and Jennings 1935), the space between the keel and muscular tubercle is the place of attachment for the longus capitis muscle. Medial to the posterior end of the muscular tubercle is a small circular fossa (“rcv” in Fig. 19), which provides an attachment surface for the rectus capitis ventralis, again based on *F. catus* (Jayne 1898; Reighard and Jennings 1935).

**AMNH 207730, Newborn.**—As in the adult, the basioccipital is six-sided (Figs. 6C–D), but its overall shape is quite different. Whereas the anterior border is the longest in the adult, it is the shortest in the newborn. The lateral margin is deeply concave and the posterior edge contributes to the jugular foramen; in the adult the lateral edge is more longitudinal and the basioccipital is excluded from the jugular foramen (based on the juvenile, AMNH 51486). The ventral surface of the basioccipital in the newborn is virtually flat, with no muscular tubercle, midline keel, or fossa for the rectus capitis ventralis yet developed.

**Others.**—We recorded the incidence of two features of the basioccipital across the study sample:

(1) Muscular tubercle height: (a) uniform along its length - AMNH 51471 (Fig. 25), 51486, 51488, 51448, CM 5157, 59495, 59496, 42725, 42726, 42282, 69365, 69366, 42728; (b) highest anteriorly - CM 42281, 2356, 59497, AMNH 51503, 134969, CM 3693, AMNH 51510, CM 16103, AMNH 51494, 51445, CM 5097, AMNH 51513; (c) highest posteriorly - CM 6371, 6374, AMNH 201513. This distribution shows no obvious correlation with geography, ontogeny, and sex.

(2) Odontoid notch: (a) present - AMNH 207730 (Figs. 4C–D), 51471, 51486, CM 6371, AMNH 51488, CM 6374, AMNH 201513, 51448, CM 5157, 2356, AMNH 51503, CM 69365, AMNH 51510, 51445, 51513; (b) absent - CM 42281, 59497, 59495 (Figs. 4A–B), AMNH 134969, CM 59496, 42726, 42282, 69366, 16103, AMNH 51494, CM 5097. This distribution shows no obvious correlation with geography, ontogeny, and sex.

We also noted that a keel on the basioccipital is absent

in the newborn, AMNH 207730 (Figs. 4C–D), and younger juveniles (AMNH 51471, 51486, CM 6371, AMNH 51488), but is present in the older juveniles and adults. In addition, a fossa for the rectus capitis ventralis (Figs. 19, 24) is present in nearly the entire study sample; it is absent in the newborn, AMNH 27730 (Figs. 4C–D, 13) and the oldest adult, AMNH 51513. Rather than a depression, three adult specimens have a raised muscle scar, AMNH 134969, CM 42725 and 5097.

#### Exoccipital (“eo” in figures)

As noted above, the paired exoccipitals are unfused with the basi- and supraoccipital in only the newborn, AMNH 207730, and two juveniles, AMNH 51471 and 51486. The descriptions in the adult are supplemented based on these specimens.

**CM 59495, Principal Adult.**—The exoccipital has a horizontal part on the skull base and a vertical part on the occiput. The horizontal part (Fig. 19) is seamlessly fused to the basioccipital anteromedially and contacts the pars canalicularis of the petrosal anteriorly and laterally. It is dominated by the prominent paracondylar process (“pcp” in Fig. 19), which in *F. catus* provides attachment for the digastric and jugulohyoid muscles (Reighard and Jennings 1935). The ventral aspect of the paracondylar process is rounded, but with a smaller, more pointed prominence in its posteroventral surface. Laterally, the paracondylar process abuts the less prominent mastoid shelf of the petrosal. The anterior face of the base of the paracondylar process contacts the petrosal lateral to the jugular foramen (“jf” in Fig. 19). On the ventromedial face of the paracondylar base is the hypoglossal foramen (“hf” in Fig. 19), which has a groove running anteriorly to join with the jugular foramen. Based on AMNH 51486, the exoccipital forms the entire posterior border of the jugular foramen, with no contribution from the basioccipital. The jugular notch of the exoccipital has an anteriorly directed spine that partially subdivides the jugular foramen into a larger anteromedial and a smaller posterolateral opening. The other prominent feature visible ventrally is the occipital condyle (“oc” in Fig. 19). The condyle in ventral view has a claw hammer-shaped outline, with the handle forming the anterior margin of the foramen magnum and the head at the posterolateral corner with the claw directed laterally. The posterior margin of the articular surface is strongly convex. Between the condyle and the paracondylar process is the deep ventral condyloid fossa (“vcf” in Fig. 19). It contains four or five small foramina of uncertain function asymmetrically arranged between the two sides.

The lateral border of the vertical part of the exoccipital contacts the mastoid exposure ventrally and the parietal on the posterior edge of the nuchal crest dorsally. On the left side, near the dorsalmost extent of the parietal on the nuchal crest, is a short, medially directed seam (“\*” in Fig. 29B), which represents a remnant of the suture between the ex- and supraoccipital. Based on the newborn (Figs. 29C–D)

and two juveniles preserving the suture, when unfused it ran obliquely ventromedially from the nuchal crest to the dorsal margin of the foramen magnum, such that the supraoccipital forms the middle third of the dorsal edge of the foramen magnum. Ventral to this sutural remnant are two small foramina; many more of these foramina are present on the supraoccipital (see below). The vertical part of the exoccipital is dominated by the occipital condyle (Figs. 29A–B). The condyle is obliquely oriented, from ventromedial to dorsolateral. It is as tall as the foramen magnum, with its ventral two-thirds forming the lateral border of that opening; its dorsal one-third diverges laterally and does not contribute to that border. Dorsal to the condyle is the dorsal condyloid fossa, a small, shallow depression (“dcf” in Fig. 29B). Within the fossa are small foramina, three on the left and two on the right, which drain into the condyloid canal (see Endocranium below). Ventrolateral to the condyle is the prominent paracondylar process, which in posterior view ends at a sharp anterolaterally directed point.

**AMNH 207730, Newborn.**—The exoccipital differs chiefly from that of the adult in relief. In ventral view (Fig. 13), the paracondylar process is a minor swelling, the occipital condyle is proportionally smaller, and the ventral condyloid fossa is shallow. In posterior view (Figs. 29C–D), the occipital condyle is not as tall as the foramen magnum and the dorsal condyloid fossa is absent. The lateral margin of the exoccipital has no bony contacts due to the lack of ossification to the pars canalicularis of the petrosal.

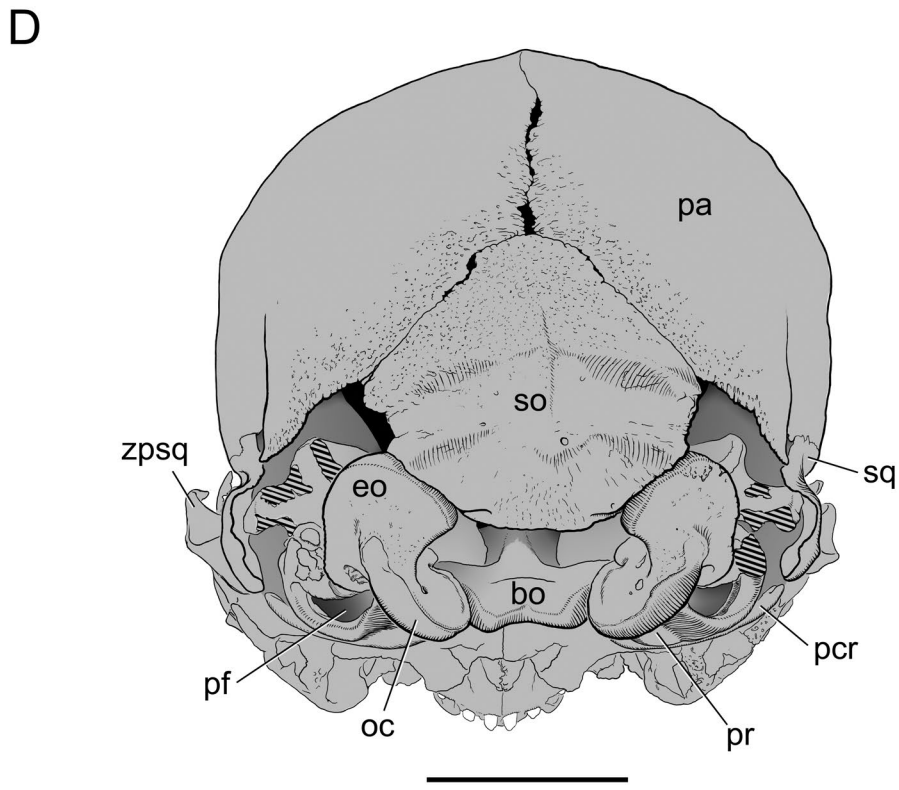
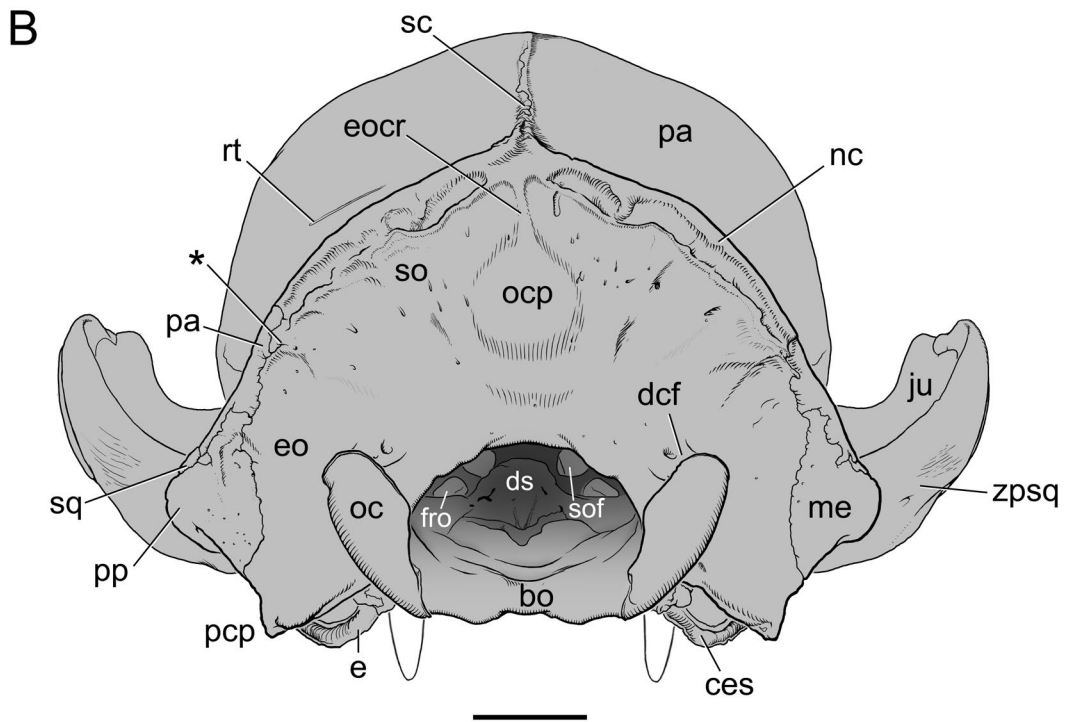
**Others.**—In the series in Figure 1, the ontogeny of the paracondylar process can be traced. The process is barely perceptible in the newborn, AMNH 207730 (see Fig. 13); the ventral extent of the process is even with the neighboring skull base in the juveniles, AMNH 51486 and CM 6374, slightly below the skull base in the younger adult, CM 59495, and well below the skull base in the older adult, CM 42728. Additionally, the occipital condyles gradually increase in height in Figure 1; they are low down on the occiput in the newborn, less than halfway up the foramen magnum in the juveniles, more than halfway in the younger adult, and about even with the dorsal aspect of the foramen magnum in the older adult.

We recorded the incidence of one feature of the exoccipital across the study sample:

(1) Separation of the hypoglossal and jugular foramina: (a) thin bar (equal to or less than the diameter of the hypoglossal foramen) - AMNH 207730 (Fig. 13), 51471 (Fig. 23), 51486 (Fig. 24), CM 6371, AMNH 51488, 201513 (Fig. 14), CM 42281, 2356, 5157, AMNH 51503, CM 59496, 42727, AMNH 51513; (b) thick bar (greater than the diameter of the hypoglossal foramen) - CM 6374, AMNH 51448, CM 59497, 59495 (Fig. 19), AMNH 134969, CM 3693 (Fig. 15), 42725, 42726, 42282, 69365, 69366, AMNH 51510, CM 16103, AMNH 51494, 51445, CM 5097. This distribution shows no obvious correlation with geography, ontogeny, and sex.



Fig. 29—Skulls of *Nandinia binotata* in occipital view. **A, B**, adult, CM 59495; **C, D**, newborn, AMNH 207730. \* indicates a remnant of the suture between the ex- and supraoccipital. Scale = 5 mm. Abbreviations: **bo**, basioccipital; **ces**, sulcus for caudal entotympanic on ectotympanic; **dcf**, dorsal condyloid fossa; **ds**, dorsum sellae; **e**, ectotympanic; **eo**, exoccipital; **eoctr**, external occipital crest; **fro**, foramen rotundum; **ju**, jugal; **me**, mastoid exposure of petrosal; **nc**, nuchal crest; **oc**, occipital condyle; **ocp**, occipital protuberance; **pa**, parietal; **pcp**, paracondylar process of exoccipital; **pcr**, posterior crus of ectotympanic; **pf**, perilymphatic foramen; **pp**, paroccipital process of petrosal; **pr**, promontorium of petrosal; **rt**, foramen for ramus temporalis; **sc**, sagittal crest; **so**, supraoccipital; **sof**, sphenorbital fissure; **sq**, squamosal; **zpsq**, zygomatic process of squamosal.



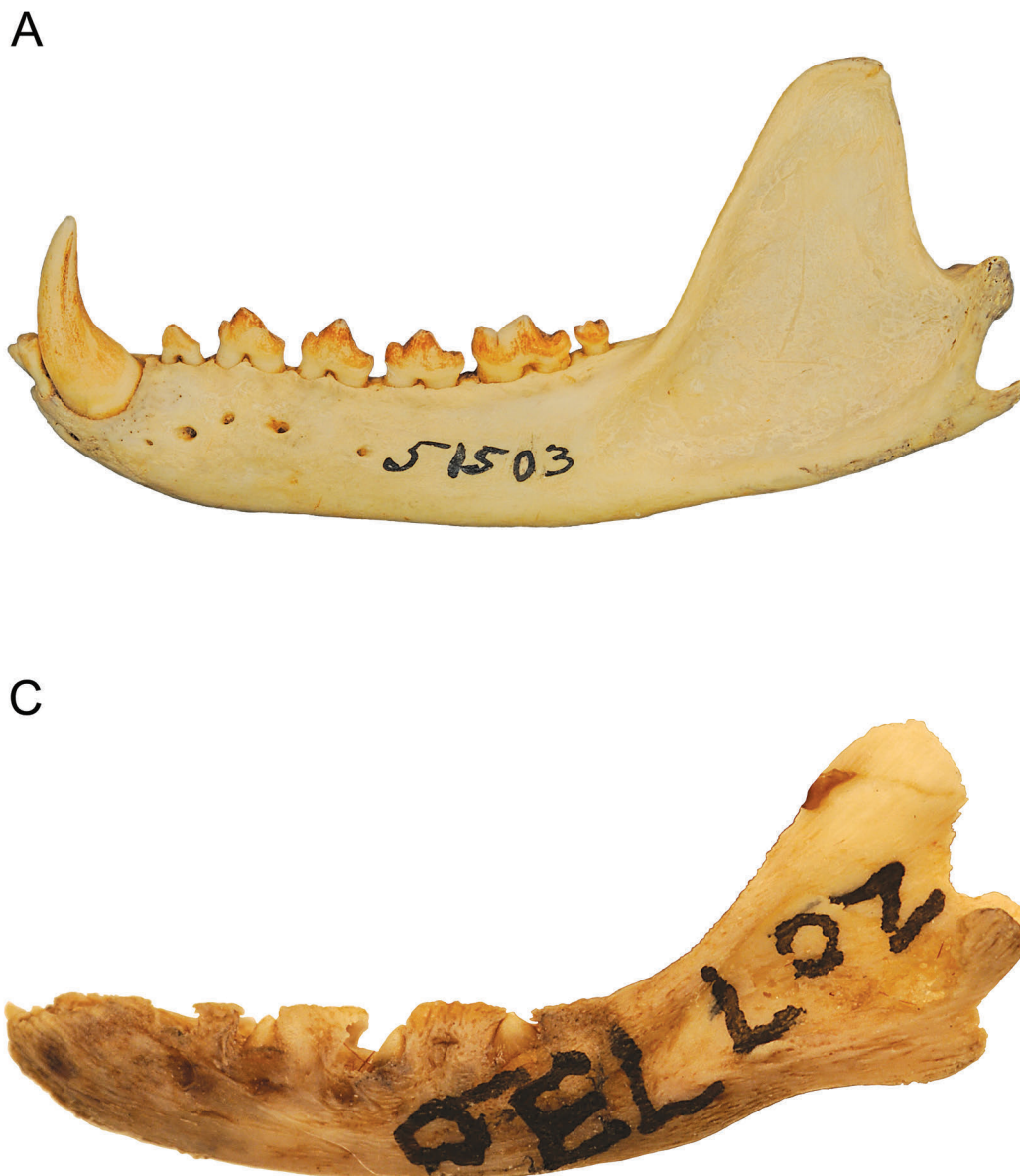
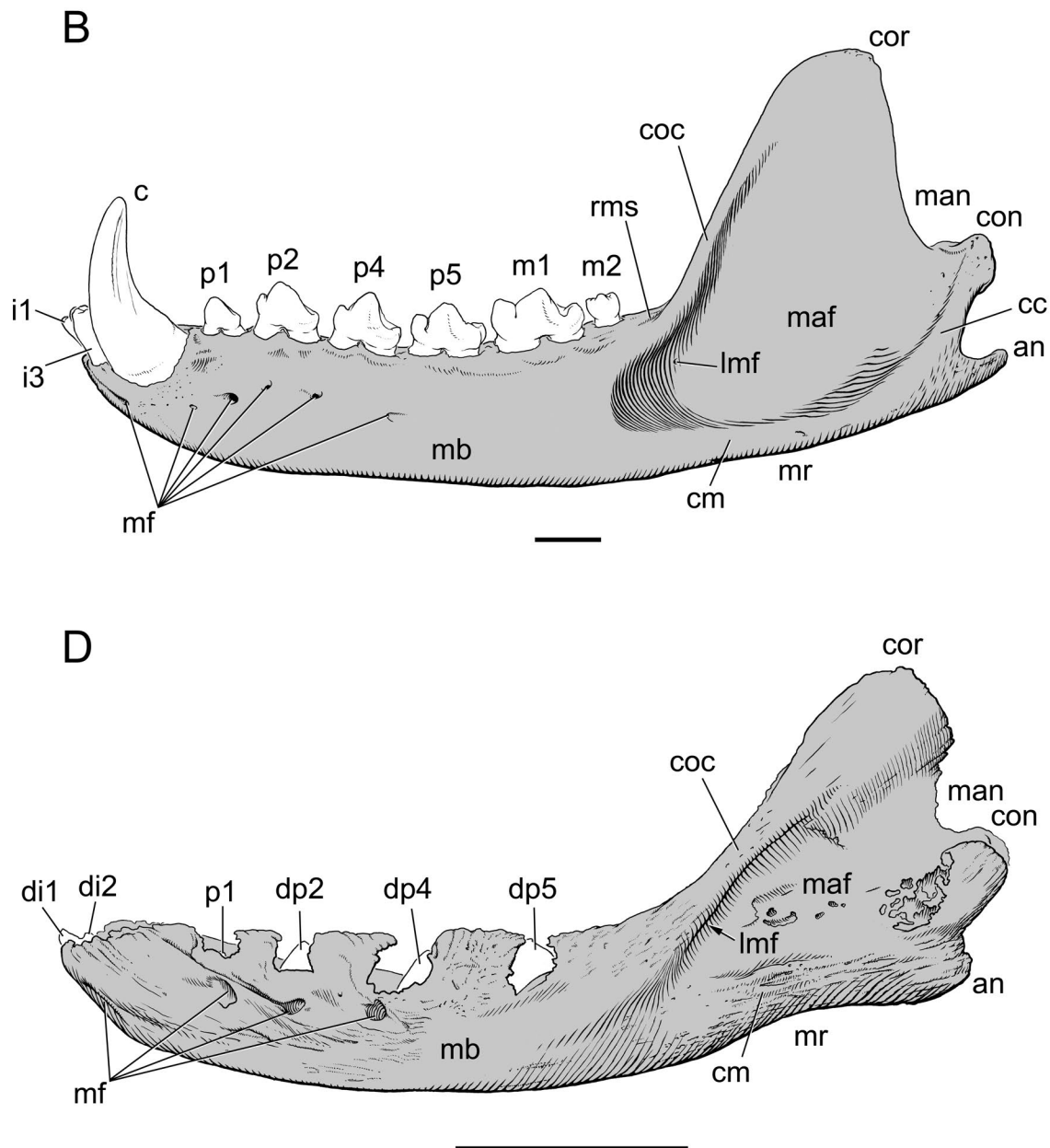


Fig. 30—Left mandibles of *Nandinia binotata* in lateral view. **A, B**, adult, AMNH 51503; **C, D**, newborn, AMNH 207730. Scale = 5 mm. Abbreviations: **an**, angular process; **c**, lower canine; **cc**, condyloid crest; **cm**, crista masseterica; **coc**, coronoid crest; **con**, condylar process; **cor**, coronoid process; **di1**, deciduous lower first incisor; **di2**, deciduous lower second incisor; **dp2**, deciduous lower second premolar; **dp4**, deciduous lower penultimate premolar; **dp5**, deciduous lower ultimate premolar; **i1**, lower first incisor; **i3**, lower third incisor; **lmf**, labial mandibular foramen; **m1**, lower first molar; **m2**, lower second molar; **maf**, massteric fossa; **man**, mandibular notch; **mb**, mandibular body; **mf**, mental foramen; **mr**, mandibular ramus; **p1**, lower first premolar; **p2**, lower second premolar; **p4**, lower penultimate premolar; **p5**, lower ultimate premolar; **rms**, retromolar space.

We also noted that most specimens have only one opening for the hypoglossal nerve on both the endo- and extracranial surfaces of the exoccipital. Only one side of one specimen has two openings externally, CM 6374(L), but the two are separated by just a thin septum. Two openings are present internally in CM 6371(R), 6374(L), 42727, and 3693.

#### Supraoccipital ("so" in figures)

As noted above, the supraoccipital is separated from the exoccipitals in only the newborn, AMNH 207730, and two juveniles, AMNH 51471 and 51486. The descriptions in the adult are enhanced via additional observations of these specimens.



**CM 59495, Principal Adult.**—In posterior view (Figs. 29A–B), the fan-shaped supraoccipital forms the dorsal half of the occiput. Its narrow ventral margin contributes to the middle third of the foramen magnum’s dorsal border. Its curved dorsal margin forms the back of the dorsal half of the nuchal crest, which is completed ventrolaterally by the parietal, exoccipital, squamosal, and petrosal. On the midline adjacent to the nuchal crest is the short but distinct

external occipital crest (“eocr” in Fig. 29B). Between the external occipital crest and foramen magnum is a prominent bulge, the occipital protuberance (“ocp” in Fig. 29B), which is the external manifestation of the vermiform impression. The bone forming the protuberance is thinner than that adjacent to it. Lateral and dorsal to the protuberance, the supraoccipital has about a dozen small foramina that are asymmetrically distributed between the two sides.

**AMNH 207730, Newborn.**—The newborn (Figs. 29C–D) differs in that the nuchal crest is not formed, the external occipital crest is broader and less distinct, the occipital protuberance is lacking, and only two or three small foramina occur.

**Others.**—The series in Figure 1 shows the development of the nuchal crest and occipital protuberance. As noted above, both structures are lacking in the newborn, AMNH 207730. The protuberance is visible in both dorsal and lateral view in the juveniles, AMNH 51486 and CM 6374, but little of the nuchal crest is evident. In the younger juvenile, CM 59495, a strong nuchal crest is present, obscuring the protuberance in dorsal and lateral view, while in the older juvenile, CM 42728, the nuchal crest overhangs the occiput.

We recorded the incidence of two features of the supra-occipital across the study sample:

(1) External occipital crest in adults: (a) absent - AMNH 51488, CM 6374, AMNH 201513, 51448, CM 42281, AMNH 51503, 134969, CM 42727, 42725, 69365, 69366, AMNH 51510, 51445, CM 42728, AMNH 51513; (b) present - CM 5157, 59497, 59495 (Figs. 29A–B), 59496, 3693, 42726, 42282, 16103, AMNH 51494, CM 5097. This crest is absent in the newborn (Figs. 29C–D) and juveniles, but its adult distribution shows no obvious correlation with geography, ontogeny, and sex.

(2) Occipital protuberance in adults: (a) present - AMNH 51448, CM 42281, 5157, 2356, 59497, AMNH 51503, CM 59495 (Figs. 29A–B), 42727, 42725, 69365, 69366, AMNH 51510, CM 42728, AMNH 51513; (b) absent - AMNH 134969, CM 59496, 42726, 42282, CM 16103, AMNH 51494, 51445, CM 5097. Although absent in the newborn, the protuberance is present in all juveniles. However, its adult distribution shows no obvious correlation with geography, ontogeny, and sex.

#### Mandible

The paired mandibles consist of a shallow, tooth-bearing horizontal part (body) anteriorly and a broad vertical part (ramus) posteriorly. An adult mandible holds ten teeth: three incisors, a canine, four premolars, and two molars. In the vast majority of specimens (22 of 28), including the newborn, AMNH 207730, and the principal adult, CM 59495, the left and right mandibles are held together by soft tissue at the mandibular symphysis; in the remaining six, the two sides are separated. We have chosen to describe a specimen with its mandibles separated, AMNH 51503, in order to illustrate the lower jaw's medial side.

**AMNH 51503.**—In lateral view (Figs. 30A–B), the inferior margin along the mandibular body and ramus (“mb” and “mr” in Fig. 30B, respectively) is gently convex. The alveolar margin is gently concave, with a breakpoint at the posterior aspect of the canine where the margin becomes considerably lower. It rises again below the incisors but

does not reach the same height as beneath the p1. The medial and lateralmost incisors, i1 and i3, are visible in lateral view, because i1 is more procumbent than is i3. The i2 is not visible as its alveolus is offset posteriorly from the others. The canines and incisors are tightly packed together, whereas the postcanine teeth are separated by small diastemata. Behind the m2 is a retromolar space (“rms” in Fig. 30B), serving to separate the body from the ramus. The postcanine teeth all have two roots except for the single-rooted m2. The mandibular body is relatively uniform in depth beneath the postcanine dentition and is deepest below the m2, followed closely by the p2. The left mandible has six mental foramina (“mf” in Fig. 30B): one below i3, two below p1, two below p2, and one below p4 (the more anterior one below p1 is smaller than the rest); the right mandible has four. The foramina below p2 on both sides are positioned more dorsally than the others. The anterior mental foramina on both sides are directed chiefly anteriorly, whereas the posteriormost one is directed posteriorly. A distinct muscle scar extends the length of the postcanine dentition ventral to the alveolar margin; it is broader below the anterior two premolars, extending to fill the space between their roots and respective mental foramina. Based on *F. catus* (Jayne 1898), this muscle scar accommodates the buccinator.

In medial view (Fig. 31), the most prominent feature on the body is the irregular surface for the mandibular symphysis (“mas” in Fig. 31) ventral to the anterior dentition, from below the posterior root of p1 to just before the anterior extent of the mandible. The dorsal margin of this surface is slightly medially elevated from the mandibular body. This relief is not uniform: the posterior margin grades smoothly into the body. The remaining surface of the body is featureless with no indication of muscle attachment or a mylohyoid line. Both the i1 and i2 are visible in medial view due to the offset of their alveoli placing the latter posteroventral to the former; they are similarly procumbent.

The mandibular ramus is dominated by three processes: the coronoid, condylar, and angular processes (“cor,” “con,” and “an” in Fig. 30B, respectively). The height of the coronoid process is more than twice the maximum depth of the body below m2. Its anterior margin rises from the body at an angle of 120° to the alveolar margin; the posterior margin is straight and nearer to the vertical. The ventral two-thirds of the anterior margin are raised as a prominent coronoid crest (“coc” in Fig. 30B), with the degree increasing slightly ventrally. The coronoid crest continues onto the body to the level of m2. The dorsal one-third of the anterior margin is slightly thickened; the posterior margin is uniformly thin. The ramal surface of the coronoid process is uniformly flat and grades into the masseteric fossa (see below).

The ventral margin of the ramus is thickened (“cm” in Fig. 30B); based on *F. catus* (Turnbull 1970), this provides an attachment surface for the pars profunda of the masseter. This masseteric crest continues posterodorsally

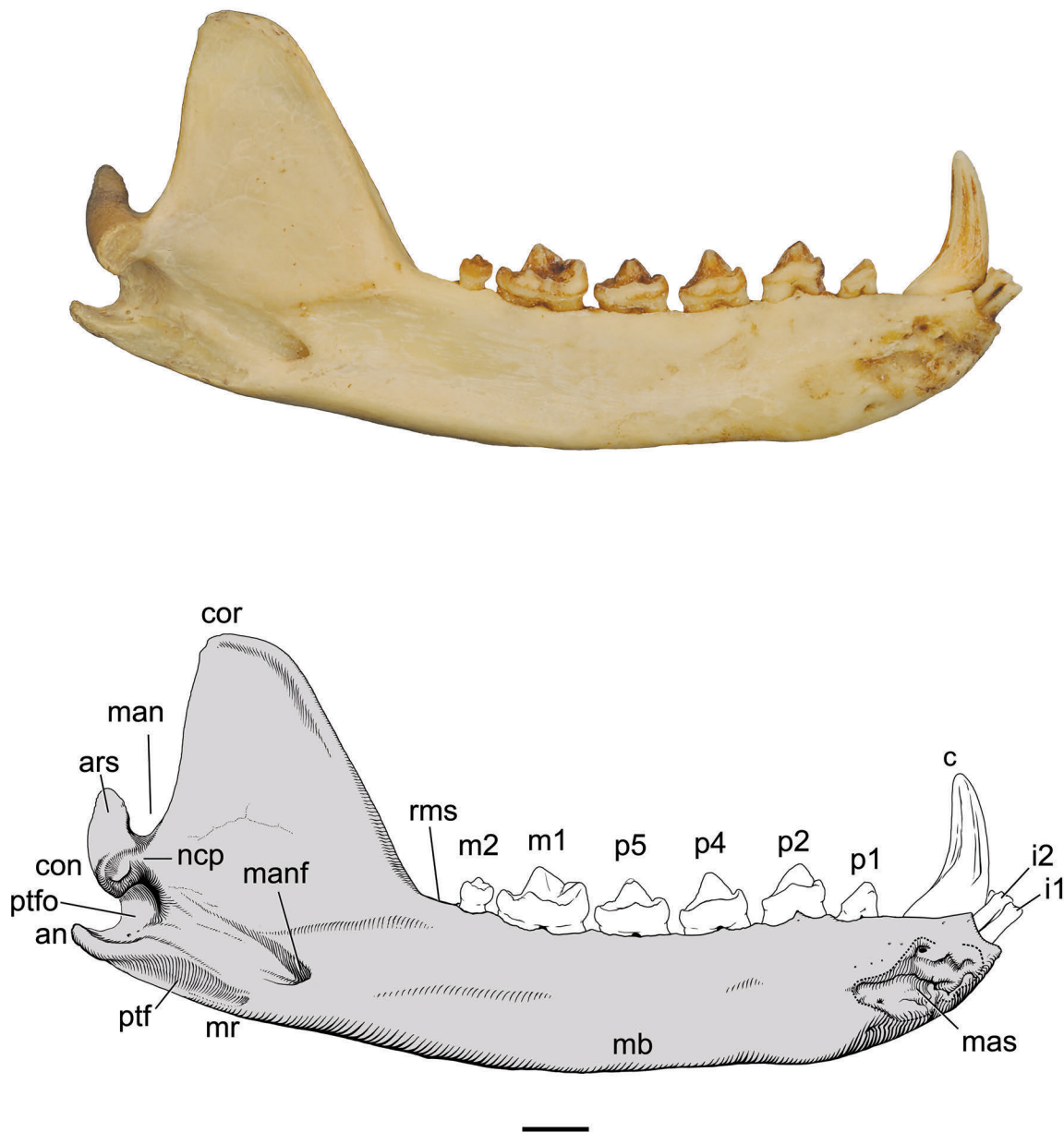


Fig. 31—Left mandible of adult *Nandinia binotata*, AMNH 51503, in medial view. Scale = 5 mm. Abbreviations: **an**, angular process; **ars**, articular surface; **c**, lower canine; **con**, condylar process; **cor**, coronoid process; **i1**, lower first incisor; **i2**, lower second incisor; **m1**, lower first molar; **m2**, lower second molar; **man**, mandibular notch; **manf**, mandibular foramen; **mas**, mandibular symphysis; **mb**, mandibular body; **mr**, mandibular ramus; **ncp**, neck of condylar process; **p1**, lower first premolar; **p2**, lower second premolar; **p4**, lower penultimate premolar; **p5**, lower ultimate premolar; **ptf**, pterygoid fossa; **ptfo**, pterygoid fovea; **rns**, retromolar space.

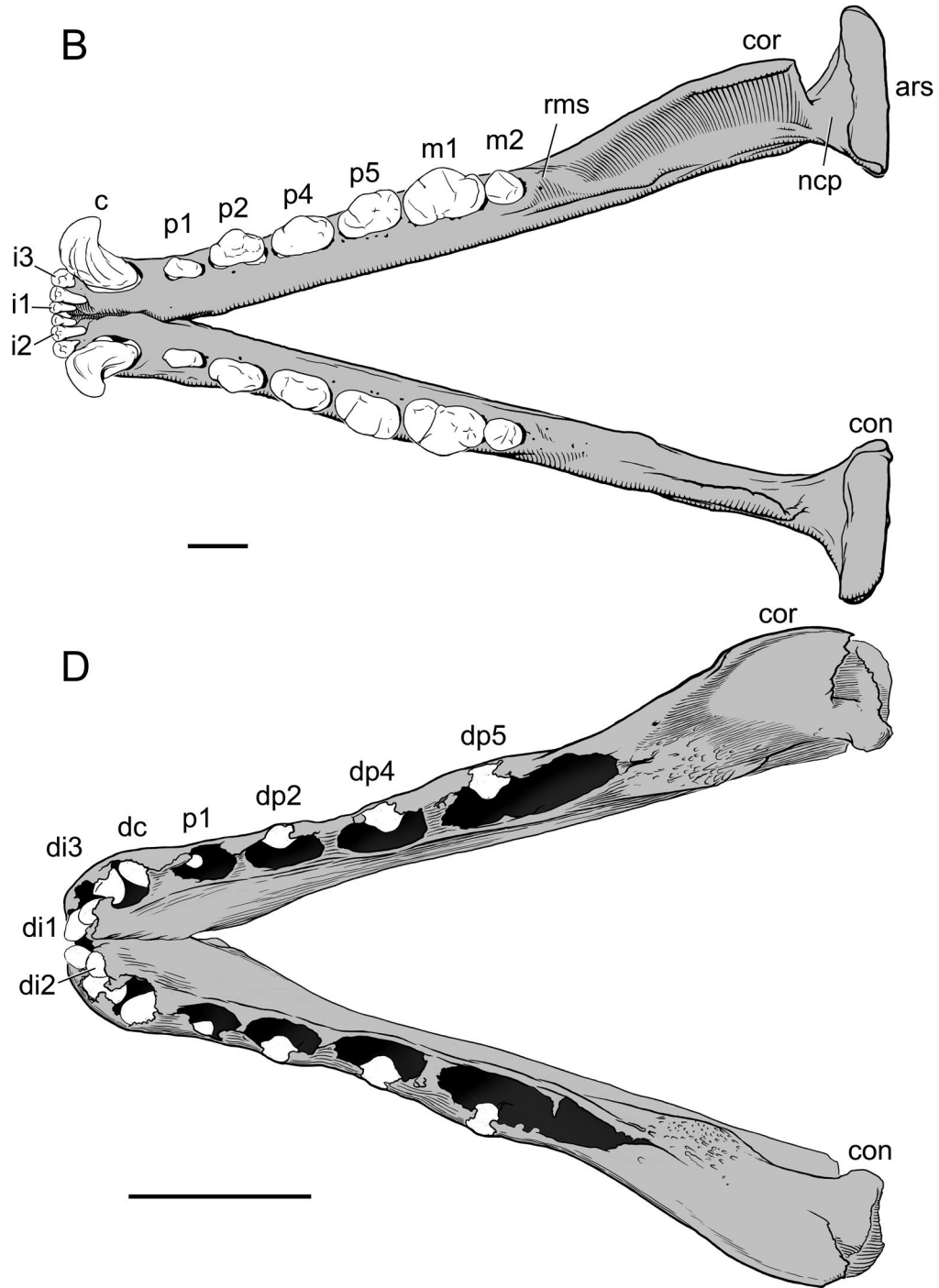
onto the condylar process as the condyloid crest (“cc” in Fig. 30B). The raised margins on the anterior, ventral, and posterior aspects of the ramus create a pocket surrounding a flat surface. This pocket is the masseteric fossa (“maf” in Fig. 30B), the site of attachment for the zygomatico-mandibularis muscle, based on *F. catus* (Turnbull 1970); the temporalis muscle inserts dorsal to this surface on the dorsal part of the coronoid process (Turnbull 1970). The masseteric fossa extends anteriorly onto the mandibular

body, ending ventral to the m2. Several tiny foramina are found in the masseteric fossa near the condyloid crest, and another tiny one is directed anteriorly into the bone near the base of the coronoid crest (“lmf” in Fig. 30B). This last opening, which is present bilaterally, is in the position of a relatively larger opening, the labial mandibular foramen, described in some Early Cretaceous eutherians (Kielan-Jaworowska and Dashzeveg 1989; see below).

The angular process is a short, blunt hook; it is directed



Fig. 32—Mandibles of *Nandinia binotata* in occlusal view. **A, B**, adult, CM 42282; **C, D**, newborn, AMNH 207730. Scale = 5 mm. Abbreviations: **ars**, articular surface; **c**, lower canine; **con**, condylar process; **cor**, coronoid process; **dc**, deciduous lower canine; **di1**, deciduous lower first incisor; **di2**, deciduous lower second incisor; **di3**, deciduous lower third incisor; **dp2**, deciduous lower second premolar; **dp4**, deciduous lower penultimate premolar; **dp5**, deciduous lower ultimate premolar; **i1**, lower first incisor; **i2**, lower second incisor; **i3**, lower third incisor; **m1**, lower first molar; **m2**, lower second molar; **nep**, neck of condylar process; **p1**, lower first premolar; **p2**, lower second premolar; **p4**, lower penultimate premolar; **p5**, lower ultimate premolar; **rms**, retromolar space.



posterodorsally in lateral view (Figs. 30A–B), continuing the general curvature of the inferior border of the ramus anterior to it. Viewed from below (not illustrated), the angle does not lie in the same exact plane as rest of the ramus; it is directed slightly medially, but it is not medially inflected as occurs, for example, in marsupials (Sánchez-Villagra and Smith 1997). The angle's lateral surface is a muscle scar, providing attachment for the pars profunda of the masseter based on *F. catus* (Turnbull 1970).

The condylar process sits atop the condyloid crest (Figs. 30A–B); there is no real distinct neck or peduncle in lateral view. A sharp point at the termination of the condyloid crest forms the lateral margin of the articular surface. The details of the articular surface are considered below with the medial and occlusal views. The condylar process is separated from the coronoid and angular processes by shallow notches; the former is the mandibular notch ("man" in Fig. 30B).

In medial view (Fig. 31), the dorsal half of the anterior margin of the coronoid process is thickened, which makes the adjacent coronoid surface slightly depressed; the remaining coronoid surface is flat. Based on *F. catus* (Turnbull 1970), the medial aspect of the coronoid provides attachment for the temporalis muscle (Jayne 1898 mistakenly identified this as being for the lateral pterygoid). A line marks the ventral margin of the temporalis attachment. The anterior half of this marking is more prominent and starts anteriorly below the retromolar space; it runs posteriorly and slightly ventrally and turns posterodorsally just behind the level of the mandibular foramen ("manf" in Fig. 31). The line terminates at the neck of the condylar process ("ncp" in Fig. 31). The posterior half of this line forms the dorsal margin of a broad sulcus leading into the mandibular foramen. The ventral margin of this sulcus marks the dorsal limit of a distinct pterygoid fossa ("ptf" in Fig. 31) for the attachment of the medial pterygoid, based on *F. catus* (Turnbull 1970). The pterygoid fossa extends onto the narrow medial surface of the angular process. The dorsal extent of the angular process marks the inferior extent of a triangular surface that reaches to the condylar process ("ptfo" in Fig. 31); based on *F. catus* (Turnbull 1970), this is the pterygoid fovea for the attachment of the lateral pterygoid muscle (Jayne 1898 mistakenly labeled this as being for the maxillo-auricular muscle). The condylar process is a mediolaterally elongate cylinder in medial view. The posterior half of the cylinder is the articular surface ("ars" in Fig. 31) for the glenoid fossa of the squamosal.

**CM 42282.**—The articulated left and right mandibles of this adult are shown in occlusal view (Figs. 32A–B). The i2 alveolus is offset posterior to those of the i1 and i3, as in AMNH 51503. However, the crowns of the three incisors are in roughly the same near transverse plane in CM 42282, whereas in the other specimen the i2 crown was also offset posteriorly. The two mandibles diverge at an angle of 28°. The retromolar space extends medial to the base of the coronoid crest and is continuous posteriorly

with the crest marking the anteroventral limit of the temporalis muscle (described above). The condylar process dominated by the cylindrical articular surface is massive compared to the thin ramus and body anterior to it, and extends farther medially.

**AMNH 207730, Newborn.**—In lateral view (Figs. 30C–D), there are four mental foramina per side: under the di1, p1, dp2, and dp4. The alveolar margin is more consistently level along the dentition; it is not lower at the incisors and canine. The inferior margin of the mandibular ramus has a concavity in it below the coronoid process and ends posteriorly at a blunt angle. The coronoid process rises at a more obtuse angle of 130°. The crests delimiting the masseteric fossa anteriorly and ventrally are relatively thicker than in the adult; the bone of the posterior (condyloid) crest is not fully formed. Whereas the masseteric fossa grades into the coronoid surface dorsal to it for the attachment of the temporalis in the adult (Figs. 30A–B), in the newborn the fossa is distinctly set off from the surface dorsal to it. A labial mandibular foramen, which is relatively larger than that in the adult, AMNH 51503, is hidden by the coronoid crest in the newborn (its position is marked by the arrow in Fig. 30D) and connects from the masseteric fossa to the back of the empty alveolus for the m1; this is double on the right side.

In medial view (Fig. 33A), a distinct Meckelian sulcus extends from the medial lip of the mandibular foramen to below the space between the dp4 and dp5. The posterior half of this sulcus is roughly twice as wide as the anterior half, with the dorsal margin more distinct. The sulcus converges on, but does not intersect the inferior margin of the mandibular body. Anterior to the end of the sulcus is a faint line that anteriorly reaches ventral to the small gap between the dp2 and dp4. We interpret this line as an indicator of where the mandible bone has closed over Meckel's cartilage. A broad sulcus extends posteriorly from the mandibular foramen to the posterior margin of the mandibular ramus. There is no pterygoid fovea, although a weak pterygoid fossa is present.

In occlusal view (Figs. 32C–D), the most striking differences are a slightly larger angle between the two mandibles, 36°, and the coronoid is not as erect but diverges dorsolaterally.

**Others.**—The series in lateral view in Figure 1 shows some general trends in the development of the mandible. The increase in the length of the mandible from newborn to adult has a larger contribution from the body than the ramus, reflecting the increased number of teeth. The height of the coronoid process increases relative to braincase height; the angle between the coronoid process and body becomes less obtuse. The mandibular angle becomes more prominent, as does the masseteric crest.

On the medial side, a faint remnant of the Meckelian sulcus is present only in several juveniles. This is ventral to the dp4 and dp5 in AMNH 51471 (Fig. 33B) and the dp5

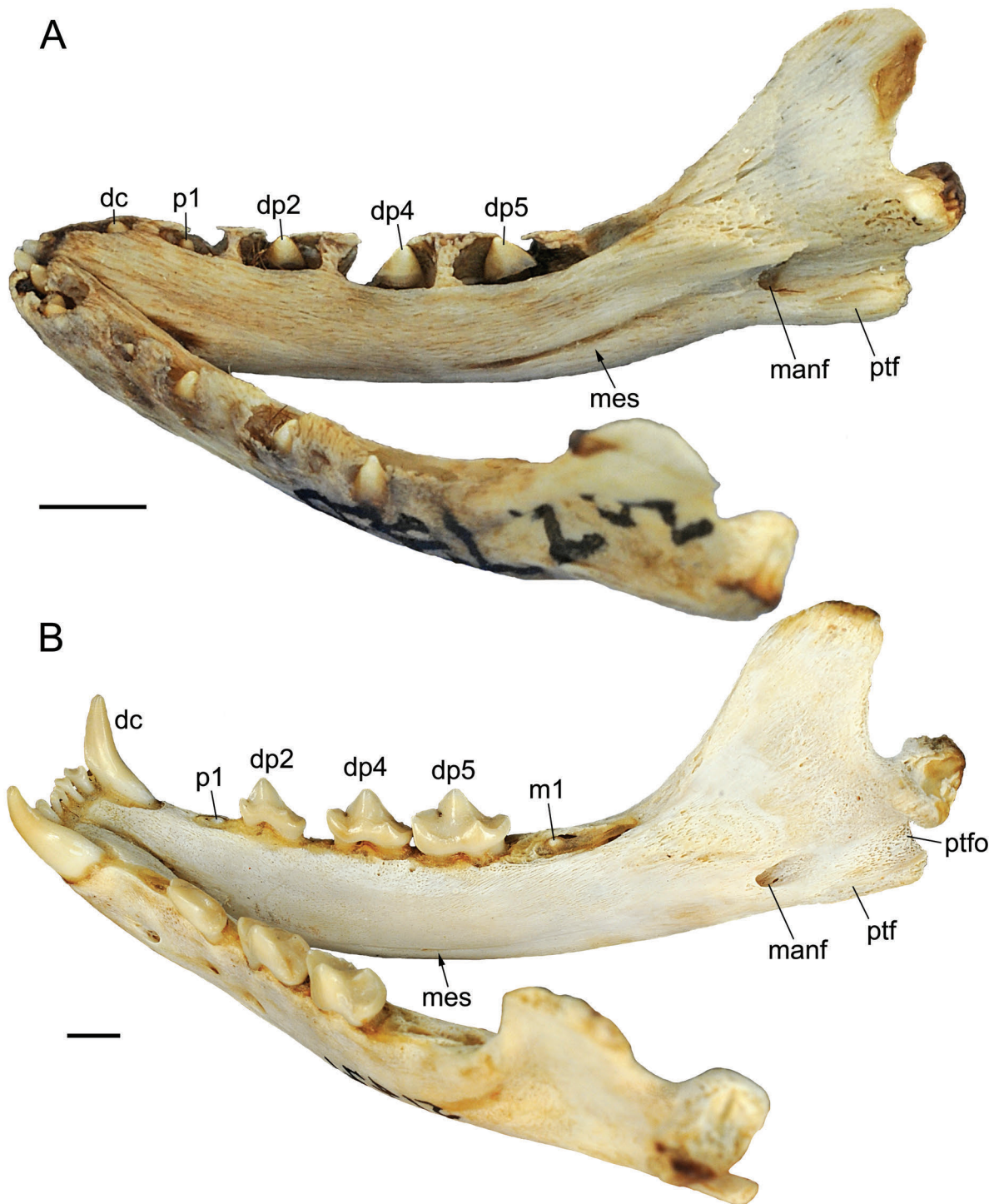


Fig. 33—Mandibles of *Nandinia binotata* in oblique lateral view. **A**, newborn, AMNH 207730; **B**, juvenile, AMNH 51471 (reversed). Scale = 5 mm. Abbreviations: **dc**, deciduous lower canine; **dp2**, deciduous lower second premolar; **dp4**, deciduous lower penultimate premolar; **dp5**, deciduous lower ultimate premolar; **m1**, lower first molar; **manf**, mandibular foramen; **mes**, Meckelian sulcus; **p1**, lower first premolar; **ptf**, pterygoid fossa; **ptfo**, pterygoid fovea.

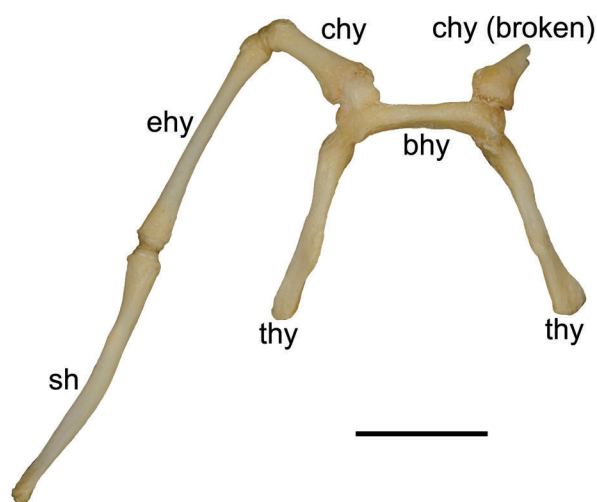


Fig. 34—Hyoid apparatus of *Nandinia binotata*, AMNH 134969, in ventral view. Scale = 5 mm. Abbreviations: **bhy**, basihyal; **chy**, ceratohyal; **ehy**, epihyal; **sh**, stylohyal; **thy**, thyrohyal.

and m1 in AMNH 51486 and CM 6371. The oldest juvenile with the sulcus, CM 6374, has the longest, stretching from the dp5 to the mandibular foramen. All juvenile and adult specimens have a pterygoid fossa and fovea, which become more distinct in the series from juvenile to adult (cf. Fig. 31 and 32B). The area housing the pterygoid fovea is not present in the newborn, as the broad sulcus running posteriorly from the mandibular foramen occupies this part of the mandibular ramus between the pterygoid fossa and condyle (Fig. 32A).

The presence of a foramen in the position of the labial mandibular foramen of Cretaceous eutherians is unexpected. With the exception of two specimens, a juvenile, AMNH 51486(R), and an adult, CM 3693, foramina, usually multiple and tiny, are found in the anterior part of the masseteric fossa throughout the study sample. However, the newborn, AMNH 207730, and two adults, CM 2356(R) and AMNH 134969(L), have openings on the same scale as those described for Cretaceous eutherians (Kielan-Jaworowska and Dashzeveg 1989; Wible et al. 2009). In light of this resemblance, we identify the openings in *N. binotata* as labial mandibular foramina.

We recorded the incidence of two features of the mandible across the study sample:

(1) Number of mental foramina: (a) three - AMNH 51471(L), CM 2356(R), 42727(R), 69365(R), 69366(L), 42728(R); (b) four - AMNH 207730 (Figs. 30C–D), 51471(R), 51486, CM 6371(L), AMNH 51488, 51448(L), CM 42281(R), 5157, 2356(L), 59497, AMNH 51503(R), AMNH 134969(R), CM 42727(L), 42725, 42726(L), 42282(R), 69265(L), 69366(R), AMNH 51510, CM 16103, AMNH 51494(R), CM 42728(L), 5097(R), AMNH 51513(L); (c) five - AMNH 51448(R), CM 59495, 59496(R), AMNH 51494(L), 51445, 51513(R); (d) six - CM 6371(R), 6374, 42281(L), AMNH 51503(L),

134969(L), CM 42282(L). The anteriormost mental foramen is ventral to the incisors in all specimens; the posteriormost is usually ventral to the p4(dp4), but is ventral to the diastema between p2 and p4 in CM 2356, 59597, 3693, 42282(R), 42728, and ventral to the p5 in CM 42282(L). The distribution of the number of mental foramina shows no obvious correlation with geography, ontogeny, and sex.

(2) Posterior margin of the coronoid process: (a) concave - AMNH 207730 (Figs. 30C–D), 51471 (Fig. 32B), 51486, CM 6371, 6374, AMNH 51448, CM 42281, 5157, 59495, 59496, 42727, 3693, 42725, 42726, AMNH 51510, 51494, CM 42728; (b) straight - AMNH 51488, CM 2356, 59497, AMNH 51503 (Figs. 30A–B), 134969, CM 42282, 69365, 69366, 16103, AMNH 51445, CM 5097, AMNH 51513. This distribution shows no obvious correlation with geography, ontogeny, and sex.

### Hyoid Apparatus

The bony hyoid apparatus is preserved in AMNH 134969 and illustrated in ventral view in Figure 34. Preserved are the basihyal, left and right thyrohyals, and the right ceratohyal, epihyal, and stylohyal; the left ceratohyal is known only from its broken ventral half, whereas the left epihyal and stylohyal are missing.

The unpaired basihyal (“bhy” in Fig. 34) is a craniocaudally compressed rod (6.5 mm wide) with its lateral ends bent dorsally. In ventral view, its rostral surface is flat and its caudal surface is slightly concave; in rostral and caudal views, its ventral surface is straight and its dorsal surface is concave. The small lateral face is a convex oval with a dorsoventral long axis. At the lateral ends, the paired ceratohyal articulates on the dorsorostral aspect and the paired thyrohyal on the dorsocaudal.

The paired thyrohyals (“thy” in Fig. 34) are gently curved, mediolaterally compressed rods (7.7 mm long) that are thickened at their ends. In lateral view, the rostral surface is slightly concave and the caudal convex, with a distinct process or angle dorsal to the midpoint (“thya” in Fig. 35). The ventral end articulates with the basihyal. On the left thyrohyal, the dorsal end is connected to the rostral horn of the thyroid by a 1 mm long element that appears to be cartilaginous (“ch” in Fig. 35), the equivalent of the chondrohyal of *F. catus* (Jayne 1898; Davison 1903). This is missing on the right side, showing that the dorsal end of the thyrohyal is concave.

The paired ceratohyals (“chy” in Fig. 34) are the shortest elements of the hyoid apparatus (5.6 mm long). The ceratohyal bears resemblance to a metacarpal, with a broad ventral base and a convex dorsal head. The concave ventral end articulates with the basihyal and overhangs it to a small degree laterally. On the right side, extra bone growth has fused the articulation between the ceratohyal and basihyal on the ventral surface. The dorsal end articulates with the epihyal.

The paired epihyals (“ehy” in Fig. 34), after the stylo-

hyals the second longest elements of the hyoid apparatus (9.3 mm long), are straight rods, slightly expanded at their rounded ends. The epihyal articulates with the ceratohyal ventrally and the stylohyal dorsally.

The paired stylohyals (“sh” in Fig. 34) are long, straight rods (11.3 mm long), slightly expanded at their ends. Its rounded ventral end articulates with the epihyal and its flattened dorsal end presumably articulates with the tympanohyal. In *F. catus* (Jayne 1898) and *C. lupus familiaris* (Evans 1993), a curved rod of cartilage connects the stylohyal to the skull base near the stylomastoid foramen; Evans (1993) identified these as the tympanohyoid cartilage and area of attachment of the tympanohyoid. *Nandinia binotata* likely has a similar arrangement, given that the end of the straight stylohyal cannot fit into the recessed attachment point on the petrosal (“th” in Figs. 19, 22), which we term the tympanohyal here.

### Larynx

Three unpaired elements of the larynx are preserved in AMNH 134969, the ossified thyroid cartilage, cricoid cartilage, and first tracheal ring. They are illustrated in lateral view in Figure 35.

Most of the ossified thyroid cartilage has smooth edges that suggest the bulk of this element is preserved. However, there are some roughened edges on the rostral margin suggesting a small amount of cartilage may have been present. The thyroid consists of left and right laminae (“lm” in Fig. 35). The laminae are roughly rectangular, ventrodorsally long and rostrocaudally narrow; their lateral surface is gently concave and together they form a U in rostral or caudal view. The laminae have a narrow midline union ventrocaudally at a rounded process, the laryngeal prominence (“lp” in Fig. 35). Projecting rostroventrally from the rostrocaudal corner of each lamina is the elongate rostral cornu or horn (“rc” in Fig. 35); the rostral horn tapers to its distal end where it articulates with the chondrohyal and thyrohyal. Projecting dorsocaudally from the dorsocaudal corner of each lamina is the shorter, more digitiform caudal cornu or horn (“cc” in Fig. 35); the medial surface of its distal end contacts the cricoid. Anterior to the caudal cornu is a small rounded process on the dorsocaudal margin of the lamina from which a subtle crest extends rostrally (“obl” in Fig. 35). Given its position, this short crest represents the oblique line, which provides attachment for the sternothyroid muscle in *C. lupus familiaris* (Evans 1993).

Caudal to the thyroid is the ossified cricoid cartilage (“crc” in Fig. 35). The left half of this element appears to be complete with finished smooth bony edges; it has the usual signet ring shape. In contrast, the right half (not figured) is severely deformed, much smaller, and with unfinished roughened edges, suggesting that more cartilage was present. The left caudal cornu of the thyroid is fused to the cricoid; there is a small, hard, white pad that is interposed between the medial side of the digitiform end of the caudal

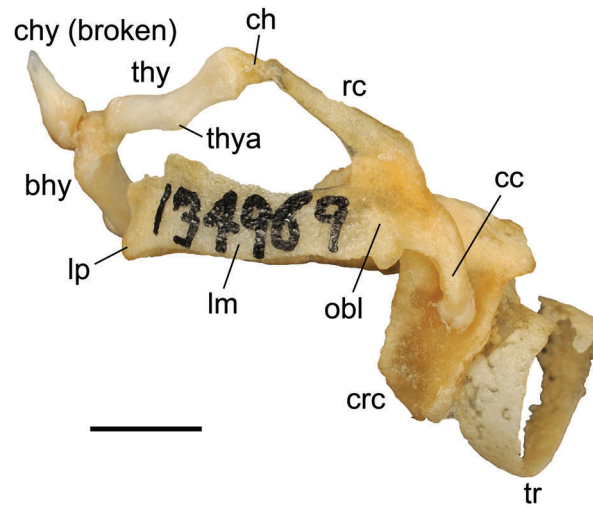


Fig. 35—Ossified larynx of *Nandinia binotata*, AMNH 134969, in left lateral view. Scale = 5 mm. Abbreviations: **bhy**, basihyal; **cc**, caudal cornu of thyroid cartilage; **ch**, chondrohyal; **chy**, ceratohyal; **crc**, cricoid cartilage; **lm**, left lamina of thyroid cartilage; **lp**, laryngeal prominence; **obl**, oblique line; **rc**, rostral cornu of thyroid cartilage; **thy**, thyrohyal; **thya**, thyrohyal angle; **tr**, first tracheal ring.

cornu and the lateral aspect of the cricoid.

Caudal to the cricoid is the ossified first tracheal ring (“tr” in Fig. 35). Some of its edges are roughened, which is evident on the right rostral margin in the figure. Nevertheless, it appears that most of the element is preserved. The ring is incomplete dorsally and of uniform dimensions except ventrally where its rostrocaudal height is less than half of the remainder.

### Endocranium

The majority of the observations on the endocranium are based on AMNH 134969, a skull in which the braincase roof was cut with a saw at some time prior to our study.

**AMNH 134969.**—The rostral and middle cranial fossae (“rcf” and “mcf,” respectively, in Fig. 36) are the endocranial spaces anterior and posterior to the annular ridge on the frontal bone (“ar” in Fig. 36). The rostral fossa is divided into a larger anterior part housing the olfactory bulbs and a smaller posterior part for the anterior surface of the cerebrum. The anterior part is the well-defined ethmoidal fossa (“etf” in Fig. 36); it is a small space, roughly 10 mm at its widest (mediolaterally) by 12 mm tall (dorsoventrally) by 5 mm deep (anteroposteriorly). Forming the bulk of the surface of the ethmoidal fossa is the cribriform plate of the ethmoid (“cpl” in Fig. 36). The cribriform plate is perforated by approximately 300 foramina of various sizes that transmit olfactory nerves. The plate midline is occupied by a line of foramina; a crista galli is lacking, but there is a weak crista frontalis on the midline of the roof (not visible in the figures). The foramina off the midline are arranged in cauliflower-shaped bundles that are presumably

associated with individual ethmoturbinates in the nasal fossa. The correspondence between foramina and particular ethmoturbinates is not a subject of this report. A specific cribroethmoidal foramen could not be identified.

The ethmoidal fossa is demarcated from the posterior part of the rostral cranial fossa by a distinct vertical ridge on the frontal bone ("vr" in Fig. 36). Dorsally, this vertical ridge converges with the annular ridge, but the latter slopes posteroventrolaterally from this convergence. The ventral end of the annular ridge is not prominent, and the rostral and middle cranial fossae are not well delimited there. Anterior to the vertical ridge is a slender exposure of frontal in the walls, floor, and roof of the ethmoidal fossa (features of the frontal in the ethmoidal fossa are not visible in the figures). In the anteroventral aspect of the lateral wall is the endocranial aperture of the ethmoidal foramen, which is formed by both frontal and ethmoid. A well-developed groove on the frontal runs dorsally from the ethmoidal foramen. It is vertical initially, but bends posterodorsally halfway up the lateral wall. At the bend is a rounded, anterior projection of the frontal that forms the base of a large cauliflower-shaped bundle of foramina in the cribriform plate. In addition, the frontals have a small spinous projection on the ventral midline that extends forward a short distance dorsal to the ethmoid. There is no indication of a midline suture between the frontals

In the floor of the posterior part of the rostral cranial fossa is the triangular jugum sphenoidale of the presphenoid ("js" in Fig. 36). It lies at a higher plane than the floor of the middle cranial fossa behind it and slopes slightly dorsally into the ethmoidal fossa. The suture between the jugum and frontals is irregular, with asymmetrically placed interdigitations. The anterior tip of the jugum extends into the ethmoidal fossa, past the ventral base of the vertical ridge on the frontal bone. The anterior tip is asymmetric, with its farthest anterior extension to the right of the midline, where it contacts the ethmoid bone; the left side is separated from the ethmoid by the frontal (not visible in the figures). Several small foramina of unknown function are present in the dorsal surface of the jugum: one is on the midline of the anterior tip with a groove leading into it from behind; a second is on the right side slightly more posteriorly positioned; and an additional three are more posteriorly placed on the left side. The posterior margin of the jugum forms the orbitosphenoid crest ("ocr" in Fig. 37).

The middle cranial fossa (Figs. 36–38), housing the rest of the cerebrum, extends from the annular ridge of the frontal to the dorsum sellae and ossified tentorium ("ds" and "tpa" in Figs. 37–38, respectively). The anterior third of the midline is formed by the presphenoid and the posterior two-thirds by the basisphenoid (Fig. 37). As on the skull exterior, the presphenoid and orbitosphenoid are not separated by sutures endocranially. The presphenoid is the sunken midline triangular area, which is flanked laterally by the orbitosphenoid wings. Distinct grooves for the optic nerves run anterolaterally across the presphenoid, separated by a low midline eminence ("son" in Fig. 37). The

grooves end at the optic foramina (Fig. 36), which are anteriorly and only slightly laterally directed. Just medial to the optic foramina is a dorsoventrally narrow connection between the two sides that housed the optic chiasm ("opc" in Fig. 36). The orbitosphenoid forms the bulk of the roof of the sphenorbital fissure, and lateral to that aperture contacts the alisphenoid and frontal. The posterior margin of the orbitosphenoids has an asymmetric projection that represents the rostral clinoid process ("rcp" in Fig. 37); this projection comes to a point on the right side but is blunt on the left.

Anteriorly, the basisphenoid has a narrow midline prominence, the tuberculum sellae ("tbs" in Figs. 36–38), which initially is at the same level as the presphenoid in front of it, but then slopes posteroventrally. The dorsal surface of the tuberculum is convex and rectangular, longer than wide. There is a slight projection from the left lateral aspect in the position of a middle clinoid process. The back of the tuberculum sellae is concave and represents the anterior aspect of the hypophyseal (pituitary) fossa ("hyf" in Figs. 37–38). The hypophyseal fossa is oval, longer than wide (4.5 x 3.2 mm), and wider posteriorly than anteriorly. It is asymmetric, with slightly more of it on the right side than the left (Fig. 37). Its anterior wall is the highest, followed by the right wall, then the left, and finally the posterior wall is the lowest. Lateral to the posterior aspect of the hypophyseal fossa on the left side is a well-developed foramen directed ventrolaterally; it is the endocranial aperture of the transverse canal foramen (arrow passes through canal in Figs. 37–38), which is entirely absent on the right side. A small gap separates the back of the hypophyseal fossa from the dorsum sellae. In this gap, slightly to the right of the midline is a small foramen, the cranial aperture of the craniopharyngeal canal ("cpc" in Fig. 37), which is larger than the corresponding aperture on the external skull base.

On either side of the tuberculum sellae and hypophyseal fossa is a gutter (Fig. 37), which represents the floor of the cavum epiptericum (Gaupp 1902, 1905). The segment of this gutter opposite the tuberculum sellae transmits structures to the sphenorbital fissure and is remarkably deep, with high medial and lateral walls. It is in the anterior part of this gutter that there is an exposure of the pterygoid bone, between the pre- and basisphenoid medially and the alisphenoid laterally. In the posterolateral aspect of the suture with the last bone is a small foramen ("ropc" in Fig. 37); it is the endocranial aperture of the pterygoid canal. The segment of the gutter opposite the hypophyseal fossa has low medial and lateral walls ("scs" in Fig. 37), and is twice as wide on the right side as on the left; this sulcus housed the cavernous sinus. Lateral to the sulcus for the cavernous sinus is another wider gutter ("smxn" in Fig. 37) that housed the maxillary nerve. Based on the positions of the bones on the skull exterior, this sulcus is on the alisphenoid. The maxillary nerve leaves the endocranium at the foramen rotundum ("fro" in Figs. 36, 38), which, after a short course through bone, opens externally lateral to

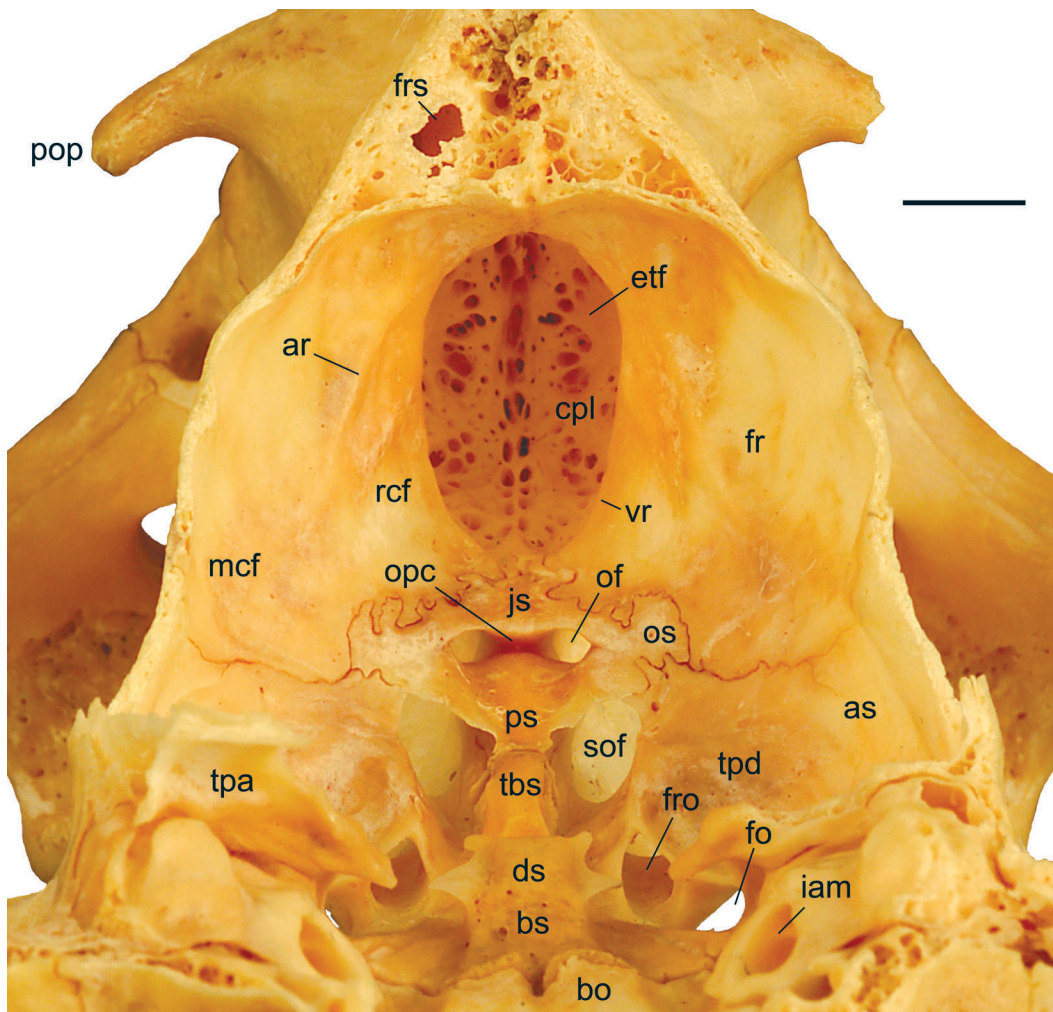


Fig. 36—Floor and anterior wall of endocranium of *Nandinia binotata*, AMNH 134969, in posterior view. The top of the skull with the main part of the ossified tentorium was removed and is figured elsewhere (Fig. 39). Scale = 5 mm. Abbreviations: **ar**, annular ridge of frontal; **as**, alisphenoid; **bo**, basioecipital; **bs**, basisphenoid; **cpl**, cribriform plate of ethmoid; **ds**, dorsum sellae; **etf**, ethmoidal fossa; **fr**, frontal; **fro**, foramen rotundum; **frs**, frontal sinus; **iam**, internal acoustic meatus; **js**, jugum sphenoidale; **mcf**, middle cranial fossa; **of**, optic foramen; **opc**, sulcus for optic chiasm; **os**, orbitosphenoid; **pop**, postorbital process of frontal; **ps**, presphenoid; **rcf**, rostral cranial fossa; **sof**, sphenorbital fissure; **tbs**, tuberculum sellae; **tpa**, tentorial process of parietal (cut); **tpd**, temporal pole depression; **vr**, vertical ridge.

the sphenorbital fissure. The foramen rotundum is joined by the alisphenoid canal (“asc” in Fig. 38); therefore, the external opening of the foramen rotundum also serves as the rostral opening of the alisphenoid canal. Posterolateral to the maxillary nerve sulcus is a large depression on the alisphenoid (“trf” in Figs. 37–38) that housed the trigeminal ganglion; the anterolateral aspect of the trigeminal fossa has a short sulcus for the mandibular nerve (“smnn” in Figs. 36–37) that leads to the foramen ovale (“fo” in Figs. 36, 38). Lateral to the trigeminal fossa, the floor of the middle cranial fossa is elevated and has a large kidney bean-shaped depression, the temporal pole depression (“tpd” in Figs. 36–38). The anterior half of this depression is formed by the alisphenoid and the posterior half by the tentorial process of the parietal. The portion of the alisphenoid

behind the foramen ovale rises to meet the tentorial process of the parietal and represents a tentorial process of the alisphenoid (“tas” in Figs. 37–38). A posterodorsolaterally directed groove for the middle meningeal artery and vein (“mma” in Fig. 37) runs across the tentorial process of the alisphenoid onto the parietal.

The endocranial surface of the roof of the middle cranial fossa is shown in Figure 39, although the portion of the ossified tentorium attached to the roof obscures the posterior part of the middle cranial fossa. The parietals are the principal elements of the middle cranial fossa roof, with some contribution from the frontals anteriorly. The sagittal suture is fused on the ventral surface of the frontals but is open in parts of the contact between the parietals. The midline is raised to form a low, broad eminence on the frontals

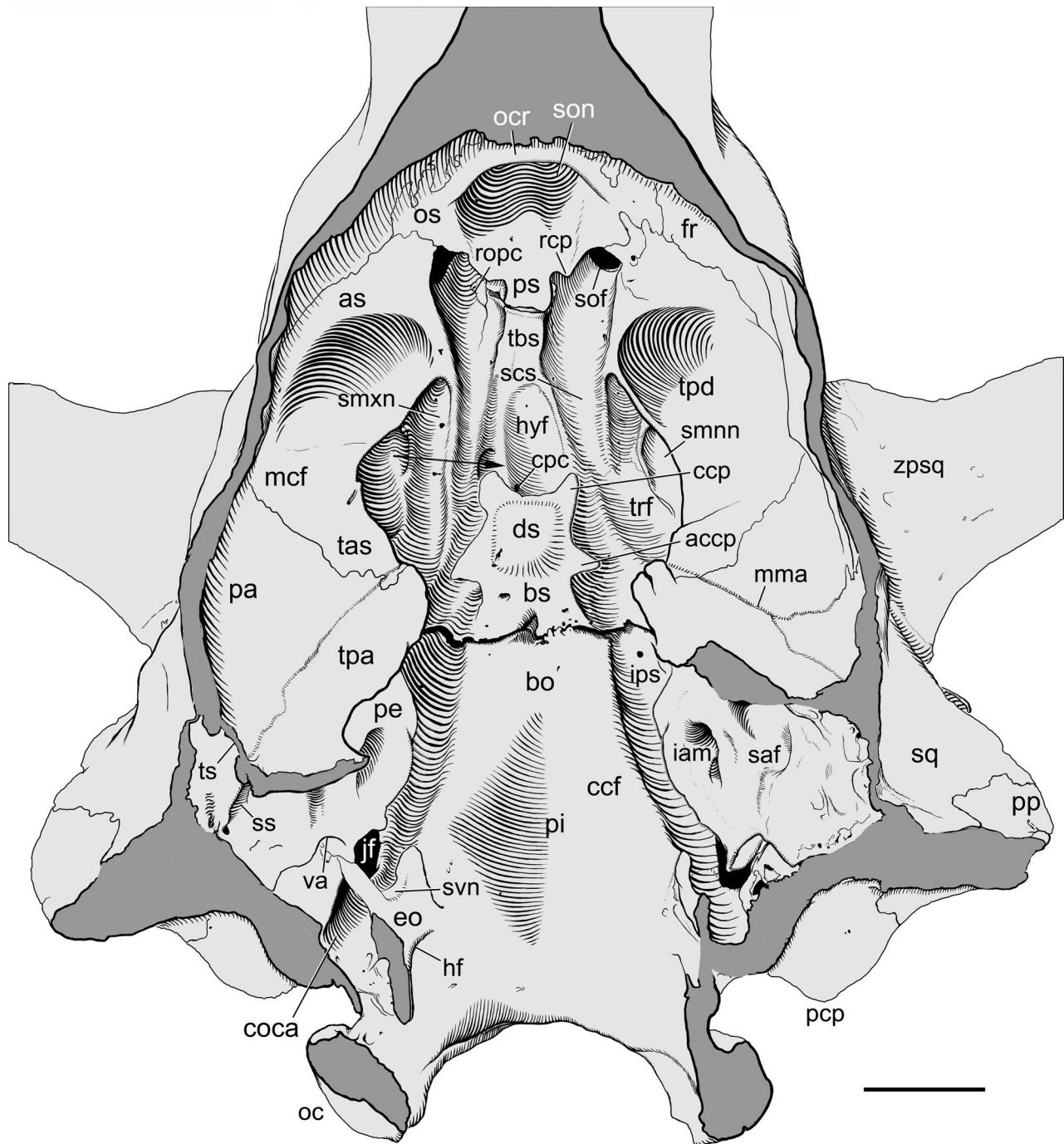


Fig. 37—Floor of endocranium of *Nandinia binotata*, AMNH 134696, in dorsal view. Unlabeled arrow on the left side, lateral to the hypophyseal fossa, is through the transverse canal, which is absent on the right side. Scale = 5 mm. Abbreviations: **accp**, accessory caudal clinoid process; **as**, alisphenoid; **bo**, basioccipital; **bs**, basisphenoid; **ccf**, caudal cranial fossa; **ccp**, caudal clinoid process; **coca**, condyloid canal; **cpc**, craniopharyngeal canal; **ds**, dorsum sellae; **eo**, exoccipital; **fr**, frontal; **hf**, hypoglossal foramen; **hyf**, hypophyseal fossa; **iam**, internal acoustic meatus; **ips**, inferior petrosal sinus; **jf**, jugular foramen; **mcf**, middle cranial fossa; **mma**, groove for middle meningeal artery and vein; **ocr**, orbitosphenoid crest; **os**, orbitosphenoid; **pa**, parietal; **pep**, paracondylar process of exoccipital; **pe**, petrosal; **pi**, pontine impression; **pp**, paroccipital process of petrosal; **ps**, presphenoid; **rcp**, rostral clinoid process; **ropc**, rostral opening of pterygoid canal; **saf**, subarcuate fossa; **scs**, sulcus for cavernous sinus; **smnn**, sulcus for mandibular nerve; **smxn**, sulcus for maxillary nerve; **sof**, sphenorbital fissure; **son**, sulcus for optic nerve; **sq**, squamosal; **ss**, sulcus for sigmoid sinus; **svn**, sulcus for vagus, glossopharyngeal, and accessory nerves; **tas**, temporal process of alisphenoid; **tbs**, tuberculum sellae; **tpa**, tentorial process of parietal; **tpd**, temporal pole depression; **trf**, trigeminal fossa; **ts**, opening for transverse sinus; **va**, vestibular aqueduct; **zpsq**, zygomatic process of squamosal.

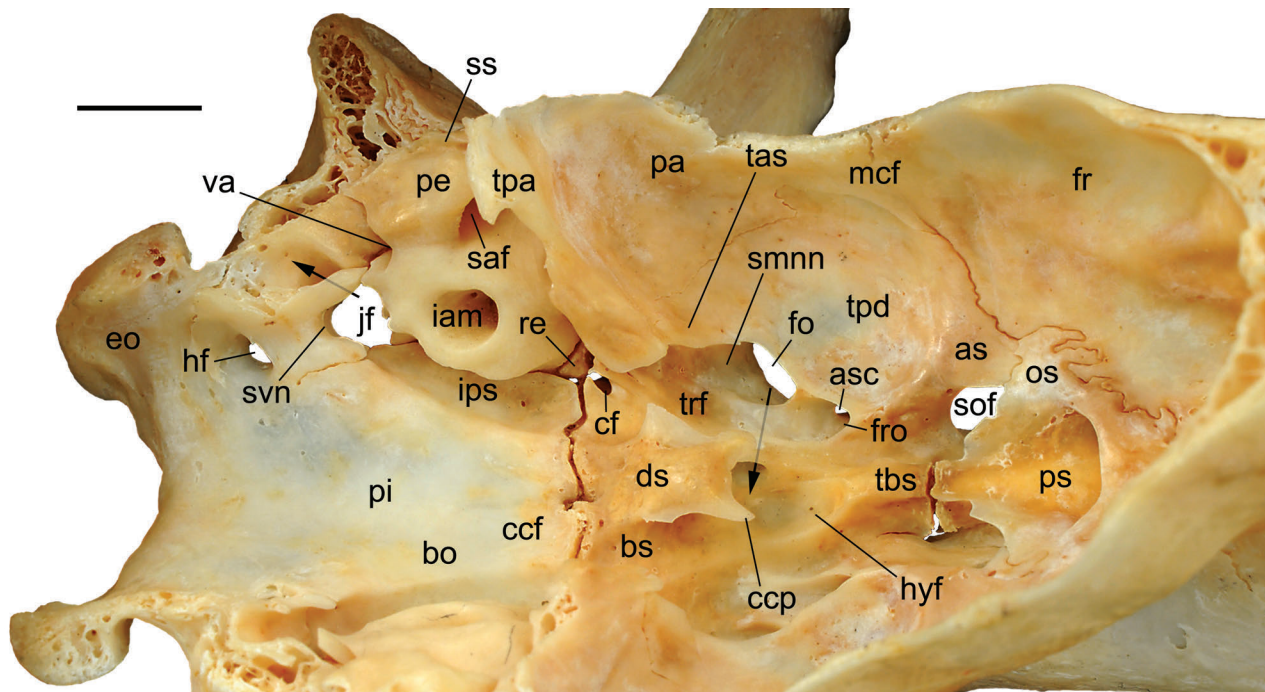


Fig. 38—Floor of endocranium of *Nandinia binotata*, AMNH 134696, in oblique ventral view. Arrow directed to the bottom of page is through the transverse canal, which is absent on the right side; arrow directed to the left is through part of the condyloid canal. Scale = 5 mm. Abbreviations: **as**, alisphenoid; **asc**, caudal opening of alisphenoid canal; **bo**, basioccipital; **bs**, basisphenoid; **ccf**, caudal cranial fossa; **ccp**, caudal clinoid process; **cf**, carotid foramen; **ds**, dorsum sellae; **eo**, exoccipital; **fo**, foramen ovale; **fr**, frontal; **fro**, foramen rotundum; **hf**, hypoglossal foramen; **hyf**, hypophyseal fossa; **iam**, internal acoustic meatus; **ips**, sulcus for inferior petrosal sinus; **jf**, jugular foramen; **mcf**, middle cranial fossa; **oc**, occipital condyle; **pa**, parietal; **pe**, petrosal; **pi**, pontine impression; **ps**, presphenoid; **re**, rostral entotympanic; **saf**, subarcuate fossa; **smnn**, sulcus for mandibular nerve; **sof**, sphenorbital fissure; **ss**, sulcus for sigmoid sinus; **svn**, groove for vagus, glossopharyngeal, and accessory nerves; **tas**, tentorial process of alisphenoid; **tbs**, tuberculum sellae; **tpa**, tentorial process of parietal; **tpd**, temporal pole depression; **trf**, trigeminal fossa; **va**, vestibular aqueduct.

and on the anterior two-thirds of the parietals. On the posterior one-third is a slight midline depression that housed the dorsal sagittal sinus. The midline has four foramina that drained into the dorsal sagittal sinus: the anteriormost one is on the frontal (the posteriormost is hidden by the ossified tentorium in Fig. 39). Where the tentorial process of the parietal meets the braincase roof is a large foramen impar (Evans 1993) just to the right of the midline (hidden by the ossified tentorium in Fig. 39). It drained the dorsal sagittal sinus into the confluence of the sinuses, which in turn drained into the transverse sinuses. Each transverse sinus runs laterally and then bends ventrally in a canal in the base of the tentorial process of the parietal (“**ts**” in Fig. 39). Off the midline are impressions for cerebral gyri and sulci: visible are the coronal, marginal (lateral), and suprasylvian sulci (“**cos**,” “**mas**,” and “**sus**” in Fig. 39). Running perpendicular to the latter two are grooves for the middle meningeal artery and vein.

The caudal cranial fossa (“**ccf**” in Figs. 37–38) is the space posterior to the dorsum sellae and the ossified tentorium. On the anterior midline is the prominent dorsum sellae of the basisphenoid. Its base is wider than the hypophyseal fossa, with several asymmetrically arranged foramina of uncertain function on its posterior surface. From the base, the dorsum sellae projects anteriorly and slightly

ventrally (Fig. 38), such that its anterior extent is even with the rear of the hypophyseal fossa. The posterodorsal surface of the dorsum sellae is raised in a pillow-shape. Extending anteriorly and slightly dorsally from the anterior corners of the dorsum sellae are horns, the caudal clinoid processes (“**ccp**” in Fig. 37–38); the left one is broader than the right. Extending laterally from the lateral aspects of the dorsum sellae is a second pair of horns, slightly larger than the caudal clinoid processes (“**accp**” in Fig. 37); we are not familiar with these in other forms and term them accessory caudal clinoid processes (the right one is preserved in Fig. 37 but is broken in Fig. 38).

Posterior to the dorsum sellae is the suture between the basisphenoid and basioccipital. At the lateral end of this suture is the juncture of five bones, with the central wedge-shaped element being the rostral entotympanic (Fig. 37). The rostral entotympanic contacts the basisphenoid anteromedially, the alisphenoid anterolaterally, the petrosal posteriorly, and the basioccipital medially. Because so much rostral entotympanic is visible endocranially, this specimen has a well-developed gap between the basisphenoid and petrosal (“**\***” in Figs. 14, 16A). Anteromedial to the rostral entotympanic is the endocranial aperture of the carotid foramen, which in AMNH 134969 is a deep incisure with a narrow opening in its posterior border (Fig. 38).

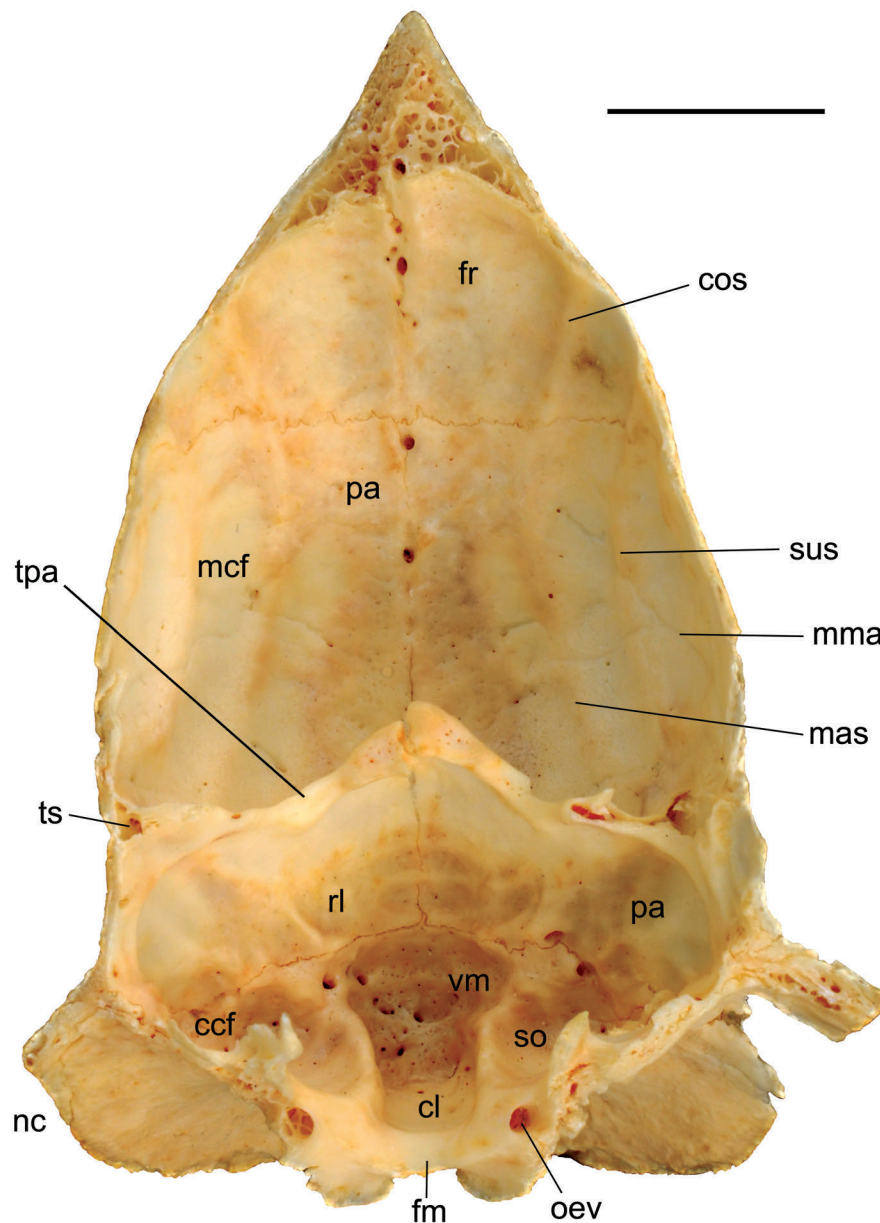


Fig. 39—Roof of endocranium of *Nandinia binotata*, AMNH 134696, in ventral view. Scale = 10 mm. Abbreviations: **ccf**, caudal cranial fossa; **cl**, vermis portion of caudal lobe; **cos**, ridge forming impression of coronal sulcus; **fm**, dorsal margin of foramen magnum; **fr**, frontal; **mas**, ridge forming impression of marginal sulcus; **mcf**, middle cranial fossa; **mma**, groove for middle meningeal artery and vein; **nc**, nuchal crest; **oev**, canal for occipital emissary vein; **pa**, parietal; **rl**, vermis portion of rostral lobe; **so**, supraoccipital; **sus**, ridge forming impression of suprasylvian sulcus; **tpa**, tentorial process of parietal; **ts**, opening for transverse sinus; **vm**, vermis.

A well-developed carotid groove runs anteromedially a short distance; it does not reach the hypophyseal fossa.

The basioccipital forms most of the floor of the caudal cranial fossa (Figs. 37–38). A broad midline concavity extends the length of the basioccipital, the pontine impression (“pi” in Figs. 37–38). The lateral margin of this depression is marked by a low, oblique ridge, which forms the medial margin of a broad gutter for the inferior petrosal sinus (“ips” in Figs. 37–38). The sulcus for the inferior petrosal sinus ends posteriorly at the jugular foramen and

can be traced forward onto the basisphenoid, lateral to the dorsum sellae, where it joined the cavernous sinus. Near the anterior end of the sulcus on the petrosal is a small foramen of uncertain function, asymmetrically arranged between the right and left sides. Medial to the left jugular foramen is what appears to be a crack in the oblique ridge, but which we interpret as the remnant of the basi- and exoccipital suture. Posterior to the suture is a U-shaped surface on the exoccipital directed towards the jugular foramen, with a short groove extending posteromedially from

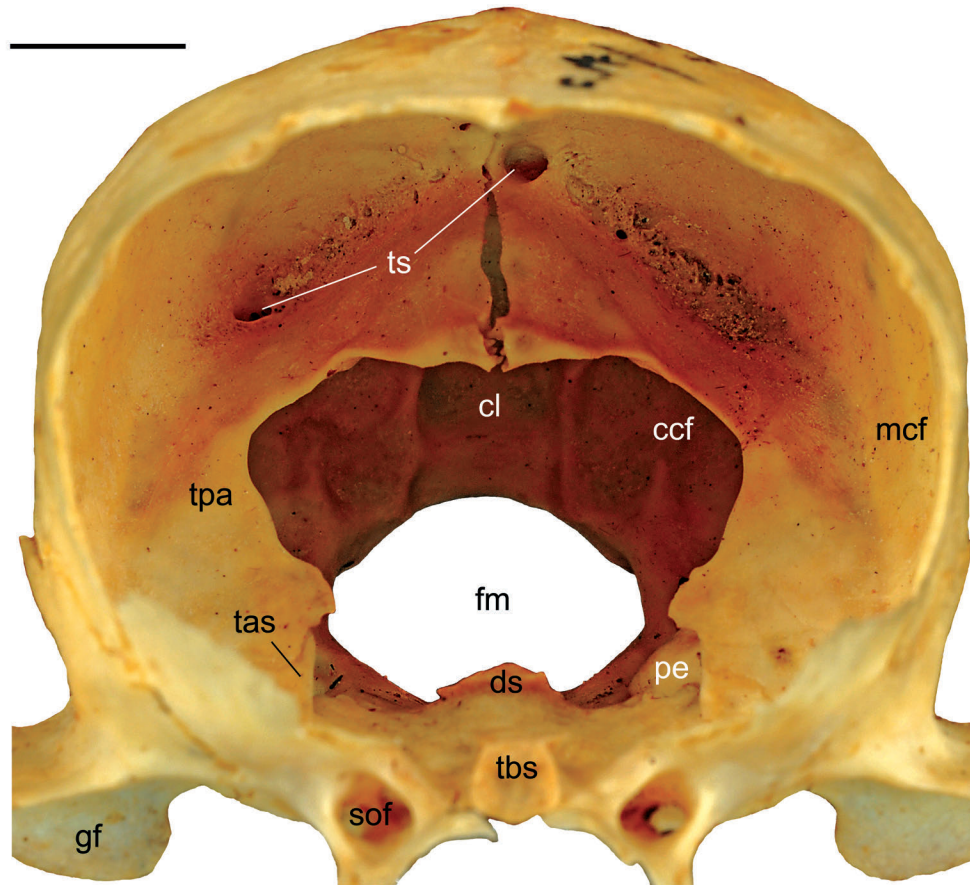


Fig. 40—Endocranium of the open braincase of *Nandinia binotata*, AMNH 201513, in anterior view, showing the anterior surface of the ossified tentorium. Scale = 5 mm. Abbreviations: **ccf**, caudal cranial fossa; **cl**, vermis portion of caudal lobe; **ds**, dorsum sellae; **fm**, foramen magnum; **gf**, glenoid fossa; **mcf**, middle cranial fossa; **pe**, petrosal; **sof**, sphenorbital fissure; **tas**, tentorial process of alisphenoid; **tbs**, tuberculum sellae; **tpa**, tentorial process of parietal; **ts**, openings for transverse sinus.

it (“svn” in Figs. 37–38); it transmitted cranial nerves IX, X, and XI (glossopharyngeal, vagus, and accessory) to the jugular foramen. Posteromedial to this sulcus is the endocranial aperture of the hypoglossal foramen in the exoccipital. Leading posterolaterally from the jugular foramen is a deep sulcus on the exoccipital for the contents of the condyloid canal (“coca” in Fig. 37). On the left side, this sulcus is roofed by a narrow piece of exoccipital (see arrow in Fig. 38) that contacts the petrosal near the vestibular aqueduct (“va” in Fig. 37–38); this is damaged on the right side.

The tentorial process of the left parietal slopes anteroventrally, covering the anterodorsal face of the petrosal (Fig. 38). The medial edge of the left parietal’s tentorial process is undamaged. The dorsal half has a concavity and the ventral half is considerably broader anteroposteriorly. The ventral-most extent is separated from the accessory caudal clinoid process by a gap.

On the dorsal aspect of the left petrosal is the sulcus for the sigmoid sinus (“ss” in Figs. 37–38). This sulcus can be traced forward to where the canal for the transverse sinus

is located in the margin of the tentorial process of the parietal (“ts” marks where it is hidden under the broken parietal edge in Fig. 37). Anterior to this junction, a sulcus for the superior petrosal sinus runs forward lateral to the low crista petrosa about halfway along the length of the pars cochlearis; the overlying tentorial process nearly encloses this sulcus in a canal (not visible in the figures). This morphology is different to that described for the isolated petrosal of AMNH 201513, where the sulcus for the superior petrosal sinus is quite short and lies medial to the crista petrosa (Fig. 21E). Visible within the cut edge of the canal for the transverse sinus are two other conduits for the vascular contents (not visible in the figures): the first continued the ventral trend of the transverse sinus and reached the postglenoid foramen, based on similar morphology in *C. lupus familiaris* (Evans 1993); the second turned anteroventromedially in the medial edge of the tentorial process and led to an opening between the tentorial processes of the parietal and alisphenoid. This opening is hidden in the figures; it lies dorsolateral to the carotid foramen and empties its contents into the area of the trigeminal fossa (Fig. 38).

The sulcus for the sigmoid sinus can be traced posteriorly onto a shallow sulcus on the part of the exoccipital bone attached to the sawed piece of the skull roof, although this continuity is not visible in Figure 39. This shallow sulcus drains into the condyloid canal, which ultimately drains out the foramen magnum, which, as described above, runs posteriorly from the jugular foramen (Figs. 37–38). Unlike the condition in *F. catus* (Reighard and Jennings 1935) and *C. lupus familiaris* (Evans 1993), the sigmoid sinus in AMNH 134969 does not exit the skull via the jugular foramen.

The roof of the caudal cranial fossa is shown in Figure 39. It closely reflects the morphology of the cerebellum. Forming the anterior wall of the caudal cranial fossa is the tentorial processes of the parietals. The middle third of tentorial processes is undamaged; the ventral edges of the lateral thirds are cut. The ventral margin of the middle third is thickened, in particular centrally, where a flat triangular surface is found on both sides of the midline. The posterior surface of the middle third is concave. This midline concavity forms the anterior aspect of a bowl-shaped depression (“rl” in Fig. 39). Posterior to the tentorial processes, the ventral surface of the braincase (here formed by the parietals) completes the bowl, which is only partially demarcated from a deep midline depression on the supraoccipital behind. On the parietal are transverse impressions for three cerebellar ridges and four sulci, all part of the vermis portion of the rostral lobe of the cerebellum.

Immediately posterior to the depression on the parietal for the rostral lobe is a slightly narrower oval depression on the supraoccipital (“vm” in Fig. 39); it too has transverse ridges and sulci but these are not as evident as on the parietal. In addition, the roof has many asymmetrically arranged foramina. This depression housed the central part of the cerebellar vermis. Posterior to this is another narrower depression with a smoother wall (“cl” in Fig. 39); it housed the vermis portion of the caudal lobe.

The surface posteroventral to the depression of the caudal lobe is the dorsal margin of the foramen magnum (“fm” in Fig. 39). On either side of this is a well-developed foramen opening dorsally and medially into the supraoccipital (“oev” in Fig. 39). This opening drains a well-developed canal that runs in the prominent lateral walls of the depressions for the caudal lobe and central vermis. Some of the foramina on the left side of the latter depression clearly drain into this canal. We interpret these foramina and canals as for the occipital emissary veins, which ultimately drain ventrally into the condyloid canals just inside the ventrolateral corner of the foramen magnum. This pattern differs from that in *C. lupus familiaris* (Evans 1993), where the occipital emissary vein drains to the sigmoid sinus.

Lateral to the midline depressions for the vermis are three obliquely oriented depressions per side for the left and right cerebellar hemispheres. The anterolateral depression is the largest, entirely on the parietal, and smooth walled (“pa” label is in this depression in Fig. 39). The posteromedial is next in size; it is entirely on the supraoccipital and has ridges and sulci (the “so” label is in this depression is

Fig. 39). The posterolateral depression is on both bones and also has ridges and sulci (the “ccf” label is in this depression in Fig. 39); the ventralmost limit of the posterior wall of this depression is on the exoccipital bone, in light of the position of the suture between the supra- and exoccipital bones in juvenile specimens (e.g., AMNH 51486).

**Others.**—Three additional damaged specimens provide details of the endocranium: AMNH 201513, 51448, and 51445. In the rostral cranial fossa, the juvenile, AMNH 201513, is the only one to show details about the bony construction of the floor. It has a very broad, bilateral contact between the presphenoid and ethmoid, with no frontal in the floor. Additionally, the anterior half of the presphenoid in the rostral cranial fossa has a midline suture, which means that at least two ossification centers are present in the anterior part of the sphenoid (pre- and orbitosphenoid). In AMNH 51445, the orbitosphenoid crest has a tiny pair of rounded bumps on either side of the midline, which project posteriorly; this crest is smooth in all other specimens, including AMNH 134969 (Fig. 37).

In the middle cranial fossa, AMNH 51445, which is the oldest specimen of those revealing endocranial features, has more prominent rostral clinoid processes than in the others, including AMNH 134969 (Fig. 37). AMNH 51445 also has prominent middle clinoid processes, as does the left side of AMNH 201513. The latter also has openings on either side of the hypophyseal fossa for the transverse sinus canal; these are lacking in the other two specimens, as on the right side of AMNH 134969 (Fig. 37). The anterior surface of the undamaged ossified tentorium of AMNH 201513 is shown in Figure 40. It confirms features described above for the damaged ossified tentorium of AMNH 134969 (Figs. 36–39), including the shape of the passageway between the middle and caudal cranial fossae and the central thickening in the tentorial process of the parietal forming the dorsal border of that passageway. However, whereas AMNH 134969 had a single opening to the left of the dorsal midline for the dorsal sagittal sinus, AMNH 201513 has paired openings for the transverse sinuses, one to the left of the midline and the other on the right side about halfway across the dorsal margin (“ts” in Fig. 40). In AMNH 201513, the dorsal sagittal sinus divided into the left and right transverse sinuses anterior to the ossified tentorium, rather than within the ossified tentorium as in AMNH 134969. The anterior surface of the ossified tentorium is also visible in AMNH 51445; it has one large opening for the transverse sinus on the right and six smaller ones on the left, which get progressively smaller laterally. In addition, there is a medium-sized foramen of unknown function on the left side near the lateral end of the tentorium with a groove leading into from in front.

In the caudal cranial fossa, the dorsum sellae is variable. In the juvenile, AMNH 201513, caudal and caudal accessory clinoid processes are absent; in the other two specimens, AMNH 51448 and 51445, the caudal clinoid processes are absent, but the accessory processes are prominent.

We recorded the incidence of one feature of the endocranium across the study sample:

(1) Number of posterior openings of the condyloid canal: (a) one - AMNH 51471(L), 51486, CM 6371, AMNH 51488, CM 6374(L), AMNH 201513, 51448(R), CM 42281, 2356, 5157(L), 59497(L), AMNH 51503, CM 59495, 59496(R), 42727, 42725, 42282, 69365(L), 69366, AMNH 51510, CM 16103, AMNH 51494, 51445, CM 5097, AMNH 51513(L); (b) two - AMNH 51471(R), CM 6374(R), AMNH 51448(L), CM 5157(R), 59497(R), 59496(L), 42726, 69365(R), AMNH 51513(R); (c) three - AMNH 207730. These openings are located on the endocranial surface of the exoccipital at the ventrolateral margin of the foramen magnum. This distribution shows no obvious correlation with geography, ontogeny, and sex.

### COMPARISONS

Family-level relationships of extant clades within the order Carnivora have been mostly well resolved by a combination of morphological and molecular studies (i.e., Flynn et al 2005; Finarelli 2008; Spaulding and Flynn 2012). Long standing controversies have been resolved, such as the position of the red panda, *Ailurus fulgens* F. Cuvier, 1825, as the sole living representative of the family Ailuridae, the monophyly of the pinnipeds, and the relationships of the Malagasy carnivorans of the family Eupleridae with Herpestidae (see discussion in Flynn et al. 2010). However, within the subclade Feliformia there remains an unresolved polytomy. While studies agree that Nandiniidae is the sister taxon to other feliforms, it is uncertain if the subsequent clade to diverge is Viverridae or Felidae. Even large-scale molecular studies have not successfully resolved these relationships (Flynn et al. 2005). The fossil record is also rather unhelpful for this phylogenetic problem, as the feliform fossil record does not begin until the late Oligocene (Goswami 2010). Representatives of extant caniform families are known in the late Eocene (Flynn and Wesley-Hunt 2005; Goswami 2010); therefore, this lack of fossil taxa represents a long ghost lineage within Feliformia.

The ghost lineage of *N. binotata* is exceptionally long; it is not only the sole living member of its family, but to date the only known taxon. The fossil record of Nandiniidae consists of a 6.1 Ma tooth of *Nandinia* sp. from Kenya (Werdelin and Peigné 2010). Thus, our knowledge of the morphology of the basalmost lineage within Feliformia entirely comes from the single extant species. It has been proposed in past literature, primarily based upon the ear region, that *N. binotata* is in some respects a “living fossil” that preserves the plesiomorphic feliform morphology (Pocock 1929; Hunt 1987, 1989, 1998, 2001; Hunt and Tedford 1993). In order to ascertain (A) if the rest of the cranial morphology is as ‘primitive’ in nature as the ear region, with its non-inflated bulla, and (B) what increased knowledge of the skull of *N. binotata* can contribute to clarifying the phylogenetic relationships near the base of Feliformia, we compare

our sample of *N. binotata* with representatives from three other extant carnivoran families, Canidae, Felidae, and Viverridae. We include four comparative figures (Figs. 41–44) that show the skulls and mandibles of *N. binotata*, the wolf, *Canis lupus* Linnaeus, 1758, the domestic cat, *F. catus*, and the common genet, *Genetta genetta* (Linnaeus, 1758). Below, we make general and detailed comparisons based on these figures.

**Skull in Dorsal View (Fig. 41).**—The overall shape of the skull in this view is remarkably similar in *N. binotata* and *G. genetta*. This includes the shape and proportions of the rostrum, braincase, nuchal crest, orbits, temporal fossae, and zygomatic arches. Detailed similarities (not present in *C. lupus* and *F. catus*) include nasals that do not extend beyond the anterior orbital rim, posterodorsal processes of the premaxillae that approximate the maxillary processes of the frontals, frontals that are much longer anteroposteriorly than the parietals, and molar roots exposed in the orbit floor.

The three feliforms differ from *C. lupus* in that the pre-orbital length is much smaller than the postorbital length, presence of prominent nasal processes of the nasals, absence of flaring of the cheeks posterior to the infraorbital foramen (presence in *C. lupus* is associated with the elongate infra-orbital canal), presence of an extensive orbital floor, zygomatic arches that are subparallel, posttympanic processes of the squamosal that are hidden in dorsal view, U-shaped (vs. V-shaped) nuchal crest, and presence of the supraoccipital on the anterior surface of the nuchal crest.

*Felis catus* is distinguished from the other taxa by its short rostrum, large orbits nearly enclosed by large postorbital processes of the frontals and frontal processes of the jugals, and squamosals that are visible in dorsal view.

**Skull in Lateral View (Fig. 42).**—As in the dorsal view, *N. binotata* and *G. genetta* share remarkable resemblances in the overall shape of the skull and the proportions of its component parts. The lateral view highlights the similarities in the size and arching of the zygoma, composition of the orbital rim, extent and shape of the entopterygoid process, and shape and orientation of the external acoustic meatus.

The three feliforms share a convex profile to the dorsal border of their skull, in contrast to the depression between the rostrum and braincase and the exaggerated sagittal crest in *C. lupus*. The feliforms are further distinguished from *C. lupus* by a short infraorbital canal, weakly bifurcated jugal, strong preglenoid process of the squamosal, jugal extending posteriorly to the preglenoid process, nuchal crest well separated from the posterior root of the zygoma, and more erect occipital profile.

*Felis catus* is distinguished by its strong anterior zygoma (related to its greater degree of orbit enclosure), ethmoid exposure in the orbit (not visible in Fig. 42), thin and posterodorsally directed alisphenoid in the temporal fossa, squamosal forming considerably more of the lateral braincase, and occiput as the posteriormost part of the skull rather than the occipital condyle. *Genetta genetta* is distinguished by its

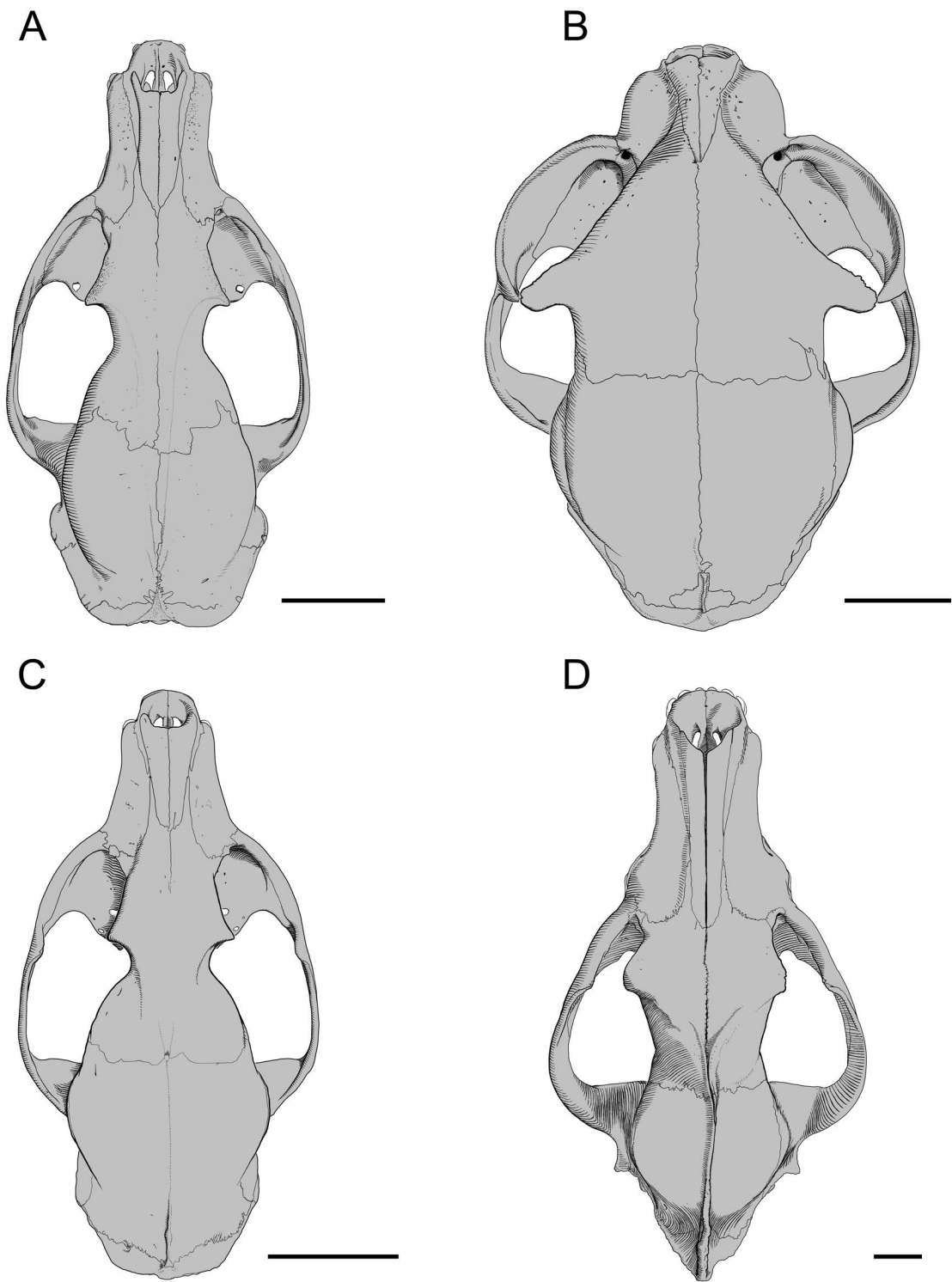


Fig. 41—Skulls in dorsal view. **A**, *Nandinia binotata*, CM 59495; **B**, *Felis catus*, CM 12910; **C**, *Genetta genetta*, CM 85593; **D**, *Canis lupus*, CM 57444. Scale = 20 mm.

strong confluence of the optic foramina. *Nandinia binotata* is distinguished by its less inflated auditory bulla. *Nandinia binotata* and *C. lupus* share a well-developed paracondylar process of the exoccipital that is directed posteroventrally, in contrast to the weaker vertical element in *F. catus* and *G. genetta*.

**Skull in Ventral View (Fig. 43).**—The remarkable resemblances between *N. binotata* and *G. genetta* noted above are also found in the ventral view. Detailed similarities include basioccipital width greater than the width at the choanae, principal major palatine foramina anterior to the palato-maxillary suture, vomer not visible in the basipharyngeal canal, absence of ectopterygoid processes, and postorbital processes not visible in the temporal fossae.

The feliforms are distinguished from *C. lupus* by incisors aligned more transversely, cheekteeth diverging posteriorly, anterior zygoma over multiple tooth positions (vs. a single tooth), infraorbital foramen on the anterior face of the anterior zygoma (vs. far anterior to the anterior zygoma), palatines contributing more to the palate, large minor palatine notches, a postdental palate, entopterygoid processes straight or diverging posteriorly (vs. converging), braincase expansion visible in the rear of the temporal fossa, and auditory bullae anteroposteriorly elongate (vs. circular). In *C. lupus*, the basicranium is anteroposteriorly compressed and the glenoid fossa is shifted posteriorly.

*Genetta genetta* is distinguished by a posterior carotid foramen well anterior to the jugular foramen; *N. binotata* and *C. lupus* share a common depression for the alisphenoid canal and foramen ovale, with the alisphenoid canal absent in *F. catus*. *Felis catus* is further distinguished by the near absence of a muscular tubercle on the basioccipital.

**Mandible in Lateral View (Fig. 44).**—In lateral view, the mandibles of *N. binotata* and *G. genetta* are very similar in the general proportions and size of the body and ramus, the shape and bordering crests of the masseteric fossa, and the shape and direction of the angular process. The few differences concern the shape of the coronoid process and the more robust angular process in *G. genetta*. In medial view (not shown), the position of the mandibular foramen of *N. binotata* and *G. genetta* is halfway between the more anterior placement in *F. catus* and the more posterior one in *C. lupus*.

The feliforms are distinguished from *C. lupus* by a convex ventral margin to the body and ramus (*C. lupus* has a concavity anterior to the angular process), masseteric fossa that extends anteriorly onto the body and is better defined by its outer crests, less robust angular process, and distinct pterygoid fovea for the attachment of the lateral pterygoid muscle (not visible in Fig. 44). The feliforms also have more mental foramina (three in *C. lupus* vs. four or more in *F. catus*, *G. genetta*, and the majority of *N. binotata*; six of 29 specimens of *N. binotata* have three on one side only).

*Felis catus* is distinguished by a more posteriorly reclined coronoid process, shorter mandibular symphysis (barely

extending posterior to the canine), and greater intermandibular angle between the left and right sides (circa 50° vs. 30°).

**Hyoid Apparatus and Larynx.**—Comparisons of *N. binotata* are made with the elements of the hyoid apparatus and larynx as described for *F. catus* (Jayne 1898; Reighard and Jennings 1935) and *C. lupus familiaris* (Baum and Zitzschmann 1936; Gasc 1967; Evans 1993). Unfortunately, we do not have access to a complete hyoid apparatus for *Genetta*. The stylohyal, epihyal, and ceratohyal are attached to the skull of *G. genetta*, CM 48670; the basihyal and thyrohyal are missing. We compared two additional feliforms, the viverrid *Viverricula indica* (É. Geoffroy Saint-Hilaire, 1803), CM 88222, which preserves the hyoid elements except the thyrohyal, and the herpestid *Herpestes javanicus* (É. Geoffroy Saint-Hilaire, 1818), CM 112473, which preserves the entire hyoid and the ossified thyroid cartilage.

The proportions of the hyoid elements are similar across the six taxa with one noteworthy exception. Although the stylohyal is the longest element in each, it is only slightly longer than the epihyal in *N. binotata* and *C. lupus familiaris*, but more than twice the length of the epihyal in the remaining taxa. The stylohyal of *N. binotata* is essentially straight (Fig. 34), but is distinctly medially bowed in the other taxa. The ceratohyal contacts the basihyal in *N. binotata*, *F. catus*, *V. indica*, and *H. javanicus* (Figs. 34–35), but both the basihyal and thyrohyal in *C. lupus familiaris*. The thyrohyal has an identifiable angle on its caudal margin in *N. binotata*, *F. catus*, and *H. javanicus* (Fig. 35), whereas this margin is straight in *C. lupus familiaris*. A chondrohyal cartilage connects the thyrohyal and the rostral cornu of the thyroid in *N. binotata*, *F. catus*, and *H. javanicus*, but not in *C. lupus familiaris*.

The thyroid is ossified in *N. binotata* (Fig. 35) and *H. indica*, but ossification has not been reported for *F. catus* and *C. lupus familiaris*. In terms of the shape and proportions of the laminae, those of *N. binotata*, *F. catus*, and *H. indica* are rectangular, whereas those of *C. lupus familiaris* are more rounded. The caudal cornu is well developed in *N. binotata* and *C. lupus familiaris*, but is weak in *F. catus* and *H. indica*. The thyroid of *N. binotata* is more similar to that of *H. indica*: they both have an elongate rostral cornu that is angled ventrally and a small, rounded process ventral to the caudal cornu. The thyroid of *H. indica* differs in two features: it has a foramen at the base of the rostral cornu and a well-developed epiglottic prominence on the rostral margin. We cannot exclude the presence of an epiglottic prominence in *N. binotata* as the rostral margin is imperfectly preserved (Fig. 35).

The only observation to make about the cricoid is that it is ossified in *N. binotata* (Fig. 35), but ossification has not been reported for *F. catus* and *C. lupus familiaris*, and the element is not preserved in the other taxa studied.

**Foramina, Canals, and Grooves.**—Preceding Appendix 1 is a glossary comparing the major cranial foramina, canals,

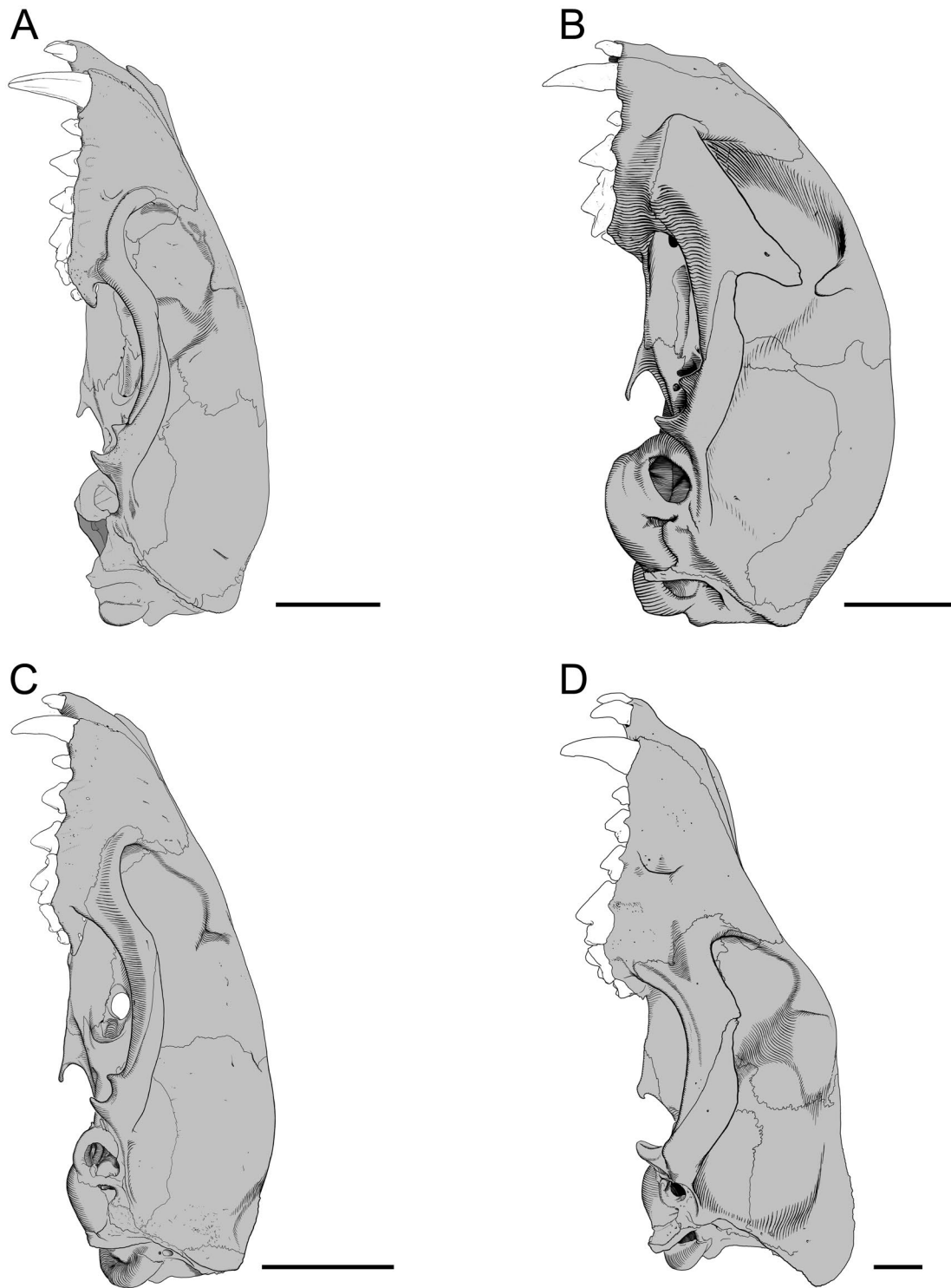


Fig. 42—Skulls in lateral view. **A**, *Nandinia binotata*, CM 59495; **B**, *Felis catus*, CM 12910; **C**, *Genetta genetta*, CM 85593; **D**, *Canis lupus*, CM 57444. In A, the caudal entotympanic (darker gray) is based on AMNH 51513. Scale = 20 mm.

and grooves of *N. binotata*, *C. lupus familiaris*, *F. catus*, and *G. genetta*. The general pattern of these structures follows that reported above, i.e., *N. binotata* and *G. genetta* are the pair sharing the most resemblances. This includes the detailed arrangement of the palatal foramina (Fig. 43), namely the composition of the incisive foramina, position of the interincisive foramina, position and number of major palatine and accessory palatine foramina, and the composition of the minor palatine notches. Both have a carotid foramen in the basisphenoid vs. one between the basisphenoid and petrosal in *F. catus* (Hunt 1974) and *C. lupus familiaris* (Evans 1993). Both have a posterior carotid foramen between the caudal entotympanic and the rostral tympanic process of the petrosal (the latter is lacking in *F. catus* and *C. lupus familiaris*). Both have a sigmoid sinus that does not exit at the jugular foramen as it does in *F. catus* (Reighard and Jennings 1935) and *C. lupus familiaris* (Evans 1993), but that enters the condyloid canal. The lacrimal fenestra is on the palatine and maxilla with no lacrimal involvement, the fenestra vestibuli is rounder, and the sphenorbital fissure is twinned with the foramen rotundum (closer to that opening than the optic foramen).

The feliforms are distinguished from *C. lupus familiaris* and *C. lupus* by caudal palatine foramina in the horizontal process of the palatine (vs. in the perpendicular process), a seam within the palatine in the dorsal border of the sphenopalatine foramen, rostral opening of the pterygoid canal in the cavum epiptericum (vs. the pterygopalatine fossa), postglenoid foramen posteromedial to the postglenoid process (vs. posterior to; Fig. 43), musculotubal canal and anterior carotid foramen continuous (vs. separated), aperture of the cochlear fossula that is half moon-shaped or round (vs. cone-shaped), absence of a trigeminal canal, endocranial inferior petrosal sinus (vs. intramural), absence of mastoid foramina, and (as noted above) shorter infraorbital canal (Fig. 42) and more mental foramina (Fig. 44).

*Nandinia binotata* is distinguished from the other taxa considered here by the stylomastoid foramen at the tympanohyal (foramen stylomastoideum primitivum vs. definitivum) and a carotid groove on the tympanic surface of the basisphenoid leading to the carotid foramen. It shares with *F. catus* a transpromontorial course for the internal carotid artery and a jugular foramen with no basioccipital involvement (the condition in *G. genetta* is unknown). *Nandinia binotata* and *C. lupus* have a narrow optic chiasm, while *F. catus* and *G. genetta* have a broad one.

**Basicranium.**—Hunt (1987, 1989, 1998, 2001; Hunt and Tedford 1993) argued that *N. binotata* expresses the primitive feliform pattern for various structures of the basicranium, including the components of the auditory bulla and their attachments to the skull, the arrangement of the bullar chambers, and the form of the petrosal. He supported this view based on the distribution of basicranial morphologies in extant feliforms and on the remarkable resemblances between *N. binotata* and the oldest known feliforms, stenoplesictines and proailurines from the late Oligocene Quercy

fissures of France. A full evaluation of Hunt's hypothesis also requires treatment of the condition in non-crown carnivoramorphans, which is beyond the scope of this report. However, we evaluate the impact of our descriptions of *N. binotata* and comparisons on Hunt's hypothesis here.

According to Hunt (1987, 1989), the primitive nature of the ectotympanic of *N. binotata* includes its small size, relatively uninflated state (vs. inflated), lack of contact with the promontorium (vs. contact separating the anterior and posterior chambers), and shallow "registration marks" for the anterior crus on the squamosal and alisphenoid (vs. deep marks for a more inflated ectotympanic). Our study here makes two corrections concerning the "registration mark" on the alisphenoid. First, in *N. binotata*, this mark (the malleolar hook facet here; Figs. 15–16) is not for the ectotympanic but for the malleolar hook of the rostral process of the malleus, and second, it is not on the alisphenoid but on the epitympanic wing of the parietal. Based on the distribution of a malleolar hook in Carnivora reported by Wible and Spaulding (2012), a registration mark for it is likely primitive for the clade. However, the occurrence of this mark on the parietal, a skull roof element, is to date unique to *N. binotata* and far from primitive. A unique feature of the ectotympanic of *N. binotata* of uncertain polarity is the well-developed sulcus on the posterior crus that houses the caudal entotympanic (Figs. 22, 26A).

According to Hunt (1987, 1989), the primitive condition of the rostral entotympanic of *N. binotata* includes its lack of contact with the ectotympanic (athetic condition of Hunt [1987] where a gap separates the two vs. thetic condition where they contact), and the course of the internal carotid artery on the lateral aspect of the rostral entotympanic. In addition, Hunt (1989) noted that the rostral tympanic process of the petrosal in *N. binotata*, stenoplesictines, and proailurines is positioned farther posteriorly than in other feliforms, which means that the rostral entotympanic also extends farther posteriorly as it contacts the anterior face of the rostral process. A unique feature of the rostral entotympanic of *N. binotata* of uncertain polarity is the well-developed sulcus that houses the caudal entotympanic (Figs. 16B, 24).

According to Hunt (1987:32), "it is not the cartilaginous composition of *Nandinia's* caudal entotympanic that suggests its bulla structure is primitive, but rather the size, form, and spatial relations of caudal entotympanic to other bullar and basicranial elements." Specifically, it does not have the usual feliform navicular shape, it is small relative to the ectotympanic and rostral entotympanic, it intervenes between the ectotympanic and rostral entotympanic but does not overgrow the latter, and it has simple edge to edge contact with the ectotympanic and rostral entotympanic. In contrast to prior authors, we characterize the caudal entotympanic of *N. binotata* as a mixture of cartilage and bone, with the latter typically in the periphery. This is reminiscent of Hough's (1953) observation, noted by Hunt (1987:17), that "in the eventually ossified yet initially hyaline cartilage caudal entotympanic of the viverrid *Viverricula*, ossification first

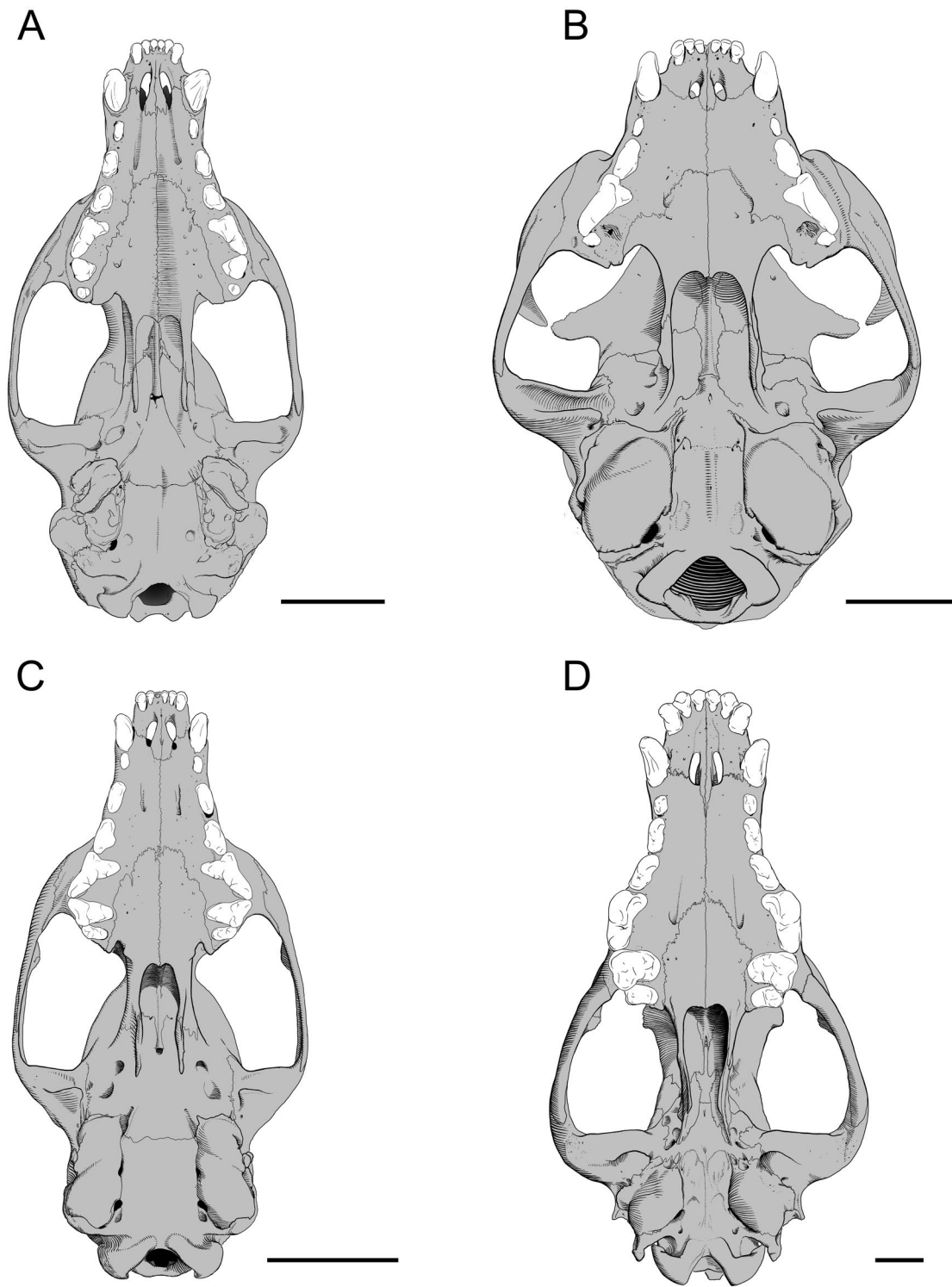


Fig. 43—Skulls in ventral view. **A**, *Nandinia binotata*, CM 59495; **B**, *Felis catus*, CM 12910; **C**, *Genetta genetta*, CM 85593; **D**, *Canis lupus*, CM 57444. Scale = 20 mm.

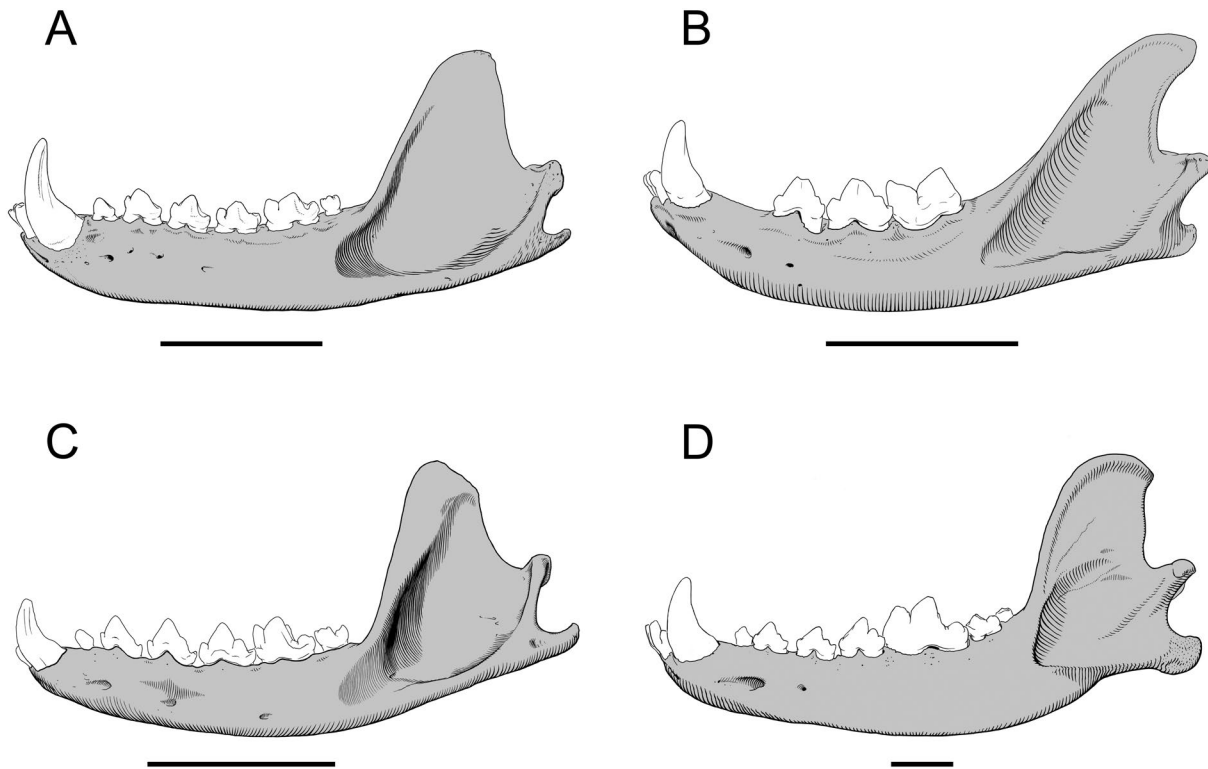


Fig. 44—Left mandibles in lateral view. **A**, *Nandinia binotata*, AMNH 51503; **B**, *Felis catus*, CM 12910; **C**, *Genetta genetta*, CM 85593; **D**, *Canis lupus*, CM 57444. Scale = 20 mm.

appears in the medial and posterior walls of the cartilaginous entotympanic, and then during ontogeny spreads to the ventral floor.” Thus, adult *N. binotata* expresses an earlier ontogenetic stage of the viverrid caudal entotympanic, showing the onset of ossification in the periphery and lack of inflation. A detail of the caudal entotympanic described here for the first time is the presence of a facet for the element on the crista interfenestralis (Fig. 15); Hunt’s (1989: fig. 7) drawings show the facet not extending anterior to the aperture of the cochlear fossula.

According to Hunt (1989), the primitive nature of the petrosal of *N. binotata* includes its robust, centrally placed rostral tympanic process (vs. gracile, anteriorly placed process or no process), lack of a facet on the promontorium for the ectotympanic, facet for the caudal entotympanic on the posterior margin, and transpromontorial course for the internal carotid artery. Hunt (1989) further noted that in most regards the petrosal of *N. binotata* is remarkably like that of the stenoplesictine *Stenoplesictis* Filhol, 1880, “including the tensor tympani fossa, epitympanic recess, bony canal for the facial nerve, mastoid geometry, and the configuration of the surrounding basicranial bones.” In light of Hunt’s descriptions and illustrations of *Stenoplesictis*, we agree with his assessment and add another similarity, the curving carotid groove on the basisphenoid leading to the carotid foramen (see Hunt 1989: fig. 8). To our knowledge,

this odd course for the internal carotid is unique to these forms among carnivorans. A difference reported by Hunt (1989) is that *Stenoplesictis* has a facet on the promontorium for the ectotympanic anterior to the aperture of the cochlear fossula, which indicates some separation between the anterior and posterior chambers. However, this apparent difference may in fact be another resemblance, as positionally this facet (see Hunt 1989: fig. 8) is similar in position to the facet we found in *N. binotata* for the caudal entotympanic (Figs. 21A, C–D, F).

Two additional features of the petrosal of *N. binotata* that are unusual compared to other placentals are the rounded, lateral bulge on the crista interfenestralis and the medially tilted crista parotica (Fig. 17), which contact in some specimens. Together, these features serve to isolate the stapedius fossa from the main tympanic cavity (Fig. 17). We found the same morphology in *Genetta cristata* Hayman in Sanborn, 1940, CM 3697, *Felis* sp., CM 10750, and *C. lupus familiaris*, CM 106574, suggesting that this may be primitive for Carnivora.

## CONCLUSIONS

Our investigation of the cranial morphology of the African palm civet, *N. binotata*, has confirmed the overall primitive nature of its ear region proposed by previous researchers

(e.g., Pocock 1929; Hunt 1987, 1989, 1998, 2001; Hunt and Tedford 1993). While in more general literature (e.g., Starck 1995; Gaubert 2009), the cartilaginous nature of the adult caudal entotympanic has received the most attention, what gives the basicranium of *N. binotata* its characteristic morphology is the lack of inflation of the bulla, not the lack of ossification of the caudal entotympanic (and in fact we have found that element to routinely have ossifications at its attachment sites), as already stated in previous studies (Hunt 1987, 1989). When the morphology of the remainder of the skull is compared to representative of three extant carnivoran families (Canidae, Felidae, and Viverridae), while many features are found that group the feliforms to the exclusion of the caniform, the greatest similarity in the study sample is found between *N. binotata* and the viverrid representative, *G. genetta* - not an unexpected result, given how for much of its taxonomic history *N. binotata* was grouped within Viverridae. Two possible conclusions can be drawn from this: 1) *N. binotata* does not retain an especially primitive overall cranial morphology and the ear region is not representative, or 2) *N. binotata* does retain a primitive morphology throughout its cranium and this is shared by modern Viverridae, extrapolating from *G. genetta*. This latter option implies that the trichotomy near the base of Feliformia (i.e., Viverridae, Felidae, and all remaining families except Nandiniidae) may be most parsimoniously resolved with the Viverridae being the first family to branch off past Nandiniidae. Whatever the far-reaching implications, it is clear that the non-basicranial morphology of the skull of *N. binotata* does not share the extremely primitive aspects found and previously commented upon in the ear region.

Within our sample of 30 individuals, from varying localities and ranging from newborn to fully matured adult forms with many fused sutures, we documented large amounts of morphological variation. Almost every cranial bone was found to vary in discrete ways, such as contacts with surrounding elements or positions and number of foramina. The bone with the largest amount of variation throughout the study sample was the lacrimal. Most of the variation seen did not follow patterns that could be attributed to ontogenetic differences, sexual dimorphism, or subspecies distinctions. Many of the structures found to vary have been used in prior phylogenetic analysis, at the level of Carnivora (e.g., Wesley-Hunt and Flynn 2005) and even Mammalia (e.g., O'Leary et al. 2013). Polymorphisms have not received much attention in the literature, as typically a single exemplar is used to represent a species (or higher-level taxon) in a phylogenetic analysis. Most descriptive studies also do not include more than one exemplar specimen, but investigations of 54 specimens of several species of the didelphid *Monodelphis* Burnett, 1830, found great variations in the distribution of cranial foramina (Wible 2003). A study of 80 specimens of an extant cryptodire turtle, the Texas river cooter, *Pseudemys texana* Baur, 1893, from a single population recovered a similar level of variation not explained by age or sex (Bever 2009), which is even more striking than our findings regarding *N. binotata*, as our study sample

ranged across Africa and included zoo specimens. Recognition of polymorphisms is not a reason to discount characters (Wiens 1995, 1999), but serves as an important reminder to survey a range of specimens when conducting phylogenetic studies or erecting systematic diagnoses.

We conclude by evaluating a recent diagnosis of *N. binotata* by Werdelin and Peigné (2010) in light of our findings. They wrote (p. 621): "Small-sized carnivoran with dental formula I 3/3, C 1/1, P 4/4, M 1-2/1-2; skull with triangular palate; primitive auditory bulla (no inflation during ontogeny, single rather than double chamber, no septum bullae, cartilaginous caudal entotympanic); paroccipital apophysis [=paracondylar process] relatively thick; lachrymal [=lacrimal] and jugal bones not in contact; anterior rim of orbit formed by frontal, maxillary and jugal; posterior carotid foramen located between the basisphenoid and the caudal entotympanic; upper incisors forming a transverse line; lingual cusp present on P3 [=P4]; M2/m2 very reduced and rounded, sometime absent; m2 with only a small buccal cusp."

Our findings suggest the following modifications to their diagnosis: caudal entotympanic partially cartilaginous; posterior carotid foramen located between the petrosal and caudal entotympanic. The following features should be removed because of their variability: lachrymal [=lacrimal] and jugal bones not in contact; anterior rim of orbit formed by frontal, maxillary and jugal; upper incisors forming a transverse line (in our sample they are gently arched). Finally, we propose the following addition: epitympanic wing of the parietal forming the facet for the malleolar hook of the rostral process of the malleus.

#### ACKNOWLEDGMENTS

This study was made possible by our access to collections of *N. binotata* and other carnivorans at two institutions: the Carnegie Museum of Natural History and the American Museum of Natural History. At the former, we thank Collection Manager Suzanne B. McLaren, and at the latter, we thank the entire curatorial staff of the Department of Mammalogy, especially Senior Scientific Assistant Eileen Westwig. The photographs were taken by the authors and the artwork was produced by Paul Bowden, Carnegie Museum of Natural History. For species identification of the genets studied here, we are grateful to Duane A. Schlitter. Robin Beck reviewed an earlier version of this manuscript, and his comments greatly improved the final product. We owe a debt to Bob Hunt for his pioneering investigations of the carnivoran ear region, which identified *N. binotata* as a taxon of considerable morphological significance. The research presented here was supported by the Carnegie Museum of Natural History, the R.K. Mellon North American Mammal Research Institute, the Rea Postdoctoral Fellowship, and National Science Foundation ATOI grant 0629959.

#### LITERATURE CITED

- ABBIE, A.A. 1939. A masticatory adaptation peculiar to some diprotodont marsupials. *Proceedings of the Zoological Society of London*, 1939:261-279.
- AGNARSSON, I., M. KUNTER, AND L.J. MAY-COLLADO. 2010. Dogs, cats, and kin: a molecular species-level phylogeny of Carnivora. *Molecular Phylogenetics and Evolution*, 54:726-745.
- ALLEN, G.M. 1939. A checklist of African mammals. *Bulletin of the Museum of Comparative Zoology at Harvard College*, 83:1-763.

- ALLEN, J.A. 1924. Carnivora collected by the American Museum Congo Expedition. *Bulletin of the American Museum of Natural History*, 47(3):73–281, pls. VI–LXXVIII.
- ANDERSEN, K. 1912. Catalogue of the Chiroptera in the Collection of the British Museum. Volume I: Megachiroptera. Trustees of the British Museum (Natural History), London. 30 pp.
- ARCHIBALD, J.D., AND A. AVERIANOV. 2012. Phylogenetic analysis, taxonomic revision, and dental ontogeny of the Cretaceous Zhelestidae (Mammalia: Eutheria). *Zoological Journal of the Linnean Society*, 164:361–426.
- BAUM, H., AND O. ZIETZSCHMANN. 1936. *Handbuch der Anatomie des Hundes*. 1. Band: Skelett- und Muskelsystem. Paul Parey, Berlin. 242 pp.
- BENSLEY, B.A. 1902. On the identification of Meckelian and mylohyoid grooves in the jaws of Mesozoic and Recent Mammalia. University of Toronto Studies, *Biological Series*, 3:75–81.
- BEVER, G.S. 2009. The postnatal skull of the extant North American turtle *Pseudemys texana* (Cryptodira: Emydidae), with comments on the study of discrete intraspecific variation. *Journal of Morphology*, 270(1):97–128.
- BININDA-EMONDS, O.R.P., J.L. GITTLEMAN, AND A. PURVIS. 1999. Building large trees by combining phylogenetic information: a complete phylogeny of the extant Carnivora (Mammalia). *Biological Reviews*, 74:143–175.
- BOYD, G.I. 1930. The emissary foramina of the cranium in man and the anthropoids. *Journal of Anatomy*, 65:108–121.
- CARLSSON, A. 1900. Ueber die systematische Stellung der *Nandina binotata*. *Zoologische Jahrbücher. Abtheilung für Systematik, Geographie und Biologie*, 13:509–528.
- CHAPUIS, G. 1966. Contribution à l'étude de l'artère carotide interne des carnivores. *Mammalia*, 30:82–96.
- CLARK, W.E. LEGRON. 1926. On the anatomy of the pen-tailed tree shrew (*Ptilocercus lowii*). *Proceedings of the Zoological Society of London*, 1926:1179–1309.
- COOPER, G., AND A.L. SCHILLER. 1975. *Anatomy of the Guinea Pig*. Harvard University Press, Cambridge. 417 pp.
- DAVIS, D.D. 1964. The giant panda: a morphological study of evolutionary mechanisms. *Fieldiana: Zoology Memoirs*, 3:1–339.
- DAVIS, D.D., AND H.E. STORY. 1943. The carotid circulation in the domestic cat. *Fieldiana: Zoology*, 28(1):1–47.
- DAVISON, A. 1903. *Mammalian Anatomy with Special Reference to the Cat*. P. Blakiston's Son & Co., Philadelphia. 250 pp.
- DE BEER, G.R. 1929. The development of the skull of the shrew. *Philosophical Transactions of the Royal Society of London*, B217:411–480, pls. 94–98.
- . 1937. *The Development of the Vertebrate Skull*. Clarendon Press, Oxford. 554 pp., 143 pls.
- EIZIRIK, E., W.J. MURPHY, K.-P. KOEPLI, W.E. JOHNSON, J.W. DRAGOO, R.K. WAYNE, AND S.J. O'BRIEN. 2010. Pattern and timing of diversification of the mammalian order Carnivora inferred from multiple nuclear gene sequences. *Molecular Phylogenetics and Evolution*, 56:49–63.
- ELLENBERGER, W., AND H. BAUM. 1891. *Systematische und topographische Anatomie des Hundes*. Paul Parey, Berlin. 646 pp.
- ELLERMAN, J.R., T.C.S. MORRISON-SCOTT, AND R.W. HAYMAN. 1953. *Southern African Mammals 1758 to 1951: A Reclassification*. Trustees of the British Museum (Natural History), London. 363 pp.
- EVANS, H.E. 1993. *Miller's Anatomy of the Dog*. W.B. Saunders, Philadelphia. 1113 pp.
- FINARELLI, J.A. 2008. A total evidence phylogeny of the Arctoidea (Carnivora: Mammalia): relationships among basal taxa. *Journal of Mammalian Evolution*, 15(4):231–259.
- FLOWER, W.H. 1869. On the value of characters of the base of the cranium in the classification of the order Carnivora, and on the systematic position of *Bassaris* and other disputed forms. *Proceedings of the Zoological Society of London*, 1869:4–37.
- . 1872. Note on the anatomy of the two-spotted paradoxure (*Nandinia binotata*). *Proceedings of the Zoological Society of London*, 1872:683–684.
- FLYNN, J.J., J.A. FINARELLI, AND M. SPAULDING. 2010. Phylogeny of the Carnivora and Carnivoramorpha, and the use of the fossil record to enhance understanding of evolutionary transformations. Pp. 25–63, in *Carnivoran Evolution: New Views on Phylogeny, Form, and Function* (A. Goswami and A. Friscia, eds.). Cambridge University Press, Cambridge.
- FLYNN, J.J., J.A. FINARELLI, S. ZEHR, J. HSU, AND M.A. NEBAL. 2005. Molecular phylogeny of the Carnivora (Mammalia): assessing the impact of increased sampling on resolving enigmatic relationships. *Systematic Biology*, 54(2):317–337.
- FLYNN, J.J., AND G.D. WESLEY-HUNT. 2005. Carnivora. Pp. 175–198, in *The Rise of Placental Mammals: Origins and Relationships of the Major Extant Clades* (K.D. Rose and J.D. Archibald, eds.). The Johns Hopkins University Press, Baltimore.
- GASC, J.P. 1967. Squelette hyobranchial. Pp. 550–583, 1103–1106, in *Traité de Zoologie*, tome XVI, fascicule I (P.-P. Grassé, ed.). Masson et Cie, Paris.
- GAUBERT, P. 2009. Family Nandiniidae (African palm civet). Pp. 50–53, in *Handbook of the Mammals of the World. Volume 1. Carnivores* (D.E. Wilson and R.A. Mittermeier, eds.). Lynx Edicions, Barcelona.
- GAUBERT, P., W.C. WOZENCRAFT, P. CORDEIRO-ESTRELA, AND G. VERON. 2005. Mosaics of convergence and noise in morphological phylogenies: what's in a viverrid-like carnivoran? *Systematic Biology*, 54(6):865–894.
- GAUPE, E. 1902. Über die Ala temporalis des Säugetierschädels und die Regio orbitalis einiger anderer Wirbeltierschädels. *Anatomische Hefte*, 19:155–230.
- . 1905. Neue Deutungen auf dem Gebiete der Lehre vom Säugetierschädel. *Anatomischer Anzeiger*, 27:273–310.
- GIANNINI, N.P., AND N.B. SIMMONS. 2007. The chiropteran premaxilla: a reanalysis of morphological variation and its phylogenetic interpretation. *American Museum Novitates*, 3585:1–44.
- GIANNINI, N.P., J.R. WIBLE, AND N.B. SIMMONS. 2006. On the cranial osteology of Chiroptera. I. *Pteropus* (Megachiroptera: Pteropodidae). *Bulletin of the American Museum of Natural History*, 295:1–134.
- GOSWAMI, A. 2010. Introduction to Carnivora. Pp. 1–24, in *Carnivoran Evolution: New Views on Phylogeny, Form, and Function* (A. Goswami and A. Friscia, eds.). Cambridge University Press, Cambridge.
- GRAY, J.E. 1830. *Spicilegium Zoologicum; or Original Figures and Short Systematic Descriptions of New and Unfigured Animals*. Treutel, Würtz and Co., and W. Wood, London. 12 pp., 11 pls.
- . 1832. On the family Viverridae and its generic subdivisions; with an enumeration of the species of *Paradoxus*, and characters of several new ones. *Proceedings of the Zoological Society of London*, 1832:63–68.
- . 1843. List of the Specimens of Mammalia in the Collection of the British Museum. British Museum (Natural History) Publications, London. 216 pp.
- . 1864. A revision of the genera and species of viverrine animals (Viverridae), founded on the collection in the British Museum. *Proceedings of the Zoological Society of London*, 1864:502–578.
- GREGORY, W.K. 1910. The orders of mammals. *Bulletin of the American Museum of Natural History* 27:1–524.
- GREGORY, W.K., AND M. HELLMAN. 1939. On the evolution and major classification of the civets (Viverridae) and allied fossil and recent Carnivora: a phylogenetic study of the skull and dentition. *Proceedings of the American Philosophical Society*, 81:309–392.
- HELGEN, K.M., C.M. PINTO, R. KAYS, L.E. HELGEN, M.T.N. TSUCHIYA, A. QUINN, D.E. WILSON, AND J.E. MALDONADO. 2013. Taxonomic revision of the olingos (*Bassaricyon*), with description of a new species, the olinguito. *ZooKeys*, 324: 1–83.
- HENSON, O.W., JR. 1961. Some morphological and functional aspects of certain structures of the middle ear in bats and insectivores. *University of Kansas Science Bulletin*, 52(3):151–255.
- HIATT, J.L., AND L.P. GARTNER. 1987. *Textbook of Head and Neck Anatomy*, Second Edition. Williams & Wilkins, Baltimore. 383 pp.
- HONACKI, J.H., K.E. KINMAN, AND J.W. KOEPLI (EDS.). 1982. *Mammal Species of the World: A Taxonomic and Geographic Reference*.

- Allen Press, Inc. and The Association of Systematics Collections, Lawrence. 694 pp.
- HOUGH, J. 1953. Auditory region in North American fossil Felidae: its significance in phylogeny. United States Geological Survey Professional Papers, 243-G:95–115.
- HOUGH, J.R. 1948. The auditory region in some members of the Procyonidae, Canidae, and Ursidae: its significance in the phylogeny of the Carnivora. *Bulletin of the American Museum of Natural History*, 92(2):67–118.
- HUNT, R.M., JR. 1974. The auditory bulla in Carnivora: an anatomical basis for reappraisal of carnivore evolution. *Journal of Morphology*, 143:21–76.
- . 1987. Evolution of the aeluroid Carnivora: significance of auditory structure in the nimravid cat *Dinictis*. *American Museum Novitates*, 2886:1–74.
- . 1989. Evolution of the aeluroid Carnivora: significance of the ventral promontorial process of the petrosal, and the origin of the basicranial patterns in the living families. *American Museum Novitates*, 2930:1–32.
- . 1998. Evolution of the aeluroid Carnivora: diversity of the earliest aeluroids from Eurasia (Quercy, Hsanda-Gol) and the origin of felids. *American Museum Novitates*, 3252:1–65.
- . 2001. Basicranial anatomy of the living linsangs *Prionodon* and *Poiana* (Mammalia, Carnivora, Viverridae), with comments on the early evolution of aeluroid carnivorans. *American Museum Novitates*, 3330:1–24.
- HUNT, R.M., JR., AND R.H. TEDFORD. 1993. Phylogenetic relationships within aeluroid Carnivora and implications of their temporal and geographic distribution. Pp. 53–73, in *Mammal Phylogeny, Volume 2. Placentals* (F.S. Szalay, M.J. Novacek, and M.C. McKenna, eds.). Springer, New York.
- JAYNE, H. 1898. *Mammalian Anatomy, A Preparation for Human and Comparative Anatomy. Part 1. The Skeleton of the Cat, Its Muscular Attachments, Growth, and Variations Compared with the Skeleton of Man*. J.B. Lippincott Company, Philadelphia. 816 pp.
- KAMPEN, P.N. VAN. 1905. Die Tympanalgegend des Säugetierschädels. *Gegenbaurs Morphologisches Jahrbuch*, 34:321–722.
- KIELAN-JAWOROWSKA, Z. 1981. Evolution of the therian mammals in the Late Cretaceous of Asia. Part IV. Skull structure in *Kennalestes* and *Asioryctes*. *Palaeontologia Polonica*, 42:25–78.
- KIELAN-JAWOROWSKA, Z., R.L. CIFELLI, AND Z.-X. LUO. 2004. Mammals from the Age of Dinosaurs: Origin, Evolution, and Structure. Columbia University Press, New York. 630 pp.
- KIELAN-JAWOROWSKA, Z., AND D. DASHZEVEG. 1989. Eutherian mammals from the Early Cretaceous of Mongolia. *Zoologica Scripta*, 18:347–355.
- KINGDON, J. 1997. *The Kingdon Field Guide to African Mammals*. Academic Press, San Diego. 465 pp.
- KLAAUW, C.J. VANDER. 1922. Über die Entwicklung des Entotympanicums. *Tijdschrift Nederlandsche Dierkundige Vereeniging*, 18:135–174.
- . 1929. On the development of the tympanic region of the skull in the Macroscelididae. *Proceedings of the Zoological Society of London*, 1929:491–560.
- . 1931. The auditory bulla in some fossil mammals with a general introduction to this region of the skull. *Bulletin of the American Museum of Natural History*, 62:1–352.
- KOYABU, D., W. MAIER, AND M.R. SÁNCHEZ-VILLAGRA. 2012. Paleontological and developmental evidence resolve the homology and dual embryonic origin of a mammalian skull bone, the interparietal. *Proceedings of the National Academy of Sciences of the United States of America*, 109(35):14075–14080.
- LUO, Z.-X., Z. KIELAN-JAWOROWSKA, AND R.L. CIFELLI. 2002. In quest for a phylogeny of Mesozoic mammals. *Acta Palaeontologica Polonica*, 47(1):1–78.
- MACINTYRE, G.T. 1972. The trisulcate petrosal pattern of mammals. *Evolutionary Biology*, 6:275–303.
- MACPHEE, R.D.E. 1979. Entotympanics, ontogeny and primates. *Folia Primatologica*, 31:23–47.
- . 1981. Auditory regions of primates and eutherian insectivores: morphology, ontogeny, and character analysis. *Contributions to Primatology*, 18:1–282.
- . 1994. Morphology, adaptations, and relationships of *Plesiorcyteropus*, and a diagnosis of a new order of eutherian mammals. *Bulletin of the American Museum of Natural History*, 220:1–214.
- MARSHALL, L.G., AND C. DE MUIZON. 1995. Part II: The skull. In *Pucadelphys andinus* (Marsupialia, Mammalia) from the early Paleocene of Bolivia (C. de Muizon, ed.). *Mémoires du Muséum nationale d'Histoire naturelle*, 165:21–90.
- MCDOWELL, S.B., JR. 1958. The Greater Antillean insectivores. *Bulletin of the American Museum of Natural History*, 115(3):113–214.
- MCKENNA, M.C., AND S.K. BELL. 1997. *Classification of Mammals Above the Species Level*. Columbia University Press, New York. 631 pp.
- MEESTER, J.A., I.L. RAUTENBACH, N.J. DIPPENAAR, AND C.M. BAKER. 1986. *Classification of Southern African Mammals*. Transvaal Museum Monograph, 5. Transvaal Museum, Pretoria. 359 pp.
- MEESTER, J., AND H. SETZER. 1971. *The Mammals of Africa: An Identification Manual*. Smithsonian Institution Press, City of Washington.
- MENG, J., AND R.C. FOX. 1995. Osseous inner ear structures and hearing in early placentals and marsupials. *Zoological Journal of the Linnean Society*, 115:47–71.
- MEREDITH, R.W., J.E. JANECKA, J. GATESY, O.A. RYDER, C.A. FISHER, E.C. TEELING, A. GOODBLA, E. EIZIRIK, T.L. SIMAO, T. STADLER, D.L. RABOSKY, R. L. HONEYCUTT, J.J. FLYNN, C.M. INGRAM, C. STEINER, T.L. WILLIAMS, T.J. ROBINSON, A. BURK-HERRICK, M. WESTERMAN, N.A. AYOUB, M.S. SPRINGER, AND W.J. MURPHY. 2011. Impacts of the Cretaceous terrestrial revolution and KPg extinction on mammal diversification. *Science*, 334:521–524.
- MIAO, D. 1988. Skull morphology of *Lambdopsalis bulla* (Mammalia, Multituberculata) and its implications to mammalian evolution. *Contributions to Geology, University of Wyoming, Special Paper*, 4:1–104.
- MIVART, ST. G. 1881. *The Cat*. Charles Scribner's Sons, New York. 557 pp.
- . 1882. On the classification and distribution of the Aeluroidea. *Proceedings of the Zoological Society of London*, 1882:135–208.
- MOORE, W.J. 1981. *The Mammalian Skull*. Cambridge University Press, Cambridge. 369 pp.
- NESSOV, L., J.D. ARCHIBALD, AND Z. KIELAN-JAWOROWSKA. 1998. Ungulate-like mammals from the Late Cretaceous of Uzbekistan and a phylogenetic analysis of Ungulatomorpha. In *Dawn of the Age of Mammals in Asia* (K.C. Beard and M.R. Dawson, eds.). *Bulletin of Carnegie Museum of Natural History*, 34:40–88.
- NOMINA ANATOMICA, 5TH EDITION. 1983. Williams & Wilkins, Baltimore. 112 pp.
- NOMINA ANATOMICA VETERINARIA, 5TH EDITION. 2005. Editorial Committee, Hannover, Columbia, Ghent, Sapporo. [http://www.wava-amav.org/Downloads/nav\\_2005.pdf](http://www.wava-amav.org/Downloads/nav_2005.pdf)
- NOVACEK, M.J. 1977. Aspects of the problem of variation, origin and evolution of the eutherian auditory bulla. *Mammal Review*, 7:131–149.
- . 1986. The skull of leptictid insectivorans and the higher-level classification of eutherian mammals. *Bulletin of the American Museum of Natural History*, 183(1):1–112.
- O'LEARY, M.A., J.I. BLOCH, J.J. FLYNN, T.J. GAUDIN, A. GIALLOMBARDO, N.P. GIANNINI, S.L. GOLDBERG, B.P. KRAATZ, Z.-X. LUO, J. MENG, X. NI, M.J. NOVACEK, F.A. PERINI, Z. RANDALL, G.W. ROUGIER, E.J. SARGIS, M.T. SILCOX, N.B. SIMMONS, M. SPAULDING, P.M. VELAZCO, M. WEKSLER, J.R. WIBLE, AND A.L. CIRRANELLO. 2013. The placental mammal ancestor and the post-KPg radiation of placentals. *Science*, 339:662–667.
- O'LEARY, M.A., AND J. GATESY. 2008. Impact of increased character sampling on the phylogeny of Cetartiodactyla (Mammalia): combined analysis including fossils. *Cladistics*, 24:397–442.
- OSBORN, H.F. 1907. *Evolution of Mammalian Molar Teeth*. The Macmillan Company, New York. 250 pp.
- OSGOOD, W.H. 1921. A monographic study of the American marsupial, *Cenolestes*. *Field Museum of Natural History, Zoological Series*, 14(1):1–162, 22 pls.

- POCOCK, R.I. 1915. On the feet and glands and other external characters of the paradoxurine genera *Paradoxurus*, *Arctitis*, *Arctogalidia*, and *Nandinia*. Proceedings of the Zoological Society of London, 1915:387–412.
- . 1916. On the course of the internal carotid artery and the foramina connected therewith in the skulls of the Felidae and Viverridae. Annals and Magazine of Natural History, Series 8, xvii: 261–269 + pl. X and XI.
- . 1929. Carnivora. Pp. 896–900, in *Encyclopaedia Britannica*, 14<sup>th</sup> Edition, Volume IV.
- POHLE, H. 1920. Zur Kenntnis der Raubtiere. II. Die Stellungen der Gattungen *Amphictis* und *Nandinia*. Gesellschaft naturforschender Freunde (Berlin), 1920(1):48–62.
- RADINSKY, L. 1978. The evolutionary history of cat brains. *Museologia*, 11:35–41.
- REIGHARD, J., AND H.S. JENNINGS. 1935. *Anatomy of the Cat*. Third edition. Henry Holt and Company, New York. 486 pp.
- ROSEVEAR, D.R. 1974. *The Carnivores of West Africa*. Trustees of the British Museum (Natural History), London. 548 pp.
- ROUGIER, G.W., J.R. WIBLE, AND J.A. HOPSON. 1992. Reconstruction of the cranial vessels in the Early Cretaceous mammal *Vincelestes neuquenianus*: implications for the evolution of the mammalian cranial vascular system. *Journal of Vertebrate Paleontology*, 12: 188–216.
- ROUGIER, G.W., J.R. WIBLE, AND M.J. NOVACEK. 1998. New specimens of *Deltatheridium*, implications for the early history of marsupials. *Nature*, 396: 459–463.
- ROWE, T.B., T.P. EITING, T.E. MACRINI, AND R.A. KETCHAM. 2005. Organization of the olfactory and respiratory skeleton in the nose of the gray short-tailed opossum *Monodelphis domestica*. *Journal of Mammalian Evolution*, 12(3/4):303–336.
- SÁNCHEZ-VILLAGRA, M.R., AND K.K. SMITH. 1997. Diversity and evolution of the marsupial mandibular angular process. *Journal of Mammalian Evolution*, 4(2):119–144.
- SÁNCHEZ-VILLAGRA, M.R., AND J.R. WIBLE. 2002. Patterns of evolutionary transformation in the petrosal bone and some basicranial features in marsupial mammals, with special reference to didelphids. *Journal of Zoological Systematics and Evolutionary Research*, 40:26–45.
- SCHALLER, O. 1992. *Illustrated Veterinary Anatomical Nomenclature*. Ferdinand Enke Verlag, Stuttgart. 614 pp.
- SEGALL, W. 1970. Morphological parallelisms of the bulla and auditory ossicles in some insectivores and marsupials. *Fieldiana Zoology*, 51:169–205.
- SIMPSON, G.G. 1945. The principles of classification and a classification of mammals. *Bulletin of the American Museum of Natural History*, 85:1–350.
- SISSON, S. 1910. *A Text-book of Veterinary Anatomy*. W.B. Saunders Company, Philadelphia and London. 826 pp.
- SMITH, T.D., AND J.B. ROSSIE. 2006. Primate olfaction: anatomy and evolution. Pp. 135–166, in *Olfaction and the Brain: Window to the Mind* (W. Brewer, D. Castle, and C. Pantelis, eds.). Cambridge University Press, Cambridge.
- SPAULDING, M., AND J.J. FLYNN. 2012. Phylogeny of the Carnivoromorpha: the impact of postcranial characters. *Journal of Systematic Palaeontology*, 10(4):653–677.
- SPAULDING, M., J.J. FLYNN, AND R.K. STUCKY. 2010. A new basal carnivoramorphan (Mammalia) from the 'Bridger B' (Black's Fork Member, Bridger Basin, Bridgerian NALMA, middle Eocene) of Wyoming, USA. *Palaeontology*, 53(4):815–832.
- STANDRING, S. (ED.). 2008. *Gray's Anatomy*. 40<sup>th</sup> edition. Churchill Livingstone. 1551 pp.
- STARCK, D. 1995. Säugetiere. Pp. 1–1241, in *Lehrbuch der Speziellen Zoologie, Band II, Wirbeltiere, Teil 5* (D. Starck, ed.). Gustav Fischer, Jena.
- TANDLER, J. 1899. Zur vergleichenden Anatomie der Kopfarterien bei den Mammalia. *Denkschriften Akademie der Wissenschaften, Wien, Mathematisch-Naturwissenschaftliche Klasse*, 67:677–784.
- . 1902. Zur Entwicklungsgeschichte der Kopfarterien bei den Mammalia. *Gegenbaurs Morphologisches Jahrbuch*, 30:275–373.
- TERRY, R.J. 1942. Osteology. Pp. 77–265, in *Morris's Human Anatomy, A Complete Systemic Treatise*, 10th ed. (J.P. Schaeffer, ed.). The Blakiston Company, Philadelphia.
- THEWISSEN, J.G.M. 1989. Mammalian frontal diploic vein and the human foramen caecum. *Anatomical Record*, 223:242–244.
- THOMAS, O. 1893. Description of a second species of the carnivorous genus *Nandinia*, from southern Nyassaland. *Annals and Magazine of Natural History*, 6(12): 205.
- TURNBULL, W.D. 1970. Mammalian masticatory apparatus. *Fieldiana: Geology*, 18(2):1–356.
- TURNER, H.N. 1848. Observations relating to some of the foramina at the base of the skull in Mammalia, and on the classification of the order Carnivora. Proceedings of the Zoological Society of London, 1848:63–88.
- VAN VALEN, L. 1963. Notes on the ear region of *Nandinia*. *Journal of Mammalogy*, 44:273.
- VÉRON, G. 1995. La position systématique de *Cryptoprocta ferox* (Carnivora). Analyse cladistique des caractères morphologiques de carnivores Aeluroidea actuels et fossiles. *Mammalia*, 59(4):551–582.
- VOIT, M. 1909. Das Primordialcranium des Kaninchen unter Berücksichtigung der Deckknochen. Ein Beitrag zur Morphologie des Säugetierschädels. *Anatomische Hefte*, 38:425–616.
- WAHLERT, J.H. 1974. The cranial foramina of the protogomorphous rodents; an anatomical and phylogenetic study. *Bulletin of the Museum of Comparative Zoology*, 146:363–410.
- WERDELIN, L., AND S. PEIGNÉ. 2010. Carnivora. Pp. 603–657, in *Cenozoic Mammals of Africa* (L. Werdelin and W.J. Sanders, eds.). University of California Press, Berkeley.
- WESLEY-HUNT, G.D., AND J.J. FLYNN. 2005. Phylogeny of the Carnivora: basal relationships among the carnivoramorphan, and assessment of the position of "Miacoidae" relative to crown-clade Carnivora. *Journal of Systematic Palaeontology*, 3:1–28.
- WIBLE, J.R. 1984. The ontogeny and phylogeny of the mammalian cranial arterial pattern. Unpublished Ph.D. dissertation, Duke University, Durham. 705 pp.
- . 1986. Transformations in the extracranial course of the internal carotid artery in mammalian phylogeny. *Journal of Vertebrate Paleontology*, 6(4):313–325.
- . 1987. The eutherian stapedial artery: character analysis and implications for superordinal relationships. *Zoological Journal of the Linnean Society*, 91:107–135.
- . 1990. Petrosals of Late Cretaceous marsupials from North America, and a cladistic analysis of the petrosal in therian mammals. *Journal of Vertebrate Paleontology*, 10(2):183–205.
- . 2003. On the cranial osteology of the short-tailed opossum *Monodelphis brevicaudata* (Didelphidae, Marsupialia). *Annals of Carnegie Museum*, 72(3):137–202.
- . 2007. On the cranial osteology of the Lagomorpha. In *Mammalian Paleontology on a Global Stage: Papers in Honor of Mary R. Dawson* (K.C. Beard and Z.-X. Luo, eds.). *Bulletin of Carnegie Museum of Natural History*, 39: 213–234.
- . 2008. On the cranial osteology of the Hispaniolan solenodon, *Solenodon paradoxus* Brandt, 1833 (Mammalia, Lipotyphla, Solenodontidae). *Annals of Carnegie Museum*, 77(3):321–402.
- . 2009. The ear region of the pen-tailed treeshrew, *Ptilocercus lowii* Gray, 1848 (Placentalia, Scandentia, Ptilocercidae). *Journal of Mammalian Evolution*, 16(3): 199–234.
- . 2010a. Petrosal anatomy of the nine-banded armadillo, *Dasyops novemcinctus* Linnaeus, 1758 (Mammalia, Xenarthra, Dasypodidae). *Annals of Carnegie Museum*, 79(1):1–28.
- . 2010b. On the hyoid and larynx of the Hispaniolan solenodon, *Solenodon paradoxus* Brandt, 1833 (Mammalia, Lipotyphla, Solenodontidae). *Annals of Carnegie Museum*, 79(1):29–38.
- . 2011. On the treeshrew skull (Mammalia, Placentalia, Scandentia). *Annals of Carnegie Museum*, 79(3):149–230.
- . 2012. The ear region of the aardvark *Orycteropus afer* Pallas, 1766 (Mammalia, Afrotheria, Tubulidentata). *Annals of Carnegie Museum*, 80(2): 115–146.
- WIBLE, J.R., AND T.J. GAUDIN. 2004. On the cranial osteology of the yellow armadillo *Euphractus sexcinctus* (Dasypodidae, Xenarthra,

- Placentalia). *Annals of Carnegie Museum*, 73(3):117–196.
- WIBLE, J.R., AND J.A. HOPSON. 1993. Basicranial evidence for early mammal phylogeny. Pp. 45–62, in *Mammal Phylogeny, Volume 1. Mesozoic Differentiation, Multituberculates, Monotremes, Early Therians, and Marsupials* (F.S. Szalay, M.J. Novacek, and M.C. McKenna, eds.). Springer-Verlag, New York.
- WIBLE, J.R., M.J. NOVACEK, AND G.W. ROUGIER. 2004. New data on the skull and dentition of the Mongolian Cretaceous eutherian mammal *Zalambdalestes*. *Bulletin of the American Museum of Natural History*, 281:1–144.
- WIBLE, J.R., AND G.W. ROUGIER. 2000. Cranial anatomy of *Kryptobaatar dashzevegi* (Multituberculata, Mammalia) from the Mongolian Late Cretaceous, and its bearing on the evolution of mammalian characters. *Bulletin of the American Museum of Natural History*, 247:1–124.
- WIBLE, J.R., G.W. ROUGIER, M.J. NOVACEK, AND R.J. ASHER. 2007. Cretaceous eutherians and Laurasian origin for placental mammals near the K-T boundary. *Nature*, 447(7147):1003–1006.
- . 2009. The eutherian mammal *Maelestes gobiensis* from the Late Cretaceous of Mongolia and the phylogeny of Cretaceous Eutheria. *Bulletin of the American Museum of Natural History*, 327:1–123.
- WIBLE, J.R., G.W. ROUGIER, M.J. NOVACEK, M.C. MCKENNA, AND D. DASHZEVEG. 1995. A mammalian petrosal from the Early Cretaceous of Mongolia: implications for the evolution of the ear and mammalia-morph interrelationships. *American Museum Novitates*, 3149:1–19.
- WIBLE, J.R., AND M. SPAULDING. 2012. Reexamination of the *Carnivora malleus* (Mammalia, Placentalia). *PLoS ONE*, 7(11):e50485.
- WIENS, J.J. 1995. Polymorphic characters in phylogenetic systematics. *Systematic Biology*, 44(4):482–500.
- . 1999. Polymorphism in systematics and comparative biology. *Annual Review of Ecology and Systematics*, 30:327–362.
- WINGE, H. 1941. *The Interrelationships of the Mammalian Genera. Volume II. Rodentia, Carnivora, Primates*. Translated from Danish by E. Deichmann and G.M. Allen. C.A. Reitzels Forlag, København. 376 pp.
- WOZENCRAFT, W.C. 1984. A phylogenetic reappraisal of the Viverridae and its relationships to other Carnivora. Unpublished Ph.D. dissertation, University of Kansas, Lawrence. 705 pp.
- . 2005. Order Carnivora. Pp. 532–628, in *Mammal Species of the World: A Taxonomic and Geographic Reference. Third Edition*. (D.E. Wilson and D.M. Reeder, eds.). The Johns Hopkins University Press, Baltimore.

## GLOSSARY

Below in alphabetical order is a treatment of the principal foramina, canals, and sulci associated with assorted soft tissues. The entries for most structures begin with the condition in the caniform *Canis lupus familiaris* and are followed by the feliforms *Felis catus*, *Genetta genetta* and/or *Genetta cristata*, and *Nandinia binotata*. Observations for the domestic dog and cat are from the literature (e.g., Jayne 1898; Davis and Story 1943; Evans 1993) supplemented by CM specimens, including *C. lupus*, CM 57444. Observations for the genets are from CM specimens and for the African palm civet are from the descriptions above.

**Accessory Palatine Foramen**—In *C. lupus familiaris*, there are one or more accessory palatine foramina (=minor palatine foramina of Evans 1993) for the accessory palatine nerves in the horizontal process of the palatine. *Canis lupus*, CM 57444, has two on the right and one on the left (Fig. 43D).

In *F. catus*, Jayne (1898:330–331) discussed variation in the openings of the horizontal process of the palatine: “[i]n some specimens there is a single large foramen in the anterior border, or just behind it; in others, one large foramen and a second smaller one much further back on the palatal surface; in others, one large foramen and two smaller posterior foramina; and more rarely, the large foramen may be accompanied by three or seven more smaller openings.” As used here, the openings in or immediately adjacent to the palatamaxillary suture described by Jayne (1898) are major palatine foramina (=posterior palatine foramina of Jayne 1898), whereas those farther back are accessory palatine foramina. *Felis catus*, CM 12910, has two on the left and one on the right (Fig. 43B).

In *G. genetta*, CM 85593, the right side has ten and the left nine accessory palatine foramina (Fig. 43C). One foramen on the right is entirely in the maxilla and another is in the platomaxillary suture; the left side has an additional foramen entirely in the maxilla.

In the study sample of *N. binotata*, between four and 13 accessory palatine foramina are present in the horizontal process of the palatine (Figs. 5, 9).

**Alisphenoid Canal**—In *C. lupus familiaris*, the alisphenoid canal (=alar canal of Evans 1993) runs through the base of the alisphenoid. Its caudal aperture (=caudal alar foramen of Evans 1993) is in a common depression with the foramen ovale (Fig. 43D) and transmits the maxillary artery and vein. Its rostral aperture (=rostral alar foramen of Evans 1993) is lateral to the sphenorbital fissure (=orbital fissure of Evans 1993) and is merged with the exit of the maxillary nerve, the foramen rotundum of this report.

An alisphenoid canal is lacking in *F. catus* (Jayne 1898; Fig. 43B), and its usual contents, the maxillary artery (=internal maxillary artery of Davis and Story 1943), run open on the ventral surface of the skull base.

In *G. genetta*, CM 85593, an alisphenoid canal is present; the rostral opening is the foramen rotundum, but the caudal opening is not in a common depression with the foramen ovale (Fig. 43B).

In *N. binotata*, an alisphenoid canal is present; the rostral opening is the foramen rotundum and the caudal open-

ing is in a common depression with the foramen ovale and the transverse canal foramina (“asc” in Figs. 11, 20).

**Anterior Carotid Foramen**—see Carotid Foramen.

**Aperture of Cochlear Fossula**—In *C. lupus familiaris*, CM 106574, the aperture of the cochlear fossula (=fenestra cochleae of Evans 1993) is a large opening in the posterior surface of the promontorium of the petrosal. It is roughly ice cream cone-shaped, with the point directed dorsally. It is directed posteriorly and slightly ventrolaterally. In the dorsolateral aspect of the aperture is a well-developed depression for the cochlear fossula. The attachment of the secondary tympanic membrane (i.e., the fenestra cochleae) is slightly internal to the aperture.

In *F. catus*, the aperture of the cochlear fossula (=fenestra rotunda of Jayne 1898:205) is “nearly circular” and “faces outward, backward, and upward.” In *Felis* sp., CM 10750, a sulcus internal to the aperture’s dorsal margin appears to be the point of attachment of the secondary tympanic membrane. A cochlear fossula is absent.

In *G. cristata*, CM 3697, the aperture of the cochlear fossula is half moon-shaped, with the dorsal margin straight and is posterolaterally directed. A sulcus internal to the lateral margin appears to be the point of attachment of the secondary tympanic membrane. A cochlear fossula is absent.

In *N. binotata* (“acf” in Figs. 15, 16, 21A–B), the aperture of the cochlear fossula is half moon-shaped, with the dorsal margin straight and is posteriorly and slightly ventrally and laterally directed. The secondary tympanic membrane inserts in a sulcus internal to the aperture. A distinct cochlear fossula is present in only a few of the studied specimens.

**Canal for Chorda Tympani**—In *C. lupus familiaris*, before emerging from the foramen stylomastoideum definitivum (=stylomastoid foramen of Evans 1993), the facial nerve gives off the chorda tympani, which runs anteriorly in its own canal (=canaliculus chordae tympani of Evans 1993) to reach the middle ear. This canal is described with the petrosal part of the temporal bone by Evans (1993), but which parts of the temporal bone form the canal is not specified. In a juvenile, CM 15205, it is between the tympanohyal and ectotympanic.

In *F. catus* (Reighard and Jennings 1935:376), “the chorda tympani is given off two or three millimeters before the emergence of the facial nerve at the stylomastoid fo-

ramen [=foramen stylomastoideum definitivum]. It passes into the tympanic cavity" via an opening between the tympanohyal and ectotympanic in a juvenile, CM 1407.

In *G. genetta*, CM 85593, there is a gap between the tympanohyal and caudal entotympanic, internal to the foramen stylomastoideum definitivum, that we interpret as the passage of the chorda tympani into the middle ear.

In *N. binotata*, the canal for the chorda tympani is a small opening between the tympanohyal and ectotympanic ("cct" in Fig. 22). It is ventral to the stylomastoid foramen (foramen stylomastoideum primitivum).

**Carotid Foramen**—In *C. lupus familiaris* (Hunt 1974; Evans 1993), the internal carotid artery crosses the basiocranium in a perbullar canal (sensu Wible 1986). There are five openings associated with this course, which have had numerous terms applied to them by various authors. (1) The artery enters the gap anterior to the jugular foramen between the caudal entotympanic, basioccipital, and petrosal that leads into a deep fissure. This fissure produces a sulcus on both the basioccipital and petrosal that also transmits the inferior petrosal sinus (=ventral petrosal sinus of Evans 1993). The fissure and the enclosed canal surrounding it are identified by Evans (1993) as the petrobasilar or petrooccipital fissure and canal. However, the gap transmitting the internal carotid artery into the fissure is not named by Evans (1993) or Hunt (1974). Following our terminology for *N. binotata*, we call the gap in *C. lupus familiaris* the posterior carotid foramen, that is, the opening that transmits the artery into the bullar wall. (2) After a short course through the fissure, the artery enters the carotid canal within the rostral entotympanic (Hunt 1974). The opening into the carotid canal is the posterior carotid foramen of Hunt (1974) and the caudal carotid foramen of Evans (1993). However, we identify it as the caudal opening of the carotid canal, reserving the posterior carotid foramen for the opening in the bullar wall. (3) The artery exits the carotid canal anteriorly at an opening within the rostral entotympanic that is recessed in from the external surface of the auditory bulla. Hunt (1974) called this opening the anterior carotid foramen and Evans (1993:620) called it the internal carotid foramen. We call it the rostral opening of the carotid canal. (4) The artery then exits the auditory bulla at an opening on the anteromedial surface of the auditory bulla between the caudal entotympanic and basisphenoid (based on CM 15205). Following our terminology for *N. binotata*, we call the opening in the bulla in *C. lupus familiaris* the anterior carotid foramen. Hunt (1974) did not name this opening and Evans (1993) called it the foramen lacerum. (5) The artery loops back into the auditory bulla through the anterior carotid foramen and turns dorsally to enter the cranial cavity between the basisphenoid and petrosal at the carotid foramen (=median lacerate foramen of Hunt 1974; =foramen lacerum of Evans 1993).

In *F. catus*, the course of the internal carotid artery begins at the posterior carotid foramen between the caudal entotympanic, basioccipital, and petrosal, anterior to the

jugular foramen (Fig. 43B). The artery enters a canal between the caudal entotympanic and petrosal, and then runs anteriorly across the promontorium and rostral entotympanic either in a groove (CM 12910) or bony tube (Hunt 1974) in the latter element. The artery turns dorsally to enter the carotid foramen (=median lacerate foramen of Davis and Story 1943) between the basisphenoid and petrosal. There is an anterior carotid foramen, an opening in the anteromedial surface of the bulla, that allows the ascending pharyngeal artery to anastomose with the internal carotid ventral to the carotid foramen; Davis and Story (1943) showed that the transpromontorial part of the internal carotid artery is a fibrous cord that does not transmit blood and that blood in the internal carotid artery at the carotid foramen comes from the ascending pharyngeal artery. The anterior carotid foramen is continuous laterally with the musculotubal canal.

In *G. genetta*, CM 85593, the posterior carotid foramen between the caudal entotympanic and rostral tympanic process of the petrosal is midway between the jugular foramen and the basisphenoid-basioccipital suture (Fig. 43C). This leads to the carotid canal, which based on *G. cristata*, CM 3697, is initially between the caudal entotympanic and rostral tympanic process, but then within the rostral entotympanic. From the rostral opening of the carotid canal, the artery turns medially to enter the carotid foramen, which is nearly entirely in the basisphenoid; its posterior border is open to the small foramen lacerum between the basisphenoid and the anterior pole of the promontorium. An anterior carotid foramen is present on the anteromedial surface of the bulla between the caudal entotympanic and basisphenoid, continuous laterally with the musculotubal canal.

In *N. binotata*, the internal carotid artery enters the posterior carotid foramen between the caudal entotympanic and rostral tympanic process, anterior to the jugular foramen (Figs. 22, 24). It runs in a short carotid canal between the same two structures and then across the promontorium (Fig. 18). After its transpromontorial course, it runs in a shallow sulcus in the rostral entotympanic (Figs. 16B, 18) and then bends sharply medially in the deep carotid groove on the basisphenoid (Figs. 13, 16A, 20). The artery then bends sharply again to enter the carotid foramen within the basisphenoid (Fig. 13, 16A, 20). The internal carotid artery is a small vessel that is joined by the ascending pharyngeal artery before it enters the carotid foramen (Fig. 18; Davis and Story 1943). To reach the internal carotid artery, the ascending pharyngeal artery passes through an anterior carotid foramen between the ectotympanic, caudal entotympanic, and basisphenoid. The anterior carotid foramen is continuous laterally with the musculotubal canal.

**Caudal Palatine Foramen**—In *C. lupus familiaris*, the caudal palatine foramen for the major palatine nerve and vessels is in the perpendicular process of the palatine, ventral to the sphenopalatine foramen (Evans 1993). In *C. lupus*, CM 57444, the caudal palatine and sphenopalatine foramina are in a common depression separated by a thin

septum.

In *F. catus*, the caudal palatine foramen (=posterior palatine foramen of Jayne 1898) is a small opening anteroventrolateral to the larger sphenopalatine foramen, in the horizontal process of the palatine. It transmits the major palatine nerve and artery (=descending palatine artery of Davis and Story 1943). Jayne (1898: 322) reported “there are, as a rule, several smaller foramina behind the principal one and external to it.”

In *G. genetta*, CM 85593, a large depression in the horizontal process of the palatine, posterolateral to the sphenopalatine foramen, has a large caudal palatine foramen anteriorly and one small foramen (two on the left) posteriorly.

In the study sample of *N. binotata*, between two and six caudal palatine foramina of differing sizes are situated lateral and posterior to the sphenopalatine foramen, in the roof of the horizontal process of the palatine (“cpf” in Fig. 8A).

**Cochlear Canaliculus**—In *C. lupus familiaris* (Evans 1993), *F. catus* (Jayne 1898), *G. cristata*, CM 3697, and *N. binotata* (“cc” in Fig. 21E), the perilymphatic duct enters the petrosal via the external opening of the cochlear canaliculus, in the anterior edge of the jugular foramen. This aperture is not visible in direct ventral view in any of these taxa.

**Condylod Canal**—In *C. lupus familiaris* (Evans 1993: 136), “the rather large condylod canal...runs through the medial part of the lateral occipital bone [=exoccipital]. There is an intraosseous passage between the condylod canal and the hypoglossal canal. Usually there is also a small passage between the condylod canal and the petrobasilar fissure.” The condylod vein, which connects the sigmoid and the basilar sinus, is the major occupant.

In *F. catus*, the condylod canal (=posterior condylod canal of Jayne 1898:173) “is sometimes absent, on one or on both sides; it is often double, presenting two anterior and two posterior openings; or it may be only partially divided, presenting two posterior and one anterior or one posterior and two anterior openings.” It transmits a vein (Jayne 1898; Reighard and Jennings 1935).

In *G. genetta*, CM 85593, and *G. cristata*, CM 3697, the condylod canal has one caudal opening posterodorsolateral to the internal opening of the hypoglossal foramen. In the dorsal wall of the canal, another canal running dorsally, presumably for the occipital emissary vein, is visible.

In the study sample of *N. binotata*, the condylod canal has between one and three caudal openings, and an opening in the dorsal wall of the canal for the occipital emissary vein.

**Craniopharyngeal Canal**—In *C. lupus familiaris* (Evans 1993:139), in the basisphenoid “occasionally the small craniopharyngeal canal...persists in the adult, particularly in Bulldogs. This midline canal is a remnant of the pharyngeal diverticulum to the hypophyseal fossa from which the

pars glandularis of the hypophysis develops.” *Canis lupus*, CM 57444, has a small midline opening in the basisphenoid posterior to the suture with the presphenoid that we interpret as a remnant of the craniopharyngeal canal (Fig. 43D).

In *F. catus*, Jayne (1898: figs. 189, 190) illustrated but did not describe a small midline opening in the basisphenoid, just posterior to the presphenoid. In adults studied by us, we found three openings in a common depression in CM 12910 (Fig. 43B), two openings in CM 1407, and one in CM 20615, 28447, and 31269. Oddly, this craniopharyngeal canal was absent in a juvenile *Felis* sp., CM 10750.

The craniopharyngeal canal is absent in *G. genetta*, CM 85593 (Fig. 43C) and 95202, and *G. cristata*, CM 3697.

In the study sample of *N. binotata*, the craniopharyngeal canal is present in eight of the 30 specimens, including the most advanced juvenile, AMNH 201513 (“cpc” in Fig. 14), and seven adults.

**Ethmoidal Foramen**—In *C. lupus familiaris* (Evans 1993), there are usually two ethmoidal foramina: a larger posterodorsal one in the frontal, for the external ethmoidal artery and vein, and a smaller anteroventral one in the suture between the frontal and orbitosphenoid, for the ethmoidal nerve.

In *F. catus*, one or two small ethmoidal foramina for the ethmoidal nerve and vessels are in or above the suture between the frontal and orbitosphenoid (Jayne 1898; Reighard and Jennings 1935). When two are present, they are termed anterior and posterior ethmoidal foramina (Jayne 1898).

In *G. genetta*, CM 85593, a dumbbell-shaped ethmoidal foramen is present, reflecting a partial division of the aperture; the anterior part is entirely in the frontal, while the orbitosphenoid contributes to the floor of the posterior part.

In the study sample of *N. binotata* (“ef” in Fig. 11), all specimens have only one ethmoidal foramen except for the right side of CM 59496, which has two. These foramina are either entirely within the frontal or in the suture between the frontal and orbitosphenoid.

**Facial Canal**—In *C. lupus familiaris* (Evans 1993), the facial canal for the facial nerve follows a straight course from its origin at the internal acoustic meatus. When it meets the thin medial wall of the fossa for the tensor tympani muscle, there is an enlargement for the geniculate ganglion (within the cavum supracochleare of Voit 1909). The canal bends posteriorly (=genu of the facial canal of Evans 1993) and opens into the middle ear lateral to the fenestra vestibuli and medial to the crista parotica. The facial nerve exits the middle ear at the foramen stylomastoideum primitivum (sensu Klaauw 1931) at the tympanohyal (based on CM 15205), but then runs in a canal between the petrosal, caudal entotympanic, ectotympanic, and squamosal to its point of exit from the skull (based on CM 106574), the foramen stylomastoideum definitivum (sensu Klaauw 1931).

The nerve is accompanied by the stylomastoid artery, a branch of the caudal auricular artery (Evans 1993).

In *Felis* sp., CM 10750, *G. genetta*, CM 95202, and *G. cristata*, CM 3697, the course of the facial nerve is essentially the same as described above for *C. lupus familiaris*. As in *C. lupus familiaris*, the facial nerve is accompanied by the stylomastoid artery at the foramen stylomastoideum definitivum in *F. catus* (Davis and Story 1943); the condition in the genets is unreported.

In *N. binotata*, the intratympanic course of the facial nerve resembles that described above for *C. lupus familiaris*, that is, initially enclosed in a canal but then in a sulcus between the fenestra vestibuli and crista parotica ("fs" in Fig. 15). However, the exit of the facial nerve of *N. binotata* differs in that it is at the foramen stylomastoideum primitivum (sensu Klaauw 1931), between the caudal entotympanic and tympanohyal (Figs. 15, 18). Wible (1984) reported a stylomastoid artery with the facial nerve in a prenatal *N. binotata*.

**Fenestra Vestibuli**—The fenestra vestibuli sits in a vestibular fossula that is deepest posteriorly in *C. lupus familiaris*, CM 106574, *Felis* sp., CM 10750, *G. cristata*, CM 3697, and *N. binotata* ("fv" in Fig. 21F). The stapedial ratio (length/width; Segall 1970) for these four taxa respectively are: 2.28, 1.96, 1.61, and 1.59 (based on CM 3693).

**Foramen for Ramus Temporalis**—The principal supply to the temporalis muscle in *C. lupus familiaris* (Evans 1993) and *F. catus* (Reighard and Jennings 1935) is via the branches of the external carotid artery. The same is inferred for *G. genetta* and *N. binotata*, because the other possible source, the stapedial system, is likewise greatly reduced (as reported for *N. binotata* by Davis and Story 1943 and for other viverrines by Tandler 1899). Nevertheless, all specimens of *N. binotata*, with the exception of two juveniles, had small foramina in the parietal or parietosquamous suture that we identified as for the ramus temporalis ("frt" in Figs. 2B, 4B). In *F. catus*, Jayne (1898:182) noted that "in some specimens a foramen may be seen near the middle of the posterior border" of the parietal; we confirm and identify these as foramina for rami temporales in CM 12910. We found similar foramina in *C. lupus*, CM 57444, but not in *G. genetta*, CM 85593, or *G. cristata*, CM 3697.

**Foramen Impar**—see Transverse Sinus Canal.

**Foramen Lacerum**—see Carotid Foramen.

**Foramen Ovale**—In *C. lupus familiaris* (Evans 1993), the obliquely-oriented foramen ovale is in the alisphenoid opposite the glenoid fossa, in a common depression with the alisphenoid canal (Fig. 43D), and transmits the mandibular nerve and a small emissary vein; a small notch or a separate foramen spinosum for the middle meningeal artery off the maxillary artery (=internal maxillary artery of Evans 1993) may occur in the posterolateral aspect of the foramen ovale.

In *F. catus* (Jayne 1898; Reighard and Jennings 1935; Davis and Story 1943), the foramen ovale is situated as in *C. lupus familiaris*, except that the alisphenoid canal is absent (Fig. 43B); the foramen transmits the mandibular nerve and the middle meningeal artery, but a separate foramen spinosum is absent. Jayne (1898:261) reported that "a small foramen is often found piercing its inner wall." We found such a tiny foramen bilaterally in one specimen, CM 28447, but its function is uncertain.

In *G. genetta*, CM 85593, and *G. cristata*, CM 3697, the obliquely-oriented foramen ovale is more posteriorly positioned, opposite the postglenoid process, and not in a common depression with the alisphenoid canal (Fig. 43C). A transverse canal foramen is in the inner wall of the foramen ovale in the former but is absent in the latter.

In the study sample of *N. binotata*, the obliquely-oriented foramen ovale is opposite the glenoid fossa in a common depression with the alisphenoid canal and transverse canal foramina ("fo" in Figs. 11, 19); Davis and Story (1943: fig. 9) identified a middle meningeal artery passing through the foramen ovale.

**Foramen Rotundum**—In *C. lupus familiaris*, the foramen rotundum (=foramen rotundum + rostral alar foramen of Evans 1993) is within the alisphenoid, lateral to the sphenorbital fissure (=orbital fissure of Evans 1993). It has an internal opening (=foramen rotundum of Evans 1993) that transmits the maxillary nerve and an emissary vein, and an external opening (=rostral alar foramen of Evans 1993) that transmits the maxillary nerve, artery, and vein. The maxillary artery and vein reach the foramen rotundum by their course in the alisphenoid canal.

In *F. catus* (Jayne 1898:260), the foramen rotundum for the maxillary nerve "lies next to the sphenoidal [=sphenorbital] fissure, and pierces the [alisphenoid] bone obliquely, passing forward, outward, and slightly downward. At the back of its inner wall is a small foramen, which appears to be constant and leads into the interior of the bone." We found this foramen in our entire CM sample and interpret it as a transverse canal foramen. An alisphenoid canal is absent.

In *G. genetta*, CM 85593, and in *N. binotata*, the foramen rotundum is as in *C. lupus familiaris*, that is, it is merged with the alisphenoid canal, and its external aperture is the common aperture for the maxillary nerve, artery, and vein.

**Foramen Stylomastoideum Definitivum**—see Facial Canal.

**Foramen Stylomastoideum Primitivum**—see Facial Canal.

**Frontal Diploic Vein Foramen**—In *C. lupus familiaris* (Evans 1993), the frontal diploic vein, an emissary vein of the diploë of the frontal bone, exits via a small foramen in the frontal, ventral to the postorbital process.

In *F. catus*, small, inconstant foramina are reported by

Jayne (1898) near the base of the postorbital process of the frontal and ventral to the supraorbital crest that lead into cancellous tissue. We found a well-developed frontal diploic vein foramen present bilaterally ventral to the supraorbital crest in CM 12910, but absent in CM 28447.

In *G. genetta*, CM 85593, a well-developed frontal diploic vein foramen is present at the base of the postorbital process; *G. cristata*, CM 3697, has two per side: one at the base of the postorbital process and the other more posteriorly placed and visible in lateral view.

In the study sample of *N. binotata*, most specimens have a single frontal diploic vein foramen on the undersurface of the root of the postorbital process (“fdv” in Fig. 10), but four specimens have two foramina on at least one side and five specimens have only several minute foramina on one side.

**Glaserian Fissure**—In *C. lupus familiaris* (Evans 1993), after its passage across the malleus, “the chorda tympani usually passes through a small canal in the rostradorsal wall of the bulla tympanica and emerges through the petrotympanic fissure (fissura petrotympanica) by a small opening medial to the retroarticular [=postglenoid] process. When the canal fails to develop, the opening is through the rostralateral wall of the tympanic bulla.” Wible and Spaulding (2012) showed that the spine of the rostral process of the malleus, the ectotympanic, and the squamosal form the exit of the chorda tympani, which, following Klaauw (1931:164-165), is the Glaserian fissure. The nerve then has an ill-defined passage anteriorly across the squamosal, medial to the glenoid fossa (Evans 1993: fig. 19–20).

In *F. catus*, Wible and Spaulding (2012) identified two openings on either side of the spine of the rostral process of the malleus; the medial opening is for the anterior tympanic artery, and the lateral is the Glaserian fissure for the chorda tympani (see Davis and Story 1943: fig. 2). The latter is between the spine, ectotympanic, and squamosal/alisphenoid. A groove on the alisphenoid rostral to the Glaserian fissure and medial to the postglenoid process indicates the further course of the nerve in some specimens (e.g., CM 12910, 28447).

In *G. genetta*, CM 85593, Wible and Spaulding (2012) reported openings on either side of the spine of the rostral process of the malleus, the anterior tympanic artery medially and the chorda tympani laterally. The latter, the Glaserian fissure, is between the spine, ectotympanic, and squamosal, and leads into a distinct groove on the squamosal, medial to the postglenoid process.

In the study sample of *N. binotata*, only a single opening is present medial to the tip of the spine (“Gf” in Fig. 23), with the remaining borders made by the ectotympanic and squamosal. This Glaserian fissure leads forward into a groove or notch on the entoglenoid process of the squamosal.

**Hiatus Fallopii**—In *C. lupus familiaris*, the greater petrosal nerve (=major petrosal nerve of Evans 1993) runs

forward from the geniculate ganglion of the facial nerve in a small canal within the petrosal (=petrosal canal of Evans 1993), dorsal to the fossa for the tensor tympani muscle. The hiatus Fallopii (=anterior opening of petrosal canal of Evans 1993) is on the endocranial surface near the petrosquamous suture.

The hiatus Fallopii of *F. catus* (Jayne 1898) and *N. binotata*, AMNH 201513 (“hF” in Figs. 21B, E), resembles that of *C. lupus familiaris*. Specimens of *G. genetta* and *G. cristata* revealing the position of the hiatus Fallopii were not available.

**Hypoglossal Foramen**—In *C. lupus familiaris* (Evans 1993), the hypoglossal foramen is in the exoccipital, posteromedial to the jugular foramen, and transmits the hypoglossal nerve and vein. It lies on the main basicranial surface of the central stem and is visible in ventral view (Fig. 43D).

In *F. catus*, the hypoglossal foramen (=anterior condyloid canal of Jayne 1898: 173) lies in the exoccipital and “may, however, be double, completely or partially, on one side or on both sides.” It transmits the hypoglossal nerve (Jayne 1898; Reighard and Jennings 1935) and caudal meningeal artery (=arteria meningeal posterior of Davis and Story 1943). In CM 12910, the hypoglossal foramen is recessed from the main basicranial surface of the central stem and partially hidden in ventral view, as it shares a well-developed posterior wall with the jugular foramen (Fig. 43B).

In *G. genetta*, CM 85593, the single hypoglossal foramen is on the main basicranial surface of the central stem; it shares its medial wall with the nearby jugular foramen (Fig. 43C).

In the study sample of *N. binotata*, most specimens have a single hypoglossal foramen in the exoccipital on the main basicranial surface of the central stem (“hf” in Figs. 23, 37). Only one specimen had two foramina externally on one side, and four had two foramina internally. The proximity to the jugular foramen varies.

**Incisive Foramen**—In *C. lupus familiaris*, the incisive foramen (=palatine fissure of Evans 1993) is mainly in the premaxilla, with the maxilla forming the posterior border medial to the canine. It transmits the nasopalatine duct, which connects the oral and nasal cavities with the vomeronasal organ, the rostral septal branch of the major palatine artery, and the nasopalatine nerve (=septal branch of the caudal nasal nerve of Evans 1993). In *C. lupus*, CM 57444, the incisive foramen is a little shorter than the alveoli of the three upper incisors (Fig. 43D).

In *F. catus*, the incisive foramen (=anterior palatine foramen of Jayne 1898) is similarly situated and sized (Fig. 43B); it transmits the nasopalatine duct (Reighard and Jennings 1935) and an anastomosis between the sphenopalatine and major palatine arteries (=anterior palatine artery of Davis and Story 1943).

In *G. genetta*, CM 85593 (Fig. 43C), and *N. binotata*

("inf" in Fig. 6), the incisive foramen differs from that of *C. lupus familiaris* and *F. catus* in that the maxilla is not confined to the posterior wall of the foramen but also contributes to the lateral margin. In *G. genetta*, CM 85593, the incisive foramen is subequal to the alveoli of the three upper incisors, while in *N. binotata*, the incisive foramen is longer than the incisors.

**Incisivomaxillary Canal**—In *C. lupus familiaris*, the incisivomaxillary canal is in the medial wall of the infrarorbital foramen and supplies nerves and blood vessels to the first three premolars, the canine, and the incisors (Evans 1993).

In *F. catus*, CM 12910, 28447, the incisivomaxillary canal is in the maxilla posteromedial to the maxillary foramen, in close proximity to the lacrimal fenestra. Jayne (1898:338) noted the presence of "many small inconstant foramina, the opening into dental canals," and one large constant one, which is the incisivomaxillary canal of this report.

In *G. genetta*, CM 85593, the incisivomaxillary canal is in the maxilla posteromedial to the maxillary foramen, near the lacrimal fenestra.

In *N. binotata*, the incisivomaxillary canal varies in its position within the maxilla: 17 are within the infraorbital canal, 11 posterior to the canal ("imc" in Fig. 8A), and two anterior to the canal ("imc" in Fig. 4D).

**Inferior Petrosal Sinus Sulcus**—In *C. lupus familiaris* (Evans 1993:710), "the ventral petrosal sinus (sinus petrosus ventralis) [=inferior petrosal sinus] extends between the caudal end of the cavernous sinus and the ventral end of the sigmoid sinus. It lies in the petrooccipital canal and is an intraosseous extension of the cavernous sinus. A smaller venous channel lies in the laterally adjacent and parallel carotid canal. It connects the same parent sinuses as does the ventral petrosal; this venous channel contains the internal carotid artery."

In contrast, the inferior petrosal sinus in *F. catus* (Reighard and Jennings 1935), *G. cristata*, CM 3697, and *N. binotata* (Figs. 37–38) runs in a deep endocranial sulcus between the basioccipital and petrosal. In *F. catus*, it connects to the sigmoid sinus internal to the jugular foramen, but in the others that connection is absent.

**Infraorbital Canal**—The infraorbital canal of *C. lupus*, CM 57444, is longer than the length of its P5, whereas in *F. catus*, CM 28447, *G. genetta*, CM 85593, and *N. binotata*, the canal is shorter than that tooth (Fig. 42).

**Infraorbital Foramen**—The infraorbital foramen, which transmits the infraorbital nerve, artery, and vein from the infraorbital canal onto the face (Reighard and Jennings 1935; Evans 1993), is dorsal to P4 in *C. lupus*, CM 57444 (Fig. 42D), *F. catus*, CM 12910 (Fig. 42B), *G. genetta*, CM 85593 (Fig. 42C), and the adult study sample of *N. binotata* (Figs. 4B, D, 42A).

**Interincisive Foramen**—In *C. lupus familiaris*, the interincisive foramen (=incisive canal of Evans 1993:148) is a midline opening in the palate between the premaxillae that "varies in size and position and occasionally is absent." Its contents are not reported. In *C. lupus*, CM 57444, the interincisive foramen is roughly halfway between the I1 and the anterior border of the incisive foramen (Fig. 43D).

In *F. catus*, an interincisive foramen is not reported in Jayne (1898). We observed the interincisive foramen in CM 12910 and 28447, where it is located posterior to the incisive foramen (Fig. 43B).

In *G. genetta*, CM 85593, the large interincisive foramen is just anterior to the posterior margin of the incisive foramen (Fig. 43C).

In the study sample of *N. binotata*, most specimens have the interincisive foramen at or anterior to the premaxillary-maxillary suture, in the lateral wall of the incisive foramen ("iif" in Figs. 5, 6D); four specimens have it posterior to that suture.

**Internal Acoustic Meatus**—In *C. lupus familiaris* (Evans 1993:143), the internal acoustic meatus "is an irregularly elliptical depression that is divided deeply by the transverse crest (crista transversa). Dorsal to the crest is the opening of the facial canal, which contains the facial nerve as well as the cribriform dorsal [=superior] vestibular area (area utriculo-ampullaris) for the passage of nerve bundles from the membranous labyrinth. Ventral to the crest is the ventral [=inferior] vestibular area (area vestibularis sacularis), through which pass additional vestibular nerve bundles that come from a deep, minute depression, the foramen singulare. The spiral cribriform tract (tractus spiralis foraminosus) is formed by the wall of the hollow modiolus of the cochlea. The perforations are formed by the fascicles of the cochlear nerve that arise from the spiral ganglion outside of the modiolus."

The internal acoustic meatus in *F. catus* (Jayne 1898:200–201), *G. cristata*, CM 3697, and *N. binotata*, AMNH 201513 (Figs. 21B, E) is arranged as in *C. lupus familiaris*.

**Jugular Foramen**—In *C. lupus familiaris* (Evans 1993), the jugular foramen lies between the petrosal and occipital (Fig. 43D), and transmits the glossopharyngeal, vagus, and accessory nerves and the sigmoid sinus. To reach the skull base, these structures pass through the petro-occipital and tympano-occipital fissures. In a juvenile, CM 15205, both the basi- and exoccipital contribute to the posteromedial border of the foramen.

In *F. catus* (Fig. 43B), the jugular foramen also transmits the glossopharyngeal, vagus, and accessory nerves and the sigmoid sinus (=termination of the sinus transversus of Reighard and Jennings 1935). In a juvenile *Felis* sp., CM 10750, it is between the petrosal and exoccipital.

In *G. genetta*, CM 85593, the jugular foramen is between the petrosal and occipital (Fig. 43C). We did not

have access to any juveniles of *Genetta*, so that the contributions of basi- versus exoccipital are not known. In *G. cristata*, CM 3697, the sigmoid sinus does not exit via the jugular foramen, but via the condyloid canal.

In *N. binotata*, the jugular foramen is between the petrosal and exoccipital based on the juvenile, AMNH 51486. The sigmoid sinus does not exit via the jugular foramen, but via the condyloid canal based on AMNH 134969.

**Labial Mandibular Foramen**—In the study sample of *N. binotata*, with the exception of two specimens, foramina, usually multiple and tiny, are found in the anterior part of the masseteric fossa (“lmf” in Figs. 29B, D). Three specimens have openings on the same scale as labial mandibular foramina described in various Cretaceous eutherians (Kielan-Jaworowska and Dashzeveg 1989; Wible et al. 2009). A similar opening has been described in various extant marsupials by Abbie (1939), who reported it to transmit a branch of the inferior dental artery (=inferior alveolar artery) to the masseter muscle. He called it the masseteric foramen, following Osgood (1921: pl. XX, fig. 2) who labeled it in *Caenolestes* Thomas, 1895, but did not describe it. It is likely that the foramen in *N. binotata* functioned in the same fashion.

In *G. genetta*, CM 85593, a small foramen in the appropriate place is present on the left side (Fig. 44C), but not the right.

Labial mandibular foramina are not reported for *C. lupus familiaris* (Evans 1993) or *F. catus* (Jayne 1898).

**Lacrimal Fenestra**—In *C. lupus familiaris* (Evans 1993:1041), the inferior oblique muscle (=musculus obliquus ventralis of Evans 1993) “originates from a small depression in the palatine bone near the junction of the palatomaxillary and palatolacrimal sutures. In prepared skulls this site may appear as a foramen [=lacrimal fenestra of this report], since the attachment plate is thin and easily lost.” In *C. lupus*, CM 57444, a large lacrimal fenestra is present at the junction of the lacrimal, maxilla, and palatine.

In *F. catus*, the lacrimal fenestra is illustrated in Jayne (1989: fig. 257), but not labeled or described. In this figure, it is a gap at the junction of the lacrimal, palatine, and maxilla on the right side and of the first two bones on the left side. In CM 12910 and 28447, the fenestra is between the three bones bilaterally.

In *G. genetta*, CM 85593, the lacrimal fenestra is between the palatine and maxilla.

In the study sample of *N. binotata*, roughly two-thirds have a lacrimal fenestra (“lacfe” in Fig. 12) and one-third an inferior oblique muscle fossa (“iomf” in Fig. 8A) that in the majority is principally on the palatine but on the maxilla in two specimens.

**Lacrimal Foramen**—In *C. lupus familiaris*, the lacrimal foramen (=fossa for lacrimal sac and lacrimal canal of Evans 1993) for the nasolacrimal duct is positioned in the

orbital process of the lacrimal, posterior to the orbital rim (Fig. 41D). The foramen is entirely in the lacrimal, but the jugal and frontal are nearby, as this part of the lacrimal is narrow mediolaterally.

In *F. catus*, the lacrimal foramen (=lachrymal canal of Jayne 1898) is posterior to the orbital rim (Fig. 41B) and usually formed by the lacrimal, maxilla, and jugal. Jayne (1898:378) reported one instance where the foramen was enclosed in the lacrimal.

In *G. genetta*, CM 85593, the lacrimal foramen is posterior to the orbital rim, between the lacrimal and jugal, the latter forming the lateral border. The maxilla nearly forms the ventral border, but is separated by a sliver of lacrimal.

In the study sample of *N. binotata*, the lacrimal foramen is always posterior to the orbital rim. It is between the lacrimal and maxilla in the majority (“lacf” in Figs. 8, 12A); it is wholly in the lacrimal in four specimens (Fig. 12B).

**Major Palatine Foramen**—In *C. lupus familiaris* (Evans 1993:150), after passage through the caudal palatine foramen and palatine canal, the major palatine nerve and vessels reach the hard palate via the major palatine foramen, “an oval, oblique opening in the suture between the palatine process of the maxilla and the palatine bone.” Extending rostrally from the foramen is the major palatine sulcus (=palatine sulcus of Evans 1993), which may reach the incisive foramen (=palatine fissure of Evans 1993). In *C. lupus*, CM 57444, there is one major palatine foramen per side, entirely within the maxilla, opposite P5 (Fig. 43D).

According to Jayne (1898:330–331), in *F. catus*, the position, number, and size of the major palatine foramina (his posterior palatine foramina) on the hard palate are variable. “In some specimens there is a single large foramen in the anterior border [of the palatine], or just behind it; in others, one large foramen and a second smaller one much farther back on the palatal surface; in others, one large and two smaller posterior foramina; and more rarely, the large foramen may be accompanied by three or even more smaller openings.” Whether all of these transmit major palatine nerves is uncertain, as “usually not more than two can be traced back to the posterior wall of the main canal.” Following the terminology employed here, the foramina in or near the palatomaxillary suture are major palatine foramina and those more posteriorly placed are accessory palatine foramina. CM 12910 (Fig. 43B) and 28447 have one major palatine foramen per side, but in the latter it is within the palatine while in the former it is between the palatine and maxilla. A short major palatine sulcus extends to the anterior limit of the palatine bone.

In *G. genetta*, CM 85593 (Fig. 43C), the anteriormost major palatine foramina are the largest, with a well-developed major palatine sulcus extending to the incisive foramen. In addition, there are eight or nine tiny foramina anterior to the palatomaxillary suture.

In the study sample of *N. binotata*, the number of major palatine foramina varies between one and seven with all anterior to the palatomaxillary suture (Figs. 5, 9). Only

one specimen has a single foramen present bilaterally. The anteriormost foramen is always the largest, with a sulcus that usually reaches to the incisive foramen.

**Mandibular Foramen**—The mandibular foramen transmits the inferior alveolar nerve, artery, and vein in *C. lupus familiaris* (=mandibular alveolar nerve, artery, and vein of Evans 1993) and *F. catus* (Reighard and Jennings 1935). In *C. lupus*, CM 57444, the foramen is situated at the anteroposterior midpoint of the coronoid process; in *F. catus*, CM 12910, it is near the anterior aspect of the coronoid process; and in *G. genetta*, CM 85593, and in juvenile and adult *N. binotata* (“manf” in Figs. 31, 33B), it is halfway between these two conditions. The condition in *F. catus* resembles that in newborn *N. binotata*, AMNH 207730 (Fig. 33A).

**Mastoid Canaliculus**—In *C. lupus familiaris* (Evans 1993:982), “the auricular branch (ramus auricularis) leaves the vagus near the jugular foramen and runs laterally through the petrous temporal bone to join the facial nerve.” In CM 106574, the mastoid canaliculus is not enclosed in the petrosal. Its medial aperture is between the petrosal, exoccipital, and caudal entotympanic, and its lateral aperture is between the petrosal and caudal entotympanic. The former opens lateral to the posterior border of the jugular foramen and the latter opens deep to the foramen stylomastoideum definitivum.

In *Felis* sp., CM 10750, the mastoid canaliculus is as reported for *C. lupus familiaris*, CM 106574. *Felis catus*, CM 28447, differs in that the medial opening is only between the petrosal and caudal entotympanic.

In *G. cristata*, CM 3697, the dried auricular ramus of the vagus is preserved on the right side, and its course is visible through the thin bone forming the roof of the posterior chamber of the bulla. It leaves the anterolateral aspect of the jugular foramen and curves laterally and then anteriorly to join the facial nerve deep to the foramen stylomastoideum definitivum. Its course is between the petrosal and caudal entotympanic.

In *N. binotata*, the auricular branch of the vagus runs between the petrosal and caudal entotympanic, leaving the lateral aspect of the jugular foramen and joining the facial nerve external to the foramen stylomastoideum primitivum (“abX” in Fig. 18).

**Mastoid Foramen**—In *C. lupus familiaris* (Evans 1993), the mastoid foramen lies on the occiput between the mastoid exposure of the petrosal and the ex- and supraoccipital; it transmits the occipital emissary vein, which connects to the sigmoid sinus.

Mastoid foramina are absent in *F. catus*, CM 1407, 3129, *G. genetta*, CM 85593, and *N. binotata* (Figs. 29A–B).

**Maxillary Foramen**—The maxillary foramen, which transmits the infraorbital nerve, artery, and vein from the pterygopalatine fossa into the infraorbital canal (Jennings

and Reighard 1935; Evans 1993), is enclosed in the maxilla in *C. lupus*, CM 57444, *F. catus*, CM 28447, *G. genetta*, CM 85593, and *N. binotata* (“mx” in Fig. 8). However, in the first three taxa, the lacrimal and jugal approximate the dorsal margin of the maxillary foramen, whereas these bones are well separated from the maxillary foramen in *N. binotata* (Fig. 8A).

**Mental Foramen**—In *C. lupus familiaris* (Evans 1993:155), there is a mental foramen “near the symphysis, ventral to the alveolus of the central incisor tooth. The largest of the mental foramina, the middle mental foramen, is located ventral to the septum between the first two cheek teeth. A small mental foramen or several foramina are present caudal to the middle opening.” These openings transmit the rostral, middle, and caudal mental nerves, arteries, and veins (Evans 1993). In *C. lupus*, CM 57444 (Fig. 44D), the anterior mental foramen is below I1, the middle below the anterior root of p2, and the posterior below the anterior root of p4.

In *F. catus*, Jayne (1898:389) reports two or more small mental foramina near the symphysis and two larger ones posterior to the canine swelling. Of the latter, “the anterior is usually larger than the posterior, and may be double; the posterior may be very small or entirely absent. There is frequently a second smaller posterior foramen below, either behind or in front of the main foramen, and there are several inconstant openings on and around the canine swelling.” In *F. catus*, CM 12910 (Fig. 44B), there are two small foramina near the symphysis, a large one below the diastema behind the canine, and two small ones below the p4.

In *G. genetta*, CM 85593 (Fig. 44C), there are two small foramina (one on the left) near the symphysis, two large foramina (below p2 and p4), and a tiny caudal foramen (below p5 on the right and p5/m1 on the left).

In the study sample of *N. binotata*, the number of mental foramina varies between three and six per side (“mf” in Fig. 30B). The anteriormost is invariably near the symphysis and the posteriormost is most often ventral to p4.

**Minor Palatine Notch**—In *C. lupus familiaris* (Evans 1993), a distinct, narrow unnamed notch (minor palatine notch here), rarely transformed into a foramen (minor palatine foramen here), in the posteriormost aspect of the palatamaxillary suture on the hard palate transmits the minor palatine artery, vein (Evans 1993), and nerve (Schaller 1992). In *C. lupus*, CM 57444, the notch is between the palatine and maxilla (Fig. 43D).

In *F. catus* (Fig. 42B), the minor palatine nerve and vessels (=postpalatine nerve and vessels of Davis and Story 1943) pass through a large, broad notch that is principally in the palatine; the maxilla makes a minor contribution to the posterolateral border.

In *G. genetta*, CM 85593, the broad minor palatine notch is entirely in the palatine (Fig. 43C). The medial border of the notch has a raised, laterally projecting ridge

that slightly constricts the occupants of the notch.

In the study sample of *N. binotata*, a well-developed minor palatine notch is present entirely in the palatine (“mpn” in Figs. 5–6). About one-third of the specimens show some degree of closure, with three having complete closure (Fig. 9). We are unsure whether the closed foramen represents a minor palatine foramen or an accessory palatine foramen.

**Musculotubal Canal**—In *C. lupus familiaris* (Evans 1993), the musculotubal canal is at the anteromedial aspect of the auditory bulla and transmits the auditory tube. Its ventral margin is formed by the styliform process of the ectotympanic (=muscular process of tympanic of Evans 1993), which provides attachment for the tensor and levator veli palatini muscles. Medial to the musculotubal canal is the anterior carotid foramen. Based on CM 15205, the musculotubal canal is between the alisphenoid, ectotympanic, and rostral entotympanic.

In *F. catus*, the auditory tube and tensor veli palatini leave the middle ear via a gap between the auditory bulla and skull base (Davis and Story 1943: fig. 2). Based on CM 1407, the musculotubal canal is between the alisphenoid, ectotympanic, and rostral entotympanic. It is continuous medially with the anterior carotid foramen.

In *G. genetta*, CM 85593, the musculotubal canal is between the alisphenoid, ectotympanic, and rostral entotympanic, and is continuous medially with the anterior carotid foramen.

In *N. binotata*, the musculotubal canal (“mtc” in Fig. 25) is between the alisphenoid, ectotympanic, and caudal entotympanic, and is continuous medially with the anterior carotid foramen.

**Optic Foramen**—In *C. lupus familiaris* (Evans 1993), the optic foramen is positioned in the posterior part of the orbitosphenoid and transmits the optic nerve, the ophthalmic artery (=internal ophthalmic artery of Evans 1993), and internal ophthalmic vein. Evans (1993:139) reported “medially, in young specimens, the two elliptical optic canals are confluent across the midline.” We found this condition in a juvenile with deciduous dentition, CM 15205, and in adult *C. lupus*, CM 57444, where the confluence is the very narrow optic chiasm.

In *F. catus*, the optic foramen is in the posterior part of the orbitosphenoid and transmits the optic nerve and ophthalmic artery (Reighard and Jennings 1935); we do not know if there are accompanying veins. In CM 28447, the optic chiasm is not a narrow, constricted space, but a broad sulcus, and the optic foramina are not confluent across the midline.

In *G. genetta*, CM 85593, the optic foramen is centrally positioned in the orbitosphenoid and is confluent across the midline (Fig. 42C), with the optic chiasm very broad.

In *N. binotata*, the optic foramen (“of” in Fig. 11) is in the posterior part of the orbitosphenoid and is confluent across the midline, with the optic chiasm narrow.

**Posterior Carotid Foramen**—see Carotid Foramen.

**Postglenoid Foramen**—In *C. lupus familiaris*, the postglenoid foramen (=retroarticular foramen of Evans 1993) is in the squamosal posterior to the postglenoid process (=retroarticular process of Evans 1993) and transmits the postglenoid vein (=retroarticular vein of Evans 1993). In *C. lupus*, CM 57444, the ectotympanic makes a small contribution to the posterior border of the postglenoid foramen (Fig. 43D).

In *F. catus* (Jayne 1989:194), “just behind the inner end of the postglenoid process is a postglenoid foramen, more or less well marked, which transmits a vessel from the diploë.” *Felis catus*, CM 12910, shows considerable left-right asymmetry: the right foramen is near the medial end of the postglenoid process, whereas the left foramen is near the lateral margin of the zygoma’s posterior root (Fig. 43B).

In *G. genetta*, CM 85593, a small postglenoid foramen is present in the squamosal, posteromedial to the postglenoid process (Fig. 43C). The position of the foramen differs between the two sides: it is lateral to the spine of the rostral process of the malleus on the left side and wholly posterior to that structure on the right.

In the study sample of *N. binotata*, between one and four small postglenoid foramina are found in the squamosal, posteromedial to the postglenoid process (“pgf” in Figs. 14–15). These are nearly obscured in some specimens by the anterior crus of the ectotympanic (Figs. 19, 22).

**Pterygoid Canal**—In *C. lupus familiaris* (Evans 1993), the pterygoid canal transmits the nerve of the pterygoid canal and occasionally a small artery off the maxillary artery. Its caudal opening is on the basicranium between the basisphenoid and pterygoid, anterior to the foramen ovale, and its rostral opening is in the pterygopalatine fossa, anteroventral to the sphenorbital fissure between the alisphenoid (=pterygoid process of the sphenoid of Evans 1993) and pterygoid. In *C. lupus*, CM 57444, the nerve of the pterygoid canal leaves the middle ear via an opening between the rostral entotympanic and basisphenoid in the dorsal aspect of the musculotubal canal, and enters a groove in the basisphenoid that ends at the caudal opening of the pterygoid canal, opposite the foramen ovale (Fig. 43D).

In *F. catus*, CM 12910 (Fig. 43B), the extracranial course of the nerve of the pterygoid canal is marked by a groove on the basisphenoid that begins posteriorly at the conjoint musculotubal canal/anterior carotid foramen. According to Davis and Story (1943), this segment of the nerve course includes an artery of the pterygoid canal off the maxillary artery. The groove for the nerve ends at the caudal opening of the pterygoid canal between the basisphenoid and pterygoid, anterior to the foramen ovale. The rostral opening is in the floor of the cavum epiptericum, deep within the sphenorbital fissure between the basisphenoid and alisphenoid. A groove leads forward from the rostral opening and ends at the ventral border of the sphenorbital fissure.

In *G. genetta*, CM 85593 (Fig. 43C), the extracranial course of the nerve of the pterygoid canal is marked by a groove on the basisphenoid exiting the middle ear at the conjoint musculotubal canal/anterior carotid foramen. The groove leads to the caudal opening of the pterygoid canal, posterior to the foramen ovale. As the pterygoid is fused to the basisphenoid on the skull base, the composition of the caudal opening is uncertain. The rostral opening of the pterygoid canal is in the floor of the cavum epiptericum, deep within the sphenorbital fissure, between the pterygoid and alisphenoid.

In the study sample of *N. binotata*, the posterior course of the nerve of the pterygoid canal is either open in a groove on the basisphenoid ("npc" in Fig. 14) or with part closed in a canal in the basisphenoid of varying lengths and positions ("npc" in Figs. 15–16, 18–19). The posterior course ends at the caudal opening of the pterygoid canal, which is between the pterygoid and basisphenoid, anterior to the foramen ovale. The rostral opening of the pterygoid canal is in the floor of the cavum epiptericum, deep within the sphenorbital fissure, between the pterygoid and alisphenoid ("ropc" in Fig. 37).

**Sigmoid Sinus Sulcus**—In *C. lupus familiaris* (Evans 1993:710), the sigmoid sinus "is the roughly S-shaped caudoventral continuation of the transverse sinus. It begins by forming an arc around the proximal end of the petrous temporal bone. The first arc is continued by the second arc, which lies medial to the petro-occipital synchondrosis. The sinus terminates after traversing the jugular foramen by continuing as the internal jugular vein." In CM 106574, a well-developed sulcus for the sigmoid sinus runs along the posterior aspect of the endocranial surface of the petrosal to the jugular foramen.

In *Felis* sp., CM 10750, a sulcus for the sigmoid sinus on both the petrosal and exoccipital leads to the jugular foramen, which confirms Reighard and Jennings's (1935) observation that the major exit of the transverse sinus is via that foramen in *F. catus*.

In *G. cristata*, CM 3697, a deep sulcus for the sigmoid sinus arcs around the petrosal posterior to the subarcuate fossa and then turns posteriorly into the condyloid canal. It does not reach the jugular foramen.

In *N. binotata*, AMNH 134969, the sigmoid sinus runs in a sulcus on the petrosal dorsal to the subarcuate fossa ("ss" in Figs. 37–38), which joins the condyloid canal posteriorly.

**Sphenopalatine Foramen**—In *C. lupus familiaris* (Evans 1993), the sphenopalatine foramen is within the perpendicular process of the palatine, dorsal to the caudal palatine foramen, and transmits the caudal nasal nerve and the sphenopalatine artery and vein. In *C. lupus*, CM 57444, the sphenopalatine and caudal palatine foramina are in a common depression.

In *F. catus*, the sphenopalatine foramen is in the perpendicular process of the palatine and transmits the same structures as in *C. lupus familiaris* (Reighard and Jennings

1935). It is not in a common depression with the caudal palatine foramen. In the CM sample (e.g., 1407, 12910, 20615, 28447), a seam within the palatine intersects the dorsal border of the foramen, suggesting the foramen forms between two processes of that bone.

In *G. genetta*, CM 85593, the sphenopalatine foramen is in the perpendicular process of the palatine and not in a common depression with the caudal palatine foramen. A seam within the palatine is present dorsal to the foramen.

In the study sample of *N. binotata*, the sphenopalatine foramen ("spF" in Fig. 8) is in the perpendicular process of the palatine and not in a common depression with the caudal palatine foramen. All specimens have a seam within the palatine dorsal to the foramen

**Sphenorbital Fissure**—In *C. lupus familiaris*, the sphenorbital fissure (=orbital fissure of Evans 1993) is between the orbito- and alisphenoid and transmits the oculomotor, trochlear, ophthalmic, and abducens nerves, the anastomotic artery connecting the maxillary artery and the Circle of Willis, and the ophthalmic venous plexus. It is situated between the optic foramen and foramen rotundum. In *C. lupus*, CM 57444, the sphenorbital fissure is in a common depression with the optic foramen and closer to that opening than to the foramen rotundum.

In *F. catus*, based on CM 1407, 12910, 20615, 28447, the sphenorbital fissure (=sphenoidale fissure of Jayne 1898; =orbital fissure of Davis and Story 1943) is not in a common depression with the optic foramen, but equidistant between that foramen and the foramen rotundum. It transmits the same structures as in *C. lupus familiaris* (Reighard and Jennings 1935), but the anastomotic artery is represented by multiple branches that connect the external rete mirabile with the internal rete mirabile and the Circle of Willis (Davis and Story 1943). The external rete surrounds the trunk of the maxillary artery between the foramen rotundum and optic foramen.

In *G. genetta*, CM 85593, the sphenorbital fissure is in a common depression with the foramen rotundum as they share a common dorsal wall. The sphenorbital fissure is nearer to the foramen rotundum than to the optic foramen.

In the study sample of *N. binotata*, the sphenorbital fissure is essentially in the same plane as the foramen rotundum and well separated from the optic foramen (Fig. 11). Davis and Story (1943) reported an anastomotic artery in the sphenorbital fissure connecting the maxillary artery with the internal rete mirabile and the Circle of Willis.

**Stylomastoid Foramen**—see Facial Canal.

**Transverse Canal Foramen**—Transverse canal foramina are not reported for *C. lupus familiaris* (Evans 1993) nor present in *C. lupus*, CM 57444.

In *F. catus*, Jayne (1898:260–261) reported small openings in the inner wall of the foramen rotundum and foramen ovale. Regarding the foramen rotundum, we found a small foramen in its inner wall bilaterally in our entire

CM sample and consider it to be a transverse canal foramen. Regarding the foramen ovale, we found only a tiny foramen in its inner wall bilaterally in one specimen, CM 28447, and do not consider it to be a transverse canal foramen.

In *G. genetta*, CM 85593, 95202, a transverse canal foramen is present bilaterally in the inner wall of the foramen ovale. It is absent in *G. cristata*, CM 3697.

In the study sample of *N. binotata*, we reported openings variable in number, size, and position associated with the foramen ovale and/or the caudal opening of the alisphenoid canal (“tcf” in Figs. 11, 20). Based on AMNH 134969 (Figs. 37–38), we interpreted these as transverse canal foramina transmitting veins. Only one specimen, CM 59496, did not have any transverse canal foramina bilaterally.

**Transverse Sinus Canal**—In *C. lupus familiaris* (Evans 1993:135), “within the dorsal part of the occipital bone [=interparietal] and opening bilaterally on the cerebral surface is the transverse canal (canalis transversus), which, in life, contains the venous transverse sinus. The transverse canal is continued laterally, on each side, by the sulcus for the transverse sinus (sulcus sinus transversi). Mid-dorsally or to one side, the dorsal sagittal sinus enters the transverse sinus via the foramen impar.” Based on Evans (1993: figs. 4–11, 4–14), the foramen impar is in the interparietal and the sulcus for the transverse sinus is in the supraoccipital and parietal.

In *F. catus*, Jayne (1898:182) reported regarding the tentorial process of the parietal that “in some specimens there is a distinct groove for the lateral sinus [=transverse sinus] leading to a foramen above the middle of the border; in others the groove is present but the sinus enters the interparietal or the occipital [=supraoccipital], and in others there is neither groove nor foramen.”

Specimens of *G. genetta* or *G. cristata* showing the anterior surface of the ossified tentorium were not available to us.

The two specimens of *N. binotata* exposing the anterior surface of the ossified tentorium exhibit differences regarding the course of the transverse sinus. In AMNH 134969, there is a single opening in the tentorial process of the right parietal just off the midline ventral to the skull roof that represents the foramen impar. The dorsal sagittal sinus enters this foramen and divides into the left and right transverse sinuses within the parietal. The canal for the transverse sinus continues ventrally in the outer edge

of the tentorial process and ends at the petrosal. In AMNH 201513, a juvenile, the dorsal sagittal sinus divides into the left and right transverse sinuses anterior to the tentorial processes of the parietals. The left transverse sinus enters an opening just off the midline, whereas the right one runs in an open groove and enters an opening about halfway down the side of the skull (“ts” in Fig. 40). We do not know if these are ontogenetic differences or variation.

**Trigeminal Canal**—In *C. lupus familiaris* (Evans 1993), the trigeminal nerve passes through a canal on the endocranial surface of the petrosal, anteroventral to the internal acoustic meatus. In CM 106574, the trigeminal canal is between the tentorial process of the petrosal, which is an enlarged crista petrosa, and the pars cochlearis of the petrosal.

In *F. catus*, CM 28447, *G. cristata*, CM 3697, and *N. binotata* (Figs. 21B–F, 37–38), the crista petrosa is not raised into a tentorial process and a trigeminal canal is absent.

**Tympanic Canaliculus**—Evans (1993: fig. 19–20) illustrated the course of the tympanic nerve in *C. lupus familiaris*, but did not describe it in detail. It is shown arising from the glossopharyngeal nerve at the jugular foramen and running laterally onto the petrosal, medial to the aperture of the cochlear fossula. In CM 106574, the tympanic canaliculus, which transmits the tympanic nerve into the middle ear, is between the caudal entotympanic and petrosal. Its medial aperture is just anterior to the mastoid canaliculus, while its lateral aperture is just medial to the aperture of the cochlear fossula.

In *F. catus*, CM 1407, and *G. cristata*, CM 3697, the tympanic canaliculus is as reported for *C. lupus familiaris*, CM 106574. We reconstructed the tympanic nerve of *N. binotata* (“tn” in Fig. 18) as in these other carnivorans, although we did not find any osteological correlates for the tympanic canaliculus.

**Vestibular Aqueduct**—In *C. lupus familiaris* (Evans 1993:143), the endolymphatic duct enters the petrosal via the vestibular aqueduct, which “is located caudodorsal to the opening of the cochlear canaliculus in a small but deep cleft in the bone.” In CM 106574, the vestibular aqueduct is medial to the subarcuate fossa, while the cochlear canaliculus is medial to the internal acoustic meatus.

In *F. catus*, CM 28447, *G. cristata*, CM 3697, and *N. binotata* (“va” in Figs. 21E, 37–38), the vestibular aqueduct (and cochlear canaliculus) is arranged as in *C. lupus familiaris*, CM 106574.

## APPENDIX 1. List of Anatomical Terms.

The terms used here are to the left; references, synonyms, and/or Nomina Anatomica Veterinaria (NAV) equivalents are to the right. (*continued on the next page*)

- Abducens Nerve (=Cranial Nerve VI)—Nervus Abducens (NAV)  
 Accessory Nerve (=Cranial Nerve XI)—Nervus Accessorius (NAV)  
 Accessory Palatine Foramen—(Wible and Rougier 2000); Middle Palatine Foramen (Novacek 1986); Minor Palatine Foramen (Evans 1993)  
 Accessory Posterior Clinoid Process—this study  
 Ala Hypochiasmatica—(De Beer 1937)  
 Alae of Vomer—Alae Vomeris (NAV)  
 Alicochlear Commissure—(De Beer 1937; MacPhee 1981)  
 Alisphenoid—Os Basisphenoidale, Ala Temporalis (NAV)  
 Alisphenoid Canal—(Gregory 1910); Canalis Alaris (NAV)  
 Alveolar Foramina—Foramina Alveolaris (NAV)  
 Alveolar Jugal—Jugal Alveolaria (NAV)  
 Alveolar Margin—Margo Alveolaris (NAV)  
 Alveolar Nerve—Nervus Alveolaris (NAV)  
 Alveolar Process of Maxilla—Os Maxillare, Processus Alveolaris (NAV)  
 Alveolar Process of Premaxilla—Os Incisivum, Processus Alveolaris (NAV)  
 Alveoli—Alveoli Dentales (NAV)  
 Ampulla of Lateral Semicircular Canal—Ampulla Ossea Lateralis (NAV)  
 Ampulla of Posterior Semicircular Canal—Ampulla Ossea Posterior (NAV)  
 Anastomotic Artery—(Davis and Story 1943; Evans 1993)  
 Angular Process of Mandible—Processus Angularis (NAV)  
 Annular Ligament of Stapes—Lig. Annulare Stapedis (NAV)  
 Annular Ridge—(Rowe et al. 2005)  
 Anterior Carotid Foramen—this study; Foramen Lacerum (Evans 1993)  
 Anterior Chamber of Auditory Bulla—(Pocock 1916; Klaauw 1931)  
 Anterior Crus (=Leg) of Ectotympanic—Annulus Tympanicus, Crus Anterior (NAV)  
 Anterior Crus of Stapes—Stapes, Crus Rostrale (NAV)  
 Anterior Pole of Promontorium—(Wible 2003)  
 Anterior Semicircular Canal—Canalis Semicircularis Anterior (NAV)  
 Aperture of Cochlear Fossula—(MacPhee 1981); Fenestra Rotunda (Jayne 1898); Fenestra Cochleae (Evans 1993)  
 Apex Parties Petrosa—(NAV); Apex Pyramidalis (Evans 1993)  
 Aqueductus Vestibuli—(NAV)  
 Artery of the Pterygoid Canal—(Davis and Story 1943; Evans 1993)  
 Ascending Pharyngeal Artery—Arteria Pharyngea Ascendens (NAV)  
 Auditory Bulla—Bulla Tympanica (NAV)  
 Auditory Ossicles—Ossicula Auditus (NAV)  
 Auditory Region—Auris (NAV)  
 Auditory Tube—Tuba Auditiva (NAV); Eustachian Tube (Jayne 1898)  
 Auricular Ramus of Vagus Nerve—Nervus Vagus, Ramus Auricularis (NAV)
- Basicranium—Basis Cranii Interna et Externa (NAV)  
 Basihyal—Basihyoideum (NAV)  
 Basilar Membrane—Lamina Basilaris (NAV)  
 Basioccipital—Os Occipitale, Pars Basilaris (NAV)  
 Basipharyngeal Canal—(Evans 1993); Nasopharyngeal Fossa (Davis 1964)  
 Basisphenoid—Os Basisphenoidale, Corpus (NAV)  
 Body of Incus—Corpus Incudis (NAV)  
 Body of Mandible—Corpus Mandibulae (NAV); Horizontal Ramus of Mandible (Clark 1926)  
 Body of Premaxilla—Corpus Osis Incisivi (NAV)  
 Brain—Encephalon (NAV)  
 Braincase—Calvaria (NAV)  
 Buccinator Muscle—Musculus Buccinator (NAV)

## APPENDIX 1. List of Anatomical Terms.

*(continued from the previous page)*

- Canal for Chorda Tympani—Canaliculus Chordae Tympani (NAV)  
 Canal for Modiolus—(Terry 1942)  
 Canines—Dentes Canini (NAV)  
 Capitular Crest of Malleus—(Henson 1961)  
 Capitular Spine of Malleus—(Henson 1961)  
 Carnassial—(Osborn 1907; Evans 1993); Dens Sectorius (NAV)  
 Carotid Foramen—(Wible and Gaudin 2004); Canalis Caroticus (NAV); Foramen Lacerum Medium (Gregory 1910; Davis and Story 1943); Middle Lacerated Foramen (Jayne 1898); Middle Lacerate Foramen (Hunt 1974); Anterior Carotid Foramen (MacPhee 1981); Foramen Lacerum (Evans 1993)  
 Carotid Sulcus—Sulcus Caroticus (NAV)  
 Cartilaginous Nasal Septum—Cartilago Septi Nasi (NAV)  
 Caudal Auricular Artery—Arteria Auricularis Caudalis (NAV)  
 Caudal Clinoid Process—Processus Clinoides Caudalis (NAV)  
 Caudal Cranial Fossa—Fossa Cranii Caudalis (NAV); Occipital Cranial Fossa (Evans 1993)  
 Caudal Horn of Thyroid—Cartilago Thyroidea, Cornu Caudale (NAV)  
 Caudal Lobe of Vermis—Cerebellum, Vermis, Pars Caudalis (NAV)  
 Caudal Meningeal Artery—(Evans 1993); Arteria Meningea Caudalis (NAV); Arteria Meningea Posterior (Davis and Story 1943)  
 Caudal Nasal Nerve—Nervus Nasalis Caudalis (NAV)  
 Caudal Opening of Alisphenoid Canal—Foramen Alare Caudale (NAV)  
 Caudal Palatine Foramen—(Evans 1993); Foramen Palatinum Caudale (NAV); Posterior Palatine Foramen (Jayne 1898); Caudal Opening of Posterior Palatine Canal (Reighard and Jennings 1935)  
 Caudal Process of Pterygoid—(Giannini et al. 2006)  
 Caudal Process of Squamosal—(Wible 2008)  
 Caudal Tympanic Process of Petrosal—(MacPhee 1981)  
 Cavernous Sinus—Sinus Cavernosus (NAV)  
 Cavum Epiptericum—(Gaupp 1902, 1905; De Beer 1937)  
 Cavum Supracochleare (=Genu of Facial Canal)—(Voit 1909; De Beer 1937); Geniculum Canalis Facialis (NAV)  
 Cavum Tympani—(NAV); Tympanum (Jayne 1898)  
 Ceratohyal—Ceratohyoideum (NAV)  
 Cerebellum—(NAV)  
 Cerebrum—(NAV)  
 Choanae—(NAV)  
 Chondrocranium—(NAV)  
 Chondrohyal—(Jayne 1898)  
 Chorda Tympani Nerve—Chorda Tympani (NAV)  
 Circle of Willis—(Evans 1993); Circulus Arteriosus Cerebri (NAV)  
 Cochlear Canaliculus—(MacPhee 1981); Apertura Externa Canaliculus Cochleae (NAV); Aquæductus Cochleæ (Jayne 1898); Aqueductus Cochleae (Evans 1993)  
 Cochlear Duct—Ductus Cochlearis (NAV)  
 Cochlear Fossula—(MacPhee 1981)  
 Common Carotid Artery—Arteria Carotis Communis (NAV)  
 Condylar Process of Mandible—Processus Condylaris (NAV)  
 Condylod Canal—(Evans 1993); Canalis Condylaris (NAV); Posterior Condylod Canal (Jayne 1898)  
 Condylod Crest of Mandible—Mandible, Crista Condylodeus (NAV)  
 Condylod Vein—(Evans 1993)  
 Confluence of Sinuses—(Evans 1993); Confluem Sinuum (NAV)  
 Coronal Sulcus—(Radinsky 1978); Sulcus Coronalis (NAV); Fissura Coronalis (Carlsson 1900)  
 Coronal Suture—Sutura Coronalis  
 Coronoid Crest of Mandible—Crista Coronoidea (Evans 1993)  
 Coronoid Process of Mandible—Processus Coronoideus (NAV)  
 Cribriform Plate of Ethmoid—Os Ethmoidale, Lamina Cribrosa (NAV)  
 Cribroethmoidal Foramen—(Moore 1981)  
 Cricoid Cartilage—Cartilago Cricoidea (NAV)

APPENDIX 1. List of Anatomical Terms.  
(continued from the previous page)

- Crista Frontalis—(NAV)  
 Crista Galli—(NAV)  
 Crista Interfenestralis—(Wible et al. 1995)  
 Crista Masseterica—(Turnbull 1970)  
 Crista Parotica—(De Beer 1937)  
 Crista Petrosa—(Wible 1990); Crista Parties Petrosae (NAV)  
 Crista Stapedis—(Henson 1961)  
 Crista Supramastoideus—(NAV)  
 Crista Tympanica—(MacPhee 1981)  
 Crura of Stapes—Stapes, Crus Rostrale + Crus Caudale (NAV)  
 Crural Sulcus of Stapes—(Henson 1961)  
 Crus Breve of Incus—Incus, Crus Breve (NAV); Superior Process of Incus (Jayne 1898)  
 Crus Commune of Semicircular Canals—(Wible 1990); Crus Osseum Commune (Evans 1993)  
 Crus Longum of Incus—Incus, Crus Longum (NAV); Inferior Process of Incus (Jayne 1898)
- Deciduous Teeth—Dentes Decidui (NAV)  
 Deep Petrosal Nerve—Nervus Petrosus Profundus (NAV)  
 Diastema—(NAV); Interdental Space (Evans 1993)  
 Digastric Muscle—Musculus Digastricus (NAV)  
 Diploë—(NAV)  
 Dorsal Condylloid Fossa—Fossa Condylaris Dorsalis (NAV)  
 Dorsal Sagittal Sinus—Sinus Sagittalis Dorsalis (NAV)  
 Dorsum Sellae—(NAV)
- Ectotympanic—(MacPhee 1981); Annulus Tympanicus (NAV); Tympanic (Gregory 1910)  
 Ectotympanic Notch—(Wible and Spaulding 2012)  
 Endocranium—Cavum Cranii (NAV)  
 Endolymphatic Duct—Ductus Endolymphaticus (NAV)  
 Entoglenoid Process of Squamosal—(McDowell 1958); Post-Glenoid (Entoglenoid) Process (Gregory 1910); Modified Entoglenoid Process (McDowell 1958; MacPhee 1981); Pseudopostglenoid (Entoglenoid) Process (Novacek 1986a); Pseudoglenoid Process (MacPhee 1994)  
 Entopterygoid Process—(Giannini et al. 2006); Medial Pterygoid Process (Clark 1926); Pterygoid Process (Davis 1964)  
 Entotympanic—(Klaauw 1922); Os Temporale, Pars Endotympanica (NAV)  
 Epiglottic Prominence—(Wible 2010b)  
 Epihyal—Epihyoideum (NAV)  
 Epitympanic Recess—(Klaauw 1931); Recessus Epitympanicus (NAV); Fossa for Malleus and Incus (Jayne 1898)  
 Epitympanic Wing of Alisphenoid—(MacPhee 1981)  
 Epitympanic Wing of Parietal—(Giannini et al. 2006)  
 Epitympanic Wing of Petrosal—(MacPhee 1981)  
 Epitympanic Wing of Squamosal—(MacPhee 1981)  
 Ethmoid—Os Ethmoidale (NAV)  
 Ethmoidal Foramen—Foramen Ethmoidale (NAV)  
 Ethmoidal Fossa—Fossae Ethmoidales (NAV)  
 Ethmoidal Nerve—Nervus Ethmoidalis (NAV)  
 Ethmoturbinates—(Smith and Rossie 2006); Ethmoturbinalia (NAV)  
 Exoccipital—Os Occipitale, Pars Lateralis (NAV)  
 External Acoustic Meatus—Meatus Acusticus Externus (NAV); External Auditory Meatus (Gregory 1910)  
 External Carotid Artery—Arteria Carotis Externus (NAV)  
 External Ethmoidal Artery—Arteria Ethmoidalis Externa (NAV)  
 External Ethmoidal Vein—Vena Ethmoidalis Externa (NAV)  
 External Lamina of Ethmoid—(Evans 1993); Os Ethmoidale, Lamina Tectoria + Lamina Orbitalis + Lamina Basalis (NAV)  
 External Nasal Aperture—Apertura Nasi Ossea (NAV); External Nasal Opening or Piriform Aperture (Evans 1993)  
 External Occipital Crest—Crista Occipitalis Externa (NAV); Occipital Crest (Jayne 1898)

## APPENDIX 1. List of Anatomical Terms.

*(continued from the previous page)*

- Facial Canal—(MacPhee 1981); Canalis Facialis (NAV); Aquæductus Fallopii (Jayne 1898)  
 Facial Nerve (=Cranial Nerve VII)—Nevus Facialis (NAV)  
 Facial Process of Maxilla—Os Maxillare, Facies Facialis (NAV)  
 Facial Process of Premaxilla—Os Incisivum, Facies Labialis (NAV); Nasal Process of Premaxilla (Reighard and Jennings 1935)  
 Facial Sulcus—(MacPhee 1981)  
 Fenestra Cochleae—(NAV); Fenestra Rotunda (Jayne 1898)  
 Fenestra Vestibuli—(NAV); Fenestra Ovalis (Jayne 1898)  
 Fontanel—(Evans 1993)  
 Footplate (=Base) of Stapes—Stapes, Basis Stapedis (NAV)  
 Foramen Acusticum Inferius—(Sisson 1910); Ventral Vestibular Area (Evans 1993)  
 Foramen Acusticum Superius—(Sisson 1910); Facial Canal + Dorsal Vestibular Area (Evans 1993)  
 Foramen Centrale Cochleare—(Terry 1942)  
 Foramen for Frontal Diploic Vein—(Thewissen 1989); Supra-Ethmoid Foramen (Gregory 1910); Frontal Diploic Foramen (MacPhee 1994)  
 Foramen for Ramus Temporalis—(Wible and Gaudin 2004); Post-Parietal Foramen, Post-Squamosal Foramen (Gregory 1910); Subsquamosal Foramen (Wible et al. 2004)  
 Foramen Impar—(Evans 1993)  
 Foramen Magnum—(NAV)  
 Foramen Ovale—(NAV)  
 Foramen Rotundum—Foramen Rotundum + Foramen Alare Rostrale (NAV)  
 Foramen Singulare—(NAV)  
 Foramen Spinosum—(NAV)  
 Foramen Stylomastoideum Definitivum—(Klaauw 1931)  
 Foramen Stylomastoideum Primitivum—(Klaauw 1931)  
 Fossa for Rectus Capitis Ventralis—this study; Fossa for Rectus Capitis Anticus Minor Muscle (Jayne 1898)  
 Fossa for Stapedius Muscle—(MacPhee 1981); Fossa M. Stapedius (Evans 1993)  
 Fossa Incudis—(MacPhee 1981)  
 Frontal—Os Frontale (NAV)  
 Frontal Diploic Vein—Vena Diploica Frontalis (NAV)  
 Frontal Eminence—(Terry 1942)  
 Frontal Process of Jugal—Os Zygomaticum, Processus Frontalis (NAV); Postorbital Process of Malar (Jayne 1898)  
  
 Geniculate Ganglion—Ganglion Geniculi (NAV)  
 Glaserian Fissure—Fissura Glaseri (Klaauw 1931); Fissura Petrotympánica (NAV); Canal of Huguier (Jayne 1898; Reighard and Jennings 1935)  
 Glenoid Fossa—Fossa Mandibularis (NAV); Glenoid Cavity (Jayne 1898); Retroarticular Fossa (Evans 1993)  
 Glossopharyngeal Nerve (=Cranial Nerve IX)—Nervus Glossopharyngeus (NAV)  
 Greater Petrosal Nerve—Nervus Petrosus Major (NAV)  
 Groove for Middle Meningeal Artery—Arborescent Groove for Meningeal Artery (Jayne 1898); Sulcus Arteriae Menigeae Mediae (Evans 1993)  
 Groove for Nerve of Pterygoid Canal—Sulcus Nervus Canalis Pterygoidei (NAV)  
  
 Hard Palate—Palatum Osseum (NAV)  
 Head of Malleus—Caput Mallei (NAV)  
 Head of Stapes—Caput Stapedis (NAV)  
 Hemisphere of Cerebellum—Cerebellum, Hemispherium (NAV)  
 Hiatus Fallopii—(Jayne 1898); Petrosal Canal (Evans 1993)  
 Horizontal Part of Exoccipital—(Wible 2003)  
 Horizontal Process of Palatine—Os Palatinum, Lamina Horizontalis (NAV)  
 Hyoid Apparatus—Apparatus Hyoideus (NAV)  
 Hypoglossal Foramen—Canalis N. Hypoglossus (NAV); Anterior Condylod Foramen (Jayne 1898); Condylar Foramen (Gregory 1910); Foramen Hypoglossi (Evans 1993)  
 Hypoglossal Nerve (=Cranial Nerve XII)—Nervus Hypoglossus (NAV)

APPENDIX 1. List of Anatomical Terms.  
(continued from the previous page)

- Hypophyseal Fossa—Fossa Hypophysealis (NAV); Pituitary Fossa (Jayne 1898)  
Hypotympanic Sinus—(Klaauw 1931)
- Incisive Foramen—Fissura Palatina (NAV); Anterior Palatine Foramen (Jayne 1898; Clark 1926; Davis 1964)  
Incisivomaxillary Canal—Canalis Maxilloincisivus (Evans 1993)  
Incisors—Dentes Incisivi (NAV)  
Incus—(NAV)  
Inferior Alveolar Artery—Arteria Alveolaris Inferior (NAV)  
Inferior Alveolar Nerve—Nervus Alveolaris Inferior (NAV)  
Inferior Alveolar Vein—Vena Alveolaris Inferior (NAV)  
Inferior Oblique Muscle—Musculus Obliquus Ventralis (NAV)  
Inferior Oblique Muscle Fossa—Pit for Inferior Oblique Muscle (Novacek 1986); Fossa Muscularis (Davis 1964)  
Inferior Petrosal Sinus—Sinus Petrosus Ventralis (NAV)  
Inferior Vestibular Area—(Terry 1942); Area Vestibularis Inferior (NAV); Inferior Cribriform Spot (Jayne 1898)  
Infraorbital Artery—Arteria Infraorbitalis (NAV)  
Infraorbital Canal—Canalis Infraorbitalis (NAV)  
Infraorbital Foramen—Foramen Infraorbitale (NAV); Infra-orbital Foramen (Jayne 1898)  
Infraorbital Margin—Margo Infraorbitalis (NAV)  
Infraorbital Nerve—Nervus Infraorbitalis (NAV)  
Infraorbital Vein—Vena Infraorbitalis (NAV)  
Infratemporal Crest—Crista Infratemporalis (NAV)  
Infratemporal Fossa—Fossa Infratemporalis (NAV)  
Interfrontal Suture—Sutura Interfrontalis (NAV)  
Interincisive Foramen—(Cooper and Schiller 1975); Canalis Interincisivus (NAV); Medial Accessory Foramen (Giannini and Simmons 2007); Stenos Foramen (Gaubert et al. 2005); Interincisive Canal (Schaller 1992)  
Intermaxillary Suture—Sutura Intermaxillaris (Evans 1993); Middle Part of Sutura Palatina Mediana (NAV)  
Internal Acoustic Meatus—Meatus Acusticus Interna (NAV); Internal Auditory Meatus (Gregory 1910)  
Internal Carotid Artery—Arteria Carotis Interna (NAV)  
Internal Carotid Nerve—Nervus Caroticus Internus (NAV)  
Interpalatine Suture—Caudal Part of Sutura Palatina Mediana (NAV)  
Interpremaxillary Suture—Sutura Interincisiva (NAV); Rostral Part of Sutura Palatine Mediana (NAV)
- Jugal—Os Zygomaticum (NAV); Malar (Jayne 1898; Gregory 1910)  
Jugular Foramen—Foramen Jugulare (NAV)  
Jugulohyoid Muscle—Musculus Jugulohyoideus (NAV)
- Labial Mandibular Foramen—(Kielan-Jaworowska and Dashzeveg 1989); Masseteric Foramen (Osgood 1921; Abbie 1939)  
Lacrimal—Os Lacrimale (NAV); Lachrymal (Jayne 1898; Gregory 1910)  
Lacrimal Fenestra—(Wible and Gaudin 2004)  
Lacrimal Foramen—Foramen Lacrimale (NAV); Lachrymal Foramen (Clark 1926); Opening of Lachrymal Canal (Jayne 1898)  
Lacrimal Fossa—Fossa Sacci Lacrimalis (NAV)  
Lateral Articular Facet of Incus—Lateral Facet of Incus (Jayne 1898)  
Lateral Laminae of Vomer—(Evans 1993)  
Lateral Palatine Process, Premaxilla—(Wible et al. 2009)  
Lateral Process of Malleus—Malleus, Processus Lateralis (NAV); Short Process (Jayne 1898)  
Lateral Pterygoid Muscle—Musculus Pterygoideus Medialis (NAV); Musculus Pterygoideus Internus (Turnbull 1970)  
Lateral Semicircular Canal—Canalis Semicircularis Lateralis (NAV)  
Lenticular Process of Incus—Incus, Processus Lenticularis (NAV)  
Lesser Petrosal Nerve—Nervus Petrosus Minor (NAV); Minor Petrosal Nerve (Evans 1993)  
Levator Veli Palatini Muscle—Musculus Levator Veli Palatini (NAV)  
Longus Capitis Muscle—Musculus Longus Capitis (NAV); Rectus Anticus Major (Jayne 1898)

## APPENDIX 1. List of Anatomical Terms.

*(continued from the previous page)*

- Major Palatine Artery—Arteria Palatina Major (NAV); Descending Palatine Artery (Davis and Story 1943)  
 Major Palatine Foramen—Foramen Palatinum Majus (NAV); Anterior Palatine Foramen (Gregory 1910); Posterior Palatine Foramen (Jayne 1898; Davis 1964)  
 Major Palatine Sulcus—Sulcus Palatinus (NAV)  
 Malleolar Hook—(Wible and Spaulding 2012)  
 Malleus—(NAV)  
 Mandible—(NAV)  
 Mandibular Canal—Canalis Mandibularis (NAV)  
 Mandibular Foramen—Foramen Mandibulare (NAV); Dental Foramen (Jayne 1898)  
 Mandibular Nerve—Nervus Mandibularis (NAV)  
 Mandibular Notch—Incisura Mandibulae (NAV); Superior or Sigmoid Notch (Jayne 1898)  
 Mandibular Symphysis—(Evans 1993)  
 Manubrial Base of Malleus—(Henson 1961)  
 Manubrium of Malleus—Manubrium Mallei (NAV); Handle (Jayne 1898)  
 Marginal Sulcus—Sulcus Marginalis (NAV); Lateral Sulcus (Radinsky 1978); Fissura Lateralis (Carlsson 1900)  
 Masseter Muscle—Musculus Masseter (NAV)  
 Masseteric Artery—Arteria Masseterica (NAV)  
 Masseteric Crest—Crista Masseterica (Turnbull 1970)  
 Masseteric Fossa—Fossa Masseterica (NAV); Coronoid Fossa (Reighard and Jennings 1935)  
 Mastoid Canaliculus—Canaliculus Mastoideus (NAV); Auricular Canaliculus (Jayne 1898); Passage for Auricular Nerve (McDowell 1958)  
 Mastoid Exposure of Petrosal—Processus Mastoideus (NAV)  
 Mastoid Shelf—this study  
 Maxilla—Os Maxillare (NAV); Maxillary (Jayne 1898; Gregory 1910)  
 Maxillary Artery—(NAV); Internal Maxillary Artery (Davis and Story 1943)  
 Maxillary Foramen—Foramen Maxillare (NAV)  
 Maxillary Nerve—Nervus Maxillaris (NAV)  
 Maxillary Process of Frontal—(Evans 1993); Nasal Process of Frontal (Jayne 1898); Frontal or Nasal Spine (Reighard and Jennings 1935)  
 Maxillary Tuberosity—Tuber Maxillae (NAV)  
 Maxilloturbinate (=Ventral Nasal Concha)—Os Conchae Nasalis Ventralis (NAV); Maxillo-turbinal (Clark 1926)  
 Meckel's Cartilage—(De Beer 1937)  
 Meckelian Sulcus—(Bensley 1902)  
 Medial Articular Facet of Incus—Medial Facet of Incus (Jayne 1898)  
 Medial Palatine Process of Premaxilla—Os Incisivum, Processus Palatinus (NAV)  
 Medial Pterygoid Muscle—Musculus Pterygoideus Medialis (NAV); Musculus Pterygoideus Externus (Turnbull 1970)  
 Median Lacerate Foramen—(Marshall and Muizon 1995)  
 Mental Foramen—Foramen Mentale (NAV)  
 Mesocranium—(Wible et al. 2004)  
 Middle Clinoid Process—(Jayne 1898)  
 Middle Cranial Fossa—Fossa Cranii Media (NAV)  
 Middle Ear—Auris Media (NAV)  
 Middle Meningeal Artery—Arteria Meningea Media (NAV)  
 Minor Palatine Nerve—Nervus Palatinus Minor (NAV)  
 Modiolus—(NAV)  
 Molars—Dentes Molares (NAV)  
 Muscular Process of Malleus—Malleus, Processus Muscularis (NAV)  
 Muscular Process of Stapes—Processus Muscularis Stapedis (Henson 1961)  
 Muscular Tubercle—Os Occipitale, Pars Basilaris, Tuberculum Musculare (NAV)  
 Musculotubal Canal—(Evans 1993); Canalis Musculotubarius (NAV); Eustachian Opening (Jayne 1898)  
 Mylohyoid Line—Linea Mylohyoideus (NAV)
- Nasal—Os Nasale (NAV)  
 Nasal Cavity—Cavum Nasi (NAV)

APPENDIX 1. List of Anatomical Terms.  
(continued from the previous page)

- Nasal Fossa—(Evans 1993)  
 Nasal Process of Nasal—(Evans 1993)  
 Nasopalatine Duct—(Clark 1926); Ductus Incisivus (NAV); Incisive Duct, Stenson's Duct (Reighard and Jennings 1901)  
 Nasopharyngeal Meatus—Meatus Nasopharyngeus (NAV)  
 Nasoturbinate, Nasal—(Smith and Rossie 2006); Crista Ethmoidalis (NAV)  
 Neck of Condylar Process—Collum Mandibulae (NAV)  
 Neck of Malleus—Malleus, Collum Mallei (NAV)  
 Nerve of Pterygoid Canal—Nervus Canalis Pterygoidei (NAV); Vidian Nerve (Jayne 1898)  
 Notch for Minor Palatine Nerve and Vessels—(Wahlert 1974); Palatine Notch (Davis 1964)  
 Nuchal Crest—Crista Nuchae (NAV); Lambdoidal Crest or Ridge (Jayne 1898);
- Occipital Artery—Arteria Occipitalis (NAV)  
 Occipital Complex—(Wible 2003); Os Occipitale (NAV)  
 Occipital Condyle—Condylus Occipitale (NAV)  
 Occipital Emissary Vein—Vena Emissaria Occipitalis (NAV)  
 Occipital Protruberance—Protuberantia Occipitalis Externa (NAV)  
 Occiput—(NAV)  
 Occlusal Plane of Teeth—Dentes, Facies Occlusalis (NAV)  
 Oculomotor Nerve (=Cranial Nerve III)—Nervus Oculomotorius (NAV)  
 Odontoid Notch—(Wible 2003); Fissura Intercondyloidea (Evans 1993)  
 Olfactory Bulb—Bulbus Olfactorius (NAV)  
 Olfactory Nerves (=Cranial Nerve I)—Nervi Olfactorii (NAV)  
 Ophthalmic Nerve—Nervus Ophthalmica (NAV)  
 Ophthalmic Venous Plexus—(Evans 1993); Plexus Ophthalmica (NAV)  
 Optic Chiasm—Chiasma Opticum (NAV)  
 Optic Foramen—Canalis Opticus (NAV)  
 Optic Nerve (=Cranial Nerve II)—Nervus Opticum (NAV)  
 Orbit—Orbita (NAV)  
 Orbital Crest—Crista Orbitalis Ventralis (NAV)  
 Orbital Fossa—Fossa Orbitalis (NAV)  
 Orbital Process of Lacrimal—Os Lacrimale, Facies Orbitalis (NAV)  
 Orbital Rim—Margo Orbitale (NAV)  
 Orbital Surface of Frontal—Os Frontale, Pars Orbitalis (NAV)  
 Orbitosphenoid—Os Presphenoidale, Ala Prbitalis (NAV)  
 Orbitosphenoid Crest—(Evans 1993); Crista Orbitosphenoidalis (NAV)  
 Osseous Lamina of Malleus—(Evans 1993); Lamina (Jayne 1898)  
 Osseous Nasal Setum—Septum Nasi Osseum (NAV)  
 Ossified Tentorium—Tentorium Cerebelli Osseum (NAV)
- Palate—Palatum (NAV)  
 Palatine—Os Palatinum (NAV)  
 Palatine Canal—Canalis Palatinus (NAV)  
 Palatine Process of Maxilla—Os Maxillare, Processus Palatinus (NAV)  
 Palatomaxillary Suture—Sutura Palatomaxillaris (Evans 1993); Sutura Palatina Transversa (NAV)  
 Paracanine Fossa—(Rougier et al. 1998)  
 Paracondylar Process of Exoccipital—Processus Paracondylaris (NAV); Paroccipital Process of Exoccipital (Gregory 1910); Jugular Process (Jayne 1898)  
 Paraflocculus of Cerebellum—Paraflocculus (NAV); Appendicular Lobe of Cerebellum (Jayne 1898)  
 Parietal—Os Parietale (NAV)  
 Parietal Eminence—(Jayne 1898; Terry 1942)  
 Parietal Foramen—(Boyd 1930)  
 Paroccipital Process of Petrosal—(Wible and Gaudin 2004); Processus Mastoideus (Schaller 1992)  
 Pars Canalicularis of Petrosal—(Wible 1990)  
 Pars Cochlearis of Petrosal—(Wible 1990)  
 Pars Processus Anterioris of Malleus—(Henson 1961); Long Process (Jayne 1898)

APPENDIX 1. List of Anatomical Terms.  
(continued from the previous page)

- Pars Profunda, M. Masseter—(NAV)  
 Pedicle of Incus—(Henson 1961)  
 Peduncle of Condylar Process—(Luo et al. 2002); Collum Mandibulae (NAV)  
 Perilymphatic Duct—Ductus Perilymphaticus (NAV)  
 Perilymphatic Foramen—(Wible and Hopson 1993)  
 Permanent Teeth—Dentes Permanentes (NAV)  
 Perpendicular Plate of Ethmoid—Os Ethmoidale, Lamina Perpendicularis (NAV)  
 Perpendicular Process of Palatine—Os Palatinum, Lamina Perpendicularis (NAV); Vertical Plate of Palatine (Jayne 1898)  
 Petrosal (=Petrus Temporal)—Os Temporale, Pars Petrosa (NAV)  
 Pharyngeal Branches of Ascending Pharyngeal Artery—Rami Pharyngei, Arteria Pharyngea Ascendens (NAV)  
 Piriform Fenestra—(MacPhee 1981); Pyriiform Fenestra (McDowell 1958)  
 Pontine Impression—Impressio Pontina (NAV)  
 Postdental Palate—(Andersen 1912)  
 Posterior Carotid Foramen—(MacPhee 1981)  
 Posterior Chamber of Auditory Bulla—(Pocock 1916; Klaauw 1931)  
 Posterior Crus (=Leg) of Ectotympanic—Annulus Tympanicus, Crus Posterior (NAV)  
 Posterior Crus of Stapes—Stapes, Crus Caudale (NAV)  
 Posterior Nasal Spine—Spina Nasalis Caudalis (NAV)  
 Posterior Semicircular Canal—Canalis Semicircularis Posterior (NAV)  
 Posterodorsal Process of Premaxilla—(Wible et al. 2009)  
 Postglenoid Foramen—Foramen Retroarticulare (NAV)  
 Postglenoid Process—Processus Retroarticulare (NAV)  
 Postorbital Constriction—Interorbital Constriction (Gregory 1910)  
 Postorbital Process—Os Frontale, Processus Zygomaticus (NAV)  
 Postpalatine Torus—(Novacek 1986)  
 Posttympanic Process of Squamosal—(Kielan-Jaworowska 1981; Novacek 1986); Processus Retrotympanicus (NAV)  
 Prefacial (=Suprafacial) Commissure—(De Beer 1937)  
 Preglenoid Process of Squamosal—(O'Leary and Gatesy 2008); Anterior Glenoid Process (Jayne 1898)  
 Premaxilla—Os Incisivum (NAV); Premaxillary (Jayne 1898; Gregory 1910)  
 Premolars—Dentes Praemolares (NAV)  
 Presphenoid—Os Presphenoidale, Corpus (NAV)  
 Primary Osseous Lamina—(Meng and Fox 1995)  
 Promontorium of Petrosal—(Evans 1993); Promontory (Jayne 1898)  
 Pterygoid—Os Pterygoideum (NAV)  
 Pterygoid Canal—Canalis Pterygoideus (NAV)  
 Pterygoid Fossa of Mandible—Fossa Pterygoideus (NAV)  
 Pterygoid Fovea—Fovea Pterygoideus (NAV)  
 Pterygoid Hamulus—Hamulus Pterygoideus (NAV); Hamular Process (McDowell 1958)  
 Pterygopalatine Fossa—Fossa Pterygopalatina (NAV)
- Ramus of Mandible—Ramus Mandibulae (NAV); Ascending Ramus of Mandible (Clark 1926)  
 Ramus Temporalis of Stapedial Artery—(Wible 1987)  
 Recessus Meatus—(Klaauw 1931; McDowell 1958)  
 Rectus Capitis Ventralis Muscle—Musculus Rectus Capitis Ventralis (NAV); Rectus Capitis Anticus Minor (Jayne 1898); Rectus Capitis Anterior Minor (Reighard and Jennings 1935)  
 Rete Mirabile—(NAV)  
 Retromolar Space—Retromolar Fossa (Hiatt and Gartner 1987)  
 Root of Teeth—Dentes, Radix Dentis (NAV)  
 Rostral Alar Foramen—Foramen Alare Rostrale (NAV)  
 Rostral Clinoid Process—Processus Clinioideus Rostralis (NAV)  
 Rostral Cranial Fossa—Fossa Cranii Rostralis (NAV)  
 Rostral Entotympanic—(Klaauw 1922)  
 Rostral Horn of Thyroid—Cartilago Thyreoidea, Cornu Rostrale (NAV)

APPENDIX 1. List of Anatomical Terms.  
(continued from the previous page)

- Rostral Lobe of Vermis—Cerebellum, Vermis, Pars Rostralis (NAV)  
 Rostral Opening of Pterygoid Canal—(Wible and Gaudin 2004)  
 Rostral (=Anterior) Process of Malleus—Malleus, Processus Rostralis (NAV); Folian Process of Malleus (McDowell 1958); Tympanic Plate of Anterior Process of Malleus (Henson 1961)  
 Rostral Septal Branch of Major Palatine Artery—Rami Septi Rostrales (Evans 1993)  
 Rostral Tympanic Process of Petrosal—(MacPhee 1981); Ventral Promontorial Process (Hunt 1987)  
 Rostrum—(NAV)
- Sacculae—Sacculus (NAV)  
 Sagittal Crest—Crista Sagittalis Externa (NAV)  
 Sagittal Suture—Sutura Sagittalis (NAV)  
 Secondary Facial Foramen—(Wible 1990)  
 Secondary Osseous Lamina—(Meng and Fox 1995)  
 Secondary Tympanic Membrane—Membrana Tympani Secundaria (NAV)  
 Semicircular Canal—Canalis Semicircularis (NAV)  
 Septal Process of Nasal—Os Nasale, Processus Septalis (NAV); Nasal Crest (Reighard and Jennings 1935)  
 Septal Process of Premaxilla—(Wible 2008)  
 Shoulder of Anterior Crus of Stapes—(Henson 1961)  
 Shoulder of Posterior Crus of Stapes—(Henson 1961)  
 Sphenoid Complex—(Wible 2003)  
 Sphenoidal Incisure of Vomer—Incisura Sphenoidalis (NAV)  
 Sphenopalatine Artery—Arteria Sphenopalatina (NAV)  
 Sphenopalatine Foramen—Foramen Sphenopalatinum (NAV); Spheno-palatine Foramen (Jayne 1898)  
 Sphenopalatine Vein—Venus Sphenopalatinus (NAV)  
 Sphenorbital Fissure—(Gregory 1910; Novacek 1986); Fissura Orbitalis + Foramen Rotundum + Foramen Alare Rostrale + Foramen Alare Parvum (NAV); Sphenoidal Fissure (Jayne 1898; Clark 1926); Orbital Fissure (Reighard and Jennings 1935; Evans 1993)  
 Spine of Tympanic Plate of Malleus—(Wible and Spaulding 2012)  
 Spiral Cribriform Tract—(Jayne 1898); Tractus Spiralis Foraminosus (NAV)  
 Squama of Frontal—Squama Frontalis (NAV); Horizontal Plate of Frontal (Jayne 1898)  
 Squamosal—Os Temporale, Pars Squamosa (NAV)  
 Stapedial Artery—(Wible 1984, 1987); Arteria Stapedia (Tandler 1899, 1902)  
 Stapedial Foramen—Obturator Foramen (Henson 1961); Stapes, Foramen Intracrutale (Fleischer 1973); Intracrutal Foramen (Wible 2003)  
 Stapedius Fossa—(Wible 1990); Fossa for Musculus Stapedius (Evans 1993)  
 Stapedius Muscle—Musculus Stapedius (NAV)  
 Stapes—(NAV)  
 Styliiform Process of Ectotympanic—(Klaauw 1931); Os Temporale, Pars Tympanica, Processus Muscularis (NAV)  
 Stylohyal—Stylohyoideum (NAV)  
 Stylomastoid Artery—Arteria Stylomastoidea (NAV)  
 Stylomastoid Foramen—Foramen Stylomastoideum (NAV)  
 Stylomastoid Notch—Foramen Stylomastoideum (NAV)  
 Subarcuate Fossa—Fossa Subarcuata (NAV); Fossa for Appendicular Lobe of Cerebellum (Jayne 1898)  
 Suboptic Foramen—(Gregory 1910)  
 Sulcus for Auditory Tube—Sulcus Tubae Auditivae (NAV)  
 Sulcus for Cavernous Sinus—this study  
 Sulcus for Inferior Petrosal Sinus—Sulcus Sinus Petrosi Ventralis (NAV)  
 Sulcus for Mandibular Nerve—this study  
 Sulcus for Maxillary Nerve—Sulcus Nervus Maxillaris (NAV)  
 Sulcus for Optic Chiasm—Sulcus Chiasmatis (NAV)  
 Sulcus for Sigmoid Sinus—(Wible 1990)  
 Sulcus for Superior Petrosal Sinus—Sulcus Sinus Petrosi Dorsalis (NAV)  
 Sulcus for Transverse Sinus—Sulcus Sinus Transversi (NAV)  
 Sulcus on Rostral Entotympanic for Caudal Entotympanic—this study

APPENDIX 1. List of Anatomical Terms.  
(continued from the previous page)

- Sulcus Septi Nasi—(Evans 1993); Sulcus Vomeris (Septalis) (NAV)  
 Sulcus Tympanicus—(NAV)  
 Superior Petrosal Sinus—Sinus Petrosus Dorsalis (NAV)  
 Superior Vestibular Area—(Terry 1942); Area Vestibularis Superior (NAV); Dorsal Vestibulari Area (Area Vestibularis Utriculo-ampullaris) (Evans 1993); Superior Cribriform Spot (Jayne 1898)  
 Supramastoid Crest—Crista Supramastoideus (NAV)  
 Suprameatal Crest—(Wible 2008); Dorsal Boundary of External Acoustic Meatus (Evans 1993)  
 Supraoccipital—Os Occipitalis, Squama Occipitalis (NAV)  
 Supra-optic Foramen—(Gregory 1910)  
 Supraorbital Crest—(Miao 1988); Supraorbital Arch (Reighard and Jennings 1935)  
 Supraorbital Margin—Margo Supraorbitalis (NAV)  
 Suprasylvian Sulcus—(Radinsky 1978); Sulcus Suprasylvius (NAV); Fissura Suprasylvia (Carlsson 1900)
- Teeth—Dentes (NAV)  
 Tegmen Tympani—(De Beer 1929); (NAV)  
 Temporal Fossa—Fossa Temporalis (NAV)  
 Temporal Line—Linea Temporalis (NAV); Temporal Ridge (Jayne 1898; Clark 1926)  
 Temporal Pole Depression—(Wible 2011)  
 Tensor Tympani Muscle—Musculus Tensor Tympani (NAV)  
 Tensor Veli Palatini Muscle—Musculus Tensor Veli Palatini (NAV)  
 Tentorial Process of Alisphenoid—(Jayne 1898)  
 Tentorial Process of Parietal—(Jayne 1898)  
 Tentorium Cerebelli—Tentorium Cerebelli Membranaceum (NAV)  
 Thyrohyal—Thyrohyoideum (NAV)  
 Transverse Canal Foramen—(Sánchez-Villagra and Wible 2002); Transverse Canal (Gregory 1910); Foramen Vesalii (McDowell 1958)  
 Transverse Crest of Petrosal—Crista Transversa (NAV)  
 Transverse Lamina—(Smith and Rossie 2006)  
 Transverse Sinus—Sinus Transversus (NAV); Lateral Sinus (Jayne 1898)  
 Transverse Sinus Canal—Canalis Sinus Transversi (NAV); Canalis Transversus (Evans 1993)  
 Trigeminal Fossa—(Wible 1990); Semilunar Recess (Rougier et al. 1992)  
 Trigeminal Ganglion—Ganglion Trigeminal (NAV)  
 Trigeminal Nerve (=Cranial Nerve V)—Nervus Trigemini (NAV)  
 Trochlear Nerve (=Cranial Nerve IV)—Nervus Trochlearis (NAV)  
 Tuberculum Sellae—(Evans 1993)  
 Tympanic Canaliculus—Canaliculus Tympanicus (NAV)  
 Tympanic Incisure—(Henson 1961)  
 Tympanic Membrane—Tympanum (NAV)  
 Tympanic Nerve—Nervus Tympanicus (NAV)  
 Tympanic Plate of Malleus—(Henson 1961)  
 Tympanic Process of Alisphenoid—(MacPhee 1981)  
 Tympanic Process of Basioccipital—(MacPhee 1981)  
 Tympanic Process of Basisphenoid—(MacPhee 1981)  
 Tympanohyal—(Klaauw 1931); Pit for Tympano-Hyal (Jayne 1898); Area of Attachment of Tympanohyal (Evans 1993)  
 Tympanohyaloid Cartilage—(Evans 1993); Tympano-hyal (Jayne 1898)  
 Tympanum—(NAV)
- Utricle—Utriculus (NAV)
- Vagus Nerve (=Cranial Nerve X)—Nervus Vagus (NAV)  
 Vascular Foramen of Lacrimal—(Giannini et al. 2006)  
 Ventral Condylloid Fossa—Fossa Condylaris Ventralis (NAV)  
 Vermis of Cerebellum—Cerebellum, Vermis (NAV)  
 Vermis Impression—Impressio Vermialis (NAV)

APPENDIX 1. List of Anatomical Terms.  
*(continued from the previous page)*

- Vertical Part of Exoccipital—(Wible 2003)  
Vestibular Aqueduct—Apertura Externa Aqueductus Vestibuli (NAV); Aquæductus Vestibuli (Jayne 1898);  
Opening for Vestibular Aqueduct (Evans 1993)  
Vestibular Fossula—(MacPhee 1981)  
Vestibulocochlear Nerve (=Cranial Nerve VIII)—Nervus Vestibulocochlearis (NAV)  
Vomer—(NAV)  
Vomeronasal Organ—Jacobson's Organ (Mivart 1881; Reighard and Jennings 1901)  
Wings of Vomer—Alae Vomeris (NAV)  
Zygoma—Arcus Zygomaticus (NAV)  
Zygomatic Process of Maxilla—Os Maxillare, Processus Zygomaticus (NAV)  
Zygomatic Process of Squamosal—Os Temporale, Pars Squama, Processus Zygomaticus (NAV)  
Zygomaticomandibularis Muscle—(Turnbull 1970)